Molecular charecterization and ageing of the sandarac resin and its principal component communic acid

Inna Kononenko

Université Pierre et Marie Curie

Physique et Chimie des Matériaux

ÉCOLE DOCTORALE 397

Laboratoire d'Archéologie Moléculaire et Structurale

Molecular charecterization and ageing of the sandarac resin and its principal component communic acid.

Par INNA KONONENKO

Thèse de doctorat de CHIMIE

Dirigée par M. Philippe Walter

Présentée et soutenue publiquement le 20 Septembre 2017

Devant un jury composé de :

Mme. Carine van HEIJENOORT, Directrice de recherche au CNRS, UPSaclay, ICSN	Rapporteur
M. Mathieu MENAGER, Maitre de Conférence, UAPV, IMBE	Rapporteur
M. Christian BONHOMME, Professeur, UPMC, LCMCP	Examinateur
Mme. Caroline TOKARSKI, Professeur, Université de Lille, MSAP	Examinateur
Mme. Jeanine TORTAJADA, directeur de recherche au CNRS, Université d'Evry, LAMBE	Examinateur
M. Philippe WALTER, directeur de recherche au CNRS, UPMC, LAMS	Directeur de thèse
Mme. Laurence de Viguerie, chargée de recherche CNRS, UPMC, LAMS	Co-directrice de thèse, membre invité

Glossary

ACN	acetonitrile
APCI	atmospheric pressure chemical ionisation
CI	chemical ionisation
CID	collision induced dissociation
COSY	correlation spectroscopy
CP	cross-polarization
Da	dalton
DCM	dichloromethane
DEPT	distortionless enhancement by polarization transfer
DMSO	dimethyl sulfoxide
DTMS	direct temperature-resolved mass spectrometry
EI electron	electron impact, electron ionisation
ESI	electrospray
eV	electronvolt
GCMS	gas chromatography-mass spectrometry
HMBC	heteronuclear multiple bond correlation
HPLC	high performance liquid chromatography
HSQC	heteronuclear single-quantum correlation
IRCP	inversion recovery cross-polarization
IS	internal standard
$M^{+\cdot}$	molecular ion
$(M+H)^{+}$	protonated molecule
MALDI	matrix-assisted laser desorption/ionisation
MAS	magic-angle-spinning
MS	mass spectrometry
MS-MS	tandem mass spectrometry
MW	molecular weight
m/z	mass/charge
NMR	nuclear magnetic resonance
SEC	size exclusion chromatography
SP	simple pulse
THF	tetrahydrofuran
TIC	total ion current
TOCSY	total correlation spectroscopy
UV	ultraviolet (light)
VIS	visible (light)

Contents

1. Introduction

In his collection of writings 'A Treatise on Painting', Leonardo da Vinci proposes a recipe for an excellent varnish based on the cypress resin: '...incise a cypress in April or May, mix the exuded liquor with nut oil and get a perfect varnish…' [1]. The term varnish designates the material deposited on the surface of the painting to protect it and to improve the saturation of the colours.

Leonardo da Vinci pointed out in his text the necessity to use a resin just exuded from the tree at the beginning of spring. So, it is important to distinguish between the fresh and aged resins. In the existing literature concerning this subject different definitions of aged and fresh resin exist. According to most of the articles, the aged resins are those that were aged on purpose by exposing the resin-based varnish to the artificial and non-artificial light [2, 3]. And the resins that were obtained by means of extraction from a plant and did not undergo any specific light treatment are called fresh resins. That can be confusing as the natural resins have tendency to be modified with time when extracted. So, the fresh resins are those that are used at once when exuded from a tree and protected from spontaneous oxidation and polymerisation on air by taking the precautions. The aged resins, in its turn, are those that were exposed to air during some period of time even without being aged on purpose. Obviously, the longer the resin is exposed to the environment the more aged it becomes and consequently harder in its consistency.

Leonardo da Vinci has certainly looked for particular materials to achieve the perfection of the surface of his painting and create realistic effects of shadows and light. He has found the right mixtures of substances to get there, certainly from many trials. Unfortunately today, without an invasive method of analysis, the nature of these binders and the organic substances used remain mysterious. The project of this thesis is therefore to study the nature and chemical properties of one of the substances that may have been used by Leonardo da Vinci, or other artists at different periods in history. From a fine characterization of their components, the molecular organization of the mixtures and their ageing will be studied using different characterization techniques.

Ageing of varnishes is one of the principal problems met by painting conservators, as it leads to yellowed products that can obscure colours, become very brittle and show a change in solubility [4]. Since these physical changes are the consequence of molecular changes in the varnish, it is significant to study these ageing processes on a molecular level. That is why

the molecular ageing process of the diterpenoid resin *sandarac* has also been investigated. The *sandarac* resin is the cypress resin, that has been widely used throughout history for artistic purposes as protective varnishes, additives to modulate the rigidity of pictorial layers and fixatives for artistic drawing [5, 6, 7, 8]. The *sandarac* resin (like copals, so-called fossil resins) consists essentially of a highly polymerized fraction of communic acid, a labdane with system of conjugated double bonds (Figure 1) that demonstrate a strong tendency to the polymerisation when executed from trees and readily reticulate as soon as it comes into contact with light and air. Initial polymerisation likely occurs starting from conjugated double bonds of the communic acid with a mechanism shown in the figure below [9].

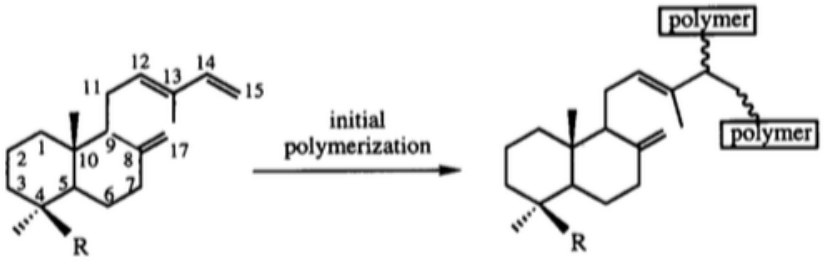

Polymerisation of communic acid [9].

Based on this background, the communic acid is chosen as a simplified model of the *sandarac* resin and thus the resin polymerisation is investigated by means of isolation of the communic acid from cones of the cypress *Cupressuss semperverins* and exploring its first stages of drying/ageing by time-resolved studies (a few hours to a week).

This strategy is justified by the fact that the natural resins are very complex mixtures of different compounds, mostly terpenoids. With ageing, the complexity increases even more. In order to understand the ageing behaviour of such complex mixtures, it is useful to first study the ageing behaviour of individual components [10].

Thus, the molecular changes in the *sandarac* resin are investigated by comparative studies of pure communic acid, artificially aged communic acid and commercial resin samples.

In the present research work a multiple analytical approach including numerous mass –spectrometric and spectroscopic techniques is applied aiming to give an informative characterization of the samples of interest.

At first, the *sandarac* resin is analyzed by gas chromatography-mass spectrometry (GC-MS) to qualitatively identify the constituent compounds of low molecular weight part of the sample. The quantitative assessment of the diterpenoid part is performed as well by the method of internal standard in order to clarify what actual part of the sample is being analyzed by this method.

However, GC-MS analysis does not provide information on the polymerization of organic compounds and their chemical modifications following their ageing. An original approach based on the study of compounds of high molecular weights is developed in order to better understand the mechanisms involved. The intact polymers and chemical modifications of their main constituent are studied by MALDI-TOF and ESI-Orbitrap mass spectrometry.

These analyses are supplemented by ^{1}H, ^{13}C 1D and 2D NMR (COSY, TOSCY, HSQC, HMBC) spectroscopy in solution to better understand the fingerprints of the different molecules that may be characteristic of each pure natural substance. This also makes it possible to evaluate the sensitivity of this technique for the study of samples of historical interest.

In order to get a complementary information on the analyzed samples, the chemical composition of the *sandarac* resin is investigated by solid-state ^{13}C NMR. Solid-state ^{13}C NMR analysis allows characterizing the insoluble in most organic solvents and cross-linked polymers, which is the case of the *sandarac* resin. The spectra are measured with a number of ^{13}C solid-state MAS NMR techniques such as SP (single-pulse), CP (cross-polarization), IRCP (inversion recovery cross-polarization).

As mentioned above, communic acid serves as a simplified reference system for the *sandarac* resin and ESI-Orbitrap is selected as the primary analytical tool to study its polymerisation/ ageing behaviour. Infrared spectroscopy technique is applied as well to follow the qualitative evolution of the communic acid with polymerisation/ ageing.

2. Bibliography

2. A. Introduction

The theme of this PhD work brings to the necessity to deeper knowledge and background on what it is already known on the *sandarac* resin and its main component communic acid.

At first, the *sandarac* resin is reviewed in its biological origin, historical aspects and its chemical composition. Particular attempt was made to reveal a misconception that exists regarding the origin of the *sandarac* resin. The resin that is commercially available today on the market and called *sandarac* is the resin that was extracted from cypresses that are planted in the region of North Africa and belong to the family Cupressaceae. Therefore, in this thesis when using word *sandarac*, we will be referring to the natural resin obtained from plant belonging to the family of Cupressaceae (*Tetraclinis Articulata*) commercially available but without information on how long the resin was stocked after its actual extraction from a tree.

After bibliographic research on the *sandarac* composition, a contradiction among the presented information on this topic was noticed. While one source reporting on *sandarac* claimed the presence of agathalic acid as a major component of the resin [3, 11], the others testified the sandaracopimaric acid being the principal component [5].

Special attention is paid to the analytical techniques that were already applied towards study on the chemical composition of the *sandarac*, since investigation of new analytical approaches and their eligibility for the chosen samples is being assessed in this research work and presents important part of this research.

A chronological research in the treatises of painting and book of recipes allowed to evaluate the occurrence of the ingredients used by artists for the development of the varnishes, and thus to emphasize their specificities. New databases, such as the one launched by the City of Music (VERNIX), facilitated access to a large number of recipes. Oil varnishes, prepared by mixing drying oils (mainly linseed or nut oils) and natural resins, have been commonly used by artists since the 11^{th} century.

Further, the instability of varnishes, that oxidize and yellow with time, is presented as a problem of major importance since yellowing obscures a painting and can considerably

change its appearance. As a consequence, varnishes have to be removed and replaced rather often, a harsh treatment that can damage the painting.

Finally, a review on chemical reactivity and properties of communic acid is accomplished, from which it can be concluded that the communic acid is frequently used as a precursor for many organic syntheses.

2. B. Diterpenoid resin – the sandarac resin: properties and applications

2. B. I. Biological origin of the *sandarac* resin

The term *resin* originated from Latin refers to a viscous and odorous substance exuded by the plants for the purpose of defence, protection and contact with their ecosystem.

Resins are secondary metabolites and play, in fact, a primary role in the physiological functioning of the plant. Composed of terpenes and sometimes phenolic compounds, resins can be secreted by different types of internal or external structures. Photosynthesis produces carbohydrates whose rupture yields pyruvate products. It is these products, which are transformed into terpenes and phenolic compounds and go throw two biosynthetic pathways involving mevalonate (MVA) or 1-deoxy-D-xylulose-5-phosphate (DOXP) [12].

The terpenes are formed from an isoprene unit (Figure 1) and are classified according to the number of carbon atoms they possess: monoterpenes (C10) and sesquiterpenes (C15) are volatile compounds, while diterpenes (C20) and triterpenes (C30) are not. According to the biosynthetic path followed, the plant produces diterpenes and / or monoterpenes or triterpenes and / or sesquiterpenes. It is therefore possible to divide the majority of resins according to the type of terpene molecules present: diterpene and triterpene resins.

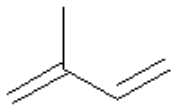

Figure 1. Isoprene molecule.

The phenolic compounds generally comprise an aromatic ring and at least one hydroxyl group. They can have different functions at the level of the plant: pigmentation of the flowers, protection against the UV, and contact with the other living organisms.

The external secretion of resin allows trapping enemies of the plant or filling wounds made to the trunk. It must also be considered that the large number of molecules of different nature prevents rapid adaptation of the harmful organisms to the plant and that certain resins will also attract the predators of these organisms. The role of resins is therefore of an ecological nature as well.

2. B. II. Historical issues on the *sandarac* resin

Due to their many properties, resins have had varied functions over time. They were frequently used for therapeutic and ritual purposes or even sometimes used as glue or to seal the hulls of ships. They were also used sometimes in the manufacture of natural varnishes. Therefore this material has been always an object of exploitation and extensive market that has even allowed economical rising of some regions of the world.

The resin market dates back at least to 1800 B.C. Just like Silk Road or a spice trade, the amber road (fossilised resin) existed as well. In the IVth century B.C., the Greek botanist Theophrastus described the usage of resins for sealing boats. This is actually how the pine resin contributed to economical growth of the North America as a necessary material for waterproofing of the Great Britain's flotilla [12, 13].

The technique of resins collection differs depending on the plant. Nevertheless, in order to collect a considerable amount of the resin the incisions are frequently applied to the bark of the tree.

a)  b) 

Figure 2. a) The resin exudates; b) Cypress *Cupressus sempervirens*.

In this work the resin of interest is the diterpene resin *sandarac* mainly used for artistic purposes. The term *sandarac* comes from the Greek sandarákê meaning also realgar. It refers

to the red colour of this arsenic sulphide or a resin from *Tetraclinis articulata*. Dissolved in heated linseed oil, it gives the *'vernice liquida'*, a recipe widely used in Italy especially in the 16th century [14, 15, 16, 17]. The *sandarac* was used from the 12th to the 15th century as an alcoholic varnish and then again as lean varnish in the 17th-18th century. Well dissolved in alcohol and castor oil (or lavender) this resin allows elaborating the so-called 'French Varnish'. Used since the Middle Ages, today it is mainly applied for wood polishing as it produces a hard and shiny varnish. It is interesting to note that the *sandarac* is a very hard resin and sometimes difficult to dissolve, which causes problems during the manufacture of *'vernice liquida'* in particular.

However, the origin of the term *sandarac* itself is problematic. Indeed, the appellation '*sandarac resin*' has undergone changes over the centuries making it difficult to interpret certain texts.

The authors of ancient manuscripts often describe the *sandarac* as Juniper resin (Juniperus). The Junipers appear in nature under different species of shrubs depending on the region. The main ones are: *Juniperus communis* found in moors and limestone and whose black 'berries' (actually cones) can be used to produce alcohol, *Juniperus oxycedrus* that is planted in garrigue and in the maquis, the *Juniperus thuriferus* threatened species that comes from the North Africa and is exploited for its wood and *Juniperus phonicea* that stretches along the Mediterranean shore.

Starting from the 16th century some authors reveal the confusion in the usage of the term '*sandarac'* [18]. However, until the end of the 19th century, this term was linked to the resin of Juniper, a common mistake. This century marks a turning point because the *sandarac* appears also under the name of resin of *Thuya articulata* that corresponds to the genus *Tetraclinis*. *Tetraclinis articulata*, due to its resemblance to the species *Callistris*, was also classified as *Callitris quadrivalvis* during a period of considerable duration [12]. Nevertheless, the Australian *sandarac* from *Callitris* trees was not exported.

The place of the resin active utilization was probably the Mediterranean region, rather in Italy and North Africa. The African *sandarac* was exported from the port of Mogador, hence the name sometimes used 'sandarac from Mogador' [12].

Hopefully, today the clearance has been reached and the distinction is now transparent. The *sandarac* resin marketed today is the one exuded from the *Tetraclinis articulata* tree, a small conifer of the *Cupressaceae* family.

As to the resin formerly used, it remains unknown whether it belonged to a species of Juniper or to *Thuya articulata*. Indeed, it was described as a species apart only starting from 1791 and would have been formerly described as Juniper. It is therefore difficult to know the true botanical origin of the *sandarac* before the 19th century, especially in the light of the fact that the term '*sandarac'* was sometimes attributed to amber or the copal resin.

Thus in the attempts to reproduce the varnish based on the *sandarac* resin, it is necessary to keep in mind this problematic concerning the resin used in accordance to the recipe of the epoch.

2. B. III. Chemical composition of the *sandarac* resin

Sandarac from *Tetraclinis articulata* is a highly odorous resin, usually light yellow in colour and with a melting point around 145 °C (Figure 3).

a)  b) 

Figure 3. a) The *sandarac* resin; b) *Tetraclinis articulata*.

The main component of the commercial *sandarac* (more than 70%) is the communic acid (Figure 4), a bicyclic diterpenoid which spontaneously polymerizes to polycommunic acid. The latter compound is responsible for the polar character and the low solubility exhibited by this resin after ageing. In *sandarac*, free diterpenoids (nearly 30%) are of the pimarane type, such as pimaric and sandaracopimaric acids, and in smaller amounts of abietane (laevopimaric acid) or phenolic products, manool or totarol [5].

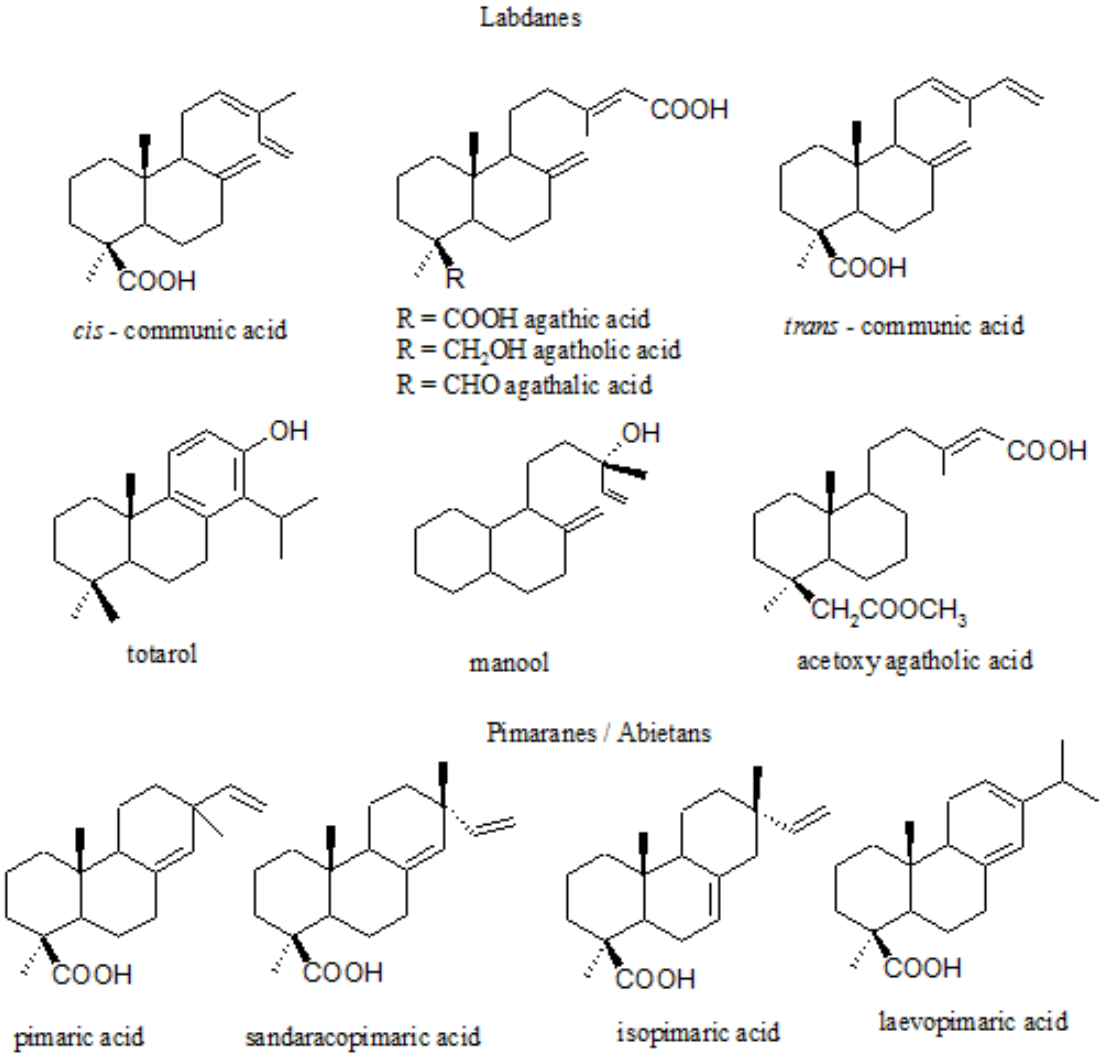

Figure 4. Chemical structures of some diterpenoid labdanes, pimaranes and abietans of the *sandarac* resin [5].

2. C. Previous analytical methods applied to the *sandarac* resin

For the time being there are very few publication consecrated solely to the analysis of the *sandarac* resin. The most extensive and multiple approach analysis of the commercially available sandarac resin has been done by Scalarone's team [11].

At first, THM-GC/MS has been applied to samples of the *sandarac* and was found to be a suitable process for the recognition of small molecules and macromolecular compounds. Its main disadvantage is that the high temperatures associated with the pyrolysis process lead to secondary degradation reactions, particularly isomerization and defunctionalisation, whose main effect is to increase the complexity of the resulting pyrograms, and thus its

interpretation. Comparison with GC/MS permitted to distinguish primary and secondary pyrolysis products.

As previously mentioned, the *sandarac* contains a highly cross-linked portion of the polycommunic acid, which is hard, resistant and almost insoluble in most organic solvents. The *sandarac* can be mixed with oils only after the subsequent heating, decarboxylation and fragmentation of the polycommunic acid.

Evidently, gas chromatography - mass spectrometry (GC/MS) has proved to be the leading technique in the analysis of a variety of di- and triterpenoid resins, but by this technique only the low molecular weight fraction, which is mainly composed of labdane molecules and sandaracopimaric acid, can be identified.

To determine the nature and composition of the cross-linked fraction, analytical pyrolysis is required. A two-step Py-GC / MS technique was applied to the *sandarac* analysis, and several diterpene compounds were identified. The procedure involves on-line derivatization at 250 °C with tetramethylammonium hydroxide (TMAH) in the first step and pyrolysis of the remaining high molecular weight fraction in the second step. The polymer fraction was found to be mainly composed of communic acid.

Further information was obtained from the DTMS. The EI-DTMS addition of the sandarac spectrum, after derivatization with TMAH, specifically highlighted polymeric nature of the samples where the methylated communic acid monomer (at m/z 316), the dimers (m/z 632) and trimers (m/z 948) were identified. Additionally, further details on the composition of the *sandarac* have been obtained from Fourier transform infrared spectroscopy (FTIR) and size exclusion chromatography (SEC), and the later supported the occurrence of bond scissions.

Another scientific group that dedicated their research to the *sandarac* analysis has applied as-well GC-MS methods [5]. Diterpenoid compounds identified in the sandarac were different from those found by [11], and included: manool, sandracopimaric acid, isopimaric acid and OH-sandaracopimaric acid. The detail to be mentioned is that in this study the resin was analysed in form of the varnish and the samples were prepared in the proportion of 100 g of resin per 200 ml of absolute ethanol.

In a recently defended thesis by C. Azemard [19] the *sandarac* was analyzed among others. The chemical composition (free diterpenoids) as well as evolution during ageing of the resin was studied in this work by GC-MS and FTIR.

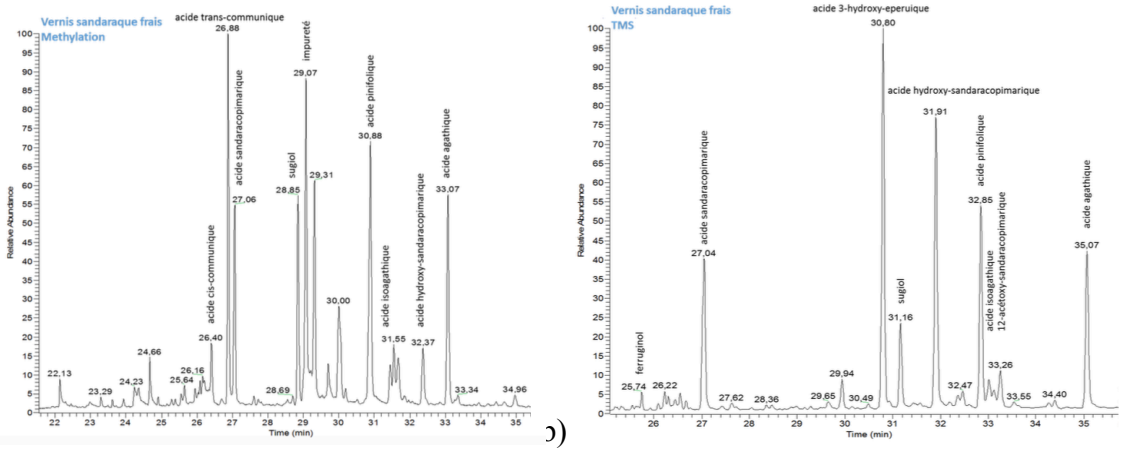

a) b)

Figure 5. Chromatograms and compounds identified in the *sandarac* after a) methylation; b) trimethylsylilation.

The compounds identified by GC-MS in this case also differ from those identified in the two works mentioned above. Moreover the different results were obtained when the derivation procedure was changed from methylation to trimethylsylilation. Thus, the extractable fraction of the *sandarac* is composed of numerous pimaranes such as sandaracopimaric, hydroxypimaric and 12-acetoxy-sandaracopimaric acids. It is also composed of labdanes like pinifolic and agathic acids. Phenols, such as sugiol and ferruginol, have also been identified (Figure 5).

Finally, the Japanese research team leaded by Tanamoto [20] aimed to identify the main constituents of the sandarac resin, to evaluate its quality as a food additive. Three constituents were isolated and identified as sandaracopimaric acid, sandaracopimarinol and 4-epidehydroabietic acid by MS and 2D-NMR. Quantification of the main constituent, sandaracopimaric acid, was performed by HPLC and its content in the product was determined to be 11.6%.

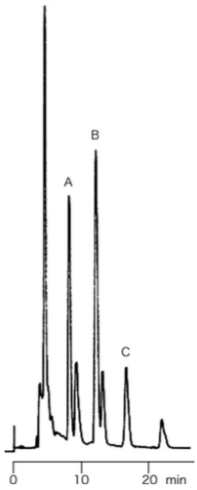

Figure 6. HPLC profile of the *sandarac* resin product. Peak A = 4-epidehydroabietic acid (3). Peak B sandaracopimaric acid (1). Peak C sandaracopimarinol (2) [20].

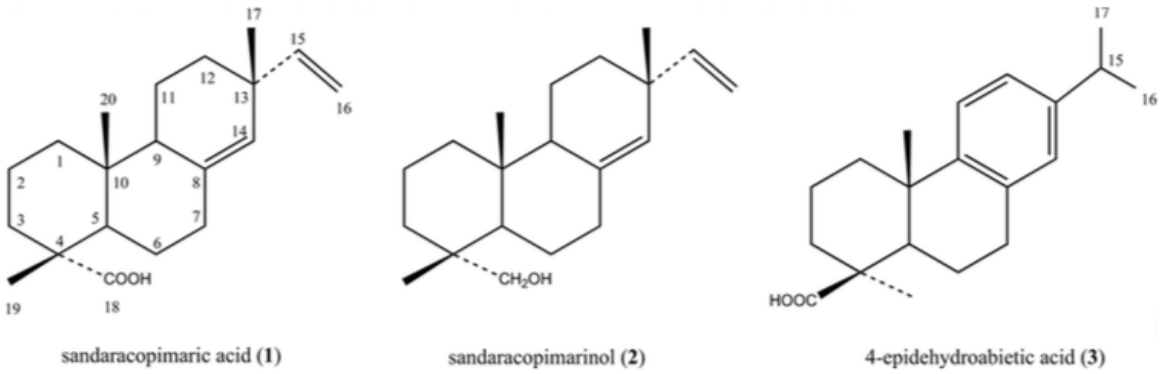

Figure 7. Structures of sandaracopimaric acid (1), sandaracopimarinol (2) and 4-epidehydroabietic acid (3) [20].

Scalarone et al. [11] has studied the accelerated photo-ageing of the *sandarac* resin when used as artistic materials. In this research the *sandarac* was subjected to an artificial exposure in order to study the processes of photo-ageing.

In [11], several mass spectrometric (GC/MS, THM-GC/MS, DTMS), chromatographic (SEC) and spectroscopic (FTIR) techniques were applied to the study of unaged and aged *sandarac* samples in order to identify their main components and to monitor changes in composition during ageing.

The *sandarac* low molecular weight fraction was identified by GC/MS, after methylation with TMS-diazomethane, while pyrolysis, applied under thermally assisted

hydrolysis and methylation (THM) conditions, was used to analyze the whole resin and isolated reticulated fraction.

To determine the nature and composition of the cross-linked fraction, pyrolysis is necessary. Thermally assisted hydrolysis and methylation, coupled with gas chromatography - mass spectrometry (THM-GC/MS), were used to identify the acid compounds. It is due to the pyrolysis, many secondary products have been recognized and distinguished from the original components of the resin. More details on the composition of *sandarac* were obtained from Fourier transform infrared spectroscopy (FTIR), size exclusion chromatography (SEC) and direct temperature - resolved mass spectrometry (DTMS). During ageing, it has been found that cross-linking and cleavage reactions have affected the chemical structure of *sandarac*, as well as minor degradation processes such as isomerization and oxidation.

According to the authors, polymerization probably begins with a radical mechanism from the conjugated double bonds of labdane-type molecules such as cummunic acid. The maturation of the polymer derived from labdanes is continued by isomerization, cross-linking and cyclization reactions.

The free diterpenoids identified by GC/MS (Figure 8) are sandaracopimaric acid (10), agathic acid and its monomethylester, agathalic acid (11) and acetoxy agatholic acid (13). *Cis*-communic acid (8) and *trans*-communic acid (9) were detected as traces in the non-aged samples and they disappear completely in the aged ones.

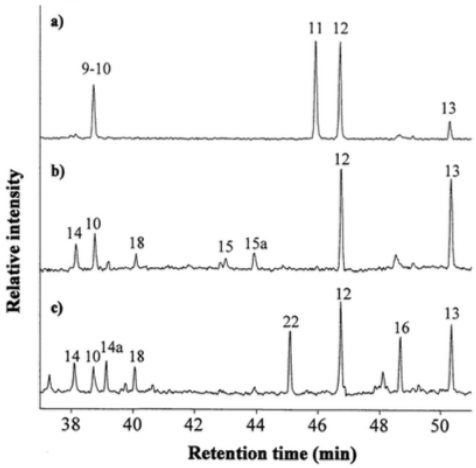

Figure 8. Total ion chromatograms of the soluble fraction of *sandarac* after derivatisation with TMS - diazomethane. (a) Unaged, (b) aged 600 h under fluorescent lamps, (c) aged 1000 h under a xenon lamp [11].

THM-GC/MS allowed the identification of high and low molecular weight components simultaneously. The pyrograms in the Figure 9 show signals of the polymer fraction, free diterpenoids and monoterpenes in the non-aged *sandarac*. The main disadvantage of this technique, particularly when compared with conventional gas chromatography, is the large number of substances that come from the pyrolysis process. Free diterpenoid acids readily undergo secondary pyrolysis, fragmentation, isomerization and recombination reactions which lead to the appearance of a large number of peaks, especially in retention times of between 35 and 50 min.

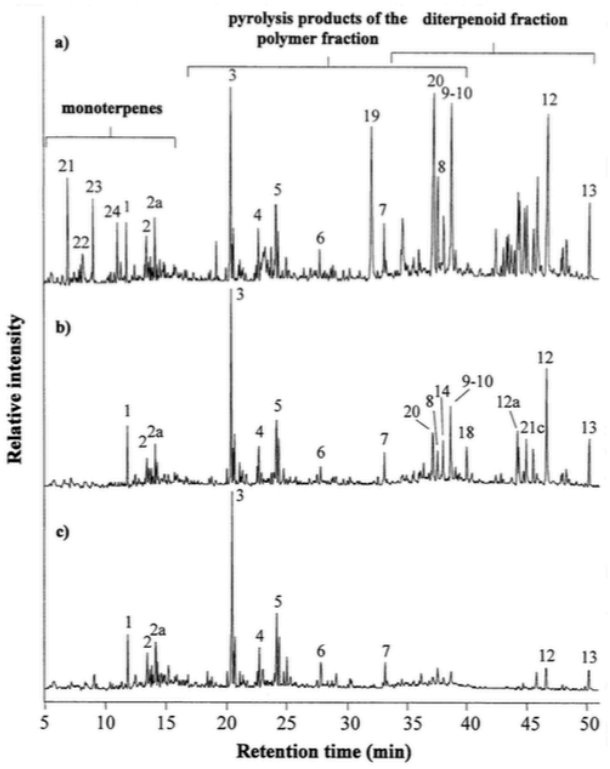

Figure 9. THM-GC/MS curves of *sandarac*. (a) Unaged, (b) aged 600 h under fluorescent lamps, (c) aged 1000 h under a xenon lamp [11].

2. D. Varnishes based on the *sandarac* resin: fabrication and applications

2. D. I. Historical review

The term '*varnish'* can be interpreted as corresponding to the material deposited on the surface of the painting to protect it and to improve the saturation of the colours. It comes

from the Medieval Latin '*veronice'*, designating the *sandarac*, or from Greek *Beronikê*, the first city that exported the resin (now Benghazi) [21].

The varnish recipes used for paintings consist of at least one film-forming resin dissolved in a solvent. Just as painting art (where oil replaced egg and water), the composition of varnishes has evolved over time as well.

Natural varnishes are made from natural resin dissolved in different media:

- in the oil, usually linseed oil, giving a fatty varnish
- in the spirit, forming a 'lean' varnish
- in the alcohol, an alcoholic varnish is then obtained

For a long time, the varnishes were called 'greasy' and consisted of an oil-resin mixture. One of the first recipes was discovered in Lucca's manuscript, dating from the eighth century; it would be the first mention of oil used for painting in the West [22]. The varnishes were prepared by dissolving resins (sandarac, putty, rosin ...) by heating in drying oils, or by first melting the resins and adding the oil thereafter.

Then, these oil varnishes were gradually replaced, from the end of the 16th century, with so-called 'lean' varnishes, with spirit, solutions of natural resins in a volatile solvent, usually spirit of turpentine.

Some recipes mention the addition of an oleoresin (natural secretion such as exudates from conifers, copaerals and elemis. It is made of a spirit and the resin resulting from the oxidation of this spirit), such as turpentine from Venice [16]. This oleoresin probably acts as a plasticizer to prevent the mixture from being too brittle [23]; the addition of a small quantity of oil to the resin / spirit mixtures would follow the same objective according to the present recipes [24].

This evolution has been followed through about fifty recipes from various sources [7, 18, 25, 26]. The use of the database developped at the Cité de la Musique (by Valéri Malecki) on the recipes of varnish of violins facilitated this research. The sources available are generally common to the different arts and there are recipes of varnish specific to musical instruments alongside those used in painting. The evolution of the different types of varnish, based on this basis, is shown in Figure 10 [27].

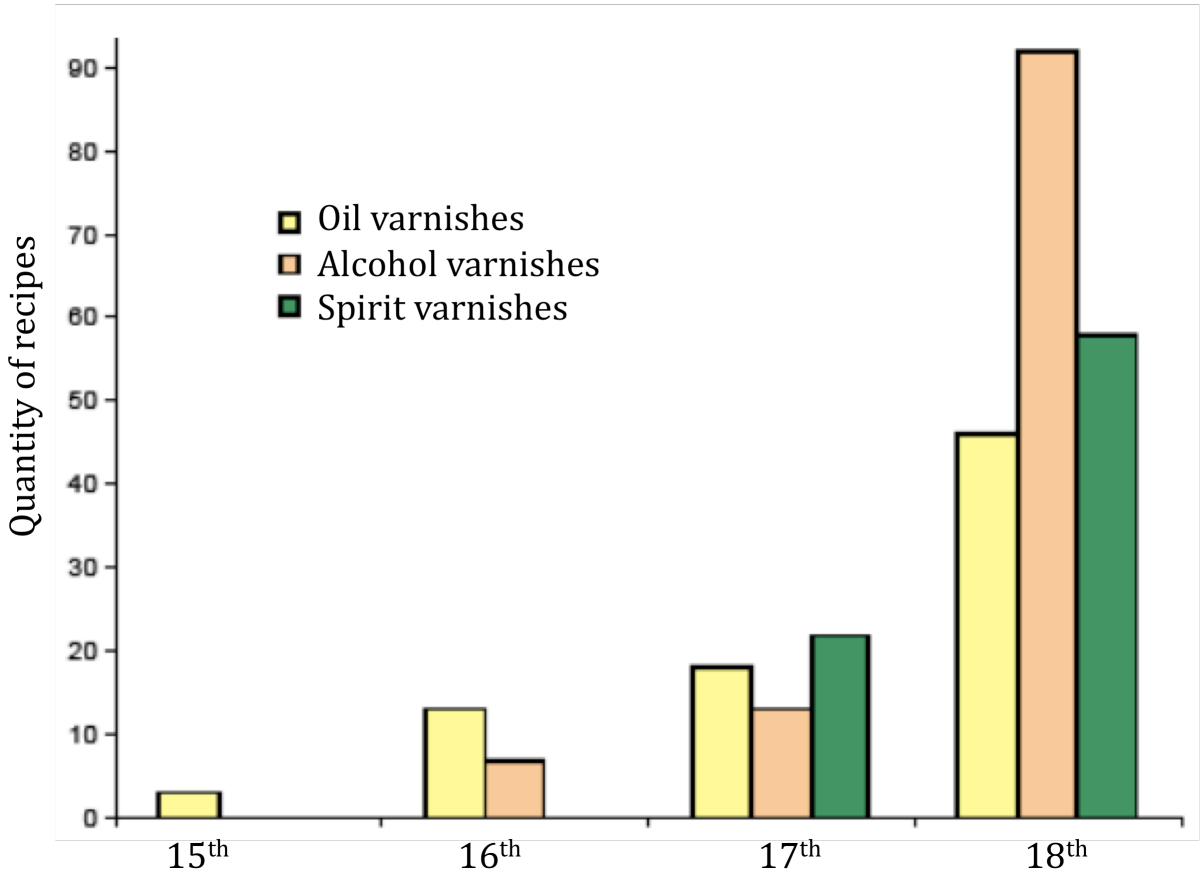

Figure 10. Evolution of types of varnish between the 15th and 18th centuries, according to the Cité de la Musique database [27].

Alcohol varnishes are not used for paintings. This example comes from the sources exploited to date and cannot therefore be considered as a general view of the evolution of the use of these varnishes.

2. D. II. Elaboration of different kinds of varnishes

2. D. II. 1. Oil varnish

As previously indicated, the varnishes based on oil are mentioned as early as the eighth century in the Lucca's manuscript [22]. The choice of the oil is the main concern for the varnish preparation. The oil has to be as light as possible, quickly drying and not to have a very strong smell. The oil-based varnishes are much more flexible and have fewer tendencies to break than the alcohol-based ones. Nevertheless, oil varnishes require a longer time to dry

and bring more pronounced colouring to the paintings. Cennini advises to apply the varnish outside by unwind weather, in the sun. In case of the absence of sunlight, the author proposes to boil the varnish at first, which allows a better drying [28].

To make the 'fat' varnishes, one technique is to heat the resin and oil separately. According to Watin [8], the resin must be previously crushed but not reduced to powder, which is in contradiction with other recipes [14]. When the resin is almost completely molten and fluid, the oil is incorporated. Another method consists in reducing the resin into fine powder and incorporating it into warmed up oil, and continuing to heat the mixture for some time [14].

Drying properties of the linseed oil and its clear colour make this oil one of the most preferred among artists. Walnut oil, poppyseed oil and lavender oil were widely used as well.

In order to improve the drying properties and transparency of oils, they were purified, degreased or clarified. The process of purification included heating oil during several hours maintaining steering. Then may follow the addition of litharge (one of the natural mineral forms of lead oxide (II) PbO) and/ or lead, white lead (the basic lead carbonate ($2PbCO_3 \cdot Pb(OH)_2$)), calcium carbonate or other compounds allowing to dry and degrease oils. The mixtures were kept heating and then allowed to settle. This procedure had a total duration of several days and oils had to 'rest' in the tank for several month to be ready for use [7, 18, 29]. Cleared oils are also called "sun oils" as they were left for days in the sun until they became clear enough.

Heating of oils raises a safety issue. Indeed, it has a tendency to inflame spontaneously when the temperature reaches approximately 360 °C, thus the control of the temperature of heating is therefore essential.

Some recipes:

A recipe of an oil-based varnish that returns very regularly in the manuscripts of the 12th century is that of the '*vernice liquida*'. This varnish consisting of linseed oil and the *sandarac* has been considered for a long time to be the best varnish. The ordinary recipe of '*vernice liquida*' comprises 2 or 3 parts of linseed oil per 1 part of the *sandarac*.

Recipe of Theophilos [30]- ‘vernice liquida’:

- Put linseed oil and finely ground *sandarac* in a container.
- Heat the mixture for several hours.

Manuscript of Marciana (1520) [7]
Quantities: 60 gr of linseed oil, 30 gr of colophony.

- Warm up the oil over low heat and gradually add the finely ground colophony.
- Add a bit of alum stone previously burnt and crushed.
- Heat and mix thoroughly (add a little oil if necessary).

2. D. II. 2. Alcohol varnish

Usage of alcohol, namely ethanol, as a solvent for varnishes, permits to obtain light, bright and transparent varnishes, sometimes called as ‘clear varnishes’. In addition, these varnishes dry quickly unlike the fatty varnishes. However, they have a tendency to break whenever applied to an artwork. Thus, the supplementary compounds are generally added to give them more flexibility. Within this fact, alcohol varnishes are more applied as musical instruments varnishes, meaning wood varnishes [8].

The resin used in making the varnish is generally sorted, washed and then powdered. It is then dissolved in alcohol in a constant temperature water bath. The proportions resin / alcohol depend on the desired result. The varnish is filtered at the end of the process in order to remove the impurities from the resin [8].

Some recipes:

Recipe of Armenini da Faenza (1587) [26].
Quantities: 30 gr of *sandarac*, 1/4 of Greek pitch (colophony), alcohol.

- Crush and sift the *sandarac* and colophony.
- Boil on low heat in alcohol.
- The varnish is left to cool and must remain covered.
- Before using, warm it over low heat.

Manuscript of Padua (17th) [7].
Quantities: 210 gr of wine spirit very rectified, 60 gr of *sandarac*, 60 gr of resin from Abies alba (the European silver fir).

- Add crushed *sandarac* to the resin from Abies alba (the European silver fir).
- Add the wine spirit and boil slowly the mixture (in a closed bowl to avoid the loss of the spirit).
- The varnish is then poured in a glass bottle, allowing the impurities to precipitate on the bottom.

Recipe of a clear varnish (1772) [8].
Quantities: 450 gr of *sandarac*, 470 gr of the wine spirit.

- Sort out the resin, wash gently with water, dry, then wash with wine spirit.

- Heat the *sandarac* in the wine spirit in bain-marie, at constant temperature.
- When the mixture is completely homogeneous the heating can be stopped.
- Pass through a cloth and leave to rest at least 24 h.

2. D. II. 3. Spirit varnish

Spirit varnishes appeared quite a while after oil and alcohol varnishes around the 16th century and today are the most used by restorers. They are elaborated from the resin dissolved in spirits, usually spirit of turpentine. Resins utilized are normally triterpenic or synthetic. Sometimes varnish is left for ageing during several months before usage. As a result, a good varnish is obtained, brilliant, hard, transparent and cheap enough. Anyway, 'lean' varnishes are more fragile than oil varnishes [8, 31].

Spirit of turpentine is known since ancient times specifically for its therapeutic properties. It's only in the 15th century that spirit is starting to be used as a varnish for paintings and then commonlu used in the 17th century [32]. In the beginning of the 16th century Leonardo da Vinci mentions usage of spirit of turpentine in picture art [33]. Spirit of turpentine is often added to oil varnishes to affine it. The principal producer of turpentine is USA. Nevertheless, in the 19th century in France the plantation of large pine forests in moors was followed by an active production development of turpentine [7].

Some recipes:

Recipe of Armenini da Faenza (1587) [26].
- Melt the resin of turpentine.
- Add the same quantity of naphta.
- Stop heating and continue stirring while the mixture is warm.

Traité théorique et pratique sur l'art de faire les vernis (1845) [34].
- Melt the resin of turpentine in the spirit of turpentine.
- Keap heating till the mixture becomes limpid.

2. E. Ageing of varnishes: intervention of photochemical reactions

The principal role of the varnish application is to protect and improve visual aspects of the artworks. However, they are sensitive to light and heat. Their ageing results in degradations that can be visually observed, colouring or embrittlement (Figure 11) [35].

All varnishes suffer more or less from yellowing depending on the conditions they are kept in and their nature. This reduces the contrast of light and the original colour. In 19th and

20th centuries this uniform colouring of the painting called the ‘golden glint’ was appreciated and the removal of the varnish by restorers was subjected to debate.

a)  b) 

Figure 11. A partially cleaned oil painting showing the result of removing a) smoke and dirt and b) yellowed varnish [10].

2. E. I. Photochemistry and reaction mechanisms

Ageing of natural resins undergo chemical and physical changes that lead to degradation phenomena, well known to conservators and restorers, ranging from discoloration to embrittlement and insolubility.

Many factors affect ageing: the nature of varnish and paint, conditions in which the artwork is kept, environment… It is expected that, after application to or on the painting, oxidative conditions will result in the formation of a number of oxidation products of the resin. Metal – promoted oxidation is expected to play an important role in the painting, whereas photochemical oxidation will be the predominant process in varnish [36].

Oxidative drying processes have been observed in the *sandarac* resin by the Scalarone’s research group [11], but no oxidised derivatives of labdane diterpenoids have been identified experimentally.

Nevertheless, during the artificial ageing process, corresponding changes were observed in the molecular weight of the *sandarac*, indicating the appearance of both cross-links and scissions.

It is known that diterpenoids with conjugated double bonds in the side chain, such as a communic acid, are polymerized into a cross-linked structure, the degree of cross-linking of which increases with ageing. The conversion of double bonds into single bonds is demonstrated by the decreasing intensity of the infrared signals at 1645 and 888 cm^{-1} (Figure 12), which were attributed to the stretching of carbon-carbon double bonds and the out-of-plain deformation of the exomethylene functionality [37].

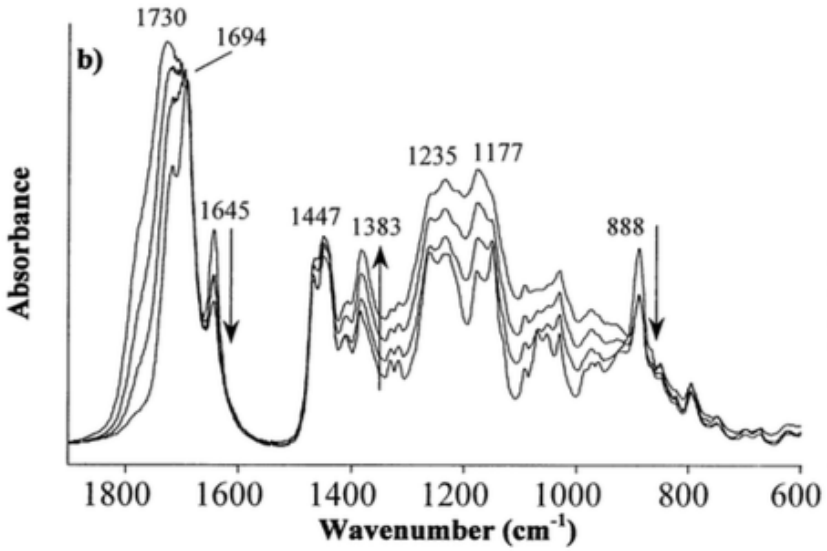

Figure 12. FTIR spectra of sandarac samples aged under a xenon lamp: 0, 25, 100 and 400 h [11].

These data as well as the simultaneous increase in peaks at 1382 and 1447 cm^{-1} due to the bending deformation of the methyl groups and to the scissoring deformation of methylene groups, respectively, can be used to control the development of cross-linking.

The on going cross-linking is also supported by the THM-GC/MS curves, shown in the Figure 9. From the peaks 1 (methyl 1,3-dimethyl-cyclohexa-2-en-carboxylate), 2 (methyl 1,2,3-trimethyl-cyclohexa-2-en-carboxylate), 2a (isomer of compound 2), 3 (methyl 1,4a,6-trimethyl-1,2,3,4,4a,7,8,8a-octahydro-naphthalencarboxylate), 4 (methyl 1,4a,6-trimethyl-5-methylene-1,2,3,4,4a,5,8,8a-octahydro-naphthalencarboxylate), 5 (methyl 1,4a,5,6-tetramethyl-1,2,3,4,4a,7,8,8a-octahydro-naphthalencarboxylate), 6 (methyl 5-ethyl-1,4a,6-

trimethyl-1,2,3,4-tetrahydro-naphthalencarboxylate), 8 (methyl cis –communate), 9 (methyl trans –communate), which represent pyrolysis fragments of the polymer component, it can be seen that the relative intensity of the communic acid (8 and 9) decreased until artificial ageing applied strengthens and disappeared completely after prolonged exposure (Figure 9c). On the other hand, the small fragments of pyrolysis still give intense peaks.

These results are in agreement with the hypothesis that the degree of cross-linking increases during ageing. As demostrated in the Figure 13, the occurrence of cross-linking on a communic acid-based polymer results in an organic network of bicyclic units and alkyl bridges. The unsaturated alky bridges are more prone to pyrolytic cleavage than cyclic structures, thus the probability of obtaining fragments 3 - 5 and their isomers is higher than that of the diterpenoid acid.

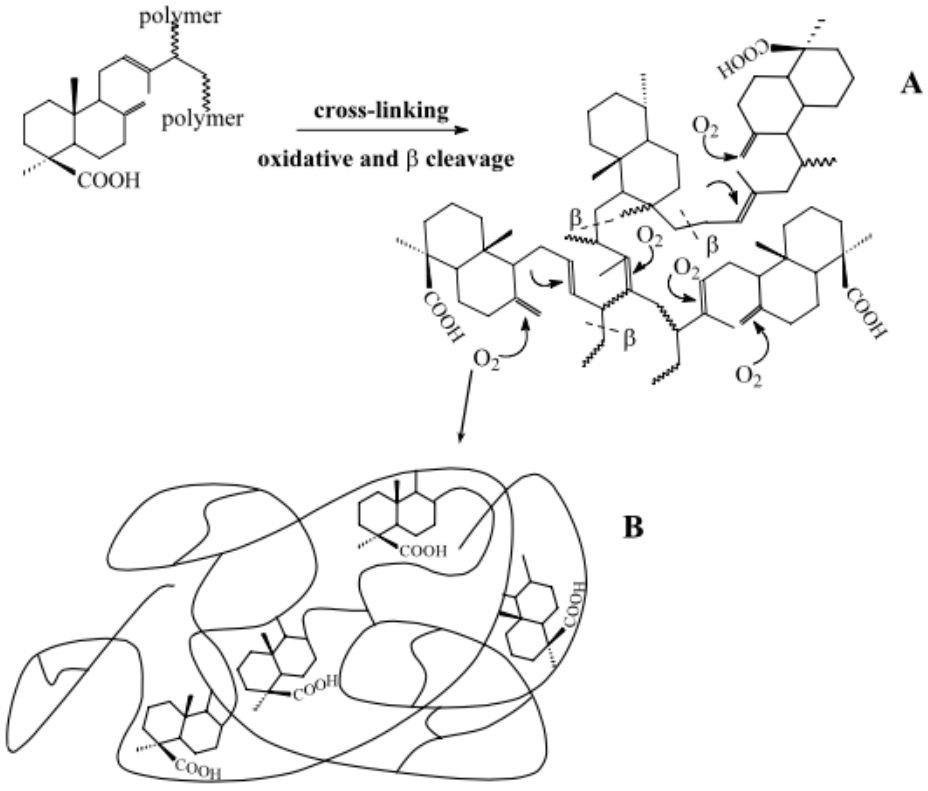

Figure 13. Degradation scheme of the communic acid-based polymer. (a) Carbon/carbon double bonds are active site for cross-linking and cleavages. Cleavage reactions occur with radical mechanisms: β-scission or oxidative scission. (b) Cross-linking proceeds further, leading to a saturated network of bicyclic units connected by a polymer chain [11].

As a complementary analysis, Scalarone et al. have accomplished DTMS (direct temperature - resolved mass spectrometry) and SEC (size exclusion chromatography) experiments that showed that the increase in cross-linking is counterbalanced by decreasing in the molecular weight of the polymeric material. The SEC showed a high signal of diterpenoids (1) and several polymer fractions (3, 4) of the unaged resins (Figure 14).

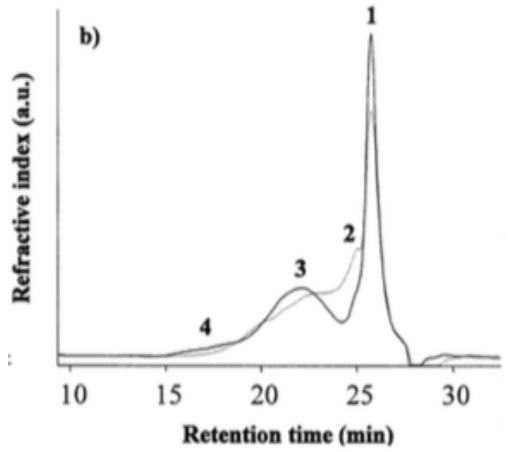

Figure 14. Size exclusion chromatograms of the *sandarac*. Unaged (full line) and aged 200 h under a xenon lamp (dotted line) [11].

While ageing the molecular weight distribution becomes narrower: the amount of diterpenoids drops down (1), new substances are detected in a range of molecular weight diterpenoid dimers (2) and the polymer fractions having a higher molecular weight (4) disappear (Figure 14). This signifies that the cross-linking process described in the previous section is in competition with the cleavage reactions. They occur probably via radical mechanisms, such as β-cleavage and oxidative cleavage (Figure 13,a), and lead to an overall decrease in molecular size. The final products of ageing are of high molecular weight, cross-linked and saturated molecules, comprising bicyclic structures of associated polymer chain (Figure 13,b).

2. F. The principal component of the *sandarac* resin – diterpenoid communic acid

2. F. I. Chemical reactivity and properties of communic acid

The communic acid (Figure 15) is also known as 8 (17), 12,14-labdatrien-19-oic acid (form *E*).

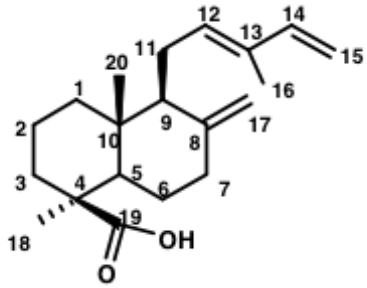

Figure 15. The structure of communic acid.

The communic acid can be isolated from the bark of five species of *Jupinerus* [38, 39, 40], and from the bark of *Cupressus arizonica* [41]. It is also present in the berries of the juniper, but also, among others in the cones of cypresses of Provence (*Cupressus sempervirens*) [42], the resin of *Agathis robusta* [43] or the pine cones of Luchu in Japan (*Pinus luchuensis*) [44].

The communic acid is also a molecule of choice for the synthesis of biologically active compounds such as oidiolactone C **13** (antifungal), nagilactone F **14** (allelopathic potential) or bruceantin **15** (pentacyclic, antitumor quassinoids) (Figure 16).

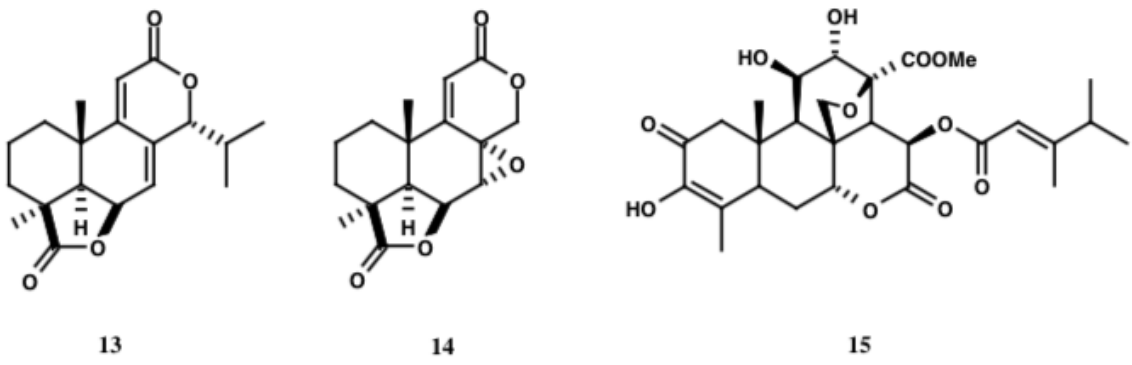

Figure 16. Examples of biologically active compounds synthesized from the communic acid.

Polymerization of the communic acid following exudation is generally thought to occur across the terminal side chain olefin C14-C15 (Figure 17) of the monomer predominantly as the sterically preferred 1,2-addition resulting in a 14,15-polylabdatriene polymer.

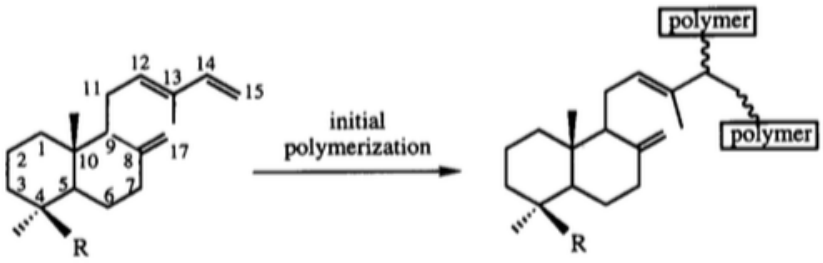

Figure 17. Polymerization of the communic acid yielding a 14,15-polylabdatrienepolymer (R = CO_2H).

The non-polymerizing compounds in the resin exudate are entrapped in the newly formed macromolecular network, resulting in a low molecular weight (LMW) resin fraction. The chemical composition of the LMW fraction of the recent and fossil resins has been well characterized due to the intrinsic solubility of its components [45].

It has been found that the components of low molecular weight fraction consist mainly of functionalized diterpenoids such as sandaracopimaric acid, agatic acid, abietic acid, communic acid and many others [46].

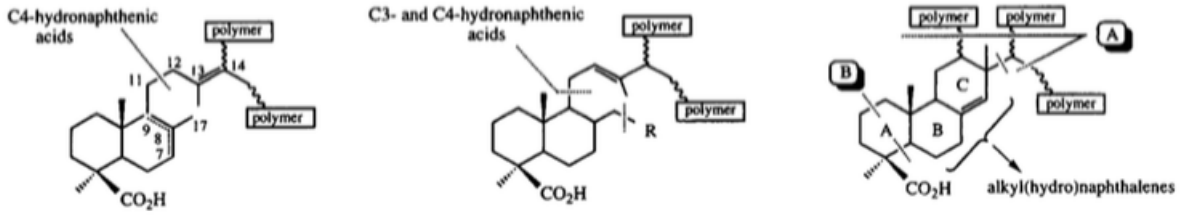

a b c

Figure 18. Maturation pathways proposed in the literature to date: (a) isomerization reactions [48]; (b) intermolecular polymerization [49]; and (c) intramolecular cyclization [49]. Dashed linesindicate most likely site of pyrolysis.

After deposition, polylabdanoid resonates are subjected to catagenetic and diagenetic processes leading to structural transformations from which it was determined that exocyclic

methylene depletion is the dominant reaction. According to the ^{13}C NMR analyses of amber by J. B. Lambert [47] the exocyclic methylene, corresponding to the C8=C17 double bond shown on the Figure 18, has tendency to diminish with the growth of the maturity degree.

Among a few mechanisms existing regarding the maturation pathways some include double bond isomerisation (Figure 18, a), intermolecular polymerization (Figure 18, b) and intramolecular cyclization (Figure 18, c).

Clifford's research team [46] analyzed a suite of polylabdanoid resinites by solid-state 13C NMR and pyrolysis-gas chromatography-mass spectrometry (py-GC-MS) to establish maturation trends indicative of structural transformations. Finally, they concluded that the mechanism probably represents a combination of three pathways, resulting in polymer condensation and possible defunctionalisation reactions. The proximity of the side chain olefins, as demonstrated for the communic acidic trimer in the Figure 19, will enable the intra-, inter- and side chain cyclization reactions, which leads to the multicyclic network having a monomer units relatively indefinite.

Thus a detailed model of the condensed polymer was not disclosed in the context of numerous cyclization, isomerization and polymerization possibilities and Clifford et al. withholded from the detailed model of mature polybdanoid resinites until additional information becomes available.

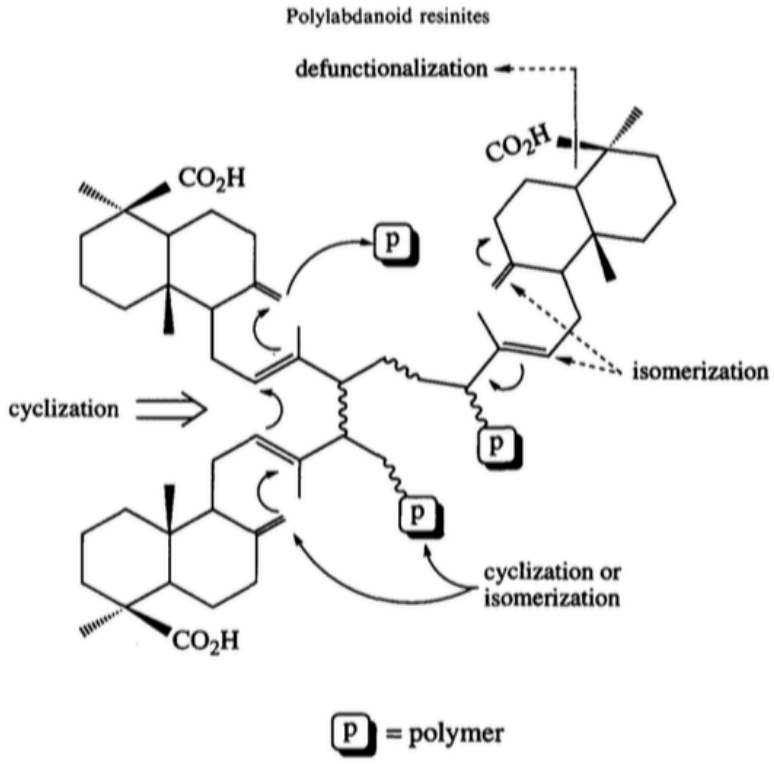

Figure 19. Polycommunic acid trimer showing possible cyclization, isomerization and defunctionalization reactions (p = polymer) [46].

2. G. References

1. da Vinci L. Traité de la peinture. Textes traduits et commentés pas André Chastel. Paris : Calmann-Lévy; 2003.
2. Scalarone D, Lazzari M, Chiantore O (2002) Ageing behaviour and pyrolytic characterisation of diterpenic resins used as art materials: colophony and Venice turpentine. J Anal Appl Pyrolysis 64: 345– 361.
3. Scalarone D, Van der Horst J, Boon JJ, Chiantore O (2003) Direct- temperature mass spectrometric detection of volatile terpenoids and natural terpenoid polymers in fresh and artificially aged resins. J Mass Spectrom 38: 607–617.
4. van Doelen GA (1999) Molecular studies of fresh and aged triterpenoid varnishes.
5. Romero-Noguera J, Martín-Sánchez I, Doménech-Carbó MT, Osete- Cortina L, López-Miras MM, Bolívar-Galiano F (2014) Analytical characterisation of the biodeterioration of diterpenoid labdanic var- nishes used in pictorial techniques: sandarac and Manila copal. Int Biodeterior Biodegrad 90:99–105.

6. Scalarone D, Duursma MC, Boon JJ, Chiantore O (2005) MALDI-TOF mass spectrometry on cellulosic surfaces of fresh and photo-aged di- and triterpenoid varnish resins. J Mass Spectrom 40:1527–1535.
7. Merrifield MP (1849) Original treatises, dating from the XIIth to the XVIIIth centuries in the arts of painting, in miniature, mosaic and on glass of gilding, dyeing, and the preparation of colours and arti- ficial gems. London.
8. Watin JF (1772) L'art de faire et d'employer le vernis, ou l'art du vernisseur. Quillau, Paris.
9. Clifford DJ, Hatcher PG (1995) Structural transformations of polylabdanoid resinites during maturation. Org Geochem 23(5): 407–418.
10. Dietemann P (2003) Towards More Stable Natural Resin Varnishes for Paintings. The Aging of Triterpenoid Resins and Varnishes.
11. Scalarone D, Lazzari M, Chiantore O (2003) Ageing behaviour and analytical pyrolysis characterisation of diterpenic resins used as art materials: Manila copal and sandarac. J Anal Appl Pyrolysis 68 – 69: 115 - 136.
12. Langenheim JH (2003) Plant resins: chemistry, evolution, ecology, and ethnobotany. Portland, Cambridge: Timber Press.
13. Clark RI (1901) A Few Notes on Varnishes and Fossil Resins. London, C. Letts & Co.
14. Eastlake SCL (2001) Methods and Materials of Painting of the Great Schools and Masters. Courier Dover Publications.
15. Perego F (2005) Dictionnaire des matériaux du peintre. Belin.
16. de Mayerne TT (1620) Pictoria Sculptoria et quae subalternarum artium, Le Manuscrit de Turquet de Mayerne présenté par M. Faidutti et C. Versini (1970).
17. Samet W (1998) Painting Conservation Catalog: Varnishes and surface coatings. Paintings Specialty Group of the American Institute for Conservation.
18. Sabin AH (1906) The industrial and artistic technology of paint and varnish. BiblioLife.
19. Azemard C (2015) Photodégradation des résines naturelles: application au domaine artistique.
20. Sugimoto N, Kuroyanagi M, Kato T, Sato K, Tada A, Yamazaki T, Tanamoto K (2006) Identification of the Main Constituents in Sandarac Resin, a Natural Gum Base. J.Food Hyg. Soc. Japan 47 (2): 76-79.
21. Maire M (2006) Du vernis en peinture.

22. Laurie AP (1910) The materials of the painter's craft in Europe and Egypt: from earliest times to the end of the XVIIth century, with some account of their preparation and use. Gyan Books Pvt. Ltd.
23. Masschelein-Kleiner L (1978) Cours de conservation. T1, Liants, vernis et adhésifs anciens, Institut royal du patrimoine artistique. Bruxelles.
24. Livache A (1896) Vernis et Huiles Siccatives. Paris Baudry & C^{ie} Editeurs.
25. Buonanni F (1723) Traité des vernis. Paris, Laurent d'Houry.
26. Armenini GB (1977) On the true precepts of the art of painting. Edited and translated by Edward J. Olszewsky.
27. Malecki V (2006) Les recettes anciennes: sources bibliographiques originales. Actes de la journée d'étude Les vernis de violon.
28. Cennini C, Tambroni G (1844) A treatise on painting. Lumley.
29. McIntosh JG (1908) The Manufacture of Varnishes and Kindred Industries Based on and Including the Drying Oils and varnishes. D. Van Nostrand Co.
30. Theophilius M (1843) Théophile, prêtre et moine. Essai sur divers arts. Cte Charles de l'Escalopier.
31. Cameron J (1886) Oils and Varnishes. J. & A. Churchill.
32. Pline l'Ancien (1848) Histoire naturelle. Edition d'Émile Littré.
33. Da Vinci Leonardo (1804) Trattato della pittura. Kessinger Publishing.
34. Tripier-Deveaux AM (1845) Traité théorique et pratique sur l'Art de faire les Vernis.
35. Berns RS, de la Rie ER (2003) The Effect of the Refractive Index of a Varnish on the Appearance of Oil Paintings. Stud. Conserv. 48: 251–262.
36. van den Berg KJ, Boon JJ, Pastorova I, Spetter LFM (2000) Mass spectrometric methodology for the analysis of highly oxidized diterpenoid acids in Old Master paintings. J. Mass Spectrom. 35: 512–533.
37. Beck CW (1986) Spectroscopic investigations of amber. Appl. Spectrosc. 22: 57-110.
38. Arya VP, Enzell C, Erdtman H, Kubota T (1961) Communic Acid, A New Diterpene Acid from Jupinerus communis L. Acta Chem. Scand. 15: 225-226.
39. Arya VP, Enzell C, Erdtman H, Kubota T (1961) Chemistry of the natural ordrer cupressales-41: The structure and stereochemistry of communic acid. Tetrahedron. 16: 255-263.
40. Arya VP (1962) Isolation of communic acid from some juniper barks. J. Sci. Ind. Res. 21: 201.

41. Erdtman H (1963) Some aspects of chemotaxonomy. Pure and applied Chemistry. 6: 679-708.
42. Ahond A, Carnero P, Gastambide B (1964) Isolement de l'acide communique des cônes d'une variété naine de cyprès. Bull. Chem. Soc. Fr. 348-349.
43. Carman RM, Dennis N (1964) The Diterpene Acids of Agathis Robusta Oleoresin Aust. J. Chem. 17: 390-392.
44. Minami T, Wada SI, Tokuda H, Tanabe G, Muraoka, O, Tanaka R (2002) Potential antitumor-promoting diterpenes from the cones of Pinus luchuensis. J. Nat. Prod. 65: 1921- 1923.
45. Lawrence BM, Bromstein AC (1974) Terpenoids in Umbellularia Californica. Phytochemistry, 13: 2009.
46. Clifford DJ, Hatcher PG (1995) Structural transformations of polylabdanoid resinites during maturation. Org. Geochem. 23(5): 407-418.
47. Lambert JB (1985) Amber from the Dominican Republic: analysis by nuclear magnetic resonance. Archaeometry. 27(1): 43-51.
48. Anderson KB, Winans RE, Botto RE (1992) The nature and fate of natural resins in the geosphere-II. Identification, classification and nomenclature of resinites. Org. Geochem. 18(6): 829-841.
49. Colombini MP, Modugno F (2009) Organic Mass Spectrometry in Art and Archaeology. Wiley.

3. Materials and methods

3. A. Materials

The samples studied by the analytical methods described in this chapter were: *sandarac* resin (*Tetraclinis articulata*) supplied by *Kremer*, *Okhra*, *Color Rare*, *La Marchande de Couleurs*, *L'Atelier Montessori*, *Hevea* and the communic acid isolated from cones of cypress *Cupressus sempervirens* purchased from *France Herboristerie* (www.france-herboristerie.com). Isopimaric acid (≥98%, GC) was purchased from Sigma-Aldrich.

3. B. Analytical technique and methods applied for the communic acid and the *sandarac* resin studies

As stated in the Introduction part several analytical approaches are applied in this research work for the molecular characterization of the *sandarac* resin and its principal component communic acid. In this chapter each of the analytical method applied is described based on the theoretical principles engaged in its technique.

3. B. I. Fourier transform infrared spectroscopy (FTIR) / Attenuated total reflectance (ATR)

3. B. I. 1. Principle

Infrared spectroscopy (IR) allows obtaining information on the atomic bonds present in the different molecules of the sample [1, 2].

The vibrational motions of the atoms in a molecule are constrained by means of the bonds and consequently the bond angles that form the molecule. A nonlinear molecule composed of N atoms has 3N independent degrees of motion freedom. These include three modes of translation (position of the molecule in space) and three modes of rotation (orientation about the center of gravity) in the three-dimensional Cartesian Coordinate system (x,y,z). This leaves 3N-6 degrees of vibrational freedom, which are known as the fundamental or normal modes of vibration. In a special case of a linear molecule that possesses only two degrees of rotational freedom, the normal modes of vibration are counted to 3N-5 [3].

Two main types of normal vibrational modes are known as stretching and bending modes. In the Figure 1 the normal vibrational modes are shown for an AX_2 functional group

located within a larger molecule (e.g. CH_2- group in an alkane). The stretching vibrations can be considered as motions involving a change in the interatomic distance along the axis of the bond and can be classified according to the symmetry of the vibration, either symmetrical (in-phase) (Figure 1a) or asymmetrical (out-of-phase) (Figure 1b).

The second type of vibrations - bending - involve a change in the bond angles between the atoms and are characterized as an in-plane asymmetrical bend or scissoring (Figure 1c), in-plane symmetrical bend or rocking (Figure 1d), out-of plane-symmetrical bend or wagging (Figure 1e), and out-of-plane asymmetrical bend or twisting (Figure 1f). Since more energy is required to stretch a bond than to bend it, stretching vibrations will always occur at higher frequencies than bending vibrations.

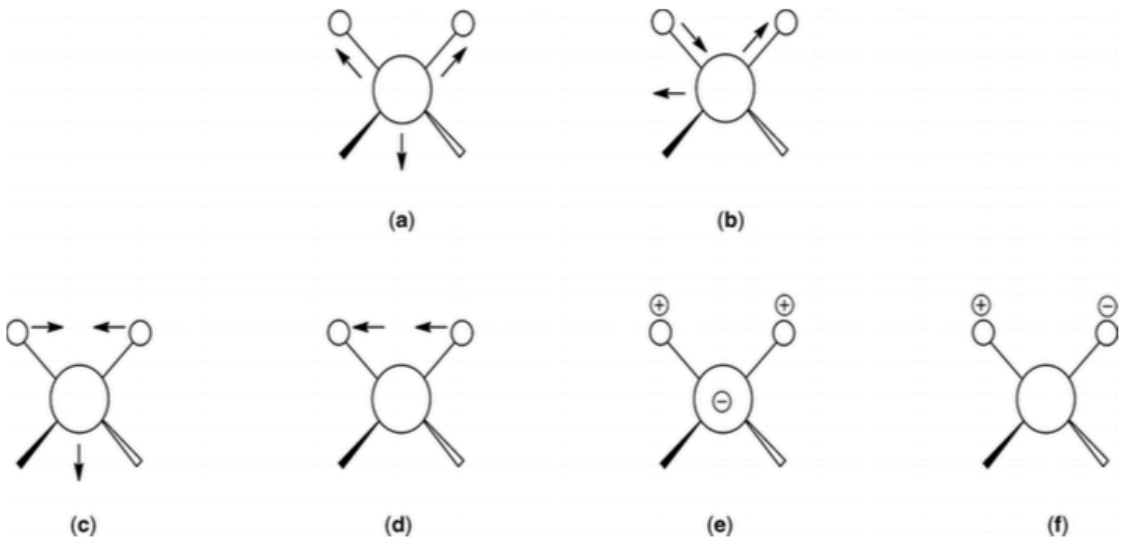

Figure 1. General types of modes of vibration for an AX_2 functional group located within a larger molecule. (a) Symmetrical stretch, (b) asymmetrical stretch, (c) in-plane asymmetrical bend or scissoring, (d) in-plane symmetrical bend or rocking, (e) out-of-plane symmetrical bend or wagging, (f) out-of-plane asymmetrical bend or twisting; $\oplus$ and θ indicates movement out of and into the plane of the page [3].

Generally, the instrument known as an optical spectrometer and applied to measure the absorption of electromagnetic radiation as a function of wavelength is composed of a source of electromagnetic radiation, a spectral analyzer, a radiation detector, and beam directing optical elements such as beam splitters and mirrors. The smallest wavelength interval that can be isolated by a spectrometer is defined as spectral resolution and depends on the spectral analyzing device used. Infrared spectrometers that use interferometers as the spectral

analyzing device are called Fourier transform (FTIR) instruments, for the reason that the interferogram is the Fourier transform of the optical spectrum [4].

As presented in the Figure 2, the radiation beam emitted from the source of the infrared spectrometer is collimated, directed through the interferometer, focused on the sample, collected, and refocused on the detector.

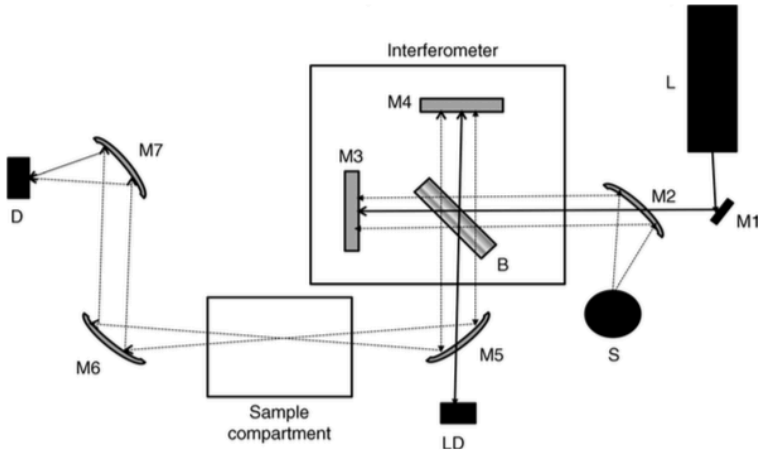

Figure 2. Optical diagram of a simple FTIR spectrometer; S = source, D = detector, L = HeNe laser, LD = laser detector, B = beam splitter, M1 = beam directing plane mirror, M2, M5, M6, and M7 = beam directing off-axis parabolic mirrors, M3 = fixed interferometer mirror, M4 = moving interferometer mirror [2].

The infrared radiation is generally sourced by hot body type. These latest are frequently composed of a solid material heated to incandescence by an electric current. The Planck blackbody equation permits the evaluation of spectral energy (I) of the source at temperature T and is given by the following formula:

$$I(v,T) = (2hv^3/c^2)\,(1/e^{hv/kT}-1)$$

where *h* is the Planck constant; *c* is the speed of light in a vacuum; *k* is the Boltzmann constant; ν is the frequency of the electromagnetic radiation. Obviously, with the increasing temperature, both the radiant power and the wavenumber of the peak emission increase.

The interferometers applied for spectral analysis in modern FTIR spectrometers are based on the original design developed by Albert Abraham Michelson in 1890 shown in Figure 3. The incoming infrared beam is collimated and directed through a beam splitter (BS), which acts as a partially reflecting mirror, transmitting half the radiation to a fixed mirror

(M1) and half to a movable mirror (M2). The two beams are reflected back to the beam splitter where they are recombined, focused, and directed to the detector [2,5].

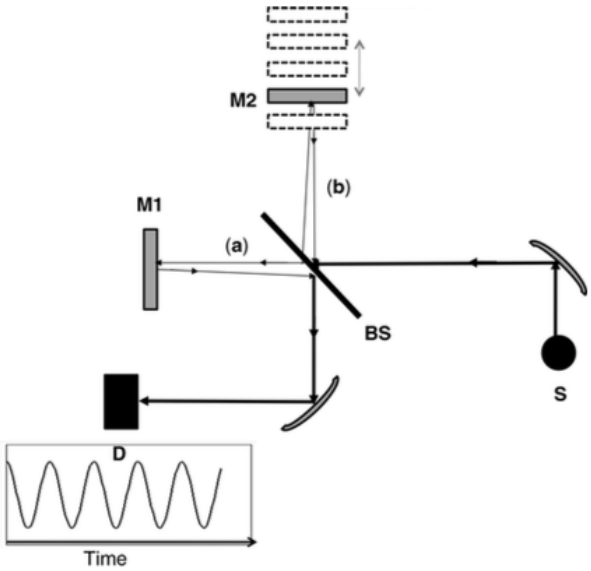

Figure 3. Basic design of a Michelson interferometer: S = source, BS = beam splitter, D = detector, M1 = fixed mirror, M2 = moving mirror, (a) = path from BS to M1, (b) = path from BS to M2. A plot of the detector output as a function of time for radiation of a single wavelength is shown below the detector. Light paths are shown offset for clarity [2].

3. B. I. 2. Total Internal Reflectance Spectroscopy

Attenuated Total Internal Reflectance (ATR) Spectroscopy is a versatile and powerful technique for infrared sampling that requires minimal or no sample preparation for rapid analysis. If an incoming beam of radiation is travelling in a transparent medium of higher refractive index (n_1) and strikes an interface with a medium of lower refractive index (n_2) at an angle greater than the critical angle ($\theta c = \sin^{-1} n_2/n_1$), the beam is totally reflected internally into the denser medium (n_1). This is known as total internal reflectance or attenuated total reflectance (ATR), and the infrared transparent denser medium is called the internal reflectance element (IRE) (Figure 4) [6, 7].

The internal reflection as a phenomenon was first observed in infrared spectroscopy in 1959. It has been discovered that in certain conditions, infrared beam entering a prism made of an infrared transmitting material with high refractive index (ATR crystal) will be totally internally reflected (Figure 5). In its turn, an evanescent wave will be created in this internal reflectance that extends beyond the surface of the crystal into the sample held in contact with

the crystal. In regions of the infrared spectrum where the sample absorbs energy, the evanescent wave will be attenuated.

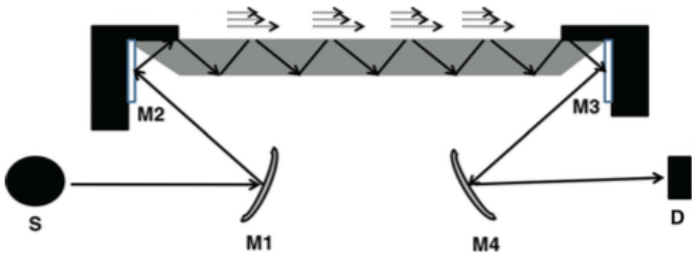

Figure 4. Diagram of a simple internal reflectance FTIR accessory showing multiple internal reflections within the IRE and the evanescent wave that penetrates into the rarer medium at each reflection. S = source, D = detector, M1, M2, M3, M4 = beam directing mirrors [7].

The valuable advantage of the evanescent wave, which makes ATR a powerful analytical method, consists in that the intensity of the wave decays exponentially with distance from the surface of the ATR crystal. Thus, the distance, which is on the order of microns, makes ATR generally insensitive to sample thickness, allowing for the analysis of thick or strongly absorbing samples.

The depth of penetration d_p can be used as a qualitative measure of the depth to which the evanescent wave extends in the sample and is defined by the following relationship in ATR spectroscopy:

$$d_p = \frac{\lambda}{2\pi n_1 \sqrt{\sin^2\theta_i - (n_2/n_1)^2}}$$

where λ is the wavelength of infrared radiation, n_1 is the refractive index of the ATR crystal, θ is the angle of incidence, and n_2/n_1 is the ratio of the refractive indices of the sample and the ATR crystal.

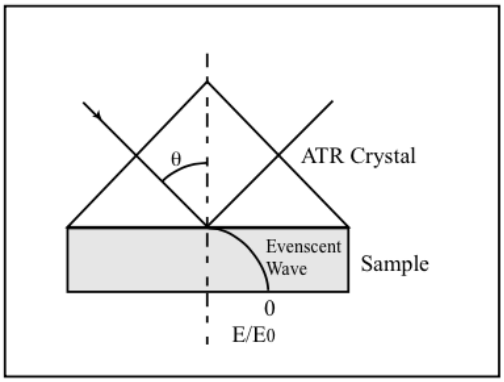

Figure 5. Total internal reflection of the infrared radiation [7].

3. B. I. 3. Experiment

The measurements were carried out at ambient temperature on a Cary 630 FTIR spectrometer from Agilent Technologies (Figure 6). The Agilent Cary 630 FTIR spectrometer uses a helium-neon laser operating in the visible region at 632.8 nanometers.

The FTIR/ATR analysis were carried out by depositing a layer of the product to be analyzed in contact with a crystal of high refractive index and is based on the existence of an evanescent wave propagating very close to the surface of the crystal, as previously described.

In case of liquid or oily samples the required contact between the ATR crystal and the sample is obtained without the need to add additional pressure.

For each preparation, 3 spectra of 20 scans are acquired, with a spectral resolution of 8 cm^{-1}.

To run the Cary 630 FTIR spectrometer the Agilent MicroLab software was used in module MicroLab PC for Microsoft Windows 7 operating system. The obtained spectra were visualized, analyzed and treated by means of OMNIC Series Software from ThermoFisher Scientific.

Figure 6. Cary 630 FTIR spectrometer from Agilent Technologies and laser signal input location.

3. B. II. Mass spectrometric analyses: electron ionization and 'soft' ionization techniques

3. B. II. 1. Electron Ionization

3. B. II. 2. Principle

Electron ionization (EI) is likely the most utilized ionization method in the research field of cultural heritage. In EI electrons induce the ionization of an atom. As shown in Figure 7, the EI source is formed by a tungsten (rhenium) filament, an anode, an ion repeller, a magnet, and a series of lenses for extracting, focusing and accelerating the ions produced [8].

The electron beam, formed by means of heating the filament, crosses the source pulled in by the anode situated before the filament. The molecules of the samples in the gas phase, presented in the source (usually heated at least at 200 °C), interact with the electron beam. As the filament–anode separation is short (1–3 cm), the electron–molecule association time ought to be greatly short. In order to increase it, one shaft of a magnet is placed behind the filament and the other behind the anode. The nearness of the magnet makes the direction of the electrons progress toward becoming helicoidal so that the distance that every electron covers significantly increases. As a result, the electron–molecule interaction time turns out to be longer in this manner causing a high ionization yield. Once the particles are produced, they are pushed out of the source towards the analyzer by the process of the extraction, centering and quickening lenses [9].

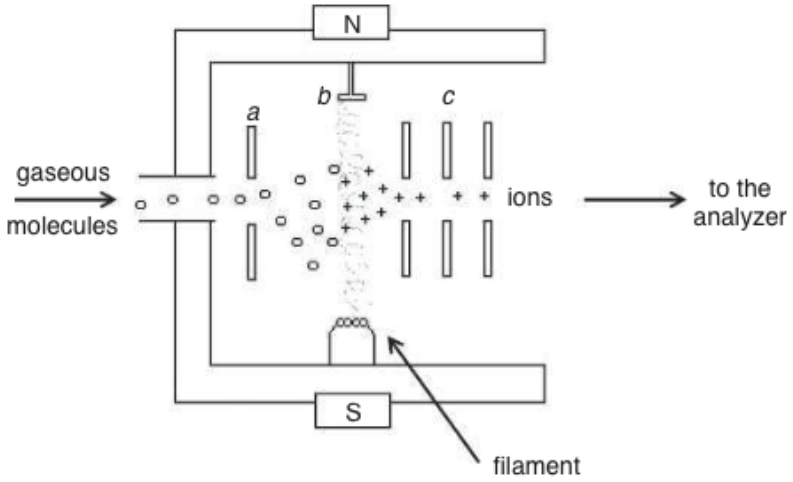

Figure 7. Schematic view of the electron ionization source. a = Ion repeller; b = anode; c = acceleration and focalization plates; N, S = magnet poles [8].

It has been evaluated that the electron–molecule interaction happens in a brief time (~10^{-16} s) and its outcome is the discharge of one electron from the molecule as in the equation on the Figure 8.

IONIZATION

Ionization technique	Molecule		Ion	
EI	$M_g + e^-$	→	$M^{+\bullet} + 2e^-$	(2.1)
CI, ESI, MALDI, APCI	$M + H^+$	→	$[M+H]^+$	(2.2)
ESI	$M + nH^+$	→	$[M+H_n]^{n+}$	(2.3)
CI, ESI, MALDI, APCI	$M - H^+$	→	$[M-H]^-$	(2.4)
ESI	$M - nH^+$	→	$[M-H_n]^{n-}$	(2.5)

Figure 8. Main ionization reactions occurring in mass spectrometry [9].

The ions so produced constitute the molecular ion ($M^{+\bullet}$) and are formed straightforwardly from the molecules yet these are positive particles. Actually, an electron has a negative charge and its expulsion from a neutral species causes the production of a positively charged ion. Furthermore, molecules are neutral species with an even number of electrons that are combined two by two in the orbitals. When one of these is expelled, there is a remaining odd number, and one electron is unpaired. Species with an unpaired electron are

called radicals. It takes after that the molecular ion is both a positively charged ion (or cation) and a radical, i.e. it is a 'radical cation'.

The electron expulsion from an atom is not an unconstrained process but rather it requires energy related to the first ionization potential (IP). For most molecules of the organic nature this value is generally around 10 eV. It became conventional to utilize a standard potential of 70 eV applied to the filament emitting electrons. This potential is considerably higher than the IP values, however there are many steps going before the energy transfer to the molecules in the gas phase, and in each stage the energy is partially lost [10].

Anyway, an overabundance of energy, negligible or extensive depending on the IP of the molecule, is conserved on the molecular ion. Being in an excited state, $M^{+\bullet}$ tends to come back to its ground state by dissipating its overabundance energy. This happens through fragmentation that comprises the breaking of covalent bonds. It leads to a mass spectrum acquired by EI, which is characterized by the presence of fragment ions, that present significant information on the structure of the analyte.

The EI technique is well established, sensitive and suitable for qualitative and quantitative applications [11].

3. B. II. 3. Experiment

Gas chromatography experiments were carried out with a GC 5890A gas chromatograph (Hewlett Packard, USA) equipped with capillary column HP-5MS cross-linked 5% Ph Me Silicone (30 m/0.25 mm/0.25 mm) and coupled with a Hewlett Packard GC 5970 mass spectrometer. The GC column temperature conditions were as follows: initial temperature of 40 °C, hold for 2 min, increased at 8 °C min^{-1} to 150 °C, increased at 3 °C min^{-1} to 280 °C. Helium gas flow was set at 1 ml min^{-1}. Mass spectra were recorded under electron impact ionisation at 70 eV electron energy, in the range from m/z 40 to 800. Derivatization of the resin samples was done using BSTFA/TMCS (80:20, v/v) for 1h at 70°C. The resulting solution was taken to dryness and dissolved in cyclohexane. Internal standard experiments were accomplished by dissolving 2.5 mg of the derivatized resin in 950 µl of cyclohexane and by subsequent addition of 50 µl of 0.25 mg/ml solution of isopimaric acid in cyclohexane.

Figure 9. Mass spectrometer from Hewlett Packard HP 5890 Series GC.

3. B. II. 4. ‘Soft’ Ionization Techniques

3. B. II. 5. Principle

The term ‘soft’ is usually applied to indicate the little amount of energy transmitted to the molecule while the ionization process. Oppositely, a large amount of energy is transmitted to the molecular ion in the case of EI (see above), what causes lots of fragmentation patterns and allows obtaining structural information. The main drawback of ‘hard’ ionization is that, however, the excessive amount of energy might lead to the loss of the molecular ion, which became undetectable. Thus the overabundance of the energy transmitted may prevent from the molecular weight determination of the analyte [12].

In the case of soft ionization approach the energy in excess that is deposited onto the ionized molecule is negligible and stable even-electron ions are produced. This allows easy determining the molecular weight of the analyte, while no structural information is available in the mass spectrum, due to the partial or complete absence of fragmentation. However, it is possible to get the structural information by causing ion fragmentation out of the source by means of tandem mass spectrometry technique [13].

In this research two methods of soft ionization were used for the analyses of the resin samples: spray ionization and desorption ionization techniques.

3. B. II. 6. Electrospray ionization (ESI)

The technique of electrospray has been yet mentioned at the beginning of the 20th century and the first description of its principle was published in 1968 [14]. The breakthrough for ESI came in the mid 1980s after publication of the research work by John Fenn [12], for which he was awarded the Nobel Prize for Chemistry in 2002. The research group of Schkurov [15] has also presented the technique of ion extraction from solutions at atmospheric pressure almost at the same time.

The meaningful features of the process are already revealed in the term electrospray: at first, what is different from the other ionization methods, in this case the ionization occurs on a spray. This is reached by forcing a liquid to pass through a capillary, close to the principle applied in usual dispensers. Millions and millions of small droplets are formed as a result. Primarily, an electric field of about 3–5 kV is applied to the capillary, which promotes the ionization (Figure 10) [16, 17, 18]. The formation of small liquid-charged droplets from which gas phase ions are formed is the final goal of the electrospray technique. This technique combines a large number of chemical and physical parameters that together determine the quality of the process. At the exit of the capillary, the liquid assumes a characteristic shape, called a Taylor cone, from which the jet of charged particles emanates (Figure 11) [19].

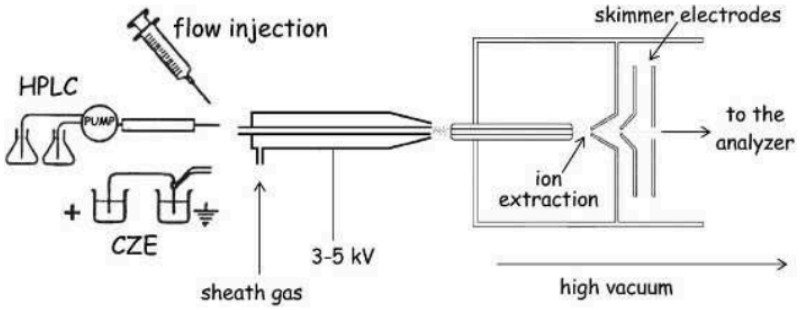

Figure 10. Electrospray ion source [8].

The electrospray process has not yet been fully understood: two theories still exist, the charge residue model (CRM) [14] and the ion evaporation model (IEM) [21].

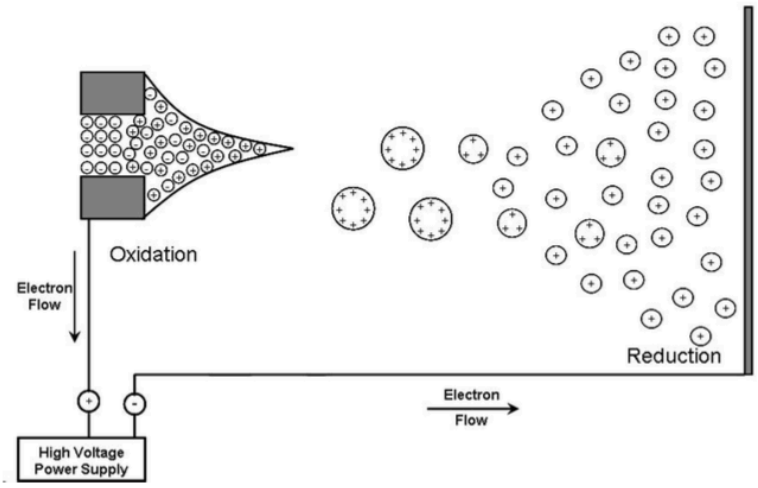

Figure 11. Representation of the electrolytic cell created between the electrospray needle (left side of the circuit) and the counter-current electrode (right side of the circuit) [20].

As previously mentioned, the charged droplets, each containing ions and solvent molecules during their travel from the exit capillary to the entrance of the high vacuum region, the distance between which is around 1–3 cm, are subjected to evaporation of the solvent with a consequent reduction of their size and, as a result, increase of the field at their surface. Consequently, due to high charge density, a so-called 'Coulomb explosion' is caused and ion escape occurs further. The ions generated this way are driven to the high vacuum region of the mass spectrometer and are directed to the mass analyzer.

It is possible to promote a protonation or deprotonation of the analyte by means of ESI. The most important for a molecule to be ionized by ESI is its polarity: nonpolar compounds cannot be ionized by this technique.

Thus, mass spectra generated from electrospray ionization are characterized by protonated/ deprotonated molecules and adduct ions, i.e. $[M + H]^+$, $[M + Na]^+$, $[M + HCOO]^-$. Among key features of the electrospray process is the production of multiply charged ions. An empirical rule states that a molecule generally takes a charge every thousand units of molecular weight. This permits the measurement of very high molecular weight molecules at low m/z values (Figure 12) [22, 23, 24].

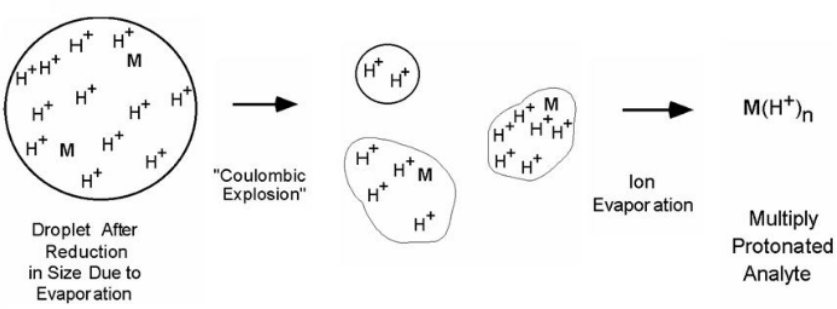

Figure 12. Illustration showing a microscopic droplet containing the analyte and an excess of positive charges (protons). After size reduction due to evaporation, the droplet disintegrates into smaller droplets due to coulombic repulsion of the charges; this process repeats until finally the analyte molecule (M) is ejected into the gas phase along with some of the excess charge (proton[s]) [25].

3. B. II. 7. Matrix Assisted Laser Desorption Ionization

To develop MS technique, many studies have been devoted to the use of laser light as an energy source for ionizing molecules. As an outcome, in the mid 1980s Matrix Assisted Laser Desorption Ionization (MALDI) [13] was introduced and quickly applied to the study of large molecules. The Nobel Prize was jointly awarded to Koichi Tanaka for Chemistry in 2002 for the study of large biomolecules by MALDI [26].

One of the remarkable features of the MALDI source, in contrast to the other ion sources, is that it may be operated under atmospheric pressure or under high vacuum. In the first case the acronym AP-MALDI (atmospheric pressure matrix assisted laser desorption ionization) is used.

The key principles of MALDI are already conveyed by its name: it is a desorption ionization, produced by a laser beam, and assisted by a matrix (Figure 13). The analyte in a concentration as low as 1 pmol or less is mixed with a suitable matrix in a proportion 1:1000 or higher molar ratio. The fist requirement for the matrix is that it has to be composed of a compound with a strong absorption at the wavelength of the laser applied. Thus, matrix excess and its strong absorption are two major factors ensuring that the energy from the laser pulse is absorbed by the matrix and not by the analyte, thus excluding the decomposition of the latest. 2,5-dihydroxy benzoic acid (2,5-DHB), sinapinic acid (SA), nicotinic acid and 2-(4-hydroxyphenylazo)benzoic acid (HABA) are some of the most commonly used matrices for MALDI.

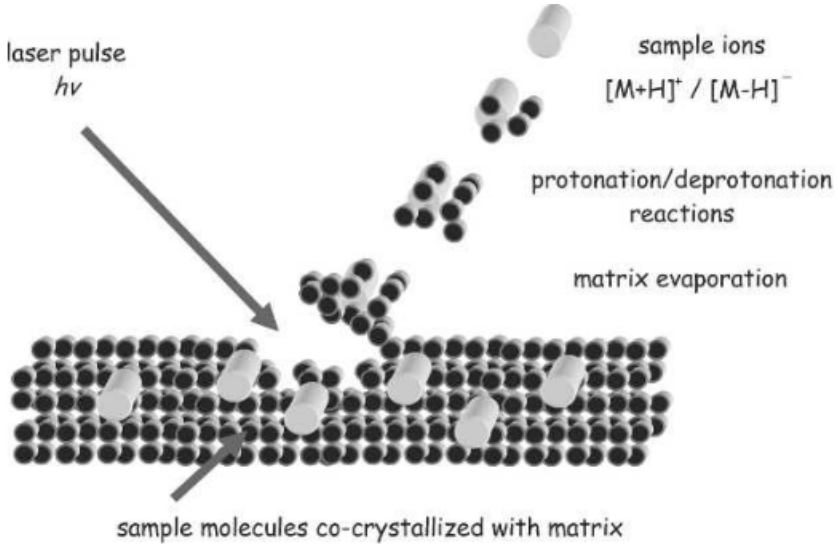

Figure 13. Schematic view of MALDI [20].

A flat metal target plate is then used as support for the deposition and spotting of solutions of the analyte and the matrix. After evaporation of the solvent, matrix and analyte have tendency to co-crystallize. The solid is further bombarded by a short laser pulses, of duration about 1–20 ns, what causes the sample and matrix to be volatilized. The formation of ions occurs by acid–base reaction between the ionized matrix molecules and the analyte molecules as shown in the Figure 13.

3. B. II. 8. Time of Flight Analyzer

In the Time of Flight Analyzer (TOF) ions are separated according to the time they spend travelling inside a flight tube (Figure 14).

The ion beam that was formed in the source is directed towards the flight tube. From the kinetic energy equation $E_k = 1/2\ mv^2$, where the kinetic energy (E_k) is related to the mass (m) and where v is velocity, it is obvious that a charged species with low molecular weight will take less time to reach the detector than a compound with high molecular weight. From the flight time it is possible to determine the m/z ratios of the ions.

Just a drift tube mainly formed the first generation of TOF analyzers that were characterized by low resolution (Figure 14a). Nevertheless, many improvements have been made over the years. Significant step towards progress in this field, that improved the TOF performances a lot, was made by the introduction of a ‘reflectron’, located at the end of the flight tube. In reality, ions with the same m/z value when accelerated in the source do not

have exactly the same kinetic energy. Thus they reach the detector at different times, provoking peak broadening and as a result low resolution. The reflectron is made up of a series of electrostatic lenses with increasing potential and provides compensation for the energy spread of the ion beam (Figure 14b). This means that ions with high kinetic energy are able to penetrate deep into the electric field generated by the lenses and consequently they cover a longer distance. In contrast, ions with the same m/z values, but with lower kinetic energy, penetrate to a less extent in the reflectron and they cover a shorter distance. As a consequence, all ions with the same m/z value will reach the detector at the same time giving a narrow peak and better resolution [27, 28, 29].

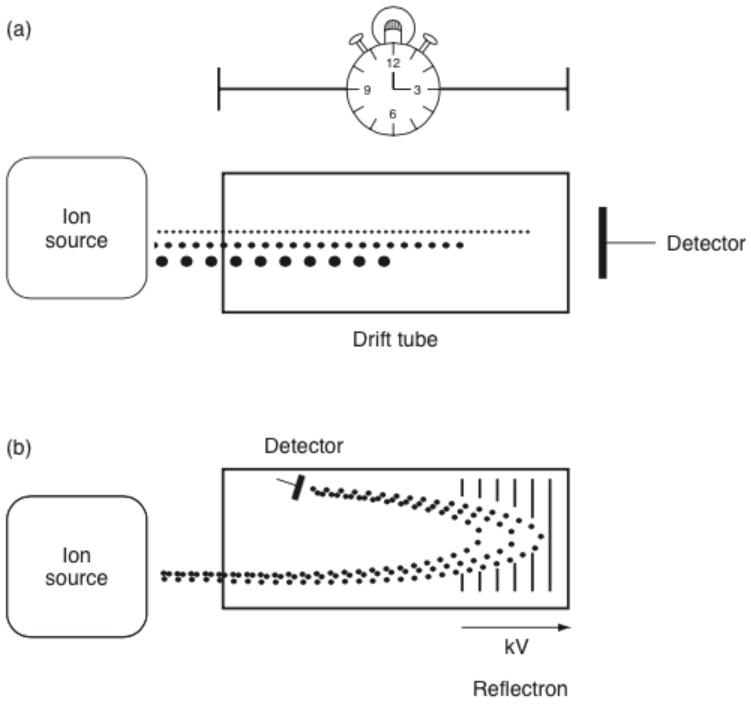

Figure 14. Time of flight analyzer: drift tube (a) and reflectron (b)

TOF analyzer is that it has no restriction on the m/z range, being able to analyze ions with m/z values ranging from a few hundred to 500000 and higher that gives great advantage to this technique. In the study of large molecules this is an important property for its coupling with MALDI. Indeed, since ions produced by MALDI are generally singly charged species, their m/z values can reach extremely high figures, what, in consequence, require an analyzer able to explore such high m/z ranges, i.e. TOF, is needed. Owing to its scan speed, high resolution and mass accuracy capabilities, TOF is currently coupled with all ionization techniques [30, 31, 32].

3. B. II. 9. The Orbitrap

In the Orbitrap analyzer, invented by Alexander Makarov [33], ions are trapped in an electrostatic field produced by two electrodes: a central spindle-shaped and an outer barrel-like electrode. A constant electric potential is imposed between these two axisymmetric electrodes (no magnetic field or oscillating electric potentials are involved). The opposing surfaces of the axisymmetric coaxial electrodes are nonparallel, as illustrated in the cross-sectional diagram in Figure 15.

In harmonic, complex spiral-like movements produced ions are moving around the central electrode while shuttling back and forth over its long axis in harmonic motion with frequencies depending only on their m/z values (Figure 15). The latter can be determined by Fourier transform treatment of the signal. From the practical point of view, the Orbitrap is simple to use and easily maintained, since neither RF nor a magnet field are applied, in contrast to other trapping analyzers.

The Orbitrap analyzer achieves a very high resolution; its resolving power in commercial instruments is 100 000 and routine mass measurement accuracies is less than 2 ppm. It finds applications in many fields, such as biology, proteomics, food chemistry and cultural heritage [34, 35].

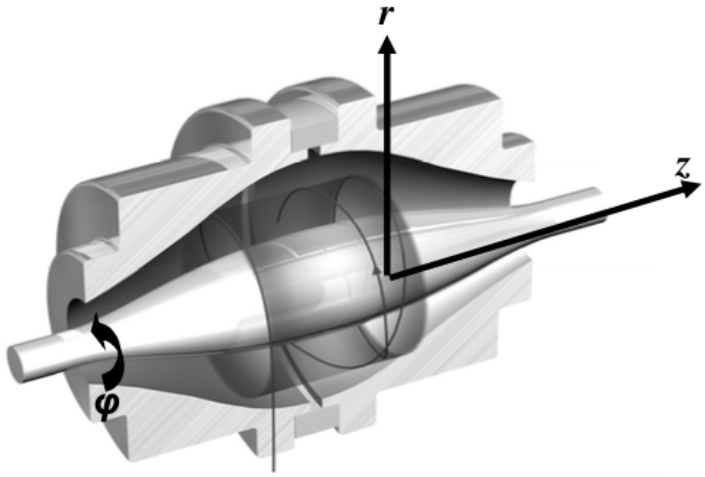

Figure 15. Cutaway of the orbitrap mass analyzer. Ions are injected at an off-axis point with a velocity perpendicular to the z-axis [from *Thermo Fisher Scientific*].

3. B. II. 10. Experiment

Measurements of the MALDI-TOF-MS mass spectra

Preparation of the *sandarac* resin solutions.

2,5-Dihydroxybenzoic acid (DHB, Aldrich, purity 98%) was used as a MALDI matrix substance. Matrix solution was prepared by adding to 15 mg of DHB 0.5 ml of acetonitrile (J.T. Baker, HPLC grade) and 0.5 ml of 0.1% trifluoroacetic acid (TFA, Aldrich 99 + %) solution in water (MilliQ). DHB matrix solution was stored sealed in the freezer.

Preparation of the *sandarac* resin solution was carried out in the following manner. A small weighed amount (0.006 g) of the *sandarac* resin powder was placed in an eppendorf tube and 0.2 ml of solvent was added with a pipette. The components were thoroughly mixed. In the case of two-component solvent mixtures, a powdered *sandarac* resin was placed in the eppendorf tube and dichloromethane (DCM) was added first, followed by the other solvent. Different volume ratios have been tested, and the most appropriate volume ratio is 1: 1.

MALDI-TOF-MS spectra acquisition

MALDI-TOF analyses were performed on MALDI-TOF ABI 4800 (Applied Biosystems, California, USA) equipped with a YAG laser with a wavelength of 355 nm and a frequency of 200 Hz. The interpretation of the MS spectra is performed with the Data Explorer software (Applied Biosystems).

The m/z values were measured in the positive mode, as more valuable information of the *sandarac* resin components are obtained from positively charged ions. In the negative ion mode, no useful mass spectra were obtained (the most intense peaks belonged to DHB).

Addition of sodium iodide, sodium carbonate and sodium acetate did not give good spectra because the formed crystals on the MALDI spot were quite large.

Measurements of the ESI-Orbitrap-MS mass spectra

Preparation of the *sandarac* resin solutions

Stock solutions of the *sandarac* resin were prepared with a concentration of approximately 1 mg/ml using various solvents. The first task involved finding a solvent system that could adequately dissolve the resin compounds and could be used with an electrospray mass spectrometer. A solvent with a 50/50 composition of DCM/EtOH worked well. Acetic acid (0.1% v/v) was added to the samples to increase the conductivity.

The ESI – Orbitrap - MS

ESI spectra were obtained on Orbitrap mass spectrometer equipped with an electrospray ionisation probe (Thermo Fisher Scientific). The mass spectrometer was operated in positive mode. Parameters of the ion source were as follows: source voltage 5 kV, capillary voltage – 40 V, tube lens voltage –250 V, capillary temperature 250°C, sheath and auxiliary gas flow (N_2) 42 and 11 (arbitrary units). The MS spectra were acquired by full-range acquisition covering 100–1400 m/z. A data-dependant scan was performed for the fragmentation study by deploying collision - induced dissociation (CID). The normalised collision energy of the CID cell was set at 35 eV.

3. B. III. Nuclear magnetic resonance spectroscopy: Liquid state ^{1}H, ^{13}C NMR 1D, 2D (COSY, HSQC, HMBC, TOCSY)

3. B. III. 1. Liquid state ^{1}H, ^{13}C NMR 1D, 2D (COSY, HSQC, HMBC, TOCSY)

Since the early 1960s, NMR spectroscopy has become an indispensable tool for the characterization of organic molecules. One-dimensional (1D) ^{1}H NMR spectroscopy remains a leading analytical technology in structural elucidation. Advantages of this approach include relatively rapid spectral acquisition and NMR resonances that provide a direct measure of organic compounds. Severe spectral congestion can, however, significantly hinder molecules identification. Two-dimensional NMR spectroscopy retains many of the benefits of 1D NMR, but additionally disperses the overlapping resonances into a second dimension, reducing signal congestions. In particular, the pairing of correlation spectroscopy (COSY) with directly detected heteronuclear correlation experiments (which link carbon atoms and nearby protons) proved to be particularly efficacious for determining structural connectivity [36].

3. B. III. 2. Principle

The principle of Nuclear magnetic resonance (NMR) spectroscopy is based on the phenomena that under certain conditions in a magnetic field a sample can absorb electromagnetic radiation in the radio frequency (rf) region at frequencies depending on the characteristics of the sample. Thus, absorption is a function of particular nuclei in the molecule.

In some nuclei the charge that they possess has tendency to 'spin' on the nuclear axis and, as a result, this circulation of nuclear charge generates a magnetic dipole along the axis (Figure 16a) [36, 37, 38]. Without an external applied magnetic field, the nuclear spins are random and spin in random directions. But, when an external magnetic field is present, the nuclei align themselves either with or against the field of the external magnet (Figure 16b). Once two energy levels for the proton have been established, it is possible to introduce energy in the form of radiofrequency radiation (ν_1) to induce a transition between these energy levels in a stationary magnetic field of given strength B_0. The fundamental NMR equation correlating the applied radiofrequency ν_1 with the magnetic field strength is

$$\nu_1 = (\gamma/2\pi)\, B_0, \text{ since } \Delta E = h\,\nu$$

The constant γ is the gyromagnetic ratio - a fundamental nuclear constant; it is the proportionality constant between the magnetic moment, μ, and the spin number, I:

$$\gamma = 2\pi\, \mu / h\, I$$

At certain radiation when the equation above is satisfied the system comes to resonance and, consequently, the proton absorbs the energy, raising it to the higher energy state [39].

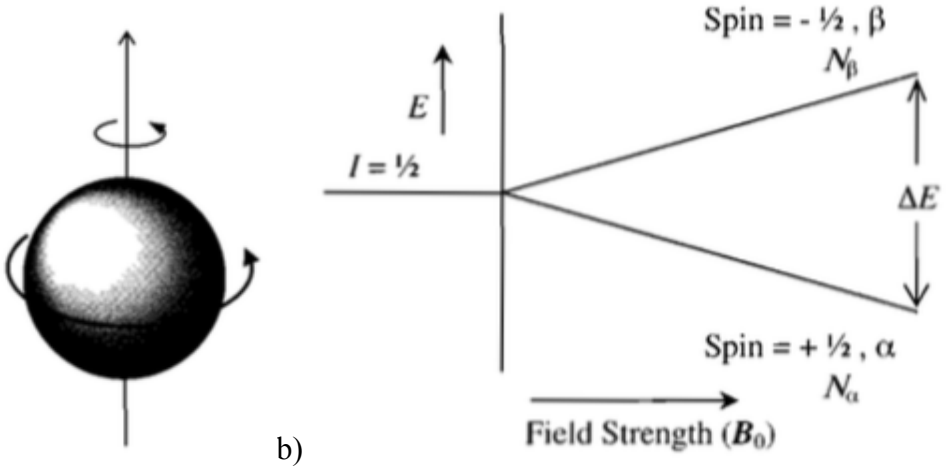

a) b)

Figure 16. a) Spinning charge on proton generates magnetic dipole; b) Two proton energy levels in a magnetic field of magnitude B_0. N is population of spins in the upper (N_β) and lower (N_α) energy states. The direction of the magnetic field B_0 is parallel to the ordinate, and field strength B_0. increases to the right. Larger B_0 fields increase ΔE [40].

For a nucleus in a magnetic field of strength B_0 with a spin I = 1/2, the nucleus' magnetic moment will precess about the z-axis defined by the direction of the magnetic field.

The angular frequency of precession is $\omega_o=2\pi\nu_o$, where ν_o is the same linear frequency as used in fundamental NMR equation, so $\omega_o=\gamma B_o$. In a real sample, a tremendous number of nuclear spins will be all precessing about the z-axis. This is shown in Figure 17 but with a much more tractable number of nuclear spins (arrows) [41].

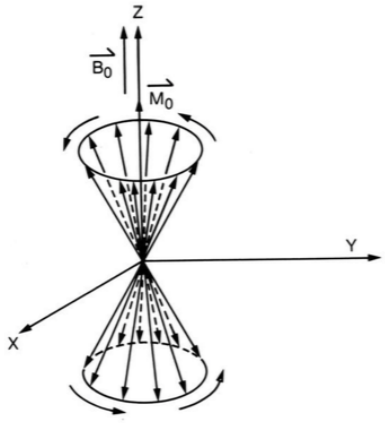

Figure 17. Orientation and precession of nuclear spins (I = 1/2) at thermal equilibrium in a stationary magnetic field B_0 that defines the z-axis. In reality, the angle between the vectors and the z-axis is much smaller than is shown for illustrative purposes. The arrows over *Mo* and *Bo* signify that they are vectors, i.e., that they have direction as well as magnitude [42].

Thus the nuclei may be oriented either parallel or antiparallel to the direction of the magnetic field. Consequently, some spins precess about the positive z-axis and some about the negative z-axis. The magnetization emanating from a real sample is simply the sum of all the individual nuclear magnetic moments (spins). From the Boltzmann statistics it is known that at room temperature, the number of spins in the lower energy level, N^+, slightly outnumbers the number in the upper level, N^- and this can be expressed by the following equation:

$$N^-/N^+ = e^{-E/kT}$$

where E is the energy difference between the spin states; k is Boltzmann's constant, $1.3805*10^{-23}$ J/Kelvin; and T is the temperature in Kelvin.

Figure 18 demonstrates the consequences of increasing magnetic field on the population of spin states, the distribution of a small number (about two million) of hydrogen nuclei, calculated from Boltzmann' Equation. The extent to which one orientation (energy state) is favoured over the other depends on the strength of the small nuclear magnet (proportional to gyromagnetic ratio) and the strength of the strong magnetic field *Bo* in which it is placed.

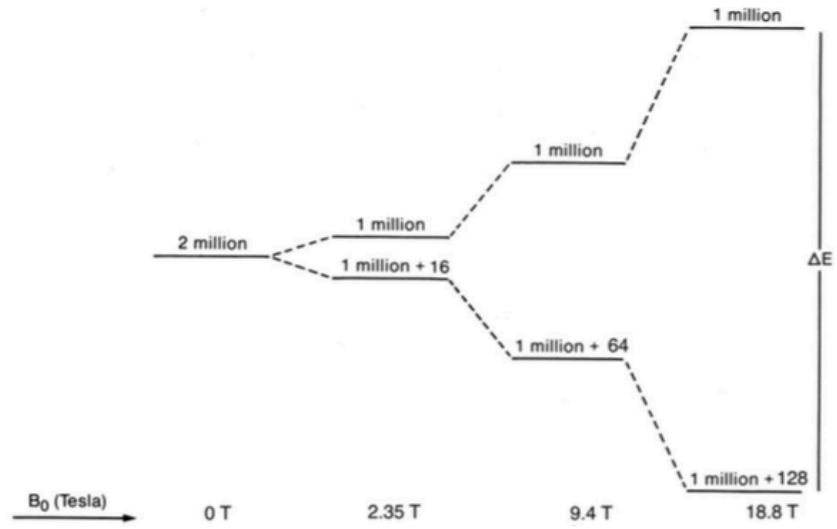

Figure 18. Dependence on magnetic field strength B_0 of the separation of nuclear energy levels (ΔE) for spin $I = 1/2$ and the relative populations of the energy levels assuming one has approximately two million protons in the sample.

Since there will be a slight excess of nuclei oriented with the magnetic field, i.e., in the lower energy state, so the sum will yield a magnetization (M_o in Figure 17) along the positive z-axis. It will be the total magnetization that determines an NMR signal – not the magnetic moment of an individual nucleus.

In order to obtain a NMR signal a strong RF pulse has to be applied at the resonance frequency. The latest is known as free induction decay (FID) and the way in which it can be observed in shown in the Figure 19. A rotating coordinate system (x', y' and z) is used in which the x'- and y'-axes are rotating about the z-axis at the NMR instrument's operating frequency (ν_0). The use of such a coordinate system enables to consider the effect of applying an RF pulse B_1, along the x'-axis and observing magnetization (and therefore a signal) along the y'-axis. Figure 19A shows the magnetization M_0 at thermal equilibrium in magnetic field B_0.

Magnetization will be rotated in a plane perpendicular to the applied B_1 pulse, i.e., y'z plane when B_1 is along x'; of course, the RF pulse B_1 must be at the appropriate frequency ν_0 as expressed by fundamental NMR equation. The angle of rotation θ depends on the gyromagnetic ratio γ of the nucleus and the amplitude B_1 of the RF pulse applied:

$$\theta = \gamma B_1$$

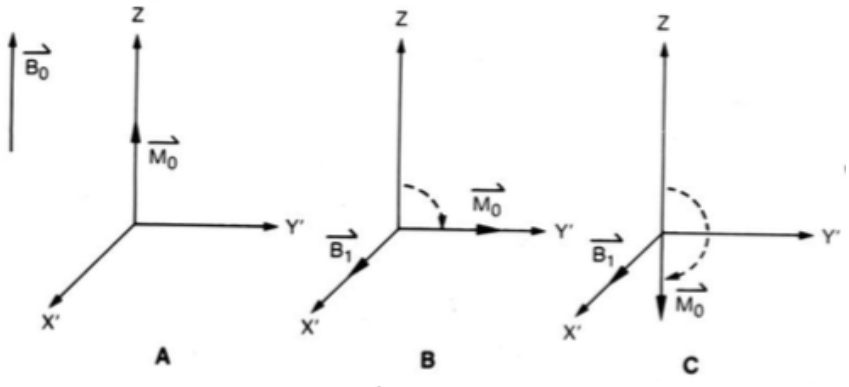

Figure 19. Rotation of the magnetization M_0 in the rotating coordinate system that rotates about the z-axis at the NMR instrument's operating frequency. (A) Spin system at equilibrium in magnetic field B_0; (B) application of a 90° (or π/2) B_1 pulse; and (C) application of a 180° (or π) B_1 pulse [43].

Figure 19B illustrates the rotation of M_0 by application of the RF pulse for sufficient time to rotate M_0 by 90° ($\theta = \pi/2$ radians). That pulse is called a 90° or π/2 pulse. Application of the B_1 field for twice as long ($\theta = \pi$ radians) will result in inversion of M_0 as shown in Figure 19C. The quantum mechanical analogs of the 90° and 180° pulses of Figure 19 are illustrated in Figure 20 using previous examples of two million protons in a 14.1 T magnetic field. The 90° pulse produces an equalization of populations in the two energy states, and the 180° pulse produces an inversion of populations so that the high energy state has a larger number of nuclear spins.

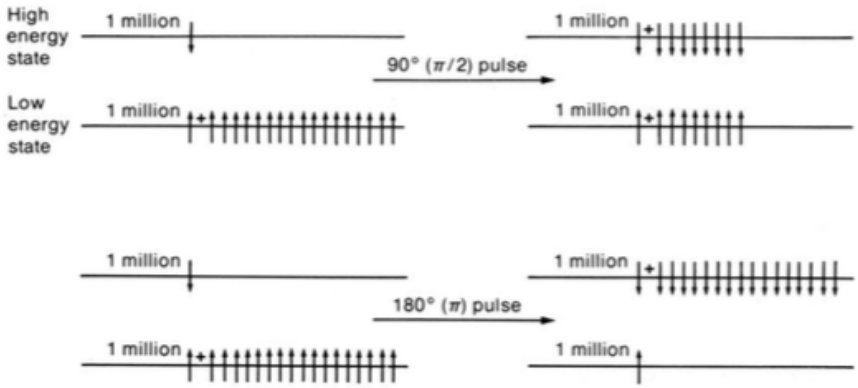

Figure 20. Effect of 90° and 180° radiofrequency pulses on the population of nuclear spins in a sample of about two million protons in a magnetic field B_0 = 2.35 T.

As a result, 1D experiment may be summarized to the scheme shown in the Figure 21.

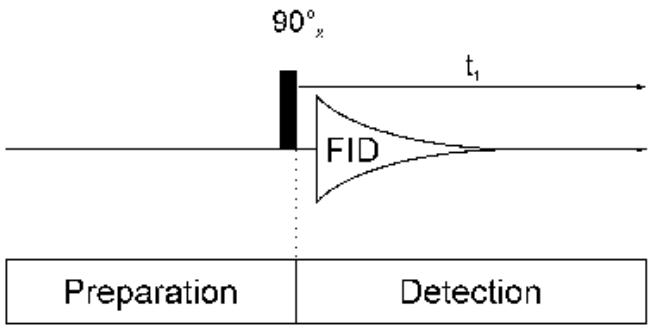

Figure 21. General sequence of 1D experiment.

Thus, every 1D NMR experiment can be conditionally divided into two parts: preparation and detection. During preparation the spin system is set to a defined state. During detection the resulting signal is recorded. In the simplest case the preparation is a 90° pulse, on x axis, for example, which rotates the equilibrium magnetization *Mz* onto the y axis (*My*). After this pulse each spin precesses with its own larmor frequency around the z axis and induces a signal in the receiver coil. Then the signal FID decays due to T_2.

Usually, the experiment is repeated several times and the data are summed up to increase the signal to noise (S/N) ratio. After summation the data are Fourier transformed to yield the final 1D spectrum.

As previously mentioned, 1D NMR spectra are sometimes far too complex for interpretation as most of the signals overlap heavily. By the introduction of additional spectral dimensions these spectra are simplified and some extra information is obtained. The invention of multidimensional spectra can be considered as the major leap in NMR spectroscopy [44].

The construction of a 2D experiment is based on that, in addition to preparation and detection already known from 1D experiments, the 2D experiment has an indirect evolution time t_1 and a mixing sequence. The general scheme of 2D experiment can be viewed in the Figure 22a.

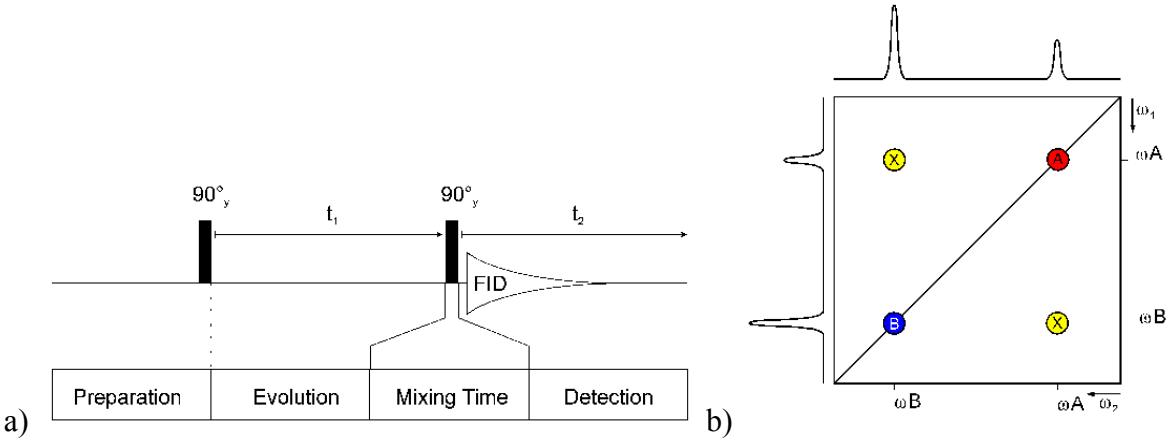

Figure 22. a) General sequence of 2D experiment; b) general topology of 2D spectrum.

After 90° pulse the spins can precess freely for a given time t_1. During this time the magnetization is labelled with the chemical shift of the first nucleus. During the mixing time magnetization is then transferred from the first nucleus to a second one. Mixing sequences utilize two mechanisms for magnetization transfer: scalar coupling or dipolar interaction (NOE). Data are acquired at the end of the experiment: during this time the magnetization is labelled with the chemical shift of the second nucleus.

Two-dimensional FT yields the 2D spectrum with two frequency axes. If the spectrum is homonuclear (signals of the same isotope (usually 1H) are detected during the two evolution periods) it has a characteristic topology as in the Figure 22b.

3. B. III. 3. Homonuclear 2D Experiments [45]

In this work two 2D spectra that are widely applied for the structure determination were used: 2D COSY (Correlation Spectroscopy) and 2D TOCSY (Total Correlated Spectroscopy).

In the COSY experiment, scalar coupling transfers magnetization. Protons that are more than three chemical bonds apart give no cross signal because the 4J coupling constants are close to 0. Therefore, only signals of protons that are two or three bonds apart are visible in a COSY spectrum (Figure 23a).

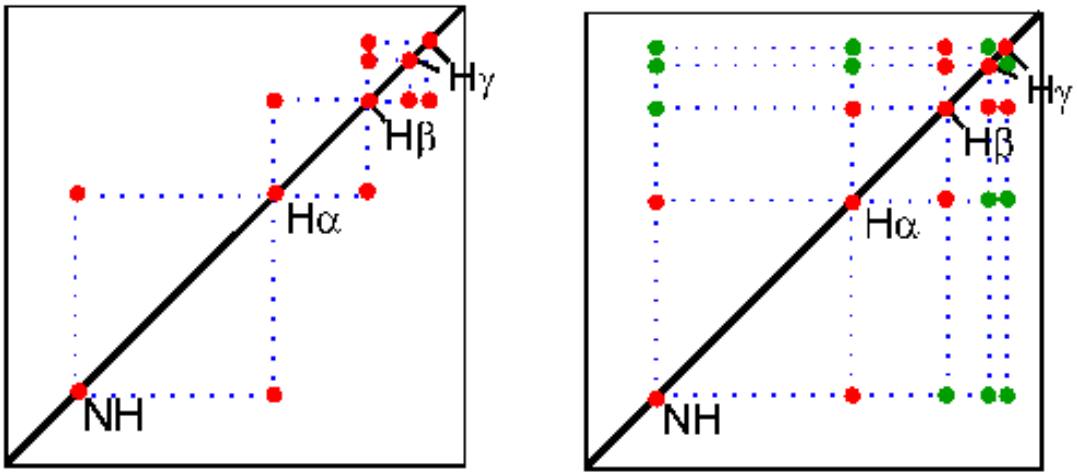

a) b)

Figure 23. a) 2D COSY; b) 2D TOCSY.

In the TOCSY (Figure 23b) experiment, magnetization is dispersed over a complete spin system of a compound by successive scalar coupling. The TOCSY experiment correlates all protons of a spin system. Therefore, not only the red signals are visible (which also appear in a COSY spectrum) but also additional signals (green) that originate from the interaction of all protons of a spin system that are not directly connected via three chemical bonds.

3. B. III. 4. Heteronuclear NMR spectroscopy

Two techniques of heteronuclear experiments have been perfomed: HSQC (Heteronuclear Single-Quantum Correlation) and HMBC (Heteronuclear Multiple Bond Correlation).

The 2D HSQC experiment permits to obtain a 2D heteronuclear chemical shift correlation map between directly bonded ^{1}H and X-heteronuclei (commonly, ^{13}C and ^{15}N). It is widely used because it is based on proton-detection, offering high sensitivity (Figure 24a) [46].

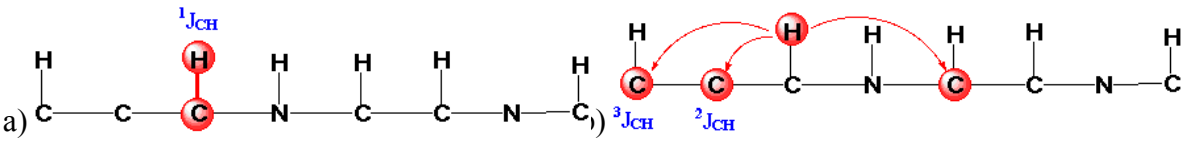

Figure 24. a) 2D HSQC; b) 2D HMBC.

The 2D HMBC experiment permits to obtain a 2D heteronuclear chemical shift correlation map between long-range coupled ^{1}H and heteronuclei (commonly, ^{13}C). It is also widely used because it is based on proton-detection, offering high sensitivity (Figure 24b).

3. B. IV. Nuclear magnetic resonance spectroscopy: Solid-state ^{13}C NMR 1D (simple pulse (SP), cross-polarisation (CP), Inversion Recovery Cross-Polarization (IRCP))

Although most NMR experiments are performed on liquid-state samples, solid-state NMR is rapidly emerging as a powerful method for the study of solid samples and materials. Modern solid-state NMR spectroscopic techniques not only produce spectra with a resolution close to that of liquid-state spectra, but also capitalize on anisotropic interactions, which are often unavailable for liquid samples [47]. With this background, in this PhD work the analysis of the resin samples were accomplished by means of some solid-state NMR spectroscopy developments, including techniques such as cross-polarization, magic-angle spinning and multiple-pulse sequences. Thus, in the present study the solid-state NMR spectroscopy is used as one of the analytical techniques to evaluate the utility of the method for the study of molecular structure of resins. The solid-state NMR of low abundance nuclei, such as ^{13}C with isotopic abundance of 1.1, suffers from low sensitivity, particularly when these nuclei also have a low gyromagnetic ratio. The second problem is the well-known fact that spin-lattice relaxation times of low abundance spin 1/2 nuclei are usually long (tens of seconds for ^{13}C in powdered organics). This is because strong homonuclear dipolar interactions, which can stimulate relaxation transitions, are largely absent, and only the much weaker heteronuclear dipolar interactions remain. The long spin-lattice relaxation time means that long delays must be left between consecutive scans. When several thousand scans are required to lower the noise to a desirable level, the spectra take a very long time to acquire.

3. B. IV. 1. CP-MAS Experiments

To enhance the signals from rare nuclei such as ^{13}C, many solid-state NMR experiments today routinely involve the transfer of polarization from abundant nuclei, such as ^{1}H, by using a technique called *cross polarization* (CP) [48, 49]. Cross-polarization (CP) from abundant spins I to low abundance spins S is a double-resonance technique that overcomes two common problems in the NMR of solids [50].

The basic CP pulse sequence is shown in the Figure 25 and the CP experiment may include the following stages:

1. Enhancement (η) of the signal of a low-gamma nucleus (*S)* by a factor on the order of the ratio of the gyromagnetic ratios:

$$\eta \propto \gamma_I/\gamma_S$$

2. Recycling of magnetization dependent upon the T_1 of the abundant, high-gamma nucleus. For organic and biological solids, the ^{1}H T_1's are much shorter (T_1 = 1–3 s) than those of ^{13}C (T_1 = 5–15 s).
3. Spectral simplification. With appropriate cycling of phases of the initial *I* spin π/2 pulse and the phase of the receiver detection of the *S* spin (termed spin-temperature alternation in the thermodynamic picture), CP results in *S* - spin signals that originate only from dipole coupled *I*-spins.

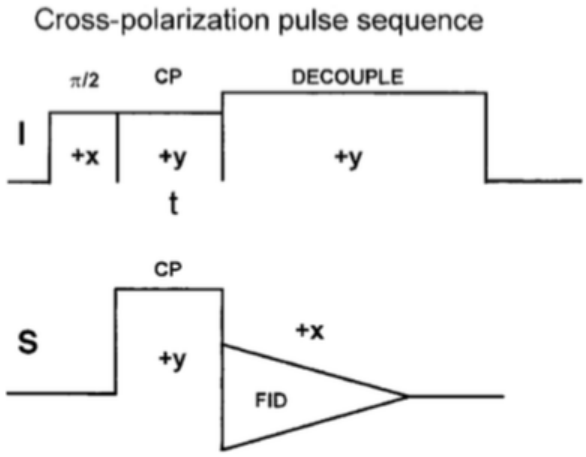

Figure 25. Basic CP pulse sequence [50].

After the preparation period, during which the sample polarizes in the magnetic field, a π/2 pulse is applied to the *I* spins along the x′ axis of the rotating frame. A long spin locking pulse of amplitude B_{1I} is then applied along the y′ axis. At the same time, a long pulse of amplitude B_{1S} applied to the *S* spins along the y′ axis. This time period, during which cross-polarization takes place, is known as the contact time, *t*. In order for the polarization transfer to be possible, the magnetizations of spins *I* and *S* must fulfil the Hartmann-Hahn condition. Thus, the amplitudes of the pulses satisfy the equation $\gamma_I B_{1I} = \gamma_S B_{1I}$. Finally, the radio frequency field applied to the *S* spins is turned off and a free induction decay of the *S* spins is observed.

Since cross-polarization is conditioned by heteronuclear dipolar interactions, it is sensitive to internuclear distances and the mobility of molecules or functional groups involved. So, in this case, CP can also be utilized to establish the connectivity between coupled nuclei and to investigate molecular dynamics in solids, a very useful feature in structural determination.

3. B. IV. 2. IRCP Experiments

A sequence, based on inversion of polarization and commonly known as inversion recovery cross polarization (IRCP) has been proposed in order to get a complete spectral editing in CP MAS NMR [51]. The principle of this sequence is presented in Figure 26. Comparing to the classical CP sequence the only difference is the introduction of a phase inversion during the contact time. The first stage consists in polarizing all of the CH_n groups during a relatively long contact time, t_c. The spin polarization will progressively invert during an inversion time, t_i, just after the phase inversion [52]. The dynamics of inversion is similar to the polarization dynamics in a standard CP sequence [53], and thus depends strongly on the ^{13}C - ^{1}H dipolar coupling: the IRCP sequence is consequently very sensitive to the local proton environment and molecular motion. A thoughtful analysis of the CP dynamics permits a clear distinction between the various $^{13}CH_x$ sites depending on the x value and also between rigid and mobile $^{13}CH_x$ sites. The principal benefit of this sequence compared to the usual CP sequence is that the magnetization begins from an optimum value, then decreases and becomes negative when increasing t_i It therefore becomes possible to point out differences in inversion dynamics of various signals especially when they overlap. The relative rates of polarization are expected to be as follows [54]:

$$CH_3 \text{ (static)} > CH_2 > CH \approx CH_3\text{(rotating)} >> C\text{(nonprotonated)}.$$

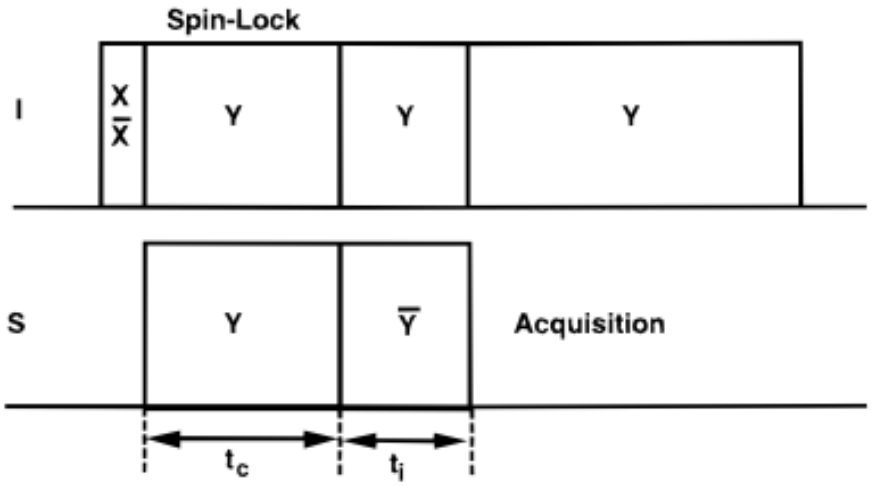

Figure 26. IRCP pulse sequence [52].

3. B. IV. 3. Experiment

Solution ^{1}H, ^{13}C 1D and 2D NMR experiments (acquisition with power-gated decoupling using a 30° flip angle) were performed on a Bruker Avance III 300 (7.05 T) spectrometer with a BBFO (X-1H) gradient coil for 5 mm tubes probe head.

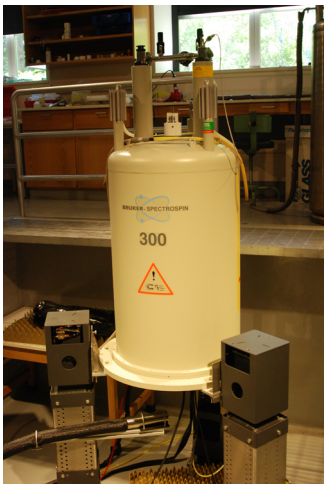

Figure 27. Bruker Avance 300 MHz (7 T) spectrometer.

^{13}C solid-state MAS NMR experiments have been acquired on a Bruker Avance 300 MHz (7 T) spectrometer using 7 mm teflon rotors spinning at a MAS frequency of ν_{MAS} = 14 kHz. ^{13}C chemical shifts were referenced relative to tetramethylsilane (TMS, δ = 0 ppm).

Single-Pulse MAS Experiments. Pulse length (90° flip angle) for ^{13}C was 3.15 μs, and the optimum recycle delays were 30 s. Two-pulse phase-modulated (TPPM) proton decoupling [55] was applied during ^{13}C acquisition (80 kHz). The number of transients (NS) was 64 for ^{13}C experiments. Spectra have been decomposed with DMFIT2004 software.35 Integration values should be considered with a 10% error coming from a trial and error methodology used in the fitting procedure.

CP-MAS Experiments. Recycle delay for all CP experiments was 3 s, and TPPM decoupling was applied during signal acquisition. CP contact time was t_{CP} = 3 ms, unless otherwise indicated. All FIDs were subjected to an exponential multiplication (EM) function with a line broadening value of 50 Hz prior to Fourier transform.

IRCP Experiments. For the IRCP experiments, a contact time, t_{CP} = 1 ms, was chosen to maximize the polarization of the ^{13}C nuclei, although 7 spectra were recorded for various inversion times, t ranging from 10 μs to 5 ms. The recycle delays between pulses were 3 s, and the number of transients was 128.

3. C. Artificial ageing

The samples of freshly extracted communic acid were dissolved in THF and equal amounts pipetted onto glass microscopic slides for artificial ageing under UV lamp with a wavelength 365 nm. The UV lamp used was LIGHTNINGCURE UV-LED spot light source LC-L1V3 from Hamamtsu.

UV lamp LC-L1V3 from Hamamtsu

3. D. References

1. Griffiths PR, de Haseth JA, Winefordner JD (2007) Fourier Transform Infrared Spectrometry. Wiley. Second Edition.
2. Gaffney S, Marley N, Jones D (2012) Fourier Transform Infrared (FTIR) Spectroscopy. John Wiley & Sons, Inc.
3. Silverstein RM, Bassler GC, Morrill TC (1991) Spectrometric Identification of Organic CompoundsJohn Wiley & Sons, New York. 5th ed.
4. Colthup NB, Daly LH, Wiberley SE (1990) Introduction to Infrared and Raman Spectroscopy. Academic Press, San Francisco, CA. 3rd ed.
5. Chalmers JM, Griffiths PR (2001). Handbook of Vibrational Spectroscopy. Wiley.
6. Introduction to Attenuated Total Internal Reflectance (ATR) (2000) Thermo Optek Corporation.
7. Averett LA, Griffiths PR (2008) Effective path length in attenuated total reflection spectroscopy. Anal. Chem. 80: 3045–3049.
8. Colombini M, Modugno F (2009) Organic Mass Spectrometry in Art and Archaeology. John Wiley & Sons, Ltd.
9. Beckey HD (1969) Field ionization mass spectrometry. Res. Dev. 20: 26–31.
10. Becker KH, Tarnovsky V (1995) Electron-impact ionization of atoms, molecules, ions and transient species. Plasma SourcesScl. Technol. 4: 307-315.
11. Lakshmi Hima Bindu MR, Angala Parameswari S, Gopinath C (2013) A review on GC-MS and method development and validation. Int J Pharm Qual Assur 4(3): 42–51.
12. Yamashita M, Fenn JB (1984) Electrospray ion source. Another variation on the free-jet theme, J. Phys. Chem. 88: 4451–4459.
13. Karas M, Hillenkamp F (1988) Laser desorption ionization of proteins with molecular masses exceeding 10,000 daltons. Anal. Chem. 60: 2299–2301.
14. Dole M, Mack LL, Hines RL, Mobley RC, Ferguson LD,. Alice MB (1968) Molecular beams of macroions. J. Chem. Phys. 49: 2240–2249.
15. Aleksandrov ML, Gall LN, Krasnov VN, Nikolaev VI, Pavlenko VA, Shkurov VA (1984) Ion extraction from solutions at atmospheric pressure – a method for mass-spectrometric analysis of bioorganic substances. Dokl Akad Nauk SSSR. 277: 379–383 (in Russian).
16. Kebarle P (2000) Overview of mechanisms involved in ESI. J Mass Spectrom. 35: 804-817.

17. Hofstadler SA, Bakhtiar R, Smith RD (1996) Instruments and Spectral Interpretation for ESI. J. Chem. Ed. 73: A82-A88.
18. Mora JF, Van Berkel GJ, Enke CG, Cole RB, Martinez-Sanchez M, Fenn JB (2000) Electrochemical processes in electrospray ionization mass spectrometry. J Mass Spectrom. 35(8): 939-952.
19. Wilm M, Mann M (1996) Analytical properties of the nanoelectrospray ion source. Anal Chem. 68(1): 1-8.
20. Watson JT, Sparkman OD (2008). Introduction to Mass Spectrometry: Instrumentation, Applications and Strategies for Data Interpretation. Wiley. Fourth Edition.
21. Iribarne JV, Thomson BA (1976) On the evaporation of small ions from charged droplets. J. Chem. Phys. 64: 2287–2289.
22. Smith JN, Flagan RC, Beauchamp JL (2002) Droplet Evaporation and Discharge Dynamics in Electrospray Ionization. Journal of Physical Chemistry A. 106(42): 9957-9967.
23. Nemes P, Marginean I, Vertes A (2007) Spraying Mode Effect on Droplet Formation and Ion Chemistry in Electrosprays. Anal Chem. 79: 3105-3116.
24. Wilm M (2011) Principles of Electrospray Ionization. Molecular and Cellular Proteomics. 10(7) : 1 – 8.
25. Duelcks T, Roellgen FW (1995) Ionization conditions and ion formation in electrohydrodynamic mass spectrometry. International Journal of Mass Spectrometry and Ion Processes 148(1/2): 123-44.
26. Tanaka K, Waki H, Ido Y, Akita S, Yoshida Y, Yoshida T, Matsuo T (1988) Protein and polymer analyses up to m/z 100 000 by laser ionization time-of-flight mass spectrometry. Rapid Commun. Mass Spectrom. 2: 151–153.
27. Mamyrin BA (2001) Time-of-flight mass spectrometry (concepts, achievements, and prospects). International Journal of Mass Spectrometry. 206(3): 251-266.
28. Mamyrin BA (1994) Reflectron TOF-MS. Int. J. Mass Spectrom. Ion Processes. 131: 1-19.
29. Scherer S, Altwegg K, Balsiger H, Fischer J, Jaeckel A, Korth A, Mildner M, Piazza D, Reme H, Wurz P (2006) A novel principle for an ion mirror design in TOFMS. Int J Mass Spectrom. 251: 73-81.

30. Cotter RJ, Gardner BD, Iltchenko S, English RD (2004) Tandem Time-of-Flight Mass Spectrometry with a Curved Field Reflectron. Analytical Chemistry. 76(7): 1976-1981.
31. Laures AMF, Wolff JC, Eckers C, Borman PJ, Chatfield MJ (2007) Investigation into the factors affecting accuracy of mass measurements on a TOF MS using Design of Experiment. Rapid Commun Mass Spectrom. 21: 529-535.
32. Brunelle A, Della-Negre S, LeBeyec Y (1992) Progress in TOF-MS. Analysis 20: 417-420.
33. Hu Q, Noll RJ, Li H, Makarov A, Hardman M, Cooks RG (2005) The Orbitrap: a new mass spectrometer. J. Mass Spectrom. 40: 430–443.
34. Hardman M, Makarov AA (2003) Interfacing the Orbitrap Mass Analyzer to ESI. Anal Chem. 75: 1699-1705.
35. Makarov A, Denisov E, Kholomeev A, Balschun W, Lange O, Strupat K, Horning S (2006) Performance Evaluation of a Hybrid Linear Ion Trap/Orbitrap Mass Spectrometer. Anal Chem 78: 2113-2120.
36. Brown DW, Floyd AJ, Sainsbury M (1988) Organic Spectroscopy. John Wiley & Sons: New York.
37. Silverstein RM, Webster FX (1998) Spectrometric Identification of Organic Compounds. John Wiley & Sons: New York. 6th ed.
38. Kemp W (1991) Organic Spectroscopy. Palgrave: New York. 3rd ed.
39. Abragam A (1961) Principles of Nuclear Magnetism. Oxford University Press, Oxford.
40. Derome A (1987) Modern NMR Techniques for Chemistry Research. Pergamon Press Press, Oxford.
41. Ernst RR, Bodenhausen G, Wokaun A (1987) Principles of Nuclear Magnetic Resonance in One and Two Dimensions. Clarendon Press, Oxford.
42. James TL (1998) Fundamentals of NMR. San Francisco.
43. James TL (1975) Nuclear Magnetic Resonance in Biochemistry. Academic Press, New York.
44. Kwan EE, Huang SG (2008) Structural Elucidation with NMR Spectroscopy: Practical Strategies for Organic Chemists. Eur. J. Org. Chem. 2671–2688.
45. Bax Ad, Summers MF (1986) ^{1}H and ^{13}C Assignments from Sensitivity-Enhanced Detection of Heteronuclear Multiple-Bond Connectivity by 2D Multiple Quantum NMR. J. Am. Chem. SOC. 108: 2094-2096.

46. Kessler H, Gehrke M, Griesinger C (1988) Two-dimentional NMR Spectroscopy: Background and Overview of the Experiments. Angew. Chem. Inf.Ed. Engl. 27: 490-536.
47. Laws DD, Bitter HML, Jerschow A (2002) Solid-State NMR Spectroscopic Methods in Chemistry. Angew. Chem. Int. Ed. 41: 3096 - 3129.
48. Pines A, Gibby MG, Waugh JS (1973) J. Chem. Phys. 59: 569-590.
49. Haeberlen U (1976) High Resolution NMR in Solids: Selective Averaging. Adv. Magn. Reson. 1 – 4.
50. Kolodziejski W, Klinowski J (2002) Kinetics of Cross-Polarization in Solid-State NMR: A Guide for Chemists. Chem. Rev. 102: 613−628.
51. Cory DG, Ritchey WM (1989) Inversion Recovery Cross-Polarization NMR in Solid Semicrystalline Polymers. Macromolecules. 22: 1611-1615.
52. Babonneau F, Maquet J, Bonhomme C (1996) ^{29}Si and ^{13}C NMR Investigation of the Polysilane-to-Poly(carbosilane) Conversion of Poly(methylchlorosilanes) Using Cross-Polarization and Inversion Recovery Cross-Polarization Techniques. Chem. Mater. 8: 1415-1428.
53. Wu X, Zhang S (1989) Selective Polarization Inversion and Depolarization in Cross Relaxation in NMR. Chemical Physics Letters. 156 (1): 79 - 81.
54. Alemany LB, Grant DM, Pugmire RG, Alger TD, Zilm KW (1483) Cross Polarization and Magic Angle Sample Spinning NMR Spectra of Model Organic Compounds. 2. Molecules of Low or Remote Protonation. J. Am. Chem. Soc. 105: 2142-2147.
55. Bennett AE, Rienstra CM, Auger M, Lakshmi KV, Griffin RG (1995) Heteronuclear decoupling in rotating solids. J. Chem. Phys. 103 (16): 6951 - 6958.

4. Study of the communic acid

4. A. Introduction: A simplification approach: the communic acid as a principal component of the sandarac resin, responsible for its polymerization

Chemically, varnish is a very complex mixture of different organic molecules combining compounds, those of oils, as well as natural resins. Ageing of varnishes is one of the major problems encountered in the field of painting art, because it leads to yellowed products, which can obscure colours, become very brittle, and show a change in solubility [1]. As these physical changes are the consequence of molecular modifications of the fresh resin, it is important to study these polymerization and ageing processes on a molecular level. This research focuses on the polymerization and further ageing processes of the diterpenoid resin *sandarac*, which is frequently used as oil painting varnishes.

Surprisingly little is known about the molecular ageing processes of the *sandarac* resin on paintings, possibly due to a number of difficulties. First, fresh diterpenoid resins are already complex mixtures of a number of compounds. Ageing on paintings results in the formation of an even larger number of compounds, which are difficult to analyse. Secondly, the investigation of the ageing of varnish by sampling from actual paintings is complicated because of the many unknown factors, such as environmental effects and the varnish recipes used [2]. All these factors seem to be a serious problem in the understanding of varnish ageing process, so a complementary approach has to be developed in which varnishes are subjected to various forms of simplifications.

The polymerisation of the *sandarac* resin is likely due to the initial presence of communic acid, also known as 8 (17), 12,14-labdatrien-19-oic acid, that has in its structure a system of conjugated double bonds, exposed to reticulation reactions (Figure 1).

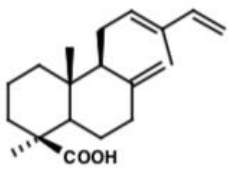

Figure 1. The structure of the communic acid.

In order to find out the manner in which natural resins exudated from plants polymerize, a simplification of the system based on the communic acid was chosen, as principal and

representative component of the fresh resin. The molecular changes are investigated by comparative studies of pure extracted communic acid, artificially aged communic acid and commercial sandarac resin.

Therefore, this thesis focuses on fundamental molecular processes that occur during ageing of diterpenoid resin *sandarac* by considering the ageing of its major compound communic acid.

In order to investigate how material has changed due to ageing both the chemical composition of the fresh starting material and the aged products must be investigated. The analysis of freshly extracted communic acid is described in the first part of this chapter, including extraction procedure and structure elucidation. Structure of the communic acid was elucidated on the basis of 1D and 2D NMR (1H, 13C-NMR, 1H–1H COSY, HSQC, TOCSY and HMBC) and IR spectroscopy, GC-MS spectrometry.

4. B. Extraction of the communic acid

Communic acid was isolated from the cones of the Mediterranean cypress (*Cupressus sempervirens*) by the method described by Ahond et al [3].

Cones of cypress *Cupressus sempervirens*

The crushed cypress cones (100 g) were placed in a column equipped with a filter and eluted with n-hexane at 25-30 ° C. A green liquid flew and the elution was continued until the flowing liquid became colourless. The n-hexane was then evaporated and green oil recovered (1.5 g). This oil was taken up in a little volume of n-hexane and a 2M solution of sodium hydroxide was added. A greenish precipitate appeared which was then filtered on Buchner

funnel by rinsing with the minimum of water. The yellow-green solid recovered (1.7 g) was then dissolved in water (pH of the solution = 13.5) and 6N HCl was added until the pH = 2 reached. A yellow precipitate appeared. Afterwards, the reaction medium was extracted with 5 x 70 mL $CHCl_3$ (the precipitate dissolves therein). The organic phases were combined, dried over anhydrous $MgSO_4$, filtered and then evaporated (Scheme 1).

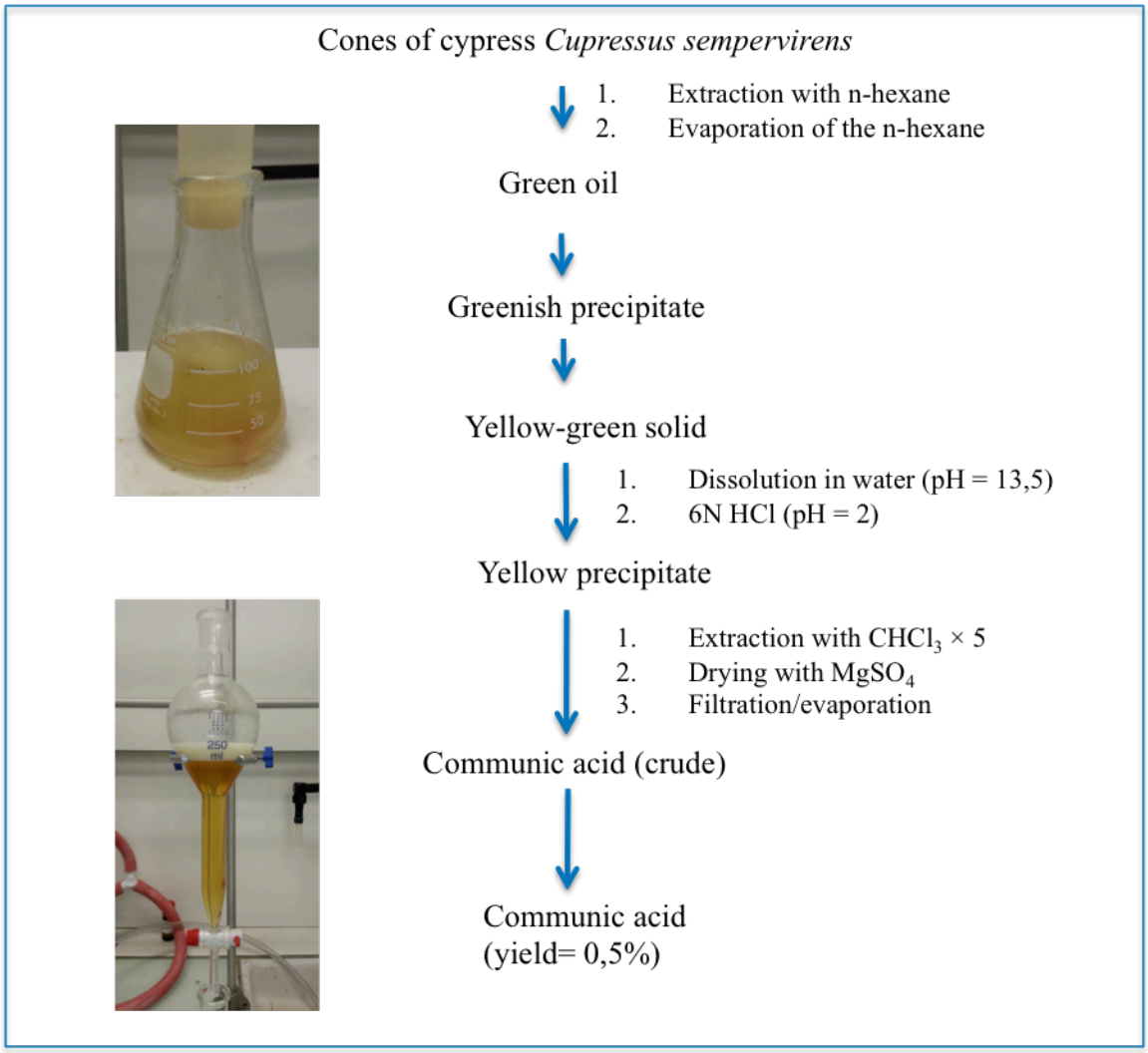

Scheme 1. The extraction of the communic acid.

The ^1H NMR of the crude product showed, in addition to the *trans*-communic acid, the presence of 13β-hydroxylabda-8(17)-14-dienoic acid. The ratio of the desired product and by-product is 1 to 0.2 (Figure 2).

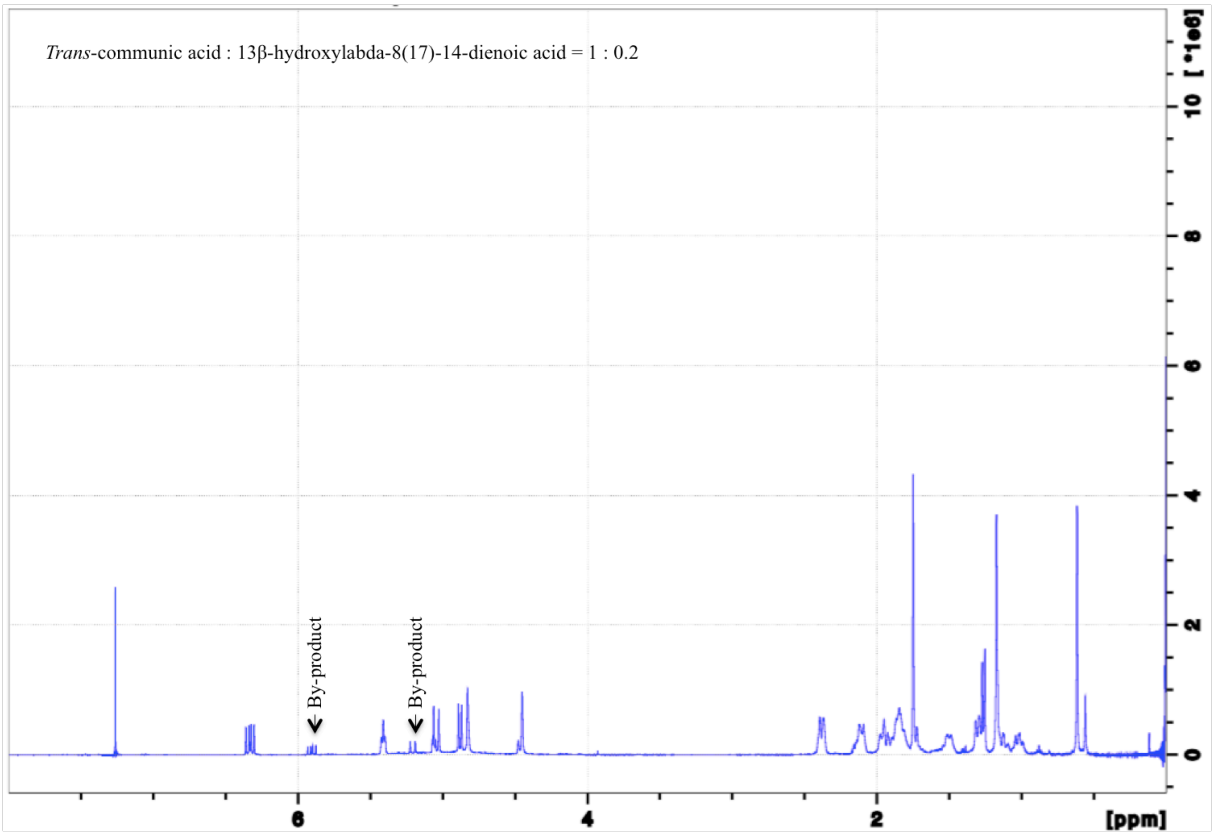

Figure 2. 500 MHz 1H spectrum of the crude mixture extracted from cypress cones (*Trans*-communic acid : 13β-hydroxylabda-8(17)-14-dienoic acid = 1 : 0.2).

The presence of the side product and its structure was proved additionally by GC-MS shown in the Figure 3. From the total ion chromatogram of the crude mixture extracted from cypress cones after derivatization with BSTFA/TMCS it is evident that there are two products present: the main product that appears the first and then followed by the minor compound. The molecular ion on the mass spectrum of the by-product at m/z 465 indicates the double trimethylsilylation that went on during the derivatization of the crude mixture with BSTFA/TMCS, and the presence in the side product of two –OH groups (Figure 3,b).

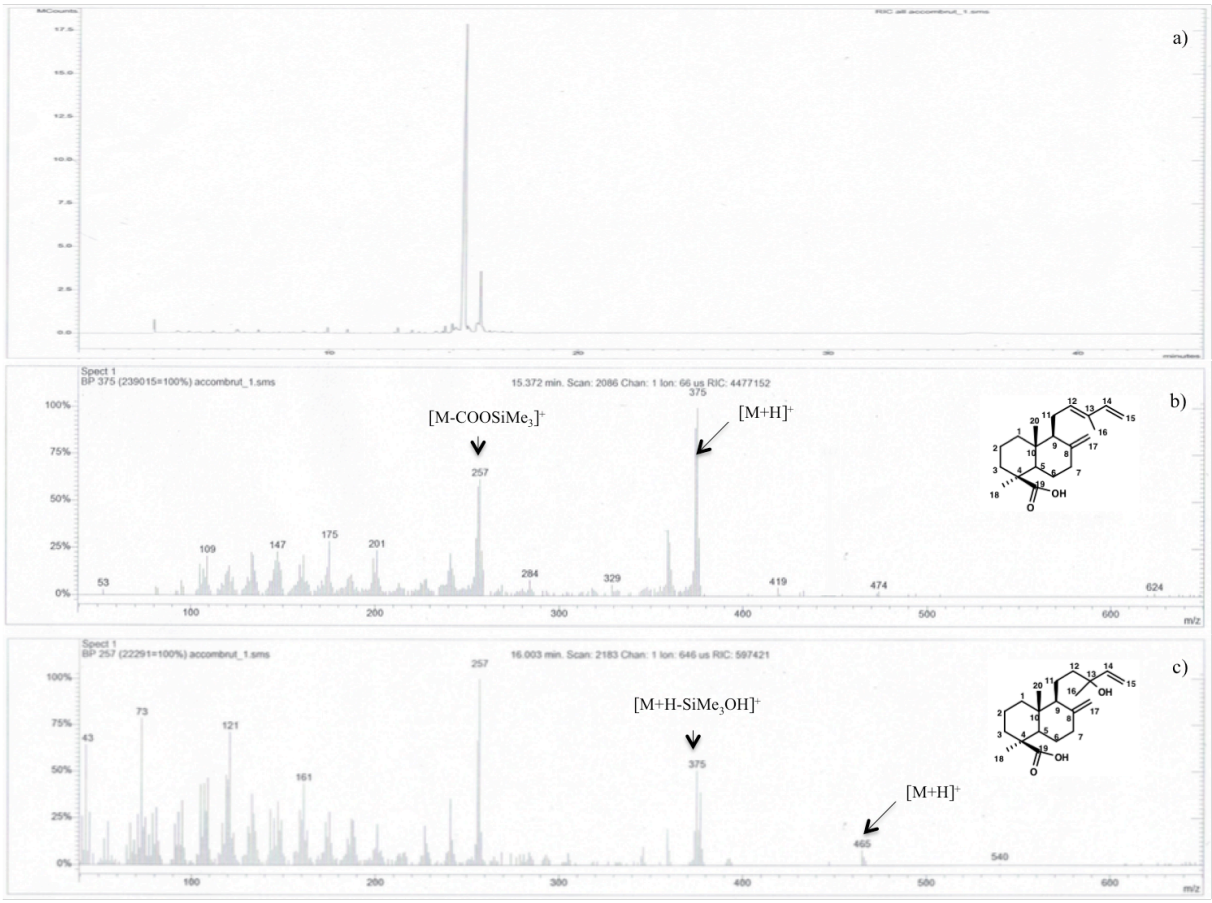

Figure 3. a) Total ion chromatogram of the crude mixture extracted from cypress cones after derivatization with BSTFA/TMCS; b) 70 eV EI-mass spectra of *trans*-communic acid; c) 70 eV EI-mass spectra of 13β-hydroxylabda-8(17)-14-dienoic acid.

The crude product was then purified by flash chromatography on silica gel (eluent: $CHCl_3$ / Hex = 80/20). The desired acid was obtained as a yellow oil with a very poor yield 0,2% (if counted from the mass of cones, 200 mg), and is stored in a freezer at -20 ° C. The molecular weight of its TMS ester derivative was determined by GC-MS at m/z 375 for the [M + H].

Preliminary ^{1}H and ^{13}C 1D NMR analyses after purification and isolation of the communic acid fraction has shown that the spectra obtained are in global accordance with spectra provided in [3]. Further, a detailed peak attribution of communic acid thought liquid state 2D NMR is provided.

4. C. Spectroscopic properties of the communic acid

4. C. I. Assignment of vibrational spectra of the communic acid

Firstly, the freshly extracted communic acid was subjected to infrared (IR) analyses in ATR mode, as that keeps the sample intact and available for further analyses. The vibrational spectroscopy also constitutes a technique of choice because it does not require any sampling preparation or destruction.

Each IR spectrum can be divided into four zones where information for identification can be found. The different regions are the OH region (3700 to 3200 cm^{-1}), the CH region (from 3200 to 2400 cm^{-1}), the carbonyl region (1800-1550 cm^{-1}) and, to complete, the fingerprint zone (1550-500 cm^{-1}).

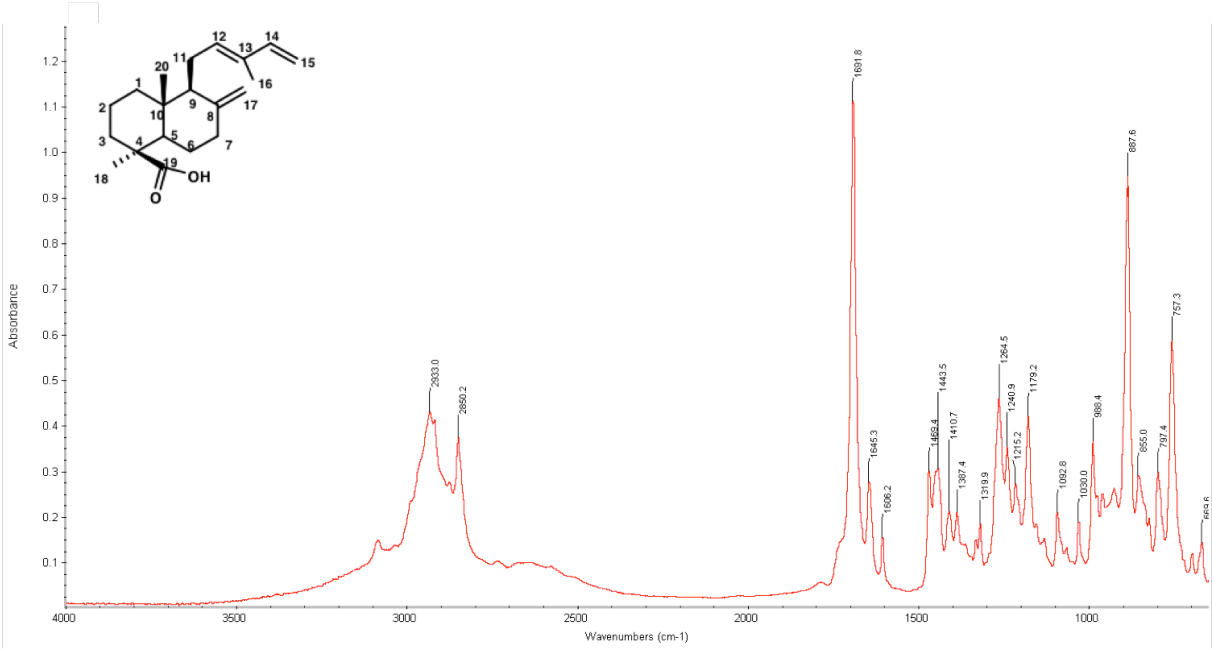

Figure 4. IR spectra of the communic acid.

The infrared spectra of the communic acid is shown in the Figure 4. O-H stretching band is observed in the range 3500 – 3200 cm^{-1} due mainly to the vibration of the hydroxyl group of the carboxyl function. The CH region has a maximum at 2933 cm^{-1} for the communic acid. A band at 3080 cm^{-1}, as well as the band centred on 2850 cm^{-1}, corresponding to the stretching vibration of the double C = C bond of the vinyl function, are characteristic bands of pimaranes [4].

The carbonyl region possess an intense infrared band at 1691 cm^{-1} that is attributed to the C=O stretching of the carboxyl group. The 1645 cm^{-1} band, assigned to the stretching vibration of the olefinic group ν(C=CH_2), together with 797 cm^{-1} band indicate a trisubstituted double bond. The band centred on 1443 cm^{-1} corresponds to the deformation of CH bonds (CH_2 or CH_3 groups). The infrared spectrum of the communic acid also showed the presence of a terminal methylene group (887 cm^{-1}) which corresponds the out-of-plain deformation of the exomethylene functionality in C8 = C17.

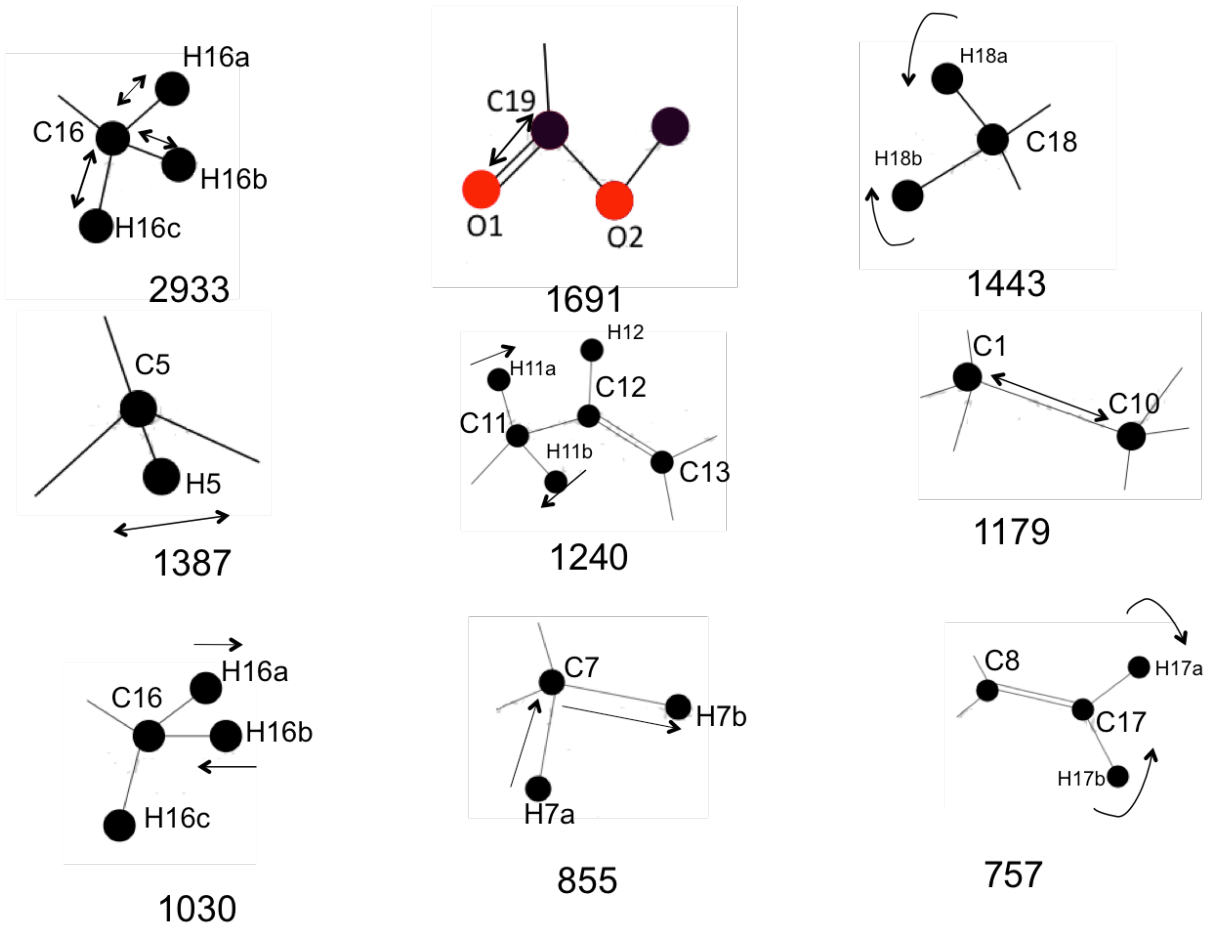

Figure 5. Selected vibrational modes and band positions for different functional groups present in the communic acid.

So, as a result, the infrared characteristic absorption bands of the communic acid are 2933 ν(C-H); 2850 ν(C-H); 1691 ν(C = O); 1645 vinyl; 1606, 1469, 1443, 1410, 1387, 1319, 1264, 1240, 1215, 1179, 1092, 1030, 988, 887, 855, 797, 757, 669 cm^{-1}, in general indicating the presence of an exomethylene group (2940 and 887 cm^{-1}), an α,β-unsaturated system (1750 and 1645 cm^{-1}) moiety, and hydroxy group (3350 cm^{-1}).

Some of the vibrational modes and band positions for different functional groups present in the communic acid are illustrated on Figure 5 for the better visualisation of the vibrations performed by the communic acid.

Peaks in the region 1030-1180 cm^{-1} are corresponding to carbon-carbon stretching vibrations, among which the C1-C10 bond vibration and the asymmetrical H-C16-H methyl stretching vibration have the most important contributions.

When two oscillators share a common atom, coupling between individual oscillators is expected, which means that the O-H stretching band (due mainly to the vibration of the hydroxyl group) has some influence of the stretching-vibration performed by the C19 – O2 bond. Analogically, the band due to C=O is coupled to the in-plane bending vibrations performed by C19 – O2 – H. The absorption band at around 797 cm^{-1} is mainly due to the methylene bending H-C7-H vibration, and band at 1387 cm^{-1} is mainly due to the symmetrical bending of the methine C5-H bond [5].

4. C. II. Detailed peak attribution through liquid state NMR 2D (COSY, HSQC, HMBC, TOCSY) of the communic acid

Even using highfield NMR-spectrometers, the analysis of the proton spectra of complex natural compounds like resin acids is not possible with conventional methods. In these cases 2D-NMR techniques have proved to be very useful for obtaining additional information [6]. In this research several of these modern techniques were used simultaneously to get an unambiguous assignment of the ^{1}H- and ^{13}C-resonances of the communic acid.

An extensive application of 1D (^{1}H, ^{13}C-NMR and DEPT) and 2D (COSY, HSQC, HMBC and TOCSY) NMR techniques was performed to characterize the structure and to establish the ^{1}H and ^{13}C resonance assignments in the extracted acid.

The ^{1}H and ^{13}C NMR data of the communic acid exhibited characteristic signals of a labdane-type structure including three methyls and an exo-methylene group. The assignment of the ^{1}H- and ^{13}C-resonances of communic acid is given in Tables l and 2 and its ^{1}H- and ^{13}C spectra respectively are presented on Figures 1 and 2.

The aliphatic region of the ^{13}C-spectrum consists of 13 well-separated peaks. The signals at 12.8, 29 and 11.8 ppm are due to the methyl groups of carbons 16, 18 and 20 respectively.

Table 1. ^{13}C-Chemical shifts of the communic acid in $CDCl_3$; δ-values are in ppm from TMS (±0.05)

C1	39.2	C11	23.3
C2	19.9	C12	133.4
C3	37.9	C13	133.9
C4	44.2	C14	141.6
C5	56.4	C15	109.9
C6	25.8	C16	12.8
C7	38.5	C17	107.7
C8	147.9	C18	29
C9	56.2	C19	184.2
C10	40.4	C20	11.8

Table 2. ^{1}H-Chemical shifts of the communic acid in $CDCl_3$; δ-values are in ppm from TMS (±0.05)

H1a	2.03 - 1,82	H11a	2.43 – 2.36
H1b	1.13	H11b	2.22 – 2.10
H2a	2.03 – 1.82	H12	5.42
H2b	1.54	H14	6.34
H3a	2.22 – 2.10	H15a	5.06
H3b	1.06	H15b	4.89
H5	1.37	H16	1.76
H6a	2.03 – 1.82	H17a	4.85
H6b	2.03 – 1.82	H17b	4.48
H7a	2.43 – 2.36	H18	1.26
H7b	2.03 – 1.82	H20	0.66
H9	1.74		

The carbon 19 of carboxyl group, the most deshielded signal of the spectrum and one of the five quaternary carbons, showed shift of δ_C184.2 (C19) typical for a carboxylic acid. Six carbons at δ_C 147.9 (C8), 141.6 (C14), 133.9 (C13), 133.4 (C12), 109.9 (C15) and 107.7 (C17) together with the corresponding signals of six vinylic protons in the ^{1}H NMR indicated the presence of three double bonds.

In the ^{1}H-spectrum the protons H-14, H-12, H-15a,b and H-17a,b show characteristic splitting patterns and are well separated. Six olefinic protons emerged in the high frequency of the ^{1}H-NMR spectrum at δ 6.34 (1H, dd, J = 17.2; 10,8 Hz), 5.42 (1H, t, J = 6.4 Hz), 5.06 (1H, d, J = 7.6Hz), 4.89 (1H, d, J = 10.7 Hz), 4.85 (1H, s) and 4.48 (1H, s).

The proton H14 is the most deshielded signal of the ^{1}H-spectrum attached to the sp2 hybridized carbon and appears as a doublet of doublets. Less deshielded proton H12 is a well-recognized triplet splitting on two neighbouring H11a and H11b protons. Two remaining protons of the conjugated system of double bonds are H15a and H15b protons each of which is splitting on the neighbouring H14. The downfield part of the spectrum is finalised by two remaining protons attached to a sp^2 hybridized carbon C17.

The assignment of the upfield region of ^{1}H-spectrum is more challenging due to the presence of numerous multiplets presenting the aliphatic region of protons connected to sp3 carbons. The three highest singlets of the shielded part are three methyl groups attached to the 16, 18 and 20 carbons, which are easily attributed.

The attribution of carbons is confirmed by DEPT (Figure 8), eliminating all quaternary carbon atoms among which C4, C8, C10, C13 and C19 and negatively inversing $–CH_2$-atoms. DEPT spectra revealed that of the 20 carbons three belonged to methyl, nine to methylene, and six to methine groups.

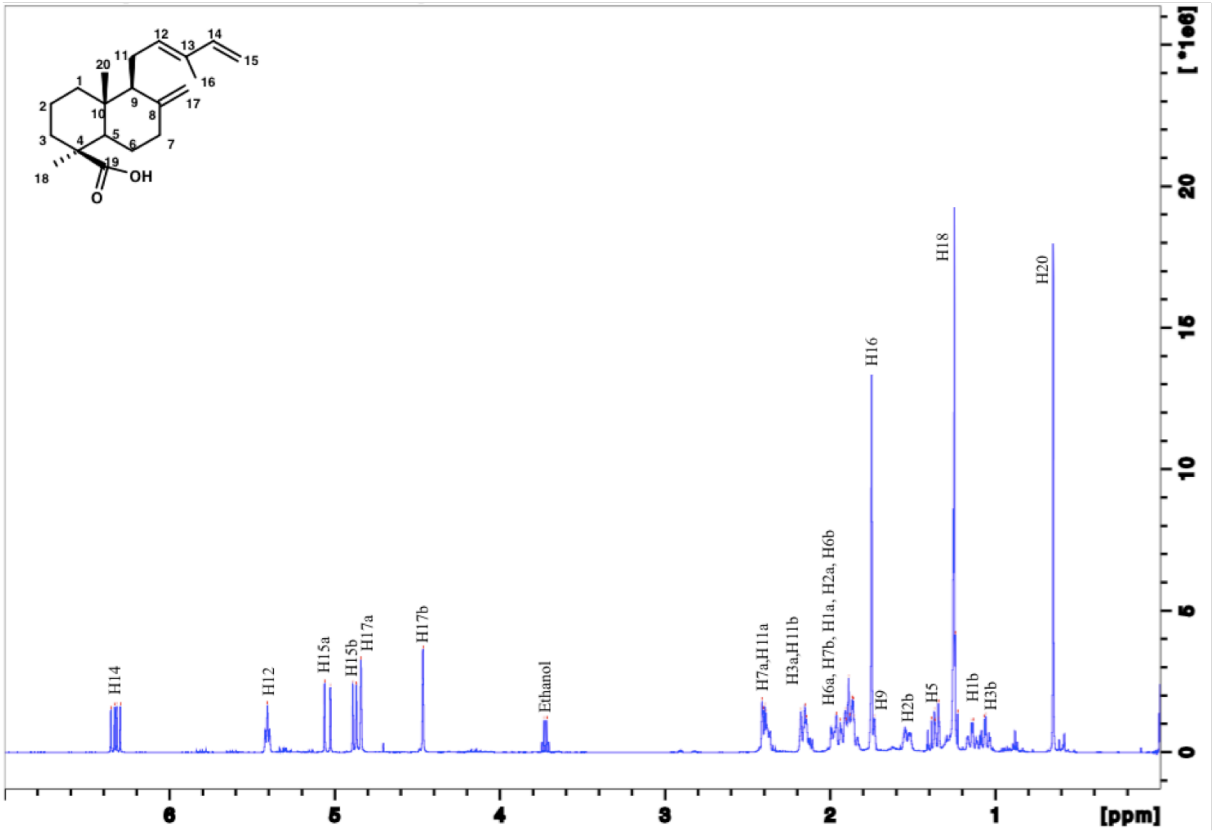

Figure 6. 500 MHz ^{1}H spectrum of communic acid in $CDCl_3$.

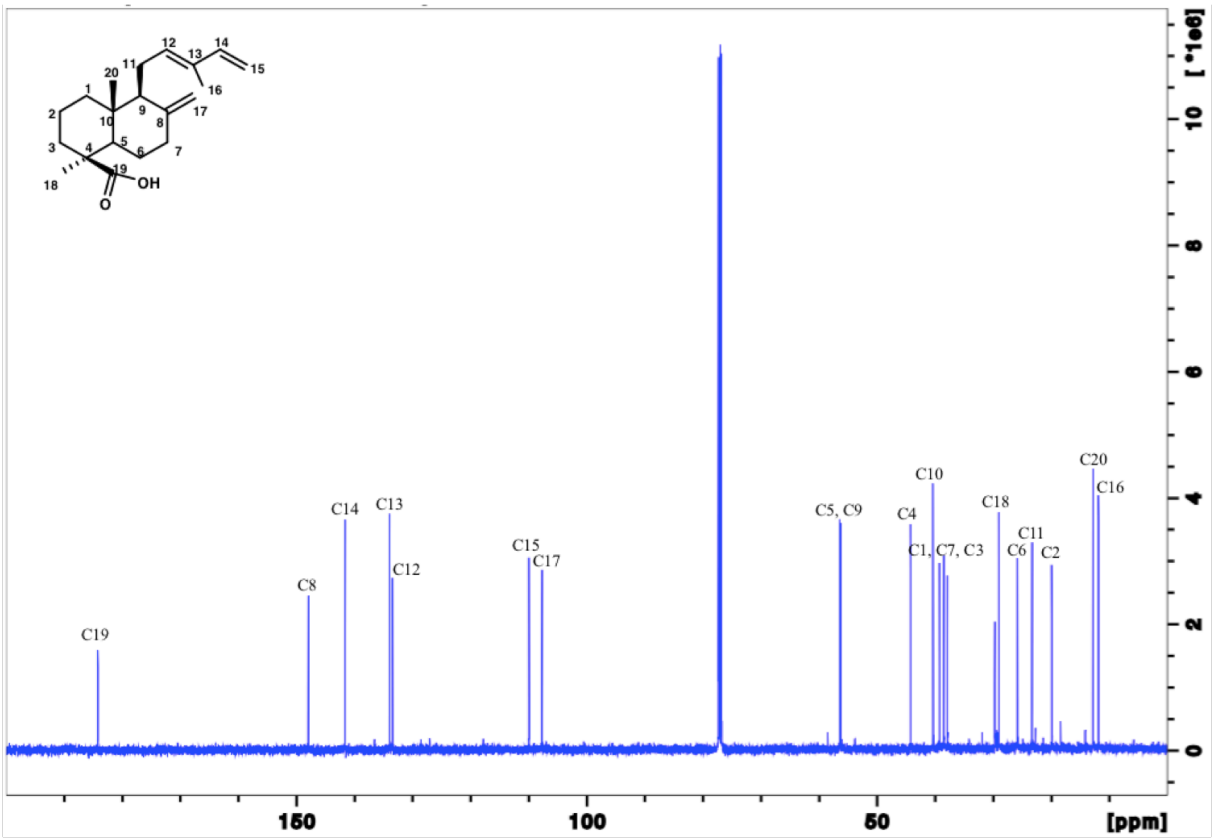

Figure 7. 500 MHz ^{13}C spectrum of communic acid in $CDCl_3$.

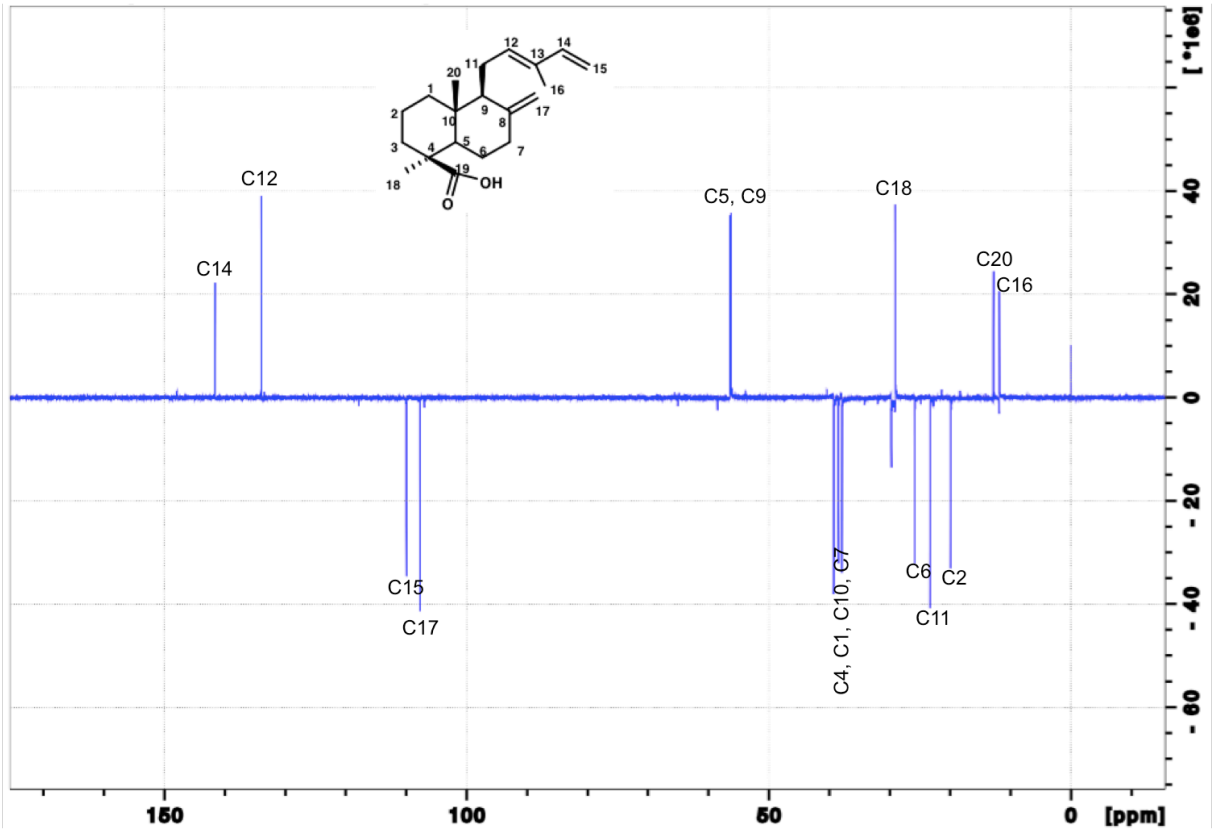

Figure 8. 500 MHz DEPT of communic acid in $CDCl_3$.

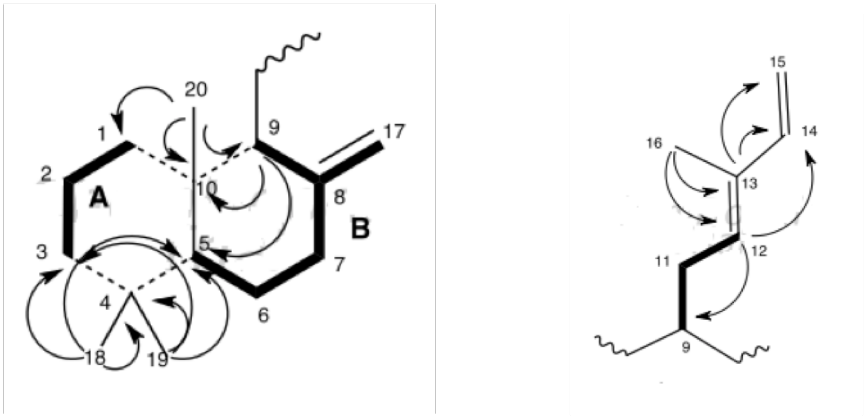

a b

Figure 9. a. Key COSY (bold) and HMBC (arrows) correlations of the trans-decalin core of the communic acid; b. key COSY (bold) and HMBC (arrows) correlations of the side chain of the communic acid.

The presence of a trans-decalin core, as depicted in Figure 9a, was highlighted from the following. Two spin systems A and B, involving protons from H1 to H3 and from H5 to H9, respectively, were identified by analysis of 1H−1H correlations observed in the COSY spectrum (Figure 10). HMBC correlations from methyl group 18 to C3, C4 and C5, and from C20 to C1, C9, and C10 supported the location of methyl groups on C4 and on C10 (Figure 11). These correlations established the junction between the two spin systems A and B.

The construction of the side chain of communic acid, as depicted in Figure 9b, was determined from the further analysis of 1D and 2D NMR data. The trans-decalin and unsaturated function are connected by an aliphatic carbon as supported by HMBC correlations from H12 to C9. The proton shift of one methyl signal at δ 1.76 and its HMBC correlations to four of the olefinic carbons (δ 141.6, 133.4 and 109.9) suggested that these two double bonds are conjugated.

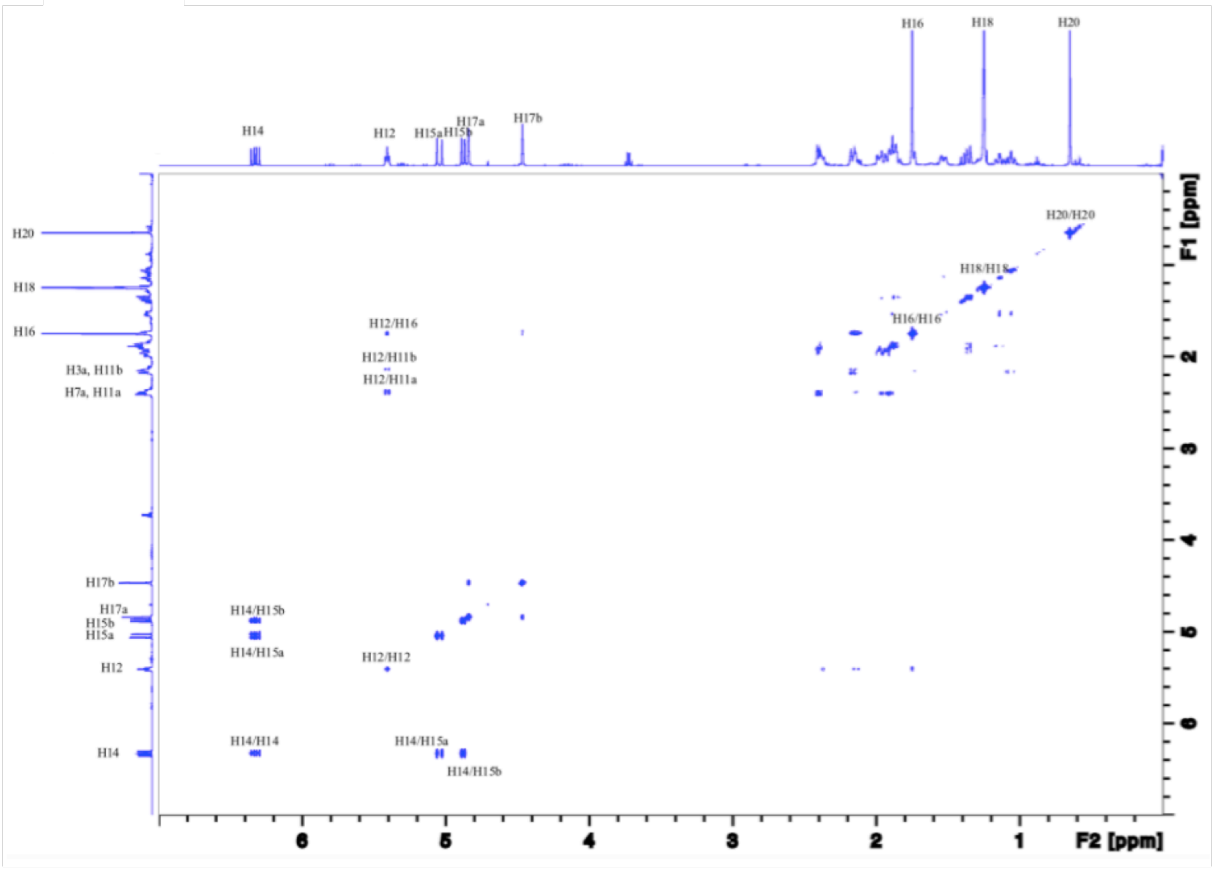

Figure 10. 500 MHz COSY of the communic acid in $CDCl_3$.

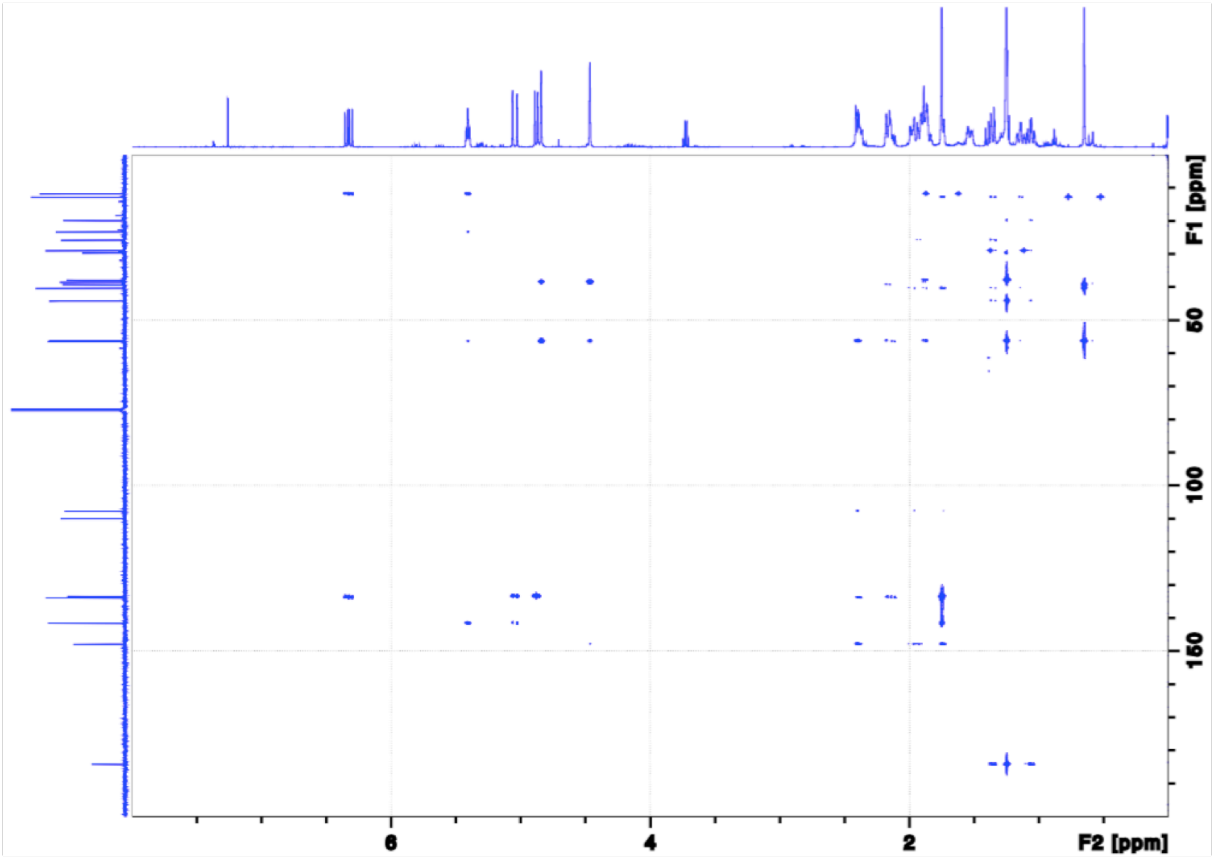

Figure 11. 500 MHz HMBC of communic acid in $CDCl_3$.

The HSQC (Figure 12) and HMBC spectra therefore allow the assignment of C14, C12, C15a,b and C17a,b. A long-range coupling of the neighbouring protons to the carboxyl carbon (δ 184.2) could be detected, namely, a HMBC cross-peak for the proton at δ 1.37 (H5) to this carbon was observed and carbon C5 (δ 56.4), to which this proton corresponds in the HSQC, showed a cross-peak with protons at δ 2.03 – 1.82, 2.43 – 2.36 (H6a,b, H7a,b).

The final attribution resolving the remaining ambiguities, concretely, the assignment of the non-equivalent protons of C15 and C17, was supported by means of TOCSY (Figure 13).

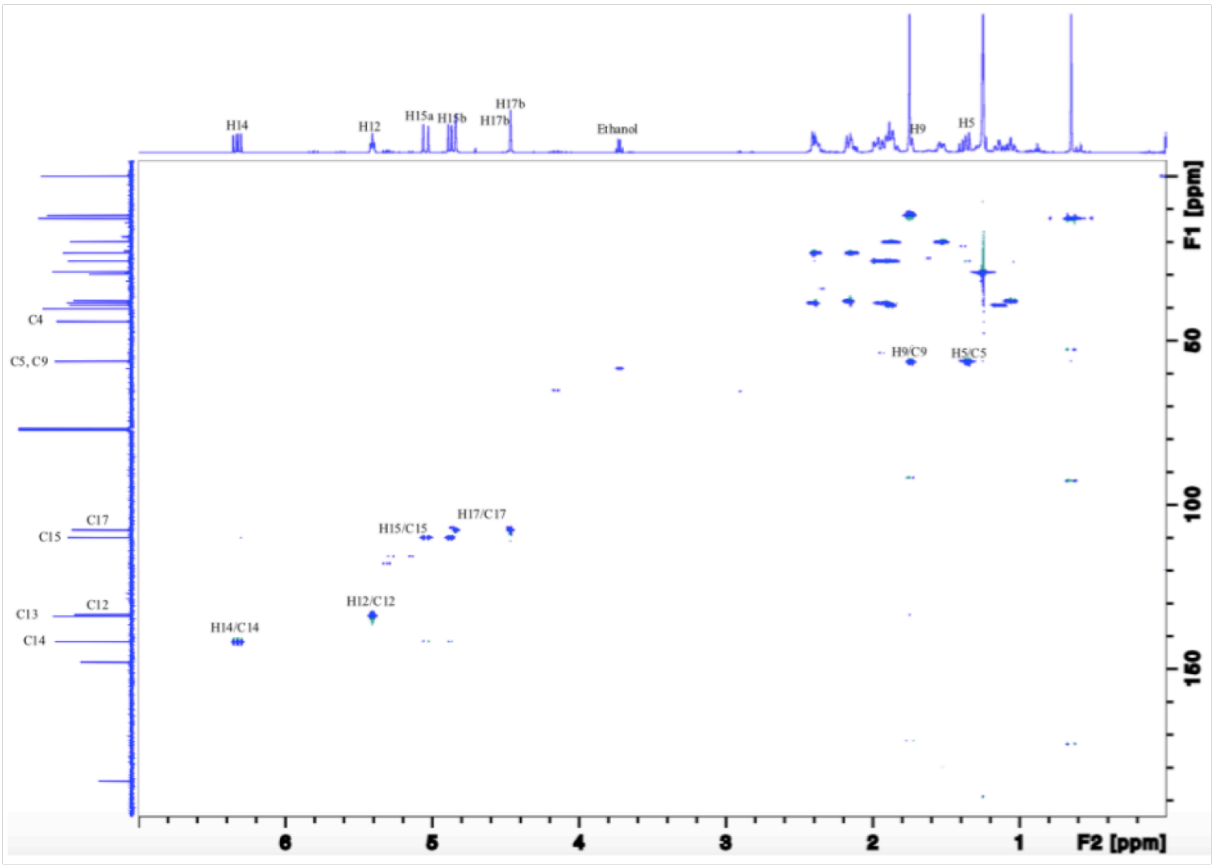

Figure 12. 500 MHz HSQC of communic acid in $CDCl_3$.

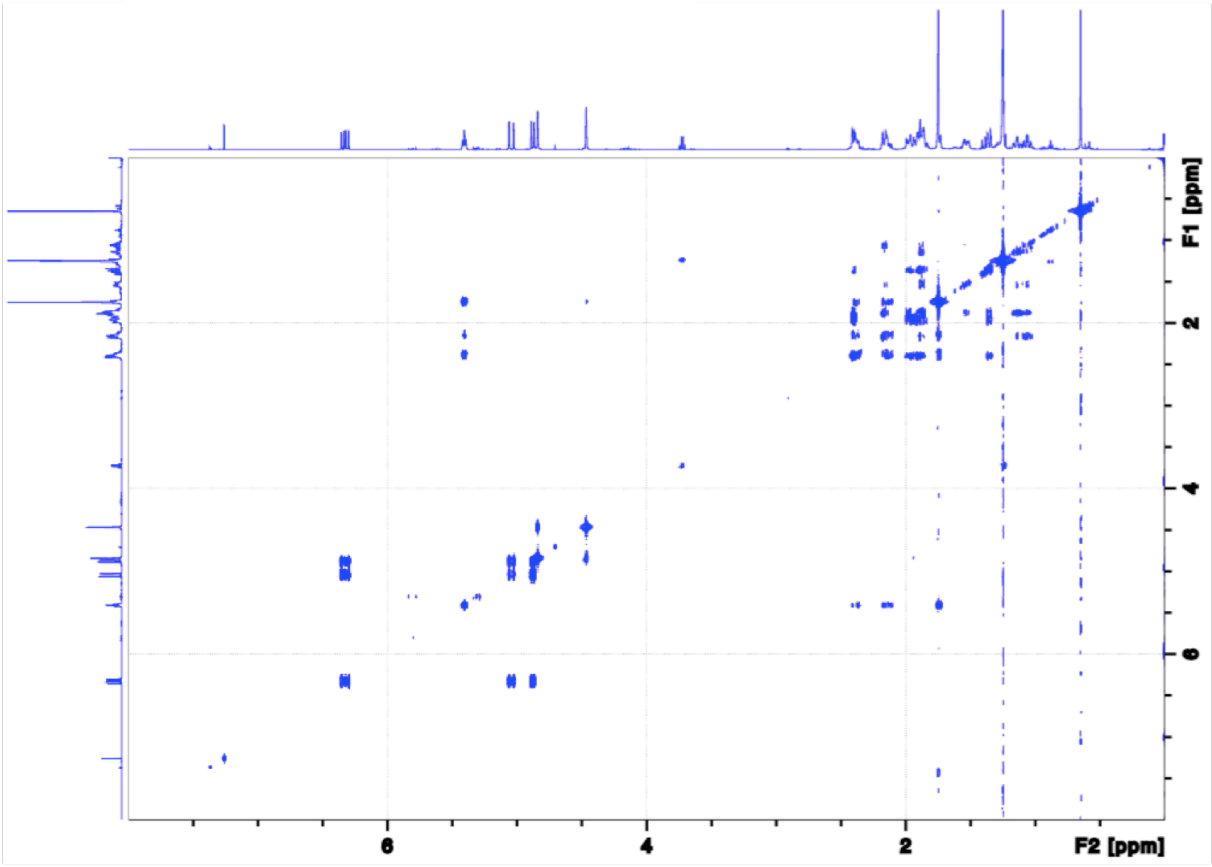

Figure 13. 500 MHz TOCSY of communic acid in $CDCl_3$.

Thus, a complete characterization of the communic acid molecule is summarized below:

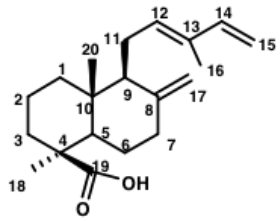

trans-Communic acid

$C_{20}H_{30}O_2$

M = 302,56 g.mol^{-1}

RMN^{1}H: δ 6.34 (dd, J=17,2; 10,8 Hz, 1H, H14), 5.42 (t, J=6,4Hz, 1H, H12), 5.06 (d, J=17,4 Hz, 1H, H15a), 4.89 (d, J = 10,7 Hz, 1H, H15b), 4.85 (s, 1H, H17a), 4.48 (s, 1H, H17b), 2.43 – 2.36 (m, 2H, H7a, H11a), 2.22 – 2.10 (m, 2H, H3a, H11b), 2.03 – 1.82 (m, 5H, H6a, H7b, H1a, H2a, H6b), 1.76 (s, 3H, H16), 1.74 (m, 1H, H9), 1.54 (m, 1H, H2b), 1.37 (m, 1H, H5), 1.26 (s, 3H, H18), 1.13 (dd, J = 14,8; 4,0 Hz, 1H, H1b), 1.06 (dd, J = 14,4 ; 4,1 Hz, 1H, H3b), 0.66 (s, 3H, H20).

RMN ^{13}C: δ 184.2 (C19), 147.9 (C8), 141,6 (C14), 133.9 (C13), 133.4 (C12), 109.9 (C15), 107.7 (C17), 56.4 (C5), 56.2 (C9), 44.2 (C4), 40.4 (C10), 39.2 (C1), 38.5 (C7), 37.9 (C3), 29.0 (C18), 25.8 (C6), 23.3 (C11), 19.9 (C2), 12.8 (C16), 11.8 (C20).

GC-MS: Rt 15.372 min; 375 $[M+H]^+$.

4. D. Studies of ageing behaviour of the communic acid

As previously mentioned, the resins are very complex mixtures of different compounds, mostly terpenoids. With ageing their complexity increases even more. To understand the ageing behaviour of such complex mixtures, it is helpful to first study the ageing behaviour of individual components. In this part of work, pure communic acid was artificially aged to investigate the changes that occur during its ageing. For direct comparison with the *sandarac* resin the communic acid was chosen as the main component and as reference diterpenoid.

The general effects of artificial or accelerated ageing have been examined by the research group of Feller [7]. Elevated doses of light of a controlled spectrum and at high temperature or humidity are used to induce chemical changes in a short period that are similar to those induced by normal ageing in a much longer time. However, natural ageing also includes thermal processes that take place in the dark and modify the products of the photolytic ageing.

Since the UV is irradiation one of the promoting factors of polymerization process [8, 9], in this research, a continuous exposure to UV light (365 nm) at room temperature was used to improve photoproduct formation. The results presented should not be considered as completely representative of the natural ageing. Nevertheless, because it is believed that the natural ageing is initiated by photolytic reactions, these results are representative of the key natural processes.

4. D. I. FTIR analysis of the communic acid ageing

First of all a study of the ageing process of the communic acid was carried out through Fourier transform infrared spectroscopy (FTIR). This study aims to provide information about which bonds are affected and unaffected, and these can be used as specific markers of the degradation of the *sandarac* resin.

A spectroscopic study of the ageing process is expected to give a valuable additional information since it can detect macromolecules and it does not require any sample treatment, such as dissolving or derivatization, to identify how molecular species are organized and which reactions or interactions exist among them.

Fresh communic acid was analysed by IR spectroscopy, specific characteristic markers of its molecular structure were identified and band assignments proposed in the previous chapter.

In order to remind, the molecule of the communic acid comprises 3 double bonds (C8 = C17, C12 = C13, C14 = C15) corresponding to the signals at 1645, 1606 and 888 cm^{-1} (Figure 1, red line) that have been attributed to the presence of conjugated C = C bonds, stretching vibration of the olefinic group of carbon - carbon double bonds ν(C=CH_2) and to the out-of-plain deformation of the exomethylene functionality in C8 = C17. Each of these double bonds can potentially participate in the stereospecific radical polymerization. Hence the greater differences are expected in the near vinyl region at 1645 cm^{-1} and 1606 cm^{-1} and for exocyclic methylene deformation at about 888 cm^{-1}. The decrease in the intensities of these peaks following the UV irradiation of the acid will be indicative in the hypothesis that the communic acid is mainly responsible for the polymerization of the *sandarac* resin.

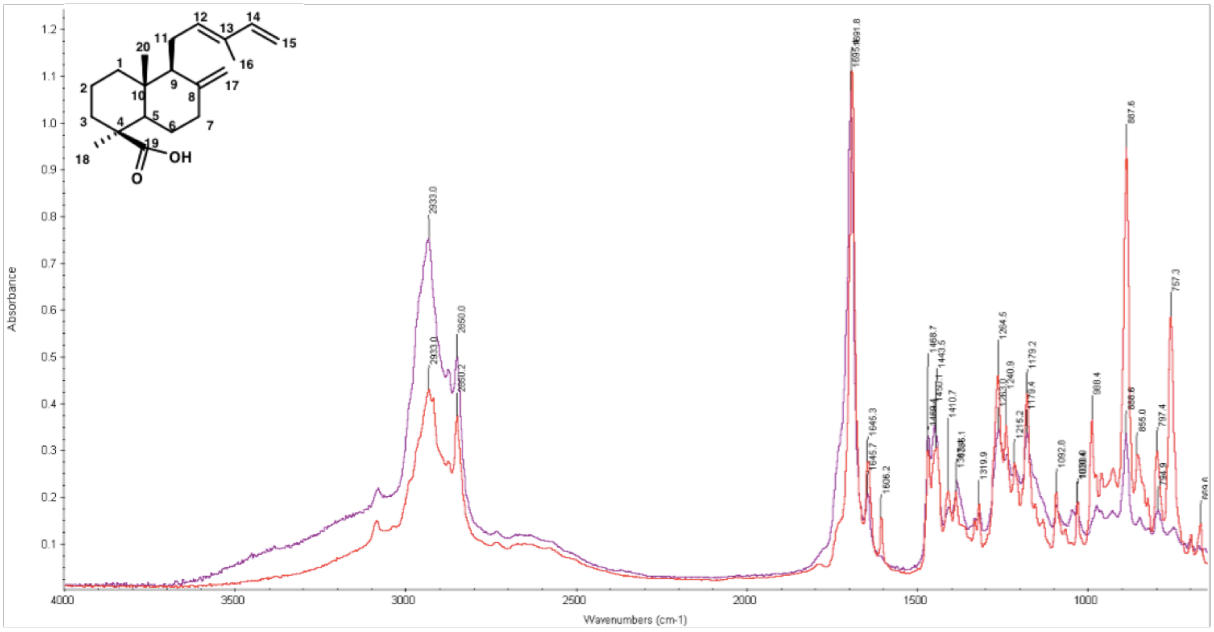

Figure 1. FTIR spectra of unaged (red) and 72h aged under 365 nm UV (purple) communic acid.

Figure 1 (purple line) shows the changes happening in the communic acid after ageing under 365 nm UV lamp during 72 hours. The most important and significant changes occur in the bands at 1691, 1645, 1606 and 888 cm^{-1}. Although the peak position and intensity of the 1691 cm^{-1} band are not affected by ageing with this irradiation period, it broadens because of the presence of a shoulder at 1725 cm^{-1} probably related to the appearance of C = O stretching indicating the oxidation took place. Additionally, the broadening of the 1691 cm^{-1} band may also be related to the presence of hydrogen bonds from the –OH and –COOH groups.

The band at 1606 cm^{-1}, corresponding to the conjugated C = C bonds, has completely disappeared, indicating that this bond is the most active. The 888 cm^{-1} band, which corresponds to the exocyclic double bond C8 = C17, decreases sharply, proving its participation in the polymerization of the resin.

In order to give a deeper insight into the ageing processes and dynamics a kinetic approach has been accomplished by means of FTIR analysis as well. Thus, the communic acid was artificially aged during 24, 72 and 168 hours under 365 nm UV lamp (Figure 2a,b).

From the Figure 2a,b the changes observed within the 24 hours of artificial ageing are minor and the only peak that was affected by UV radiation is at 1606 cm^{-1}, indicating the prior engagement of the conjugated C = C bonds. After a week of ageing this characteristic peak completely disappears. The broadening of the 1691 cm^{-1} band becomes very prominent within 168 hours with appearance of the shoulder at around 1725 cm^{-1}, showing the on going oxidation processes. Significant decrease of the peak corresponding to the exocyclic methylene deformation at 888 cm^{-1} demonstrates that this double bond partially participates in the ageing mechanisms.

Other changes observed during the kinetic studies are the increasing intensities of the bands around 2850 and 2932 cm^{-1} which is explained by the increase in the chemical variability around the –COOH groups. The regions 1400–1200 and 1050–900 cm^{-1} where skeletal vibrations appear show an increased absorption, which also can be related to the formation of other types of molecules as a result of ageing.

Finally, the communic acid is compared to the *sandarac* resin in the Figure 3, which shows that the communic acid while ageing approaches the *sandarac* resin and is the initial product of the polymerisation. Thus, from the comparison of the communic acid and the resin it can be concluded that the *sandarac* resin spectrum can be explained by the polymerization of the communic acid (Figure 3).

a)

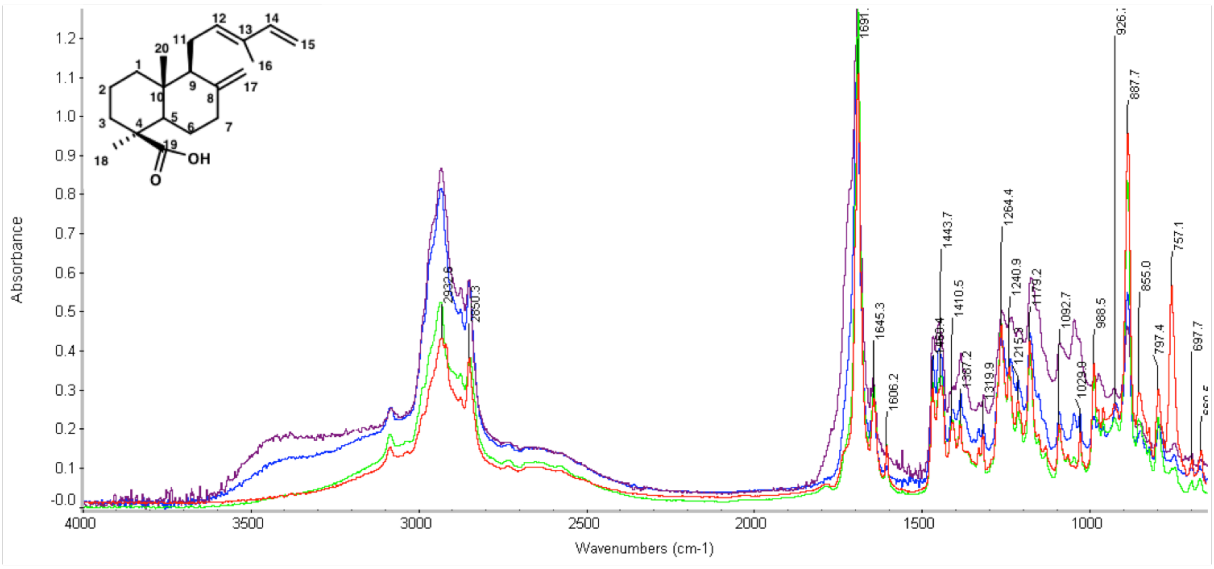

b)

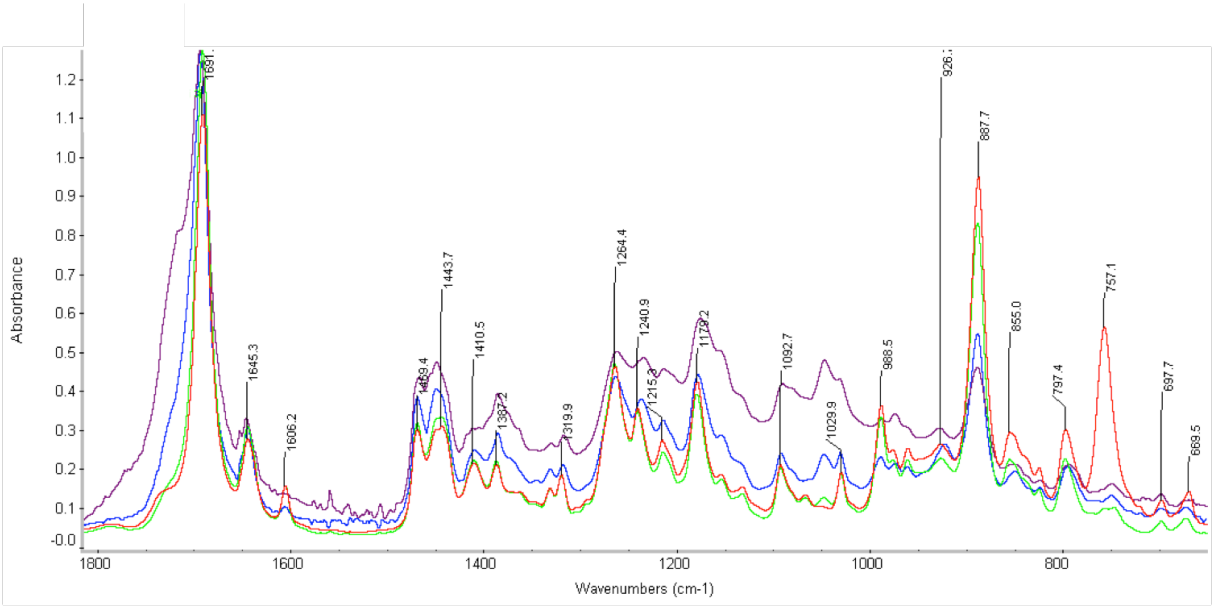

Figure 2. FTIR spectra of unaged (red), 24h (green), 72 (blue) and 168h (purple) aged under 365 nm UV communic acid: a) full spectrum; b) 1800 – 700 cm^{-1}.

In the FTIR spectra the *sandarac* resin shows higher concentrations of oxidized compounds, i.e. a more advanced degradation. The bands related to the hydroxyl and carbonyl groups, which are found in the oxidized compounds, increase in intensity. The bands associated with the hydroxyl groups appear at approx. 3400 cm^{-1} (O–H stretching) and approx. 1245 cm^{-1} (O–H deformation); those related to the carbonyl appear at approx. 1725 cm^{-1} (C = O stretching).

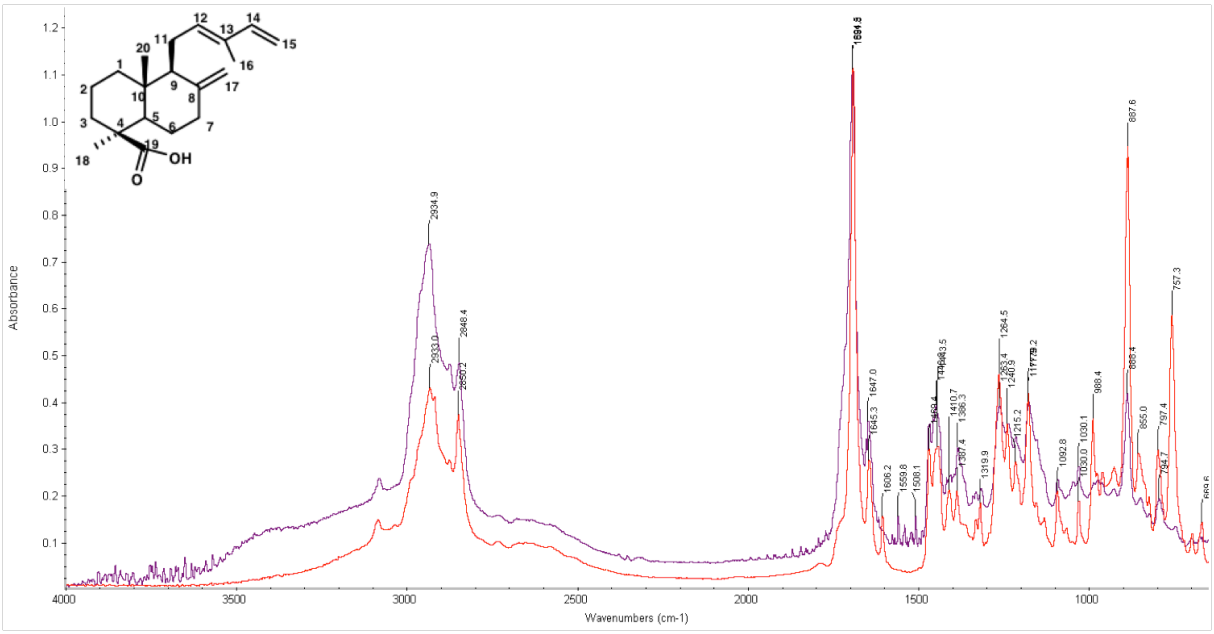

Figure 3. FTIR spectra of unaged (red) communic acid and the *sandarac* resin (*Kremer*) (purple).

Thus evolution of the IR spectra of the communic acid during ageing is subjected to the following eminent tendencies: (1) a strong increase of the OH stretchable band to ~ 3500 cm^{-1}; (2) a strong increase of the carbonyl band, just above 1700 cm^{-1}; The band also widens and moves slightly upward in energy with ageing; (3) a strong increase in intensity in the region near 1200 cm^{-1}, including the appearance of distinct bands at 1240 and 1034 cm^{-1}.

These trends support the model whereby photoageing leads to an increase in acid groups, peroxy acids and hydroperoxides [10, 11, 12]. The presence of COOH and COOOH groups corresponds perfectly to the growth, widening and shift of the carbonyl band.

4. D. II. ESI – Orbitrap analysis of the communic acid ageing

Further, unaged and aged samples of the communic acid were analyzed by ESI-Orbitrap mass spectrometry. This method is satisfactory suitable for direct analysis of simple compounds as well as complex mixtures such as *sandarac* resin, providing a good spectra of starting materials, as well as oxidation, polymerization and degradation products and yields intact molecular ions. It therefore provides a detailed and informative picture of the composition of fresh and aged diterpenoid or resin samples, although the reproducibility of spectra sometimes is a problem in general.

The ageing of diterpenoids results in a remarkable variety of products, indicating multiple points of radical attack and a gradual reaction of the initial products. H-Abstraction by attacking peroxylated radicals ($ROO\cdot + RH \rightarrow ROOH + R\cdot$) would preferentially produce the most stable radicals in tertiary, allylic or oxygenated positions, leading first to a relatively small number of abundant products [13]. With progressive oxidation, a diterpenoid will be oxidized in many different places because abstraction is not completely specific. A large number of oxygen atoms can thus be incorporated, and a wide variety of aging products is expected. Such a complex scheme has been found for UV aged communic acid measured by ESI-Orbitrap-MS. When the intensity of the initial communic acid signal decreases, groups of signals with mass increments of 16 or 14 Da are developed (Figure 4). Different numbers of O-atoms are incorporated, resulting in signals with a mass difference of 16 Da. The simultaneous loss of H (e.g., by allylic oxidation or oxidation of alcohols to acids) results in mass increases of 14 Da. Different combinations of 14 and 16 Da increments result in groups of signals becoming wider and less distinct with the mass increase.

Thus the differences between the ESI-Orbitrap spectra of non-aged and aged communic acid, the number and relative intensity of the signals with mass increments compatible with the proposed oxidation mechanisms and comparison with studies on the *sandarac* resin (see chapter 'Analyses of the high molecular mass part of the *sandarac* resin by MALDI-TOF and ESI-Orbitrap') have shown that ESI-Orbitrap-MS can be applied to the study of ageing processes of natural diterpenoids.

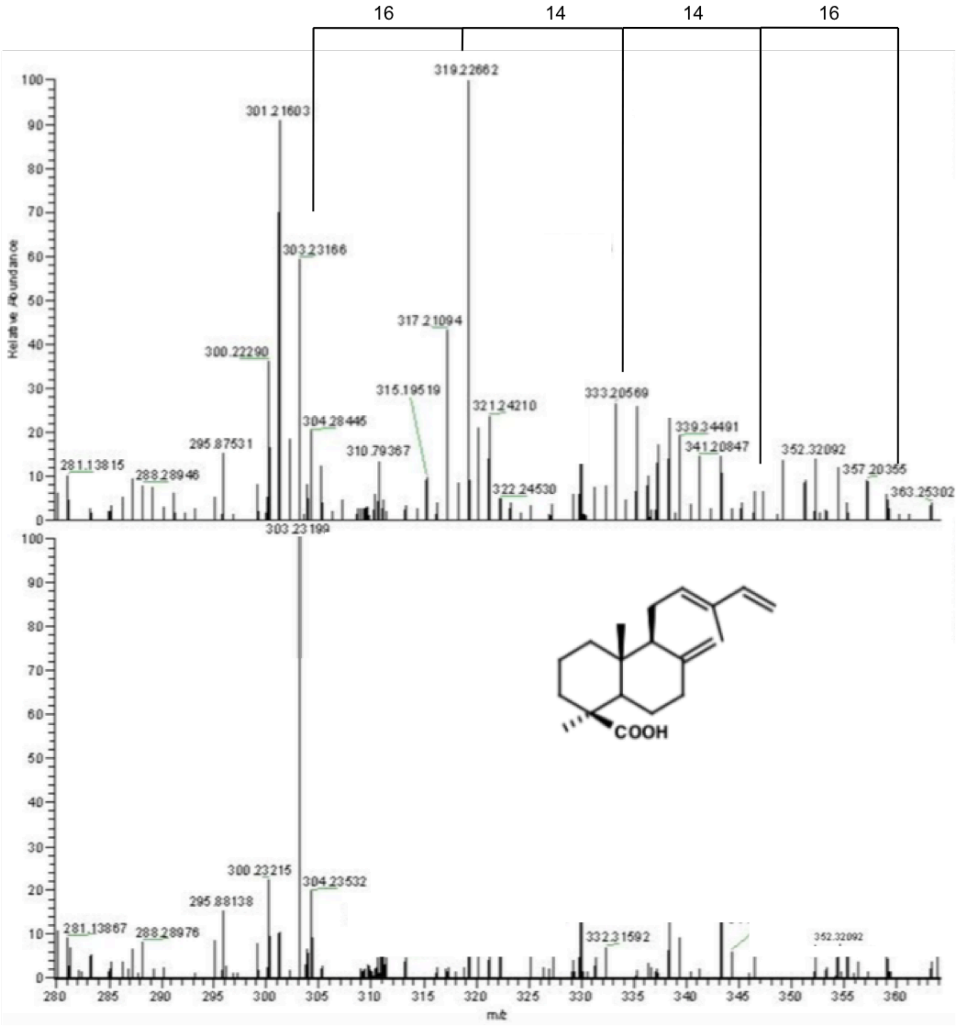

Figure 4. ESI – Orbitrap mass spectra of unaged (lower) and 24h aged under 365 nm UV (upper) communic acid. The $(M + H)^+$ signal is at m/z 303; a large amount of M + 16 appears at m/z 319. The typical oxidation pattern of a diterpenoid can be seen: groups of signals with mass increments of 14 and 16 Da, which indicate an incorporation of oxygen, a loss of hydrogen, and decomposition products due to cleavage reactions (m/z <300).

4. D. III. 1D Liquid – state NMR analysis of the communic acid ageing

In order to maintain a multi-analytical approach to the characterisation of ageing of the communic acid, a high-resolution 1D liquid-state NMR spectroscopy is used in an effort to highlight the effect of UV radiation on the diterpenoid of interest.

The liquid-state NMR spectroscopy was chosen as a technique of analysis of communic acid ageing instead of the solid-state NMR methods mainly due to the limited amounts of the communic acid at disposal, conditioned by very poor yields of the acid after its extraction from the cones. Within ageing communic acid showed a considerable decrease

in its solubility, primarily in the $CDCl_3$ used as a solvent in NMR analyses. The attempts to resolve the solubility problem with alternative solvents (Dimethyl sulfoxide-d6, Ethanol-d6) only aggravated the results. Thus, a poor solubility of the aged communic acid led to minimal results obtained with liquid-sate NMR.

The ^{13}C liquid-state NMR spectra of unaged and 168 hours aged under 365 nm UV communic acid are presented in the Figure 5. Prominent in the unaged sample are the acid peak at 184 ppm and the double-bonded carbons at 100-150 ppm. Below 60 ppm are the remaining aliphatic carbons. Notable in the aged spectrum is that ageing leads to appearance of the carbonyl peak. A low intensity ketone or aldehyde carbon (> δ 200) is detected in the aged sample at 214 ppm. So, ageing of this extent lead to production of carbonyls. Three new well-defined peaks appear in the region of unsaturated carbons at 127.2, 128.0 and 128.9 ppm, supporting the changes with carbon double bonds observed in FTIR analyses. Thus the C=C region is affected by ageing; there is even some loss of relative intensity, proving that the instauration is strongly enhanced by initial photolysis. The most readily apparent effect of ageing is intensity decrease of exomethylene functionality of ^{13}C resonances at 108 and 148 ppm. The aliphatic region becomes more congested and less resolved, indicating that polymerization and photolysis have occurred largely due to a radical attack on the hydrocarbon backbone followed by subsequent chain cleavage at the oxidized photoactive sites.

In a week-aged sample thirteen new peaks can be clearly distinguished in the aliphatic region between 0 and 50 ppm (Figure 5b) at δ 12.91, 14.25, 15.86, 15.95, 18.34, 19.82, 22.62, 23.05, 25.86, 31.92, 38.00, 44.32 and 58.53. Thus the number of signals in the up-field region has been doubled, indicating that new compounds are formed besides the peaks of the communic acid that remained without changes. Remarkably, the newly appearing peaks in the aged sample correspond to the traces of compound yet found in the spectrum of the pure communic acid. This means that the ageing of communic acid has started right after its isolation and was just accelerated by the light ageing conditions chosen.

The kinetic studies of the communic acid ageing show considerable changes in the ^{13}C spectra only after 168 hours of UV irradiation (Figure 6). Meanwhile the IR analyses have demonstrated significant changes in the spectrum within 24 hours of ageing. This can be explained by a low solubility of the ageing products and their low concentration on the early stages of ageing. Within a week of ageing the problem of the solubility is slightly resolved by the increase of the concentration of photoproducts in the aged sample.

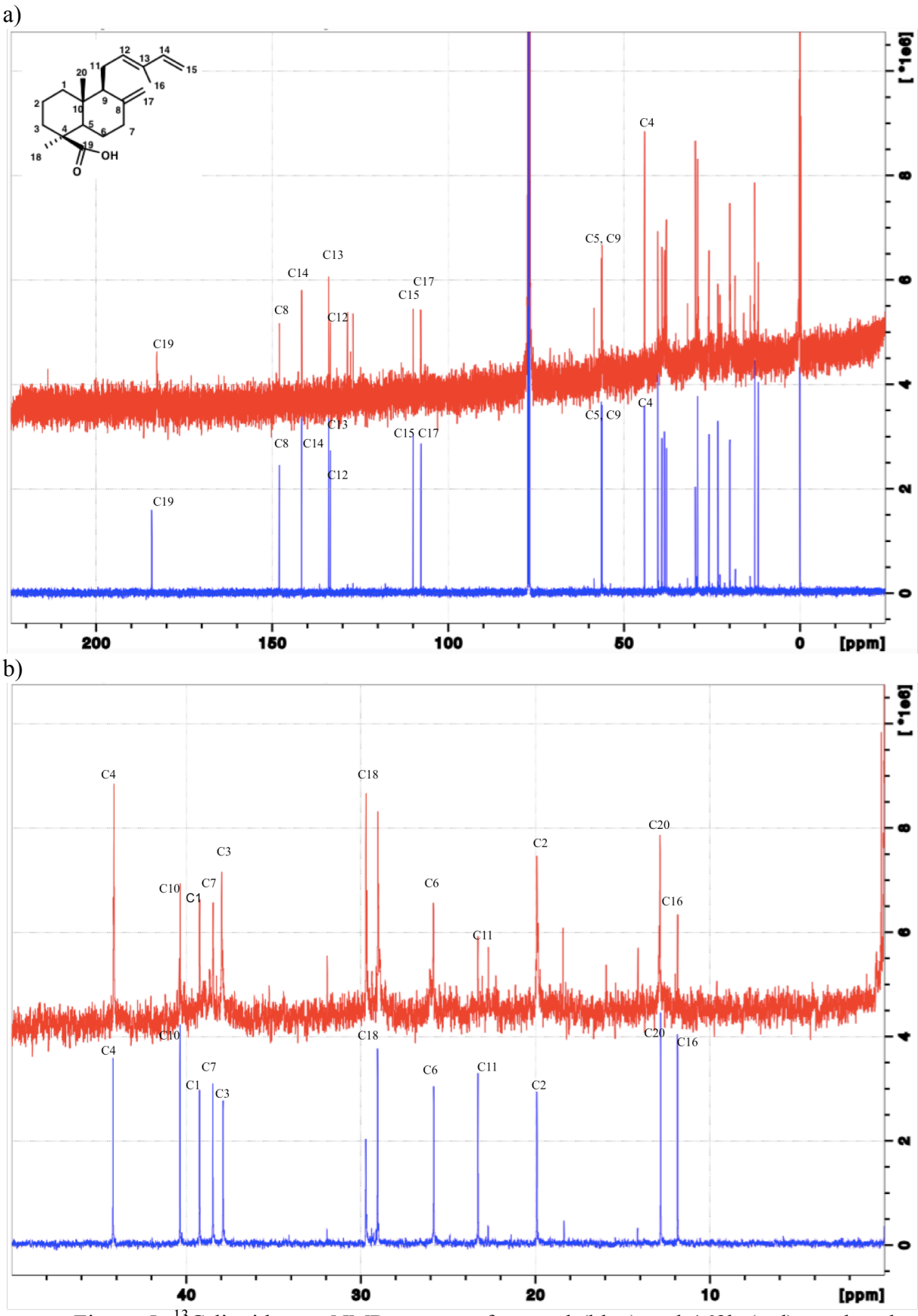

Figure 5. ^{13}C liquid-state NMR spectra of unaged (blue) and 168h (red) aged under 365 nm UV communic acid: a) full spectrum; b) 0 – 50 ppm.

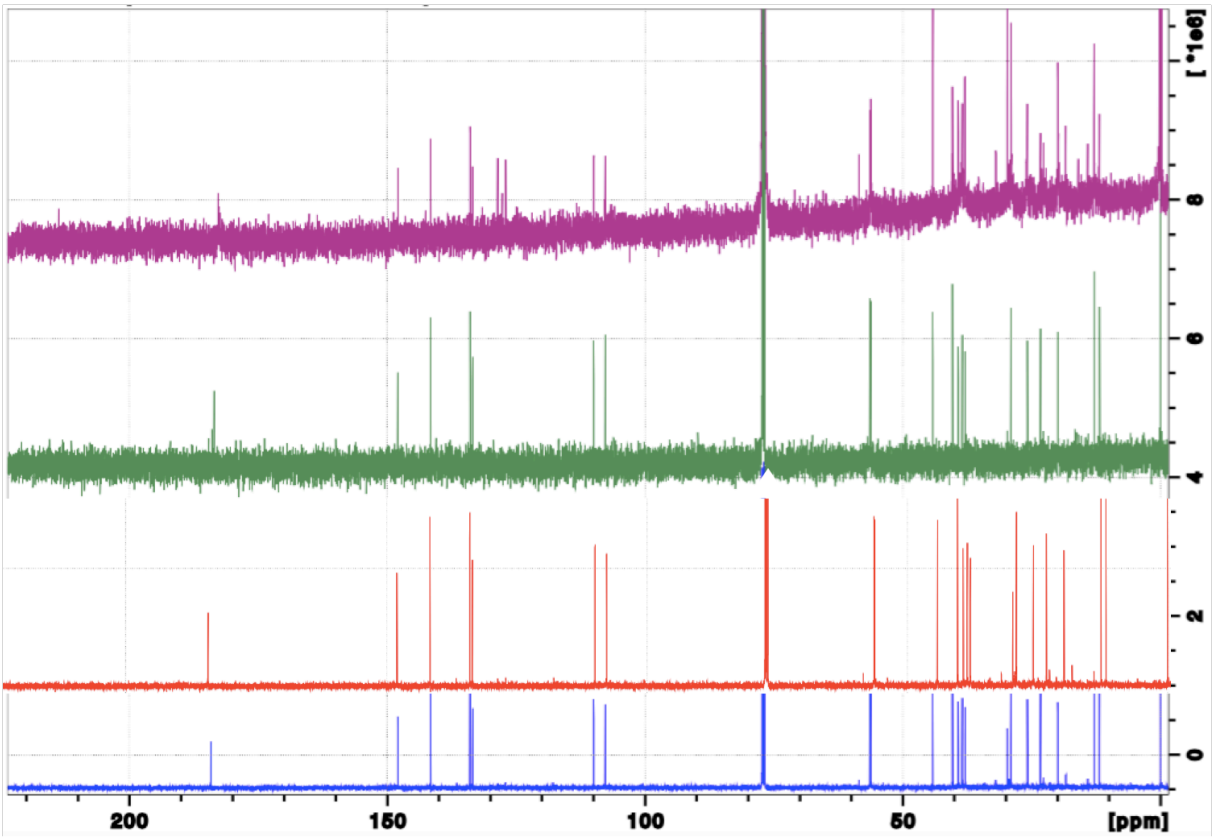

Figure 6. ^{13}C liquid-state NMR spectra of unaged (blue), 24h (red), 72 (green) and 168h (purple) aged under 365 nm UV communic acid.

The comparison of the ^{1}H NMR spectrum of the communic acid with the *sandarac* resin (*Kremer*) via weekly aged diterpenoid, clearly shows that the communic acid is the starting material of the resin (Figure 7).

The saturated region of the aged communic acid ^{1}H spectrum (Figure 7, red) provides an immediate distinction from the unaged sample since it is no more dominated by a single peak at δ 1.2, accompanied by other singlets of lower intensity at δ 1.34 and 1.38. The electron-withdrawing region is nearly empty as in the starting material, while the alkenic region becomes more pronounced, containing broad multiplet at δ 5.4 and chain of multiplets at δ 5.6 – 5.9.

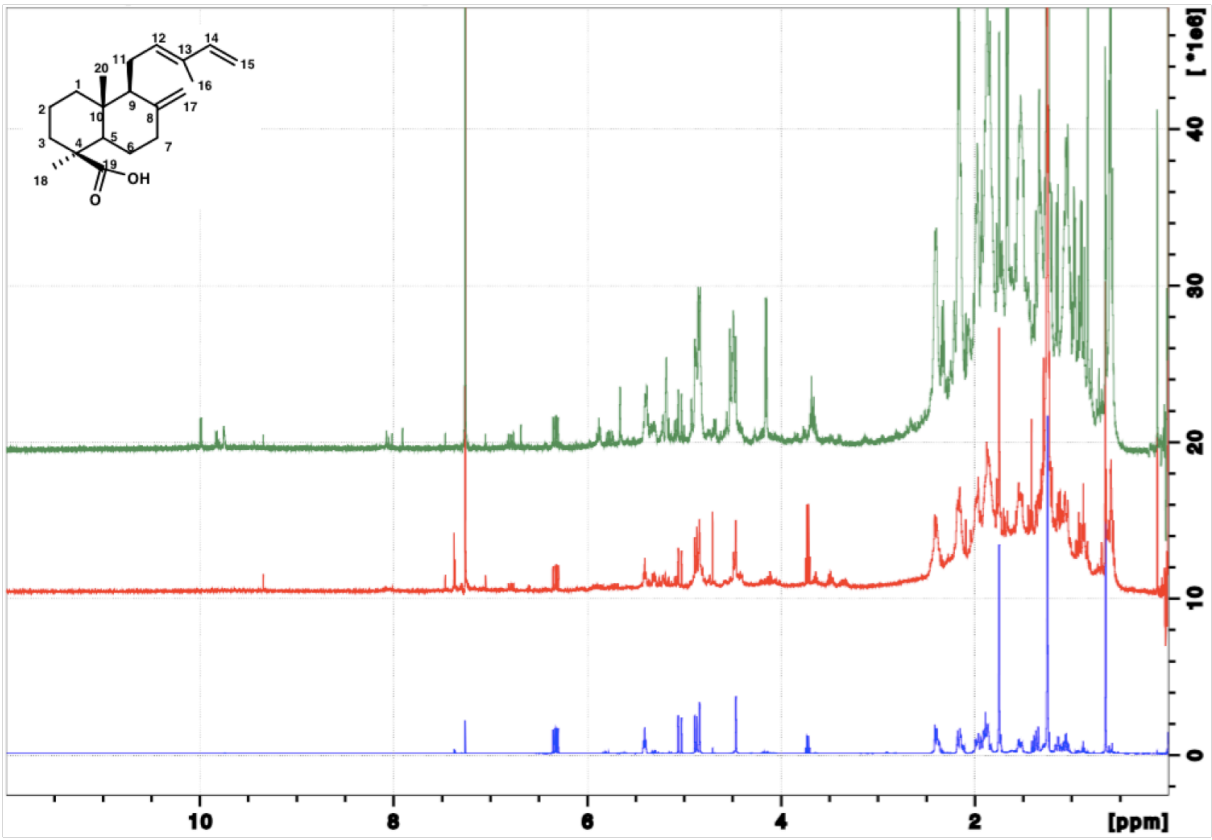

Figure 7. ^{1}H liquid-state NMR spectra of unaged (blue), 168h (red) aged under 365 nm UV communic acid and the *sandarac* resin (*Kremer*) (green).

The unsaturated region is the most important for distinguishing diterpenoid resins and provides specific information on the predominant diterpenoids skeleton involved. The most characteristic peak of the communic acid at 6.34 ppm corresponding to H14 is easily found in the aged acid and the *sandarac* resin, indicating that the diterpenoid responsible for the polymerisation remains partially as a free compound. Signals at 4.48 ppm and 4.85 ppm that has been assigned to exocyclic methylene group at C8=C17, together with peaks at 4.89 ppm, 5.06 ppm and 5.42 ppm are related to C14=C15 terminal double bond and H12 triplet, can be found in the spectra of aged commuinc acid and of the *sandarac* resin as well.

The hallmark of the *sandarac* spectrum is three dominate sets of peaks in the saturated region (δ 0.0–2.0), at δ 0.6–1.0, 1.2 and 1.5–1.8 (Figure 7, green). The second grouping is the most intense. The first and third sets are wide multiplets, and the second is a narrow multiplet. There are trailing peaks from δ 1.8 to 2.5. The *sandarac* resin spectrum contains small resonances in the aromatic region (δ 6.5–8.5), at δ 7.0 and 7.4. Another outstanding characteristic of the spectrum is a pair of relatively strong peaks at δ 3.6 and 4.1,

accompanied by smaller peaks at d 3.4 and 4.2. All these patterns are starting to be revealed in the intermediate spectrum of 7 days aged communic acid.

Thus, the choice of the communic acid as a reference compound to follow the early stages of the *sandarac* resin polymerization was justified by the results obtained. Artificial ageing of the communic acid with UV light resulted in strong oxidation of initial compounds. The general pattern of oxidation is marked by different numbers of oxygen atoms incorporated while hydrogen is eliminated. This results in a large number of compounds with mass increments of 14 or 16 Da.

5. Study of the *sandarac* resin

5. A. Analyses of the lower molecular mass part of the sandarac resin by GC-MS

At first, this part of the research aims at analysing by gas chromatography – mass spectrometry (GC-MS) the molecular composition of the *sandarac* resin and to give new insights on the markers that can be used for its identification. Secondly, we will evaluate the quantity of the sample being analysed by GC-MS. The quantitative analysis of *sandarac* resin is realized by means of an internal standard. And, finally, the different sandaracs will be compared in order to conclude how strongly differs the chemical content of the commercial resin from one supplier to another. As mentioned previously in the bibliographic research on the *sandarac* composition a contradiction among the presented information on this topic was noticed.

The *sandarac* resin sold today by artist's suppliers is an aged resin, hard, highly oxidized and polymerized and then not suitable for being used as a source for oil varnishes. Although the scientific literature concerning the *sandarac*, as an art material is limited, it is known that *sandarac* consists of a polymer fraction and of lower molecular weights compounds, the most characteristic being diterpenoid acids of labdanic structure [14]. Such acids with labdane skeletons with its system of conjugated double bonds demonstrate a strong tendency to the polymerization when executed from trees and readily reticulate as soon as they come into contact with light and air. The exudates of the resin, after having been exposed to the outer atmosphere form a solid protective layer covering the exposed plant tissues [15]. Initial polymerisation probably occurs with a radical mechanism starting from conjugated double bonds of labdatriene molecules such as communic acid (Figure 1).

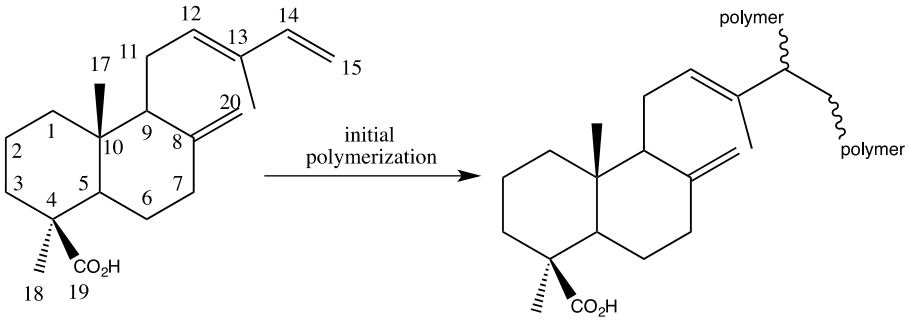

Figure 1. Polymerisation of communic acid.

Moreover, a misconception exists regarding the origin of the *sandarac* resin. The resin that is commercially available today on the market and called *sandarac* is the resin that was

extracted from cypresses that are planted in the region of North Africa and belong to the family Cupresaceae. Therefore, in this study when using word *sandarac* we will be referring to the natural resin obtained from plant belonging to the family of Cupresaceae (Tetraclinis Articulata) commercially available but without information on how long the resin was stocked after its actual extraction from a tree.

5. A. I. Qualitative analysis of the sandarac resin

Several GC-MS as well as Pyrolisys – GC-MS studies have been previously made in order to define molecular composition of *sandarac* resin and presented in the literature. Scalarone's team applying both techniques accomplished the most complete research on this topic: GC-MS for low molecular weight compounds analyses and Py-GC-MS to characterize the composition of polymerized part of the resin [16]. According to them, free diterpenoids identified by GC-MS are sandaracopimaric acid, agathic acid and its monomethyl ester, agathalic acid and acetoxy agatholic acid. *Cis*-and *trans*-communic acids have been detected in traces. Further, to determine the nature of the high molecular weight fraction, the pyrolysis was required. The THM-GCMS (Thermally assisted hydrolisys and methylation, coupled with gas chromatography – mass spectrometry) approach was used to identify the cross-linked part. This technique results in a large number of substances that are originated from the pyrolysis process, which is considered to be its main disadvantage. Fragmentation, isomerisation, recombination and other secondary pyrolysis reactions produced a large number of peaks. J.Romero-Noguera et al. have also analysed commercial resin *sandarac* applying GC-MS analysis and have identified that the composition of sandarac resin is presented by following diterpenoids: manool, sandaracopimaric acid, isopimaric acid and OH-sandaracopimaric acid [14]. As it can be concluded the results found by two research groups significantly differ, although they were both aimed to analyse the same type of natural resin.

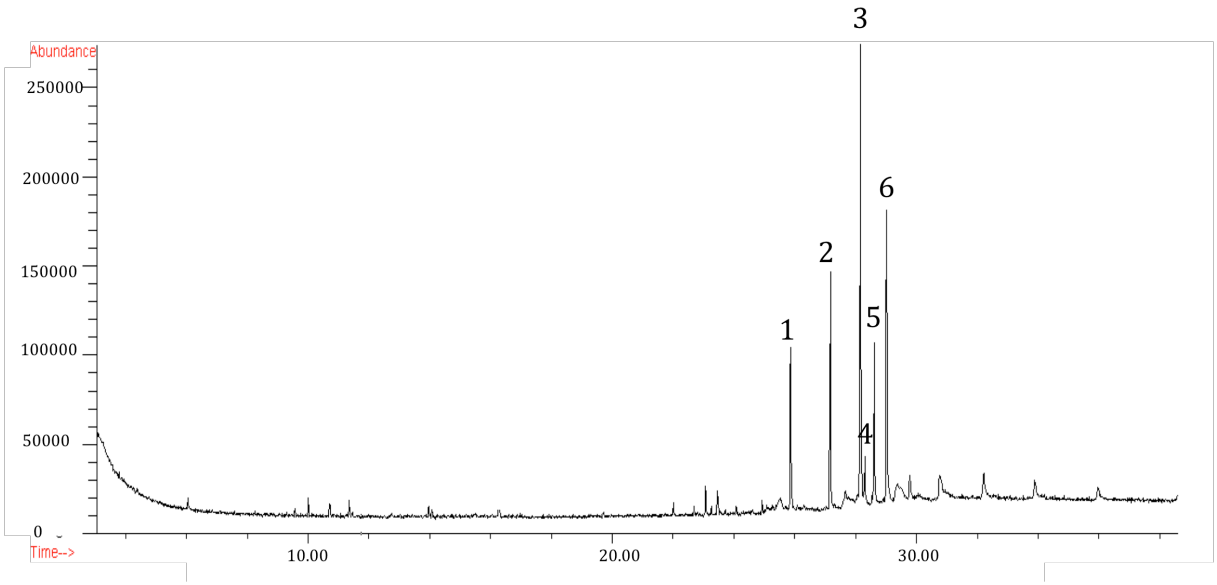

Figure 2. Total ion chromatogram of the *sandarac* resin after derivatization with BSTFA /TMCS (*Kremer*).

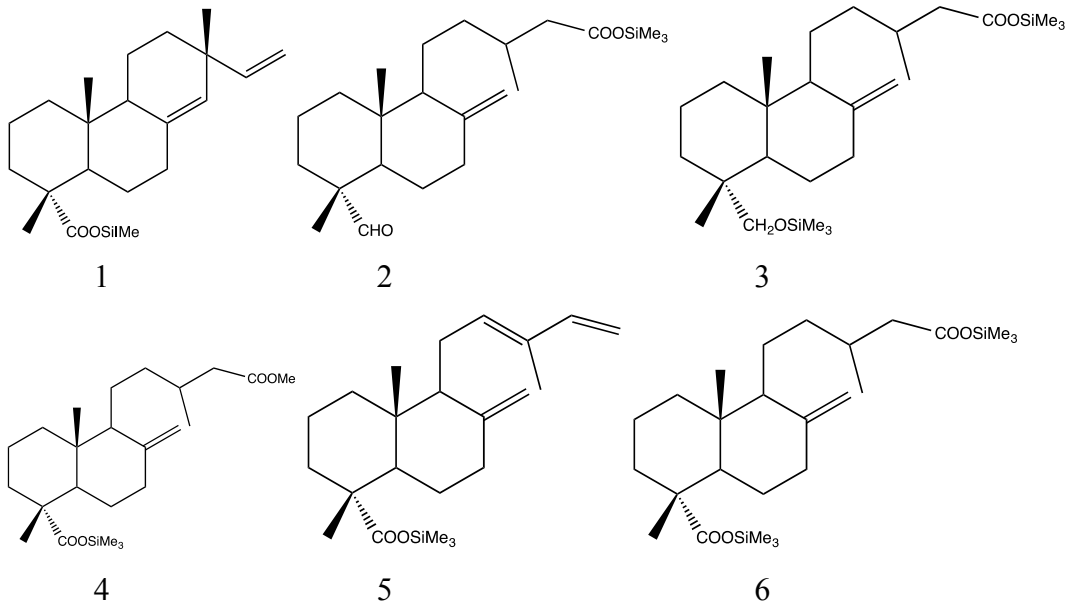

Figure 3. Structures of diterpenoids identified in the sandarac resin by GC-MS.

Here we will first discuss the qualitative analysis of sandarac resin sold by 6 companies by GC-MS. GC-MS is an established technique for the analysis of complex mixtures, holding a prime position in analytical chemistry because of its combination of sensitivity, wide range of applicability and versatility [17, 18].

In this study diterpenoid acids of sandarac were identified by GC-MS, after trimethylsilylation with BSTFA/TMCS. The free diterpenoids identified in the 6 samples by

GC-MS (Figure 2) and listed in Table 1 are sandaracopimaric acid (1), dihydroagathalic acid (2), dihydroagatholic acid (3), methyl pinifolic acid (4), communic acid (5) and dihydroagathic acid (6). Interpreting their mass spectra has identified most of the labdanoids present in sandarac [16, 19, 20, 21].

The molecules that have a molecular weight of 374 g/mol show similar fragmentation patterns dominated by fragments m/z 241 and 257. In the case of trimethylsilylation, the loss of carboxyl groups (-HCOOTMS (118 Da), which generally start with a hydrogen positioned in beta or gamma position (possibility of double bond formation) and of hydroxyl groups (-OTMS (90 Da)) are observed.

Table 1. Diterpenoids identified in the *sandarac* resin by GC-MS and their characteristic fragments.

No.	Name of compound	t_R	$M^{+\cdot}$	$[M-CH_3]^+$	$[M-COOSi(CH_3)_3]^+$	$[M-HCOOSi(CH_3)_3-CH_3]^+$
1	Sandaracopimaric acid, TMS ester	25.864	374	359	257	241
2	Dihydroagathalic acid, TMS ester	27.173	392	377	275	259
3	Dihydroagatholic acid, TMS ester	28.163	466	451	349	333
4	Methyl pinifolic acid, TMS ester	28.303	422	407	305	289
5	Communic acid, TMS ester	28.621	374	359	257	241
6	Dihydroagathic acid, TMS ester	29.027	480	465	363	347
7	Isopimaric acid, TMS ester	26.409	374	359	257	241

Thus, the fragmentation of pimaranes undergoes two main stages as illustrated in the Figure 5, using sandaracopimaric acid as an example. The loss of –COOTMS functionality and demethylation of trimethylsilyl group lead to the fragment of m/z 241.

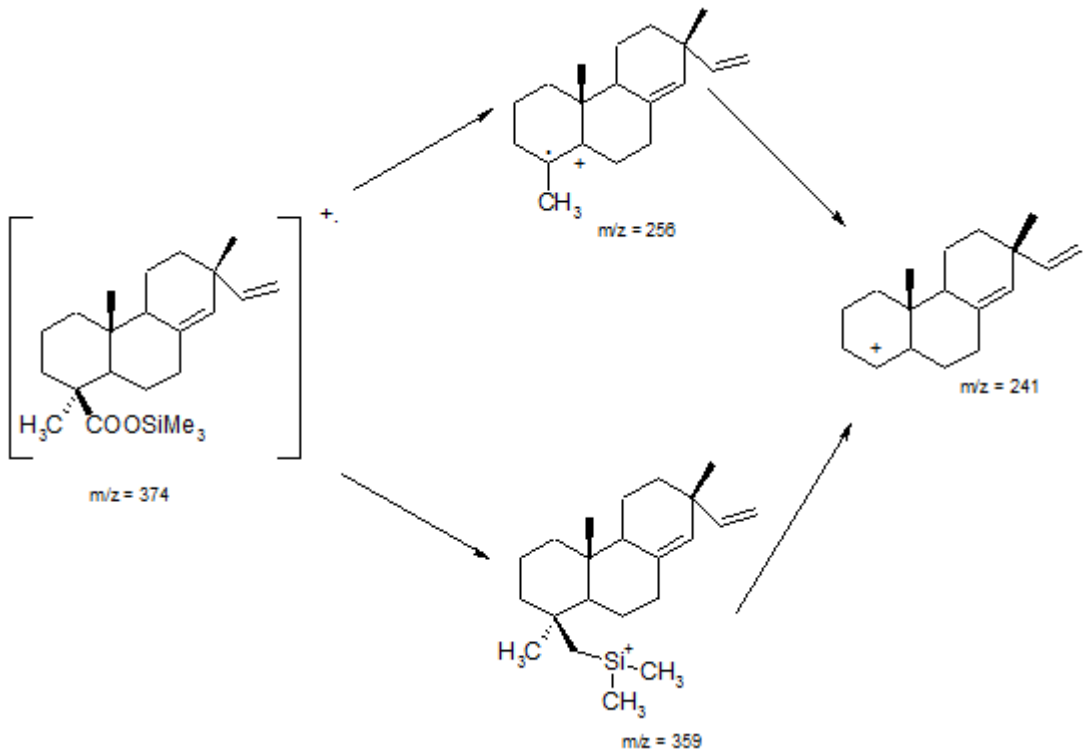

Figure 5. The fragmentation of sandaracopimaric acid.

Characteristic peaks in the EI-mass spectra result from the molecular ions, from cleavage of the functional groups and from the loss of the side chain. For the sandaracopimaric acid, TMS ester characteristic peaks are the molecular ion at m/z 374 and the fragment ions at m/z 359, obtained by loss of a methyl group $[M-15]^+$, at m/z 257 by loss of the trimethylsilyl ester $[M-117]^+$ and loss of formic acid trimethylsilyl ester and a methyl group $[M-133]^+$ (Figure 6).

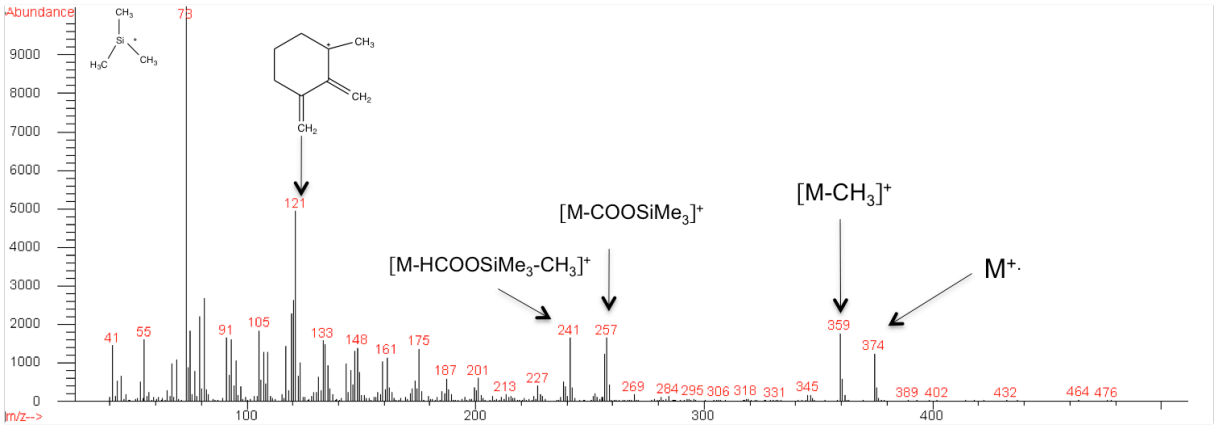

Figure 6. 70 eV EI-mass spectra of sandaracopimaric acid, TMS ester.

The rest of the compounds identified in the *sandarac* resin are labdanes. All the diterpenoids of labdane type that were found show a typical bicyclical structure with one or two functional groups situated in the ring A (R_2) or in the side chain (R_1) (Figure 7).

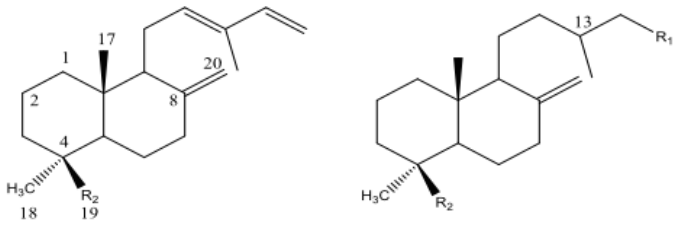

Figure 7. Bicyclical structures of diterpenoids of labdane type.

The major ion fragment at m/z 121 is found in all mass spectra and is characteristic for all diterpenoids found in the resin. The possible mechanism of the ion formation involves an intermediate fragment found at m/z 238 and is proposed in the Figure 8.

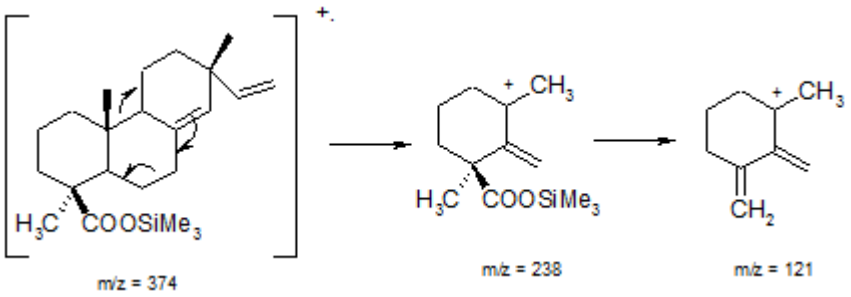

Figure 8. Possible mechanism of the m/z 121 ion formation.

A characteristic pick for communic acid, TMS ester is m/z 175. According to the fragmentation pattern on the Figure 9, it results by the loss of formic acid trimethylsilyl ester $[M-118]^+$, followed by the cleavage of a side-chain.

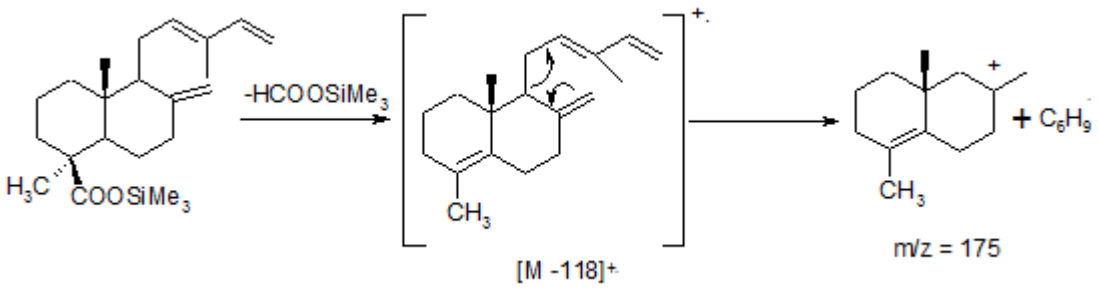

Figure 9. Structure and formation of m/z 175 ionic fragment of communic acid.

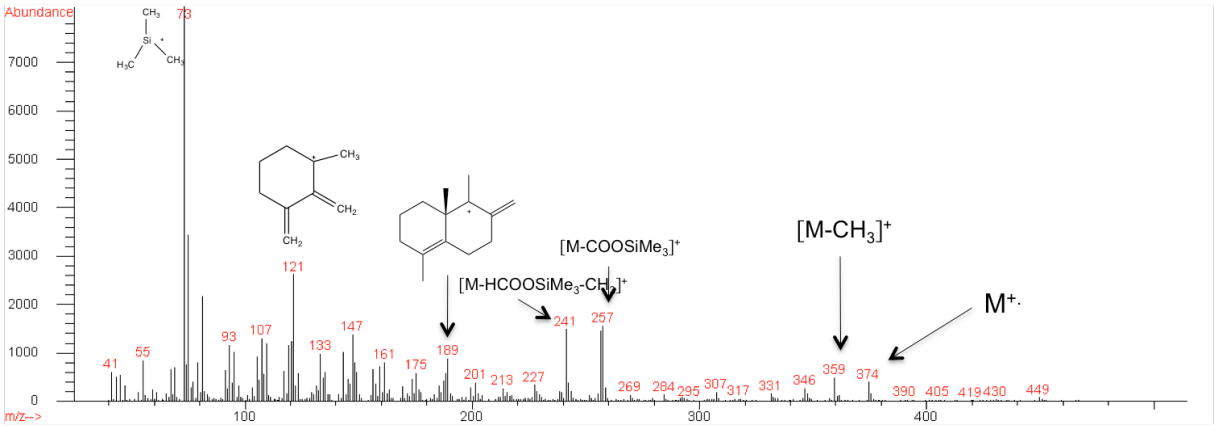

Figure 10. 70 eV EI-mass spectra of communic acid, TMS ester.

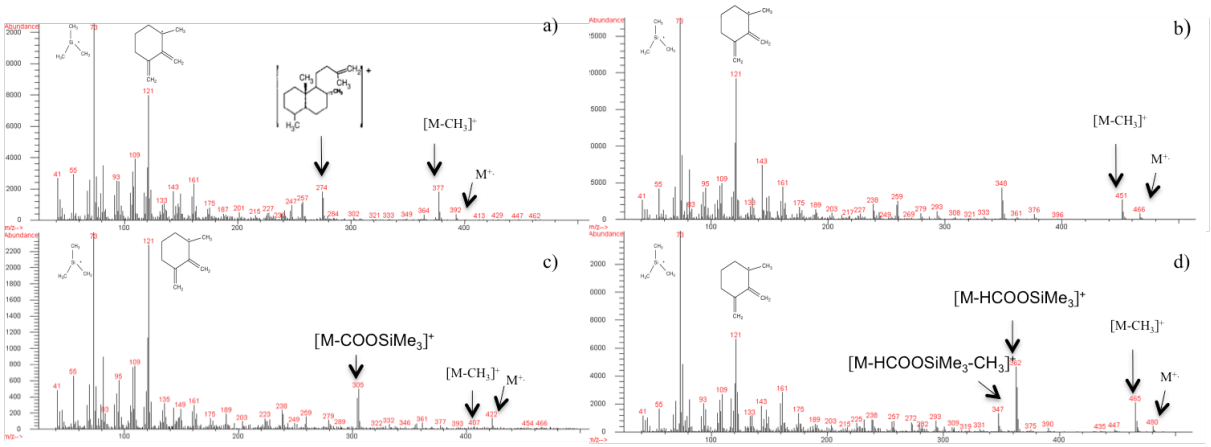

Figure 11. 70 eV mass spectra of diterpenoid TMS-esters of the sandarac resin (Kremer): a) Dihydroagathalic acid, TMS ester ; b) Dihydroagatholic acid, TMS ester ; c) Methyl pinifolic acid, TMS ester ; d) Dihydroagathic acid, TMS ester.

The mass spectrum of the communic acid is presented in the Figure 10 and the mass spectrometric behaviour of the rest indentified compounds is shown in the Figure 11.

5. A. II. Quantitative analysis of the sandarac resin

Although the *sandarac* resin is still being widely used as a source for varnishes, no quantitative analysis was realized. With the study presented hereby the quantitative assessment of the diterpenoid part has been made for the fist time by the method of internal standard method that is widely used as an efficient quantitative approach in analytical chemistry [22]. An internal standard is a chemical substance that is added in a known amount to the sample in order to calculate the relative quantity of the compounds present in the

sample and that is very similar, but not identical to the chemical species of interest in the samples.

The isopimaric acid was used as an internal standard due to its chemical similarity of the diterpenoids identified in the resin and to its commercial availability. Table 2 lists the diterpenoids identified in the *sandarac* resin from different suppliers by GC-MS and their relative quantity.

Although relative amount of each particular diterpenoid varies in a wide range depending on the supplier, it comes evident from the table that almost all sandaracs except that from La Marchande de Couleurs consist of the same diterpenoids. The sandarac purchased from La Marchande de Couleurs stands out exceptionally in comparison with other suppliers. Dihydroagathic and dihydroagatholic acids are not identified in their sandarac at all. Methyl pinifolic and dihydroagathic acids in its turn are found only in traces. On the other hand, the sandarac from La Marchande de Couleurs has the highest concentration of communic acid. Indeed, in all other five sandaracs the percentage of communic acid doesn't exceed 4%. Meanwhile, this value in case of La Marchande de Couleurs is almost twice bigger. For the other resins the qualitative composition is the same: all six diterpenoids are found in the rest five samples.

Table 2. The quantitative assessment (in %) of each identified diterpenoid by GC-MS.
*Not Detected

No.	Name of the compound	% of the compound in the sample of resin (2.5 mg)					
		Kremer	Okhra	Color Rare	La Marchande de Couleurs	L'Atelier Montessori	Hevea
1	Sandaracopimaric acid, TMS ester	1.4	2.8	7.6	3.2	7.9	6.5
2	Dihydroagathalic acid, TMS ester	3.1	3.4	2.1	n.d.*	5.6	3.6
3	Dihydroagatholic acid, TMS ester	6.7	7.8	4.6	n.d*	6.2	3.1
4	Methyl pinifolic acid, TMS ester	7.8	6.2	4.7	0.4	1.1	2.8
5	Communic acid, TMS ester	3.7	3.4	1.8	6.9	2.0	0.1
6	Dihydroagathic acid, TMS ester	7.1	8.3	0.8	0.3	3.7	5.0
	Total percentage	29.8	31.9	21.6	10.8	26.5	21.1

It is remarkable that *sandarac* resins delivered by Kremer and Okhra have very close quantitative composition. They are both characterized by weak concentration of

sandaracopimaric and communic acid, and at the same time by relatively high percentage of agathic acid's derivatives. The overall percentage of diterpenoids present in the resins from these two suppliers reaches 30%, which is the highest concentration of the diterpenoid acids among the other resins. The total amount of pimaranes and labdanes in the case of Color Rare, L'Atelier Montessori and Hevea ranges in the average of 20 – 25%. And eventually, La Marchande de Couleurs stands here alone as well, showing the presence of only 10% of diterpenoids.

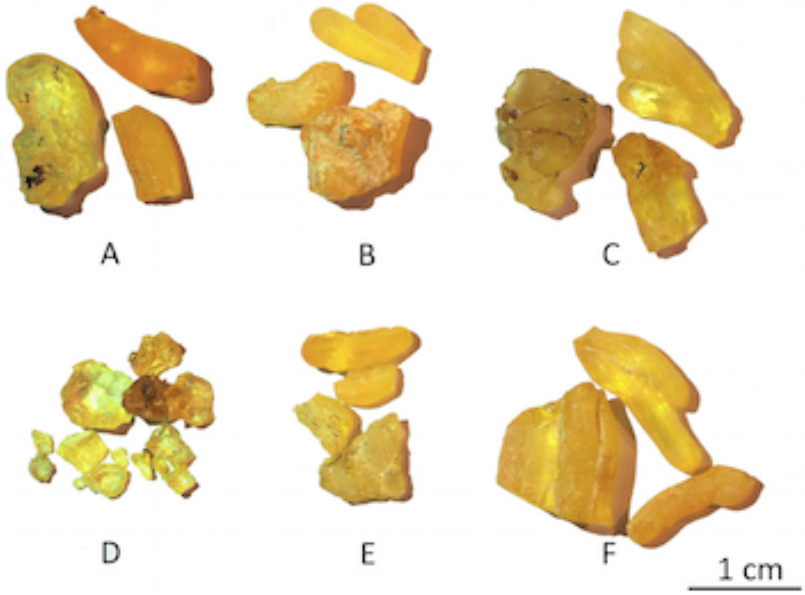

Figure 12. Lumps of the resins from six different suppliers (Kremer (A), Okhra (B), Color Rare (C), La Marchande de Couleurs (D), L'Atelier Montessori (E), Hevea (F)).

The Figure 12 presents the lumps of the resins from six different suppliers to show how the resin solidifies when exposed to the air and comes to commerce in the form of small solid chips, translucent, and having a delicate yellow tinge. The lumps of resin from five suppliers, having similar chemical composition, are visually close as well, while the resin from La Marchande de Couleurs, standing out with its particular composition, shows different shade and shape properties.

Previous research on the chemical composition of the *sandarac* resin, as outlined earlier in the introduction, showed different results presenting diterpenoids that were not identified here. The only compound that was found in common was sandaracopimaric acid. Compounds such as manool, isopimaric acid or OH-sandaracopimaric acid were not found in the six samples analysed here, whereas they have been found by name [14]. The reason for

such radical difference in results might be hidden in different methods of resin's derivation. Indeed, GC-MS analysis on the *sandarac* resin was accomplished after methylation of samples with trimethylammonium hydroxide that produced diterpenoid's methyl esters. In the current study the trimethylsilylation was chosen as the method of *sandarac* derivation. Anyway, it remains an open question if two different ways of the resin derivation could lead to such a great difference in results for the same type of resin.

Following the hypothesis widely supported in the literature that the communic acid is the first diterpenoid to be responsible for the polymerisation of the *sandarac* resin the *sandarac* from La Marchande de Couleurs is the freshest resin among the others. That means that the *sandarac* from this supplier still contains communic acid in an excessive quantity relatively to other analysed resins. Therefore, the *sandarac* resin purchased from Hevea might be the oldest one having the lowest percentage of communic acid that had probably completely polymerised.

Lacking the information on the actual origin of the resin purchased, on the method and conditions of its treatment it is difficult to judge if the difference in chemical composition of the *sandarac* (mainly quantitative) is due to the difference of trees' species and if an important factor can be the time during which the resin was stored. Actually, even the fact that the resin is originated from the same tree species is not yet the guarantee of the identical chemical composition of its resin.

The results presented in the Table 2 demonstrate that the total amount of the diterpenoids that we can analyse by this method is between 10 and 30 %, depending on the sample. The rest of the sample is probably a polymerized fraction of the resin, proving once again the fact that the sandarac is a highly reticulated resin.

Conclusion

The chemical composition of *sandarac* resin was investigated qualitatively and quantitatively by gas chromatography-mass spectrometry (GC-MS). Six compounds with labdane and pimarane skeletons were identified in the resin. The obtained mass spectra were interpreted and the mass spectrometric behaviour of these diterpenoids under EI conditions was described. Quantitative analysis by the method of internal standard revealed that identified diterpenoids represent only 10 - 30% of the analyzed sample.

The *sandarac* resin from different suppliers was analyzed (from Kremer, Okhra, Color Rare, La Marchande de Couleurs, L'Atelier Montessori, Hevea). The analysis of different

lumps of resins showed that the chemical composition differs from one lump to another, varying mainly in the relative distributions of the components.

Sandaracopimaric and communic acids are present in all resins. The rest of the diterpenoids are found in the different *sandarac* analysed with various proportions. Dihydroagathic acid was not identified in the *sandarac* from La Marchande de Couleurs, but communic acid is present in a larger quantity compared to other resins. The *sandarac* from L'Atelier Montessori demonstrated only traces of methyl pinifolic and dihydroagathic acids. We show here a wide range of composition for resins from different suppliers, which can explain the difference existing in the literature concerning sandarac. The contradiction that appeared in the two previous studies [14, 16] can be explained by this variability. Another explanation would rely on the potential influence of the resin derivation method. In order to deeper the existing knowledge, it would also be interesting to investigate the true impact of the derivation methods.

Systematic analyses on the natural products that are sold to artists on the market can provide them with a better insight on the materials they are using. Of course, the composition of natural products on the molecular level may differ notably depending on many factors such as geographic, climatic, etc; differences that would impact drastically the artist's work. That is why artists prefer to stay with one particular art supplier.

5. B. Analyses of the sandarac resin after thermal treatment by GC-MS

For the time being no research has been done on the investigation in the way the *sandarac* resin modifies with thermal treatment. In this part of the study, the *sandarac* resin was aged by heating for a long duration (1 month) and then analyzed by gas chromatography - mass spectrometry (GC-MS).

According to one of the recipes of varnish preparation described in the bibliography, heating of the system (resin + oil) is frequently inevitably due to the low solubility of the resins in oils [23, 24, 25]. During the preparation of a varnish based on the *sandarac* resin, particularly with the use of linseed oil, a preliminary heating of the resin and then the subsequent heating of the mixture as a whole, after addition of the oil, is necessary. Thus, analyses of the aged *sandarac* by means of thermal treatment would give an insight of how the molecular composition of the resin changes already on the stage of varnish preparation.

As indicated previously (in the bibliographic part), there is an assumption that prior heating is required in order to break the *sandarac* reticulated fraction. Therefore, analyses of the ion chromatogram and the mass spectra of the heated *sandarac* and the comparison of

results with the fresh resin could give an image of the evolution of the chemical composition of the *sandarac* as a result of thermal treatment. Moreover, the study of the chemical modification of the *sandarac* during heat treatment would help to better understand and propose the possible mechanisms that take place.

5. B. I. Identification of the compounds resulted from the thermal treatment of the *sandarac* resin

Compounds of thermally aged *sandarac* were identified by GC-MS, after trimethylsilylation with BSTFA/TMCS. Interpreting their mass spectra has identified most of the labdanoids present in heated resin [16, 19, 20, 21, 26].

The free diterpenoids and their degradation products identified by GC-MS (Figure 1) and listed in Table 1 are as follows: sandaracopimaric acid (1), dihydroagathalic acid (2), dihydroagatholic acid (3), methyl pinifolic acid (4), communic acid (5), dihydroagathic acid (6), agathic acid (7), 19-norlabda-8(17),13-dien-15 - oic acid (8), agathalic acid (10), 1,4a,5,6-tetramethyl-1,2,3,4,4a,7,8,8a-octahydro-naphthalencarboxylic acid (12), 1,4a,6-trimethyl-5-methylene-1,2,3,4,4a,5,8,8a-octahydro-naphthalencarboxylic acid (13), 1,3-dimethyl-cyclohexa-2-en-carboxylic acid (14). A considerable number of isomers are included, but since the mass spectra of the diterpene acids correspond perfectly to those of the corresponding isomers, they cannot be distinguished under the applied analytical conditions.

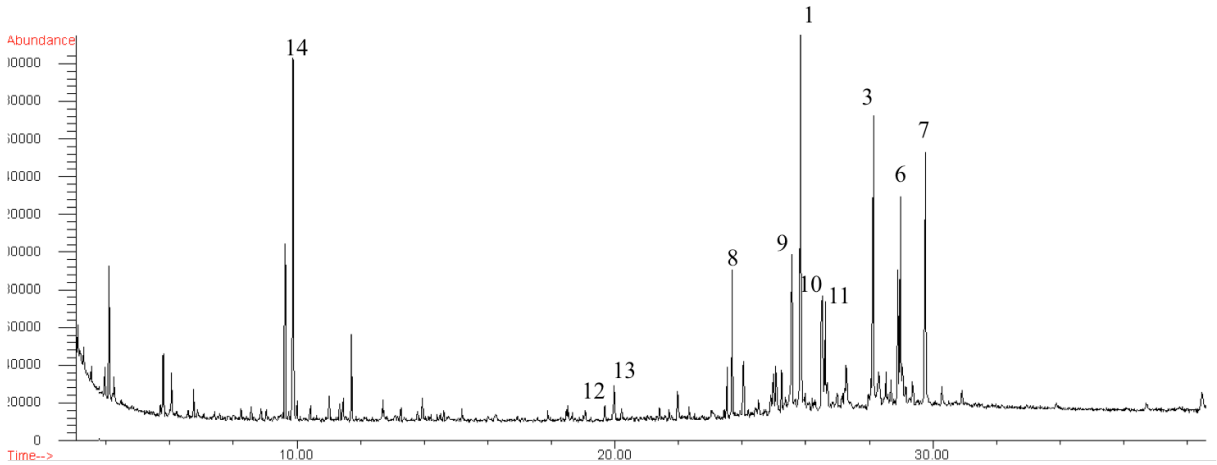

Figure 1. Total ion chromatogram of the *sandarac* resin (*Kremer*) aged at 60 °C for 1 month after derivatization with BSTFA/TMCS.

The total ion chromatogram of the heated *sandarac* is characterized by two groups of peaks. The first, with a retention time between 9 and 26 min, contains the fragments of the

thermal degradation of the cross-linked fraction. The second group, between 26 and 30 min, consists of free diterpenoids, three of which were found in the unaged *sandarac*. Thus, sandaracopimaric (1), dihydroagatholic (3) and dihydroagathic (6) acids remained in the resin aged by heating.

The most important products of the *sandarac* thermal degradation include both free diterpenoids and degradation fragments of the polycommunic acid fraction. Among free diterpenoids the most abundant ones are sandaracopimaric acid, agathic acid, agathalic acid and its isomer. Free communic acid is present only in traces, as demonstrated by comparison with GC/MS data of unaged *sandarac* (Figure 2a,b). The main degradation products of polycommunic acid include the monomer, communic acid, and bicyclic acids, such as 1,4a,6-trimethyl-5-methylene-1,2,3,4,4a,5,8,8a-octahydro-naphthalencarboxylic acid and 1,4a,5,6-tetramethyl-1,2,3,4,4a,7,8,8a-octahydro-naphthalen-carboxylic acid, generated by breakage and loss of the unsaturated side chain of the communic acid.

Table1. Compounds identified in the thermally aged *sandarac* resin (*Kremer*) by GC-MS and their characteristic fragments.

No.	Name of compound	t_R	$M^{+\cdot}$	$[M-CH_3]^+$	$[M-COOSi(CH_3)_3]^+$	$[M-HCOOSi(CH_3)_3-CH_3]^+$
1	Sandaracopimaric acid, TMS ester	25.864	374	359	257	241
2	Dihydroagathalic acid, TMS ester	27.173	392	377	275	259
3	Dihydroagatholic acid, TMS ester	28.163	466	451	349	333
4	Methyl pinifolic acid, TMS ester	28.303	422	407	305	289
5	Communic acid, TMS ester	28.621	374	359	257	241
6	Dihydroagathic acid, TMS ester	29.027	480	465	363	347
7	Agathic acid, di-TMS ester	29.758	478	463	361	345
8	19-norlabda-8(20),13-dien-15-oic acid, TMS ester	23.712	362	347	245	229
9	Isomer of compound 8	24.042	362	347	245	229
10	Agathalic acid, TMS ester	26.494	390	375	273	257
11	Isomer of compound 10	26.621	390	375	-	257
12	1,4a,5,6-tetramethyl-1,2,3,4,4a,7,8,8a-octahydro-naphthalencarboxylic acid, TMS ester	19.685	308	293	191	175
13	1,4a,6-trimethyl-5-methylene-1,2,3,4,4a,5,8,8a-octahydro-naphthalencarboxylic acid, TMS ester	19.977	306	291	189	173
14	1,3-dimethyl-cyclohexa-2-en-carboxylic acid, TMS ester	9.879	226	211	109	93

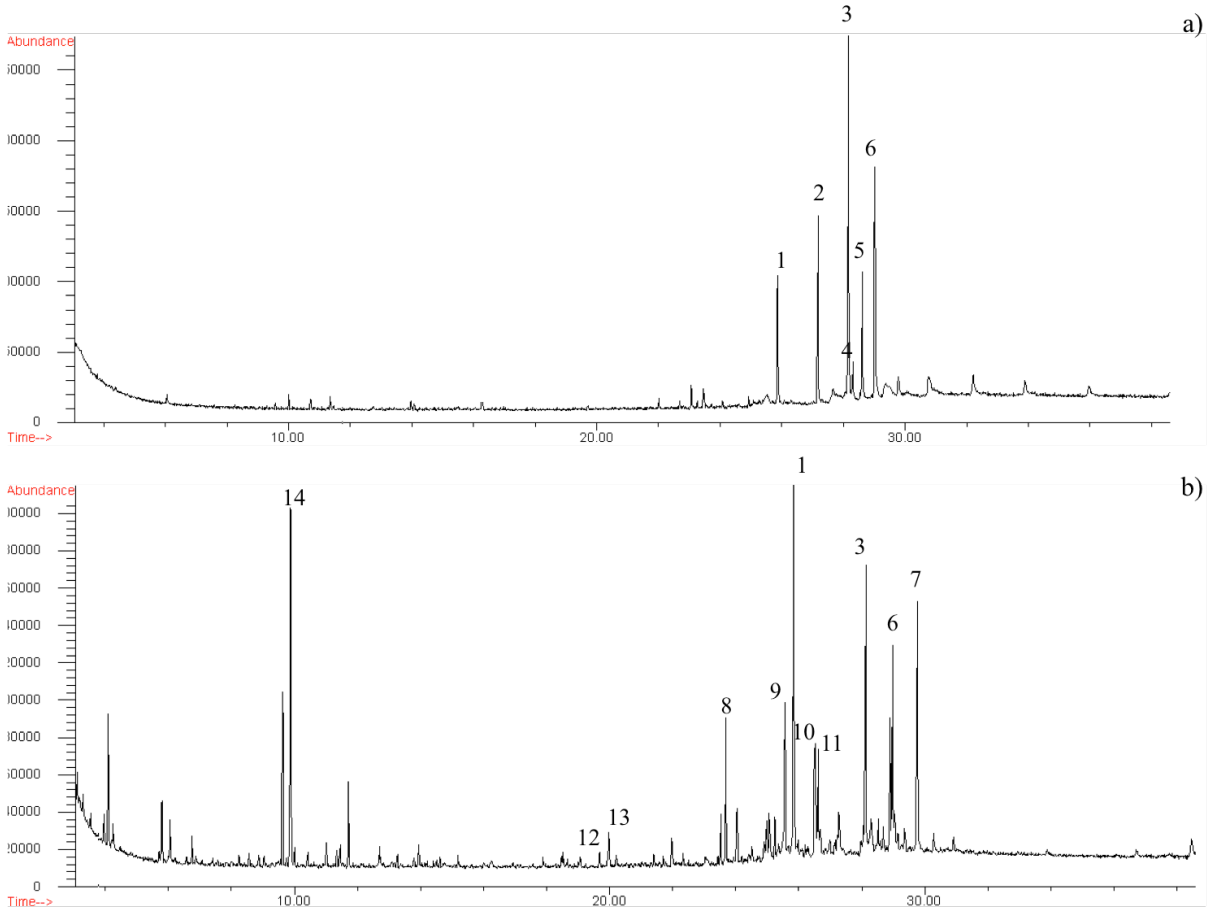

Figure 2. Total ion chromatogram of the *sandarac* resin (*Kremer*) after derivatization with BSTFA/TMCS a) unaged; b) aged at 60 °C for 1 month.

From the total ion chromatogram of the heated *sandarac* after derivation (Figure 1), almost complete disappearance of the dihydroagathalic acid (2) signal is observed and a new intense peak of agathic acid (7) appear in the chromatogram. Its mass spectrum is shown in the Figure 3.

The characteristic peaks for agathic acid, di-TMS ester are the molecular ion at m/z 478 and the ionic fragment at m/z 463, obtained by loss of a methyl group $[M-15]^+$, at m/z 346 by the loss of the trimethylsilyl ester and a methyl group $[M\text{-}COOTMS\text{-}CH_3]^+$ and at m/z 244 by the loss of two trimethylsilyl esters $[M\text{-}COOTMS\text{-}COOTMS]^+$.

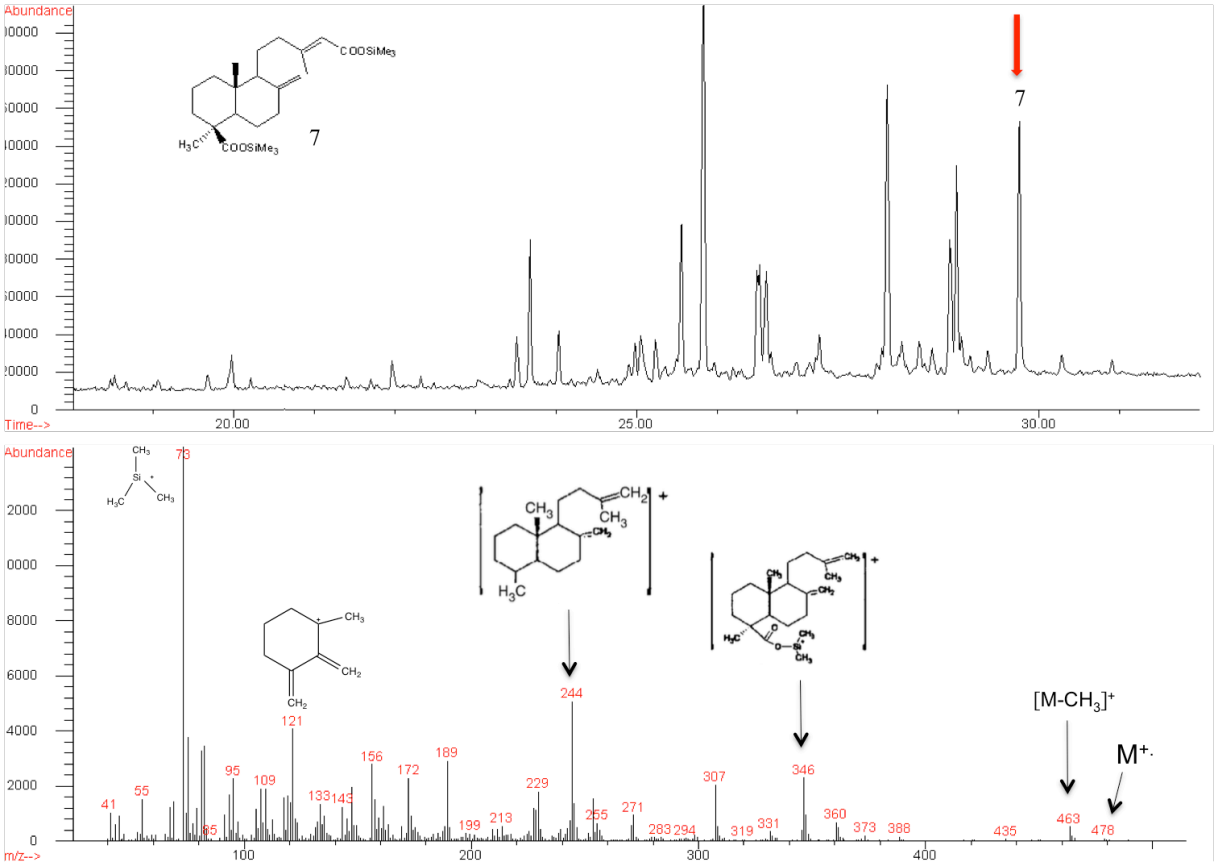

Figure 3. 70 eV mass spectra of agathic acid, di-TMS ester (7).

The mass spectrometric behaviour of the rest indentified compounds is presented in the Figure 4.

The appearance of agathalic acid (10) in the spectrum of the heated *sandarac* is very remarkable, in view of the fact that in the unaged resin there was no trace of this unsaturated compound. The formation of a double bond is one of the outcomes of oxidation processes. Thus, the formation of agathalic acid (10) from dihydroagathalic (2) can be explained by the elimination of two hydrogen atoms in C13-C14 position (Figure 5).

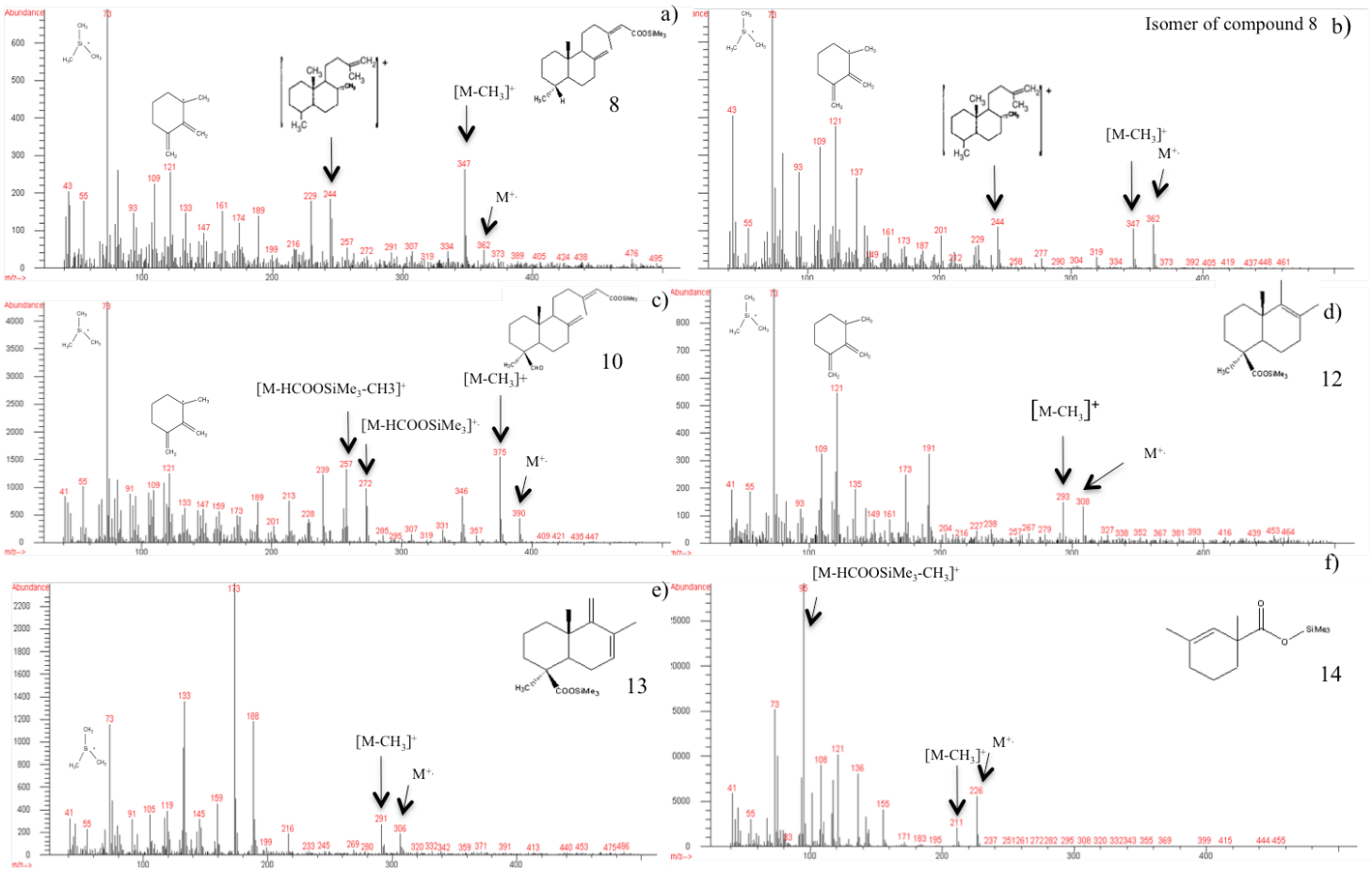

Figure 4. 70 eV mass spectra of diterpenoid TMS-esters and compounds from the thermal degradation of the polymerized part of the sandarac resin (Kremer): a) 19-norlabda-8(20),13-dien-15-oic acid, TMS ester (8); b) isomer of compound 8 (9); c) agathalic acid, TMS ester (10); d) 1,4a,5,6-tetramethyl-1,2,3,4,4a,7,8,8a-octahydro-naphthalencarboxylic acid, TMS ester (12); e) 1,4a,6-trimethyl-5-methylene-1,2,3,4,4a,5,8,8a-octahydro-naphthalencarboxylic acid, TMS ester (13); f) 1,3-dimethyl-cyclohexa-2-en-carboxylic acid, TMS ester (14).

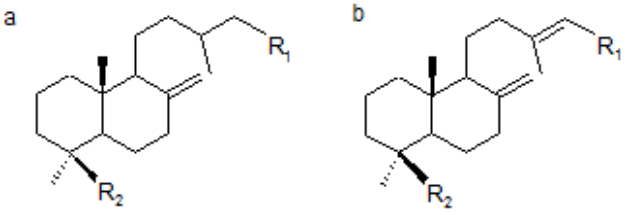

Figure 5. Labdane derivatives a) saturated; b) unsaturated.

On the other hand, the disappearance of the dihydroagathalic acid (2) and the appearance of the agathic acid (7) signal of the same intensity can be explained by the oxidation reaction of the aldehyde group to the carboxylic acid (Figure 6).

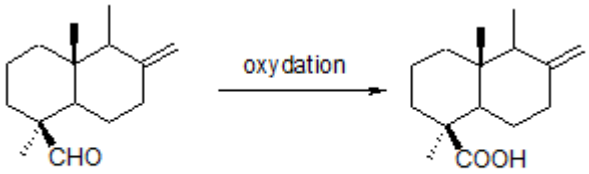

Figure 5. Proposed oxidation of labdanes with aldehyde functionality to carboxylic acid.

Conclusion

Sandarac, being a fossil resin, which, apart from free diterpenoids, consists of a highly polymerized fraction of polycommunic acid, can be mixed with oils only after heating and subsequent decarboxylation and depolymerization of polycommunic acid.

Electron impact (EI) ionization gas-chromatography mass spectrometry (GC-MS) was used to characterize thermally aged *sandarac*. Compositional differences were highlighted by the identification of low molecular mass diterpenoid compounds and components from polymeric part, polycommunic acid. Oxidation and cross-linking reactions were found to affect diterpenoid abietane and pimarane molecules. Evidence is given indicating the occurrence of cleavages in the cross-linked polycommunic structure of thermally aged *sandarac*.

5. C. Analyses of the high molecular mass part of the *sandarac* resin by MALDI-TOF and ESI-Orbitrap

In the previous chapter the *sandarac* resin was analysed by GC – MS technique. This method allows identifying only the low-molecular weight fraction, which is mainly composed of labdane-type molecules. In order to determine the nature and composition of the cross-linked fraction an analytical pyrolysis is frequently required [16].

In this part of the research work, as an alternative to pyrolysis, the technique of high-resolution mass spectra obtained with Time of Flight (TOF) mass spectrometer using matrix-assisted laser desorption/ionization (MALDI) and with an ion trap mass spectrometer

(Orbitrap) using electrospray ionisation (ESI) were explored as the appropriate techniques for the analyses of intact polymers.

MALDI became one of the most important mass spectrometric methods for rapid analysis of a wide range of compounds [27]. Despite of this fact, only few studies have been dedicated to matrix-assisted laser desorption ionization time-of-flight mass spectrometry (MALDI-TOF-MS) based techniques analysis of organic materials used in atworks such as diterpenoid resins up to date. Two principal publications have been dedicative to this approach, the first of which studied artificial photoageing of triterpenes by graphite-assisted laser desorption/ionization mass spectrometry [13] and the other one analyzed dammar resin with MALDI-FT-ICR-MS [28].

MALDI and ESI are complementary ionization sources for the analysis of *sandarac* resin and both are relatively soft ionization methods. They produce the molecular ions (in the form of adducts with H^+, Na^+ or other cations, i.e. $[M+H]^+$, $[M+Na]^+$, etc.) with little (ESI) or almost no (MALDI) fragmentation [29].

Because of the high complexity of the *sandarac* resin its mass spectrum that has been obtained without additional separation of components is expected to be immensely complex. If the resolution is not sufficient, then peaks of ions with the same nominal m/z ratio will overlap, thereby, seriously reducing the usefulness of the spectrum. High-resolution (HR) MS is able to separate peaks of the same nominal m/z ratio and has a distinct advantage here. The ion trap mass spectrometer (Orbitrap) offers a high resolution and m/z measurement accuracy.

In spite of the mentioned advantages of the analytical methods chosen, that match very well with needs of complex mixture analysis, MALDI-TOF-MS and ESI–Orbitrap-MS have found limited use in analytical studies related to cultural heritage for the time being. In particular, the high molecular mass region of the *sandarac* resin (up from approximately 600 Da) has remained almost unexplored.

Thus, the main goals of this part of the research were to study and to evaluate the capability and usefulness of MALDI-TOF and ESI-Orbitrap in measuring and analyzing extensively oxidized *sandarac* resin and to obtain good quality mass spectra.

In order to maintain analyses of high-molecular weight fraction by high-resolution mass spectrometry the development of the methodology is required first of all, i.e. optimization of the right analytical conditions such as the conditions for sample preparation, choice of solvents, capillary temperature, spray voltage in the case of ESI-Orbitrap and extraction delay, grid voltage, laser intensity for MALDI.

Thus, at first the optimisation of sample preparation and analytical conditions allowing obtaining informative spectra with a good signal-to-noise ratio was undertaken.

5. C. I. Measurements of the MALDI-TOF-MS mass spectra

5. C. I. 1. Preparation of the *sandarac* resin solutions

The MALDI method relies on the availability of a suitable matrix material for each class of analyte. These matrixes have been developed or discovered in an empirical fashion, and there is currently no method to systematically select an appropriate matrix for a new class of analytes [30]. For the *sandarac* resin samples a suitable matrix / sample preparation method has only been found after substantial effort was invested.

As a result, in the case of the *sandarac* resin, 2,5-dihydroxybenzoic acid (DHB, Aldrich, 98% purity) was used as the MALDI matrix substance. The matrix solution was prepared by adding to 15 mg of DHB 0.5 ml of acetonitrile (J.T. Baker, HPLC grade) and 0.5 ml of 0.1% trifluoroacetic acid (TFA, Aldrich 99+%) solution in water (MilliQ). Sealed DHB matrix solution was stored in the freezer.

The selection of the solvent for the deposition of the MALDI spots is not simple in the case of the *sandarac* resin as well. *Sandarac* resin is a complex natural mixture and is not completely soluble in many common solvents. One of the objectives of this work was to test different solvents and solvent systems to evaluate the solvents' capacity to dissolve *sandarac* resin and its compatibility with DHB.

A suitable solvent system is one which (1) easily dissolves the resin, (2) easily dissolves DHB and (3) is volatile. Table 1 lists the solvents and solvent systems that were used for the preparation of sample solutions, as well as information on the solubility of the *sandarac* resin in these solvents.

Preparation of the *sandarac* resin solution was carried out in the following manner. A small weighted amount (0.006 g) of the *sandarac* resin powder was placed in an eppendorf tube and 0.5 ml of solvent was added with a pipette. The components were thoroughly mixed. In the case of two-component solvent mixtures, a powdered *sandarac* resin was placed in the eppendorf tube and dichloromethane (DCM) was added first, followed by the other solvent. Different volume ratios have been tested, and the most appropriate volume ratio is 1: 1.

Table 1. The solvents tested (and solvent systems) and the solubility of the *sandarac* resin (*Kremer*)	
Solvent systems	Solubility
Dichloromethane (DCM)	Partially soluble
Ethanol (EtOH)	Soluble
Acetone	Partially soluble
Toluene	Insoluble
Acetonitrile	Insoluble
Chloroform	Partially soluble
Acetone: DCM (1: 1)	Partially soluble
EtOH: DCM (1: 1)	Soluble
Toluene: DCM (1: 1)	Partially soluble
Acetonitrile: DCM (1: 1)	Partially soluble

5. C. I. 2. Sample spotting and mass spectra measurement

MALDI is mainly based on laser desorption and ionization of solid mixture of matrix and sample deposits. In general, the sample is co-crystallized with a matrix material. A process of 'dried droplets' is often used: 1) mixing the sample and the matrix solutions together; 2) identifying the mixture on the MALDI target plate; and 3) allowing to dry. But is not suitable for identifying solutions of the *sandarac* resin. It was observed that the best results were obtained when the matrix and sample solutions were added separately to the target plate. The following spotting technique was used: one drop of the DHB matrix solution (0.7 μl) was spotted on the MALDI sample plate, and the solvent was allowed to evaporate under atmosphere pressure and at room temperature. Next, on the solid matrix crystals, a large drop of the sample solution (1 μl) was applied. The DHB crystals partially dissolved in the sample solution and recrystallized again, together with the sample. The spot was allowed to dry at room temperature. After the droplet was dried, the MALDI plate was inserted into the MALDI chamber of the mass spectrometer for analysis.

To obtain a good MALDI mass spectrum of the *sandarac* resin:

• the sample solution should be in excess of the matrix solution;

• the sample solution should not be highly concentrated. If the concentration of the solution is too high, then after evaporation of the solvent, a glossy resin film is formed on the MALDI plate and a poor spectrum is obtained;

• the crystals on the MALDI spot should be small and homogeneous.

5. C. I. 3. MALDI-TOF-MS spectra acquisition

MALDI-TOF analyses were performed on MALDI-TOF ABI 4800 (Applied Biosystems, California, USA) equipped with YAG laser with a wavelength of 355 nm and a frequency of 200 Hz. The interpretation of the MS spectra is performed with the Data Explorer software (Applied Biosystems).

The m/z values were measured in the positive mode, as more valuable information of the *sandarac* resin components are obtained from positively charged ions. In the negative ion mode, no useful mass spectra were obtained (the most intense peaks belonged to DHB).

Addition of sodium iodide, sodium carbonate and sodium acetate did not give good spectra because the formed crystals on the MALDI spot were quite large.

5. C. I. 4. Study of solvent mixtures suitable for analysis with MALDI-TOF-MS

A total of ten different solvents and two-component solvent mixtures were tested. The appropriate solvent would be that which completely dissolves the *sandarac* resin and DHB and leaves small crystals of the matrix upon evaporation when the solution is applied to the MALDI plate and supports cocrystallization of the sample with the matrix.

Ethanol completely dissolves the *sandarac* resin, including the cross-linked fraction and gives a clear solution. However, this solvent is not very appropriate for use with the DHB matrix. When the solvent is evaporated, quite large DHB crystals appear, and the sample is spread around the DHB crystals. The matrix and the analyte do not cocrystallize in the MALDI spot.

Dichloromethane only partially dissolves the *sandarac* resin, but combined with ethanol, the solubility improves. During preparation of the solutions it was found out that, first, the resin should be dissolved in DCM then ethanol should be added. Adding ethanol to the DCM solution turns slightly misty. Thus it was remarked that the *sandarac* resin almost completely dissolves in the DCM–ethanol solvent mixture. This solvent mixture is compatible with DHB, leaving small crystals upon evaporation when the solution is applied on the MALDI target plate. The spectrum analyzed in this work has been obtained using the DCM–ethanol solvent system (Figure 1).

5. C. I. 5. Analysis of the MALDI-TOF mass spectra of the *sandarac* resin

The peaks in the MALDI-TOF spectrum correspond to protonated molecules and the spectrum as a whole consists of clusters. The occurrence of oxidation in the *sandarac* resin is demonstrated by appearance of groups of signals with mass differences ranging from 14 to 18. The addition of oxygen to the saturated structures produces mass increments of 16 Da. Thus, increments of 16 Da are expected when the oxidation results in hydroxides and mass increments of 32 Da when hydroperoxides are formed. Since hydroperoxides are known to be highly unstable and readily decomposed to alkoxy and hydroxy radicals, mass increments of 32 are generally attributed to the incorporation of two oxygen atoms in different points of the molecule.

While the number of oxygen atoms increases, the degree of unsaturation also changes. The introduction of oxygen and the simultaneous loss of hydrogen result in mass increments of 14 Da. When oxidation occurs with the addition of hydrogen, mass differences of 18 Da are observed.

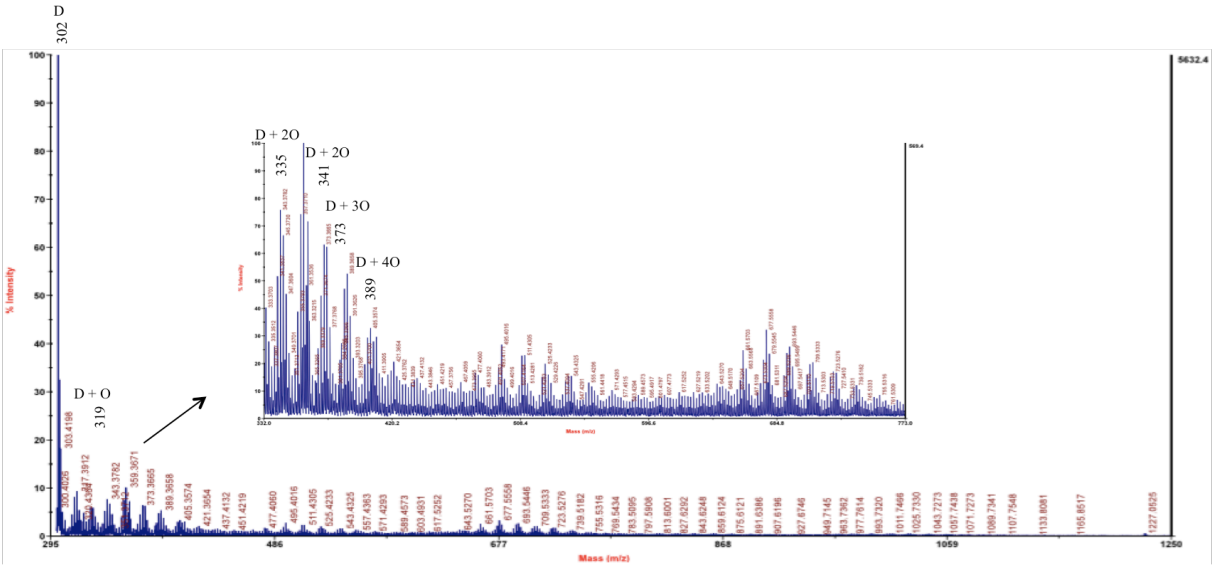

Figure 1. MALDI – TOF mass spectrum of the *sandarac* resin (*Kremer*). D indicates the diterpenoid molecules constituting the fresh resin and diterpenoids with two oxygen atoms. Their oxidation products are labeled as D + nO.

Characteristic marker compounds are sandracopimaric, communic and isopimaric acids (M = 302), dihydroagathalic acid (M = 320), methyl pinifolic acid (M = 350), dihydroagatholic acid (M = 394) and dihydroagathic (M = 408). These molecules were found

to be easily desorbed and ionized under optimised analytical conditions, giving MALDI spectra with intense peaks. Diterpenoid acids were detected as $[M + H]^+$, while their oxidation products with at least two more oxygen atoms than their nominal composition were desorbed as sodium adducts $[M + xO + Na]^+$. Therefore, peak at m/z 303 is attributed to abietane and pimarane acids with molecular weight of 302 Da. The intense signal at m/z 302 is due to the molecular radical cations $[M]^{+\cdot}$ of diterpenoid acids.

Peak at m/z 319 corresponds to oxidized diterpenoid acid molecules obtained by addition of one oxygen atom. With further oxidation, peak at m/z 335 is obtained. m/z 341 was assigned to the sodium adduct of oxidized diterpenoid acids $[M + O + Na]^+$ and at higher m/z values groups of signals with mass differences ranging from 14 to 18 suggest that diterpenoids with up to six oxygen atoms are present.

In the MALDI spectra of the *sandarac* the relative intensity of the peaks assigned to oxidized molecules is considerable and diterpenoid dimers with various oxidation degrees were observed (Figure 2). Peaks at m/z 645, 661, 677, 693, 709 and 647, 663, 679, 695, 711 represent subclusters of the cluster in the range m/z 620 – 740 and are characterized by mass differences of exactly 16 Da and for each signal parent peaks at ± 2Da indicate the presence of different oxidized groups.

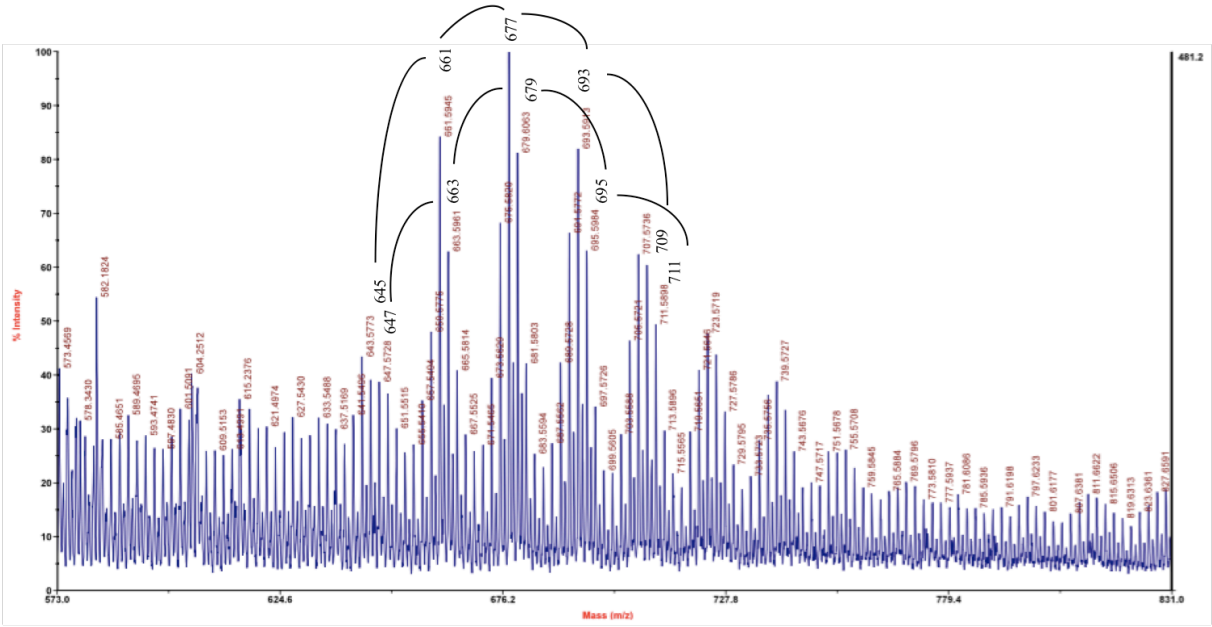

Figure 2. MALDI – TOF mass spectrum of the *sandarac* resin (*Kremer*) of the cluster in the range m/z 640 – 720.

As the oxidation progresses the number of possible combinations of increments increases, resulting in many groups of signals. With respect to the *sandarac* resin, which in turn is a mixture of diterpenoids with similar molecular weight, the situation is much more complicated and complete identification of the compound seems difficult.

Nevertheless, this approach brought to visualizing spectra with thee clusters of peaks in the m/z range of 300–900. It's highly possible that the mass range of the polymer fraction is much greater than the one was actually observed, but the difficulties with the sample ionization don't allow observing the polymer higher than m/z 900.

5. C. II. Measurements of the ESI-Orbitrap-MS mass spectra

5. C. II. 1. Preparation of the *sandarac* resin solutions

Stock solutions of the *sandarac* resin were prepared with a concentration of approximately 1 mg/ml using various solvents. The first task involved finding a solvent system that could adequately dissolve the resin compounds and could be used with an electrospray mass spectrometer. A solvent with a 50/50 composition of DCM / EtOH worked well. Acetic acid (0.1% v/v) was added to the samples to increase the conductivity.

5. C. II. 2. The ESI – Orbitrap – MS

ESI spectra were obtained on Orbitrap mass spectrometer equipped with an electrospray ionisation probe (Thermo Fisher Scientific). The mass spectrometer was operated in positive mode. Parameters of the ion source were as follows: source voltage 5 kV, capillary voltage – 40 V, tube lens voltage –250 V, capillary temperature 250°C, sheath and auxiliary gas flow (N_2) 42 and 11 (arbitrary units). The MS spectra were acquired by full-range acquisition covering 100–1400 m/z. A data-dependant scan was performed for the fragmentation study by deploying collision - induced dissociation (CID). The normalised collision energy of the CID cell was set at 35 eV.

5. C. II. 3. Analysis of the ESI - Orbitrap mass spectra of the *sandarac* resin

The Orbitrap mass spectrum of the *sandarac* resin using the ESI ionization mode is presented in Figure 3. In the first cluster, peaks are detectable from the m/z value 300 to 460, in some cases fragmented by the loss of H_2O.

Most of the peaks in the ESI-Orbitrap-MS spectrum correspond to the protonated molecules of the diterpenoid compounds, and some correspond to fragments. Like in the MALDI spectra an intense peak at m/z 303 correspond to diterpenoid acids with molecular weight of 302 Da. In the lower mass range from 300 to 460, there are numerous peaks in the ESI spectrum that are missing in the MALDI spectrum and are interpreted as fragments.

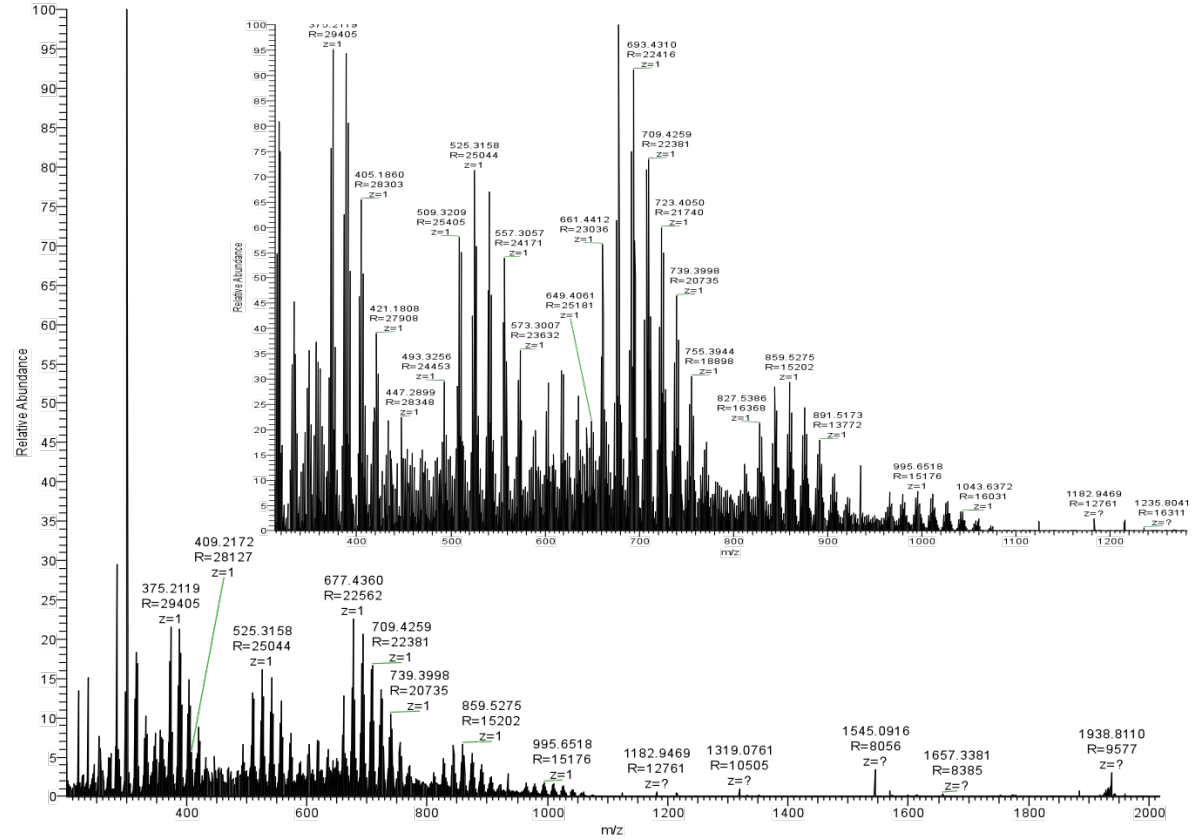

Figure 3. ESI – Orbitrap mass spectra of the *sandarac* resin (*Kremer*) obtained using a 50/50 DCM / EtOH.

Through analyses of the *sandarac* resin using gas chromatography followed by electron impact mass spectrometry six major components were found: sandracopimaric, communic and isopimaric acids (M = 302), dihydroagathalic acid (M = 320), methyl pinifolic acid (M = 350), dihydroagatholic acid (M = 394) and dihydroagathic (M = 408). Including minority components, up to 10 compounds may be found in the spectrum of the *sandarac*, but the ESI mass spectrum of Figure 4 (lower) can be interpreted as largely due to the sodium adducts of the oxidized main components, their fragments and their oxidation products.

Comparing with the ESI spectra of the communic acid (Figure 4, upper) m/z 303 is assigned as the protonated molecular ion of the communic acid and its diterpenoid isomers with molecular weight of 302 Da. Singly oxidized and protonated labdane and pimarane acids are at m/z = 319.

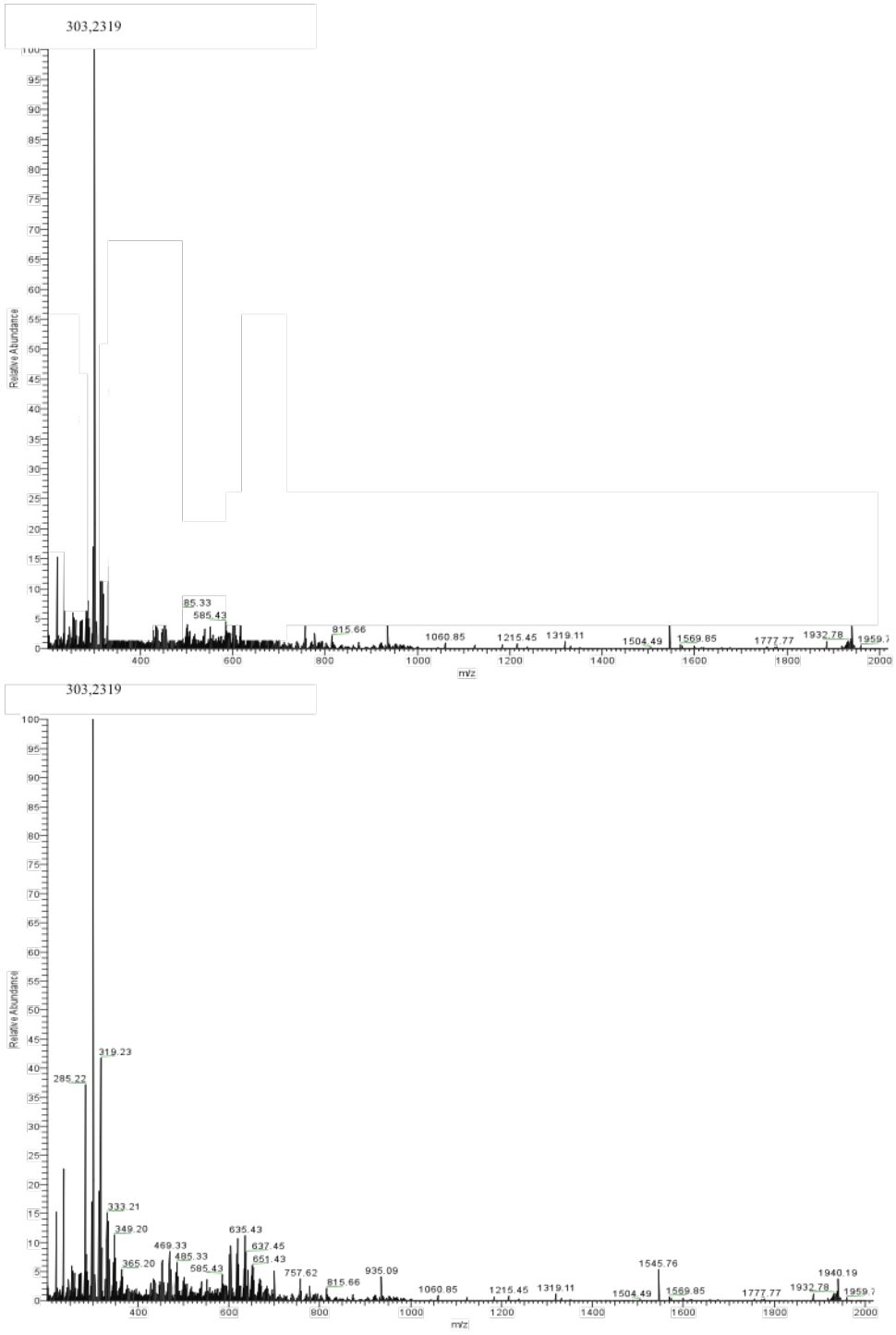

Figure 4. Comparison between the ESI – Orbitrap mass spectra of the *sandarac* resin (*Kremer*) obtained using a 50/50 DCM/EtOH (lower) and the communic acid (upper).

ESI spectra of the *sandarac* also consist of clusters and these large clusters are, in turn, composed of subclusters separated by 16 Da. The oxidation of the components of the resin leads to an increase in the number of oxygen atoms in the molecules. Attachment of an oxygen atom to a diterpenoid compound results in a mass increment of 16 Da. These subclusters correspond to oxidation products of the respective diterpenoids containing different numbers of oxygen atoms.

In the m/z range of 580 – 760 the peaks are grouped into nine subclusters (Figure 5).

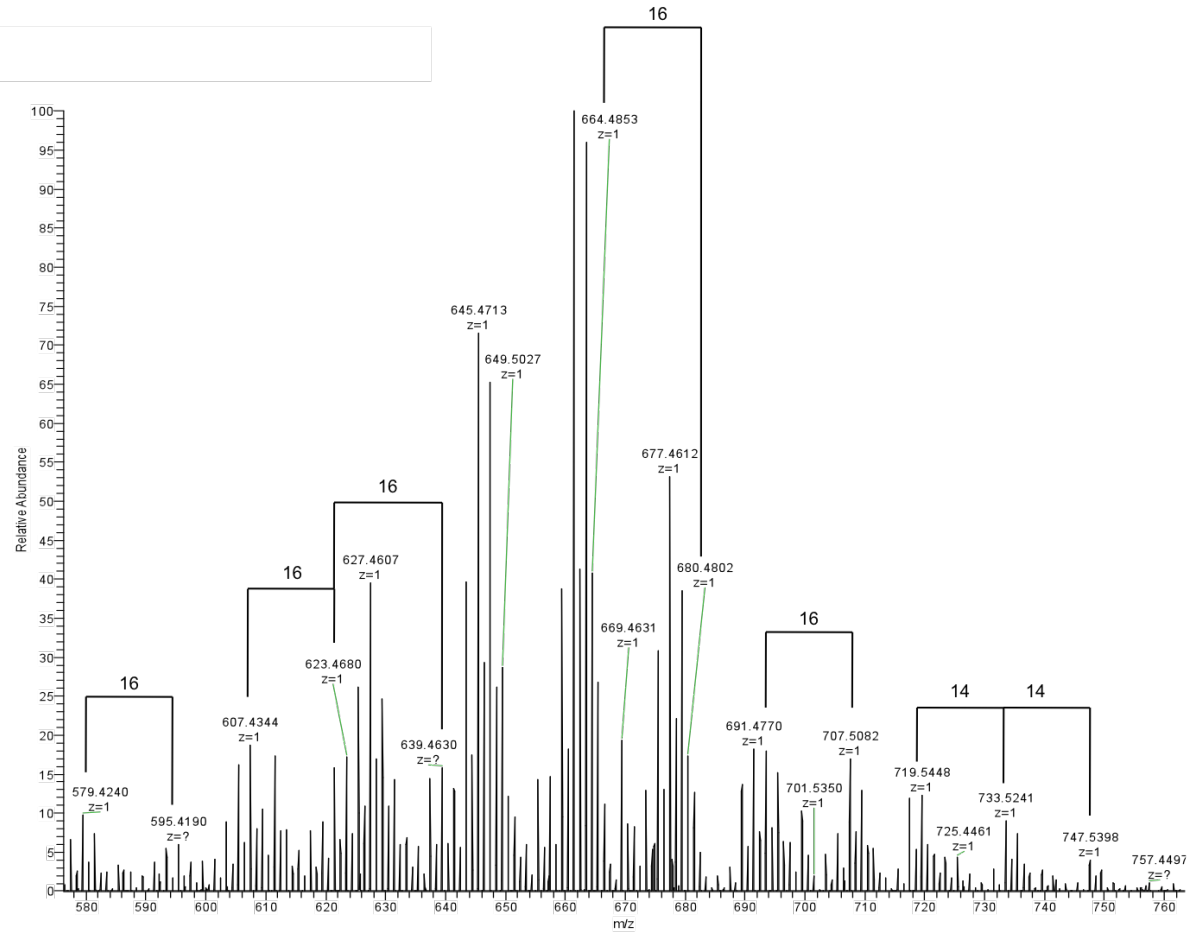

Figure 5. The cluster of peaks 580 – 760 m/z in the ESI – Orbitrap mass spectra of the *sandarac* resin (*Kremer*) obtained using a 50/50 DCM / EtOH.

Oxidation is often accompanied by a simultaneous loss of two or a multiple of two hydrogen atoms, resulting in a mass increase of 16 - 2•n Da (e.g., allylic oxidation or oxidation of an alcohol to carboxylic acid). Accordingly, within the clusters subclusters are observed (Figure 5), each corresponding to the attachment of the next oxygen atom, as well as a possible simultaneous loss of 2 n hydrogen atoms. The number of oxygen atoms in the

molecules observed in the mass spectrum generally extends from 2 to 11, depending on the cluster.

Thus, ESI technique permitted to go even farther in the mass range detection of the *sandarac* polymer part than the MALDI method, reaching m/z 1100.

Conclusion

Thus, the complexity of the *sandarac* resin is well reflected by the MALDI-TOF and ESI-Orbitrp mass spectra. The obtained MALDI-TOF mass spectrum contains thee clusters of peaks in the m/z range of 300–900, and the obtained ESI-Orbitrap mass spectrum contains five clusters of peaks in the m/z range of 300–1100.

Matrix-Assisted Laser Desorption/Ionization Time-of-Flight mass spectrometry (MALDI-TOF-MS) is shown to be a suitable method for examining highly oxidized diterpenoids, which are otherwise too difficult to determine by other techniques. By crystallization of a 2,5-dihydroxybenzoic acid (DHB) matrix and the sample solution, spectra with good signal/noise ratios are obtained and no significant interferences due to matrix ions or cluster ions were produced, at least not in the range of m/z values of interest (>300 Da). Diterpenoid compounds, being very sensitive towards photo-oxidation, were found as oxidized molecules. Diterpenoid dimers and their oxidation products were also detected. As high polarity and molecular weight prevent these compounds to be eluted and identified by gas chromatography, other techniques must be used. In this respect, Matrix-Assisted Laser Desorption/Ionization Time- of-Flight (MALDI-TOF) mass spectrometry proved to be a good choice.

During condition optimization in the case of ESI-Orbitrap analyses, very different spectra were obtained with contaminant peaks and at the beginning the polymer profile was not observed. After a number of tests, a polymer has been first observed. The best results were demonstrated by mixing solvents DCM / EtOH = 50/50 with formic acid (0.1%) for ESI-Orbitrap. With these conditions the spectra are rather complex, but nevertheless polymer is recognizable. In the massif the components are in the state of oxidation and between each two peaks there is a difference of 16 (indicating the oxygen). The presence of polymer was detected up to molecular weights above 1300 Da.

5. D. ^{13}C Solid-state NMR analyses of the *sandarac* resin

The resin exudates from plants in general may be characterized chemically by solid-state ^{13}C nuclear magnetic resonance (NMR) spectroscopy very efficiently [31]. In light of that the solubility of resins varies from high to negligible, the best solution is presented by the solid-state method that permits examination of all classes of compounds found in natural plant exudates. Solid-state NMR spectroscopy examines all the material used to record the spectrum, so the results are characteristic of the bulk and not just the portion that happens to be soluble or volatile. Meanwhile, GC/MS characterization has been very successful at identifying small molecules in either a soluble fraction or a pyrolysate. Our further goal is to examine the solid-state ^{13}C NMR spectrum of bulk resins, with different modes of decoupling.

In this part of the research the structure of the *sandarac* resin is characterized by using a combination of advanced solid-state ^{13}C NMR techniques. To study this specific material, whose spectroscopic signature is relatively complex, we explore if solid state NMR is a good candidate technique and if it provides a satisfactory spectral resolution. The great advantages of NMR are the possibility of using selective pulse sequences to identify and separate chemical species without ambiguity.

5. D. I. Combination of analytical techniques used in solid-state NMR analyses

A number of ^{13}C solid-state MAS NMR techniques (single-pulse (SP), cross-polarization (CP), inversion recovery cross-polarization (IRCP)) were combined to retrieve information on the resin of interest.

5. D. I. 1. Single-Pulse MAS Experiments

The single pulse experiment is the simplest one-dimensional NMR experiment (Figure 1). It contains three parts: pulse delay (measured in seconds), pulse length (measured in microseconds) and acquisition time (measured in seconds).

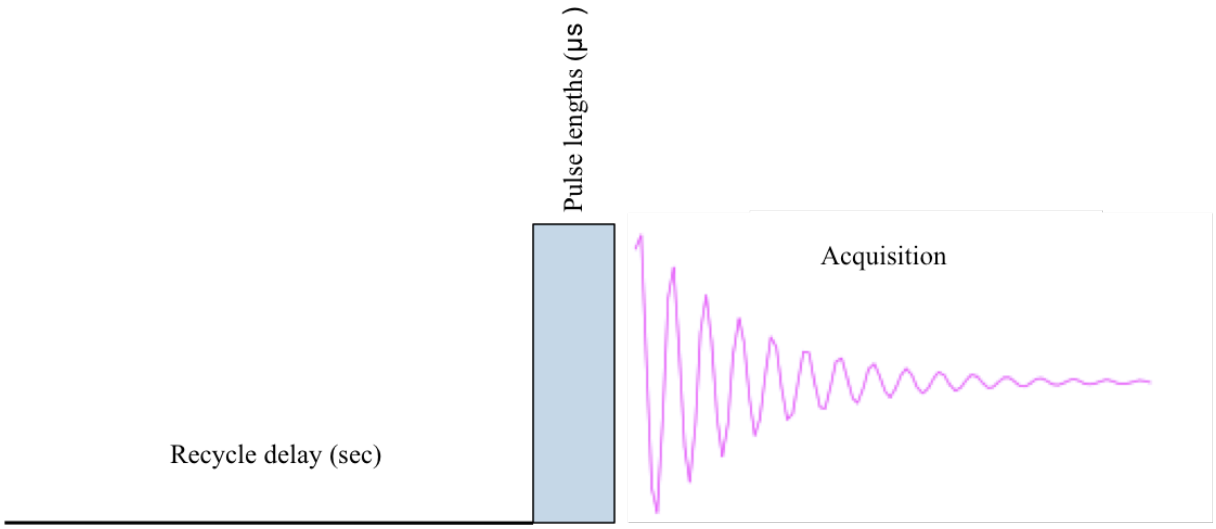

Figure 1. The Single-Pulse sequence utilized.

In the SP experiment the pulse lengths (90° flip angle) for ^{13}C was 3.80 µs and the optimum recycle delay was 30 s. Two-pulse phase - modulated (TPPM) proton decoupling was applied during ^{13}C acquisition (80 kHz). A simple two-pulse phase modulation TPPM scheme greatly reduces the residual line widths arising from insufficient proton decoupling power in double resonance magic angle spinning MAS experiments [32]. Optimization of pulse lengths and phases in the sequence produces substantial improvements in both the resolution and sensitivity of ^{13}C spins over a broad range of spinning speeds at high magnetic field. The number of transients (NS) was 64 for ^{13}C experiments.

Figure 2 illustrates a solid-state ^{13}C spectrum of the *sandarac* resin (*Kremer*) obtained with parameteres indicated above. There are several notable features to the spectrum. First of all, the carboxylic acid resonance at δ ca. 186 is diagnostic of the *sandarac*. And what is remarkable, there are no carbonyl resonances from aldehydes and ketones above δ 200. Secondly, the most intense resonances are found in the saturated region, δ 0 – 60. These are from saturated carbons typical of terpenoid hydrocarbons. Ten strong peaks in the saturated region at δ 12, 20, 27, 29, 32, 38, 41, 44, 47 and 57 dominate the alkane portion of the ^{13}C spectrum. There are weaker resonances in the region (δ 60–110) in which saturated carbon that is substituted with electron-withdrawing groups such as oxygen functionalities resonates. Finally, the unsaturated region δ 100 – 160 contains resonances from carbons of double bonds. The significant resonances in the alkene region are five broad peaks at δ 108, 116, 134, 144 and 148.

Singly substituted alkene carbons (C—HC=CH—C) resonate in the range δ 120–145, unsubstituted alkene carbons ($C=CH_2$) at δ ca. 110, and disubstituted alkene carbons (>C=C)

at δ ca. 150. All such substitution patterns are present in the spectrum of Figure 2, and the peaks at both δ 108 and 148 strongly suggest the presence of an exomethylene or terminal group (>C=CH_2).

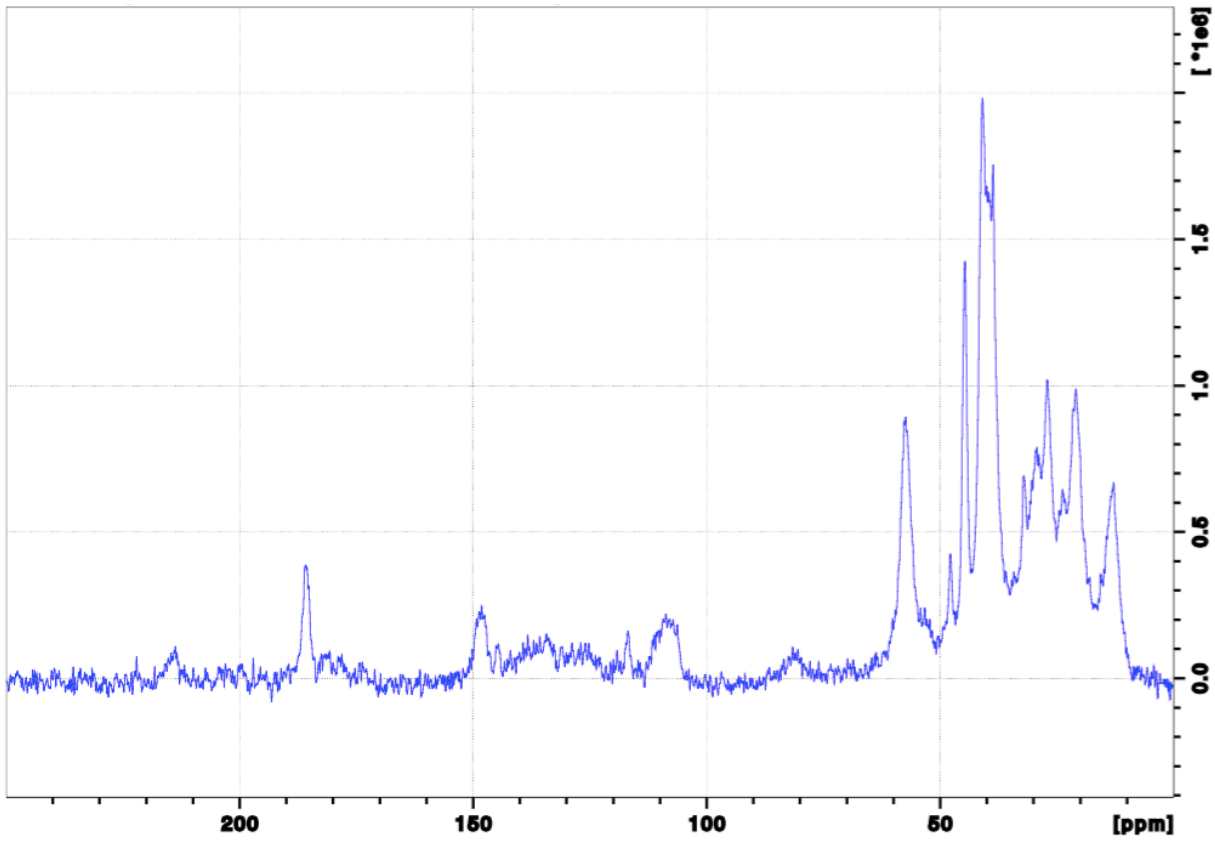

Figure 2. The ^{13}C spectrum of the *sandarac* resin (*Kremer*) with Single-Pulse MAS.

5. D. I. 2. CP-MAS Experiments

Single-pulse (SP) experiments, which are generally more favoured than CP (cross-polarization) for quantification, are frequently time - consuming. The presence of paramagnetic centres can also be a complicating factor leading to a signal broadening.

The ^{13}C cross-polarization (CP) technique combined with magic angle spinning (MAS) has become one of the most standing out one-dimensional solid-state nuclear magnetic resonance (NMR) experiments. It offers high-sensitivity spectra of natural abundance ^{13}C in solids by polarization transfer from abundant proton spins and by eliminating broadening from chemical shift anisotropy and dipolar coupling. The CP technique for ^{13}C usually is the method of choice over a simple single-pulse experiment for the sensitivity enhancement,

which is caused by both the polarization transfer from the protons to the carbons and to the shorter relaxation times of protons.

Unfortunately, quantification using CP is more difficult than in a single-pulse experiment because of the more complicated spin dynamics. Nevertheless, cross-polarization at one single contact time is, in general, the fastest approach to obtain preliminary information about chemical composition.

Figure 3 shows the ^{13}C solid-state CP-MAS NMR spectra of the *sandarac* (*Kremer*) recorded using a contact time of τ_{CP} = 1 ms.

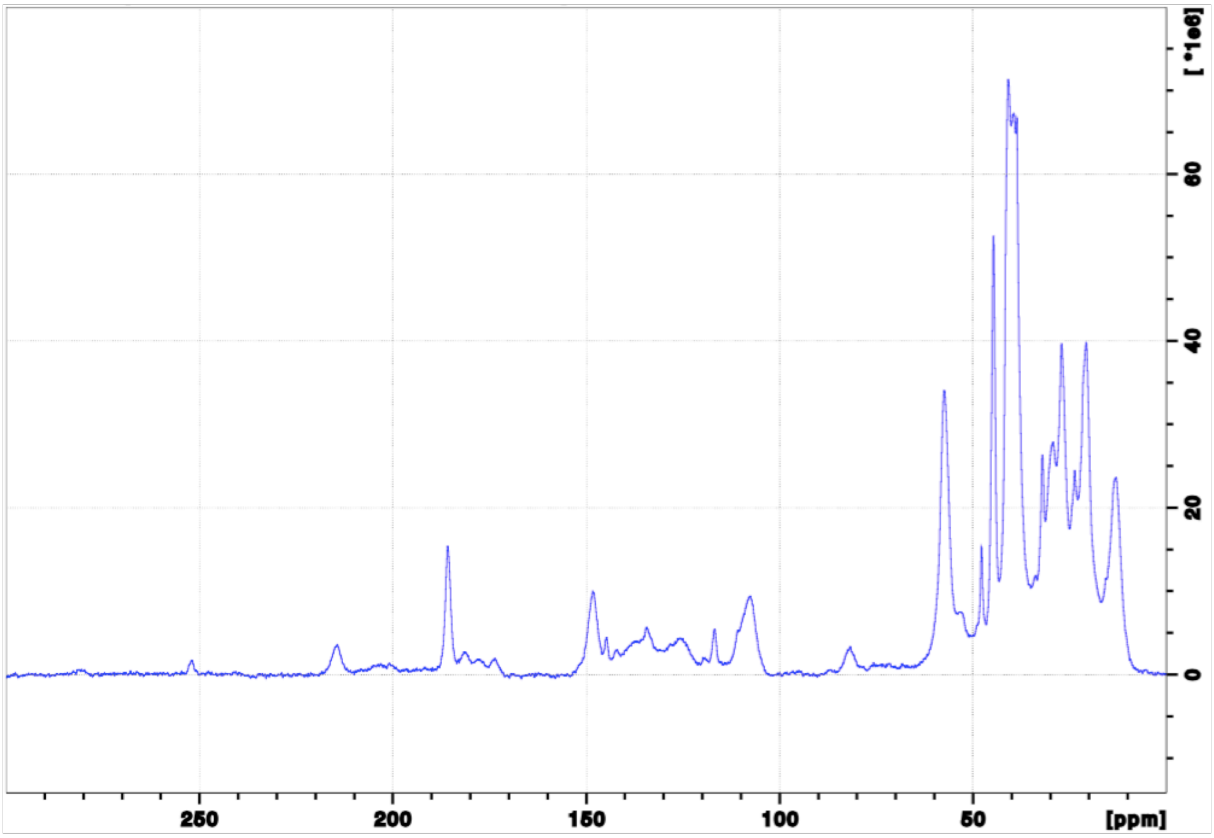

Figure 3. Carbon-^{13}C CP-MAS NMR of the *sandarac* resin (*Kremer*) obtained with contact time τ_{CP} = 1 ms.

For the further analyses the obtained spectra at different contact times (from short (τ_{CP} = 25 μs) to long values (τ_{CP} = 1 ms)) have been decomposed with DMFIT2004 software, allowing the complete simulation of solid-state NMR experiments. This program is more oriented towards users of solid-state NMR experiments as a tool for the characterization of materials [33]. The peak height alone was allowed to vary, and a Gaussian line shape was chosen. As a result, 35 peaks were modulated in order to approach the fit with real spectrum (Figure 4).

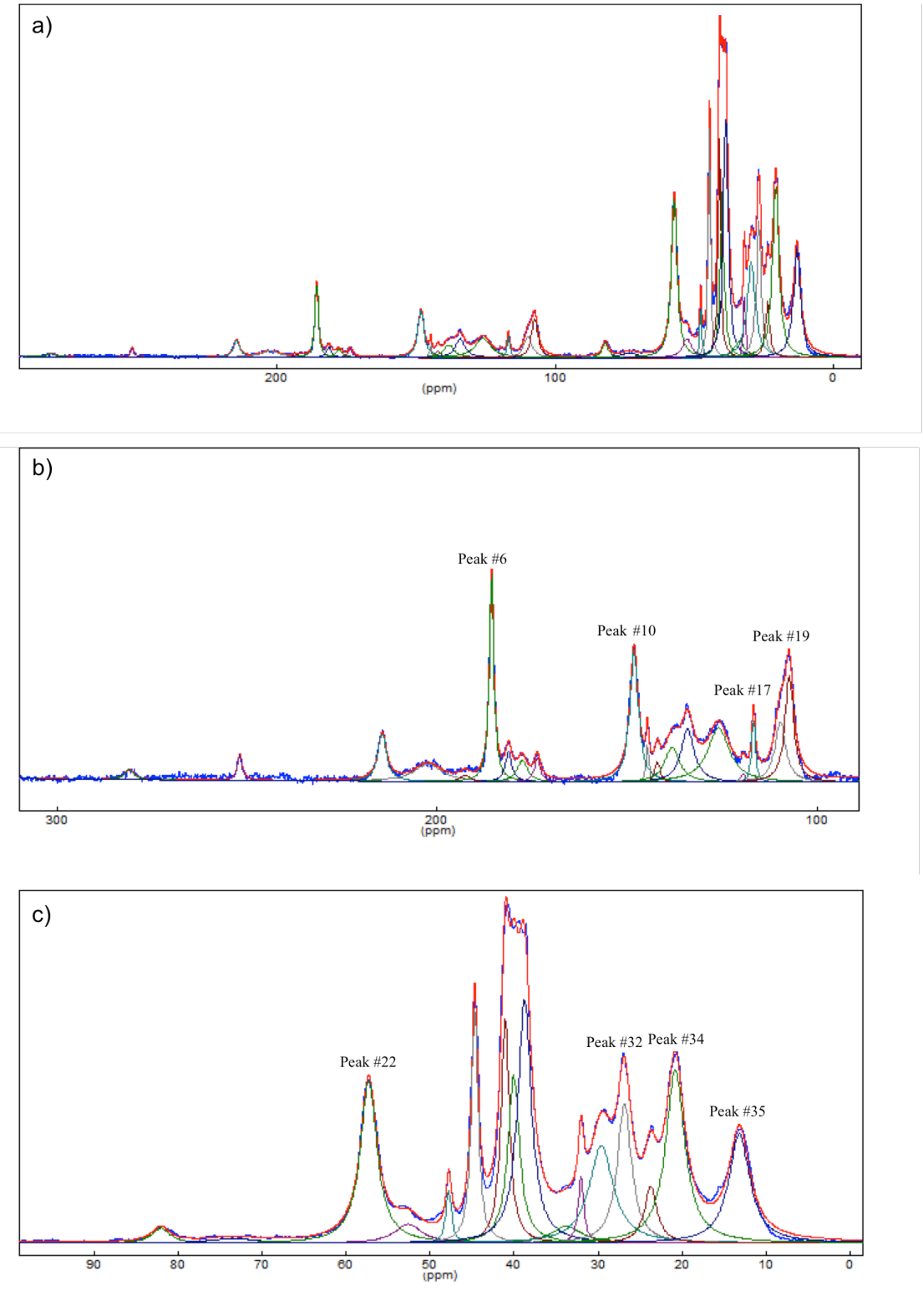

Figure 4. Simulation of CP spectra (blue) of the *sandarac* resin (*Kremer*) at contact time τ_{CP} = 1 ms. a) Full spectrum; b) ~ 100 – 300 ppm; c) ~ 0 – 100 ppm. Blue envelope corresponds to experimental data, while red one refers to simulation.

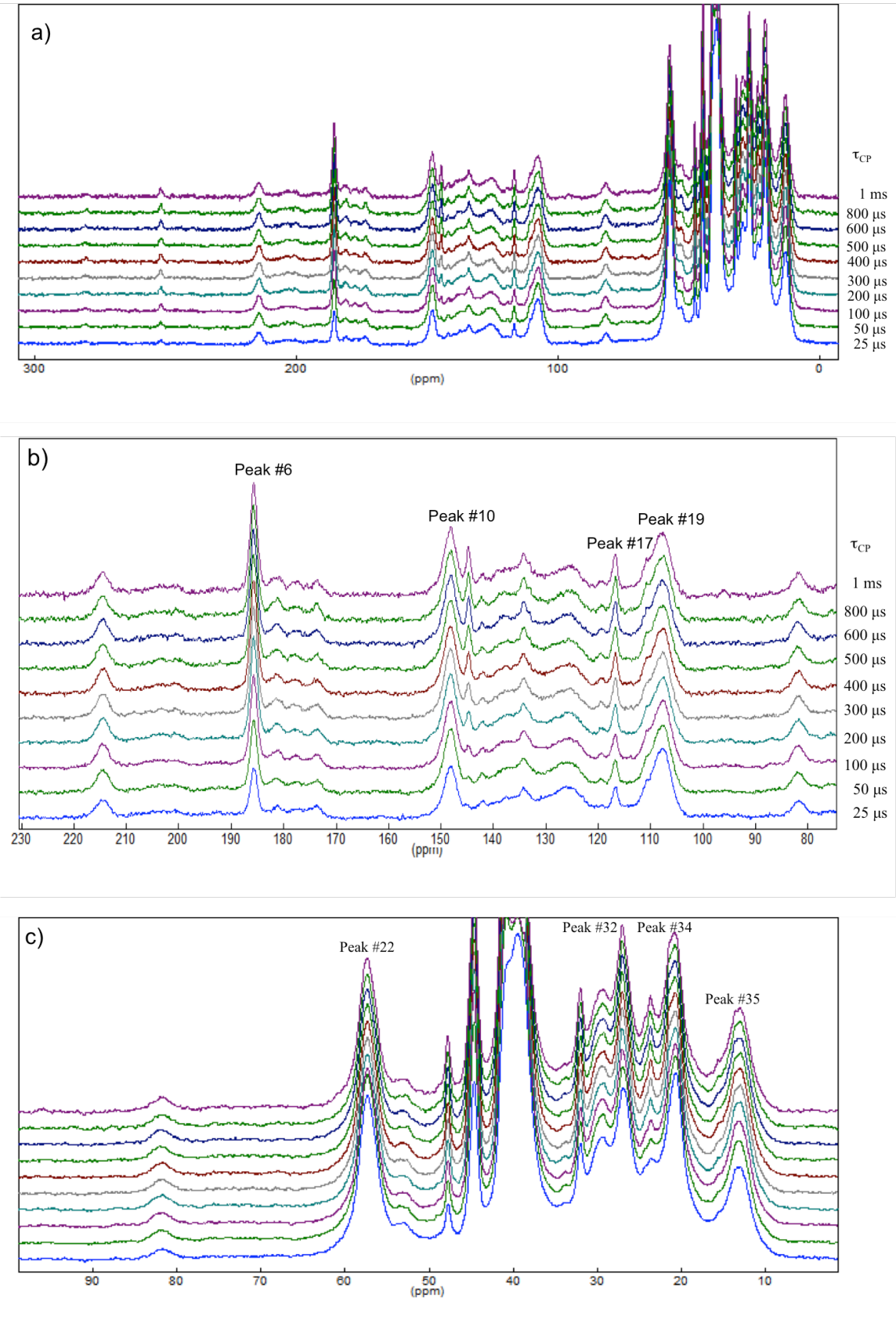

Figure 5. Evolution of ^{13}C CP-MAS spectra recorded on the *sandarac* resin (*Kremer*) for different contact times (full spectrum). a) Full spectrum; b) ~ 100 – 300 ppm; c) ~ 0 – 100 ppm.

Figure 5 shows ^{13}C CP-MAS spectra recorded at various contact times from very short (τCP = 25 μs) to long values (τCP = 1 ms). The spectrum recorded at τCP = 25 μs mainly reveals aliphatic carbons. This is expected since, for a short contact time, magnetization transfers only occur across strong dipolar couplings corresponding to short C - H distances characteristic of C-Hx bonds [34]. The aliphatic zone (10 - 80 ppm) of the CP-MAS spectra shows a very complex shape composed of several unresolved resonances for which more insight will be provided by the IRCP experiments further. However, interesting insights can be actually gained in the region 100 - 160 ppm.

In the spectrum with very short contact time τ_{CP} = 10 only signals in the region of methylene carbon resonances are clearly observed. Rotating methyls, quaternary carbons but also aromatic CH carbons need longer τ_{CP}.

The rate of cross-polarisation of particular carbons is, in first approximation, proportional to the number of directly bonded protons and the following relative rates are usually observed: CH_3 (static) > CH_2 > CH > CH_3 (rotating) > C (non-protonated).

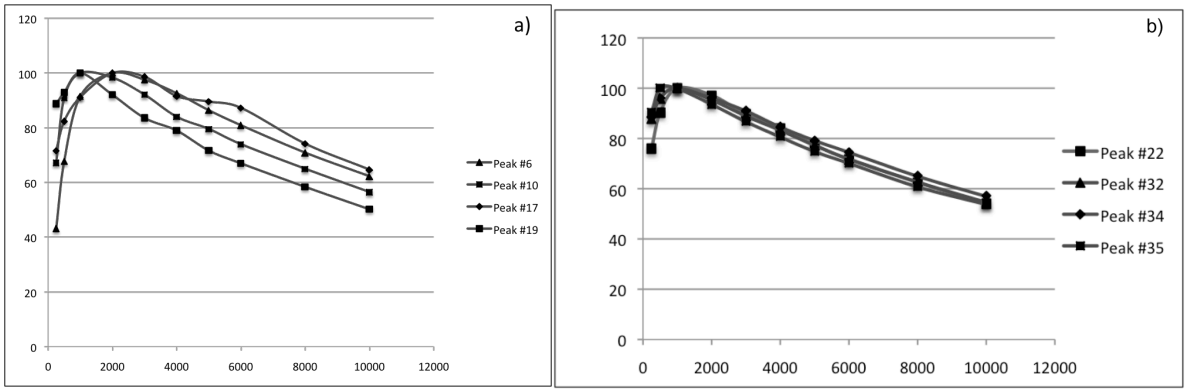

Figure 6. Variation of peak intensities of a) region ~ 100 – 300 ppm; b) region ~ 0 – 100 ppm as a function of the contact time.

Four main peaks (#6, 10, 17 and 19) of the downfield region are evidenced, and the corresponding evolution of the integrated area of these peaks as a function of cross-polarization time is shown in Figure 6a. Interestingly, peaks #6, 10 and 17 show the same polarization behaviour, typical of a quaternary carbon, whereas peak #19 shows a very fast increase in intensity, which is typical of a protonated carbon. The peak #17, which was expected to have a chemical nature similar to that of peak #19 on the basis of their very close

^{13}C chemical shifts, could not be assigned to protonated carbon as peak #19 and is dominated by quaternary species.

The variation of peak intensities for the peaks #22, 32, 34 and 35 in the region ~ 0 – 100 ppm is given in the Figure 6b. These four representative peaks of aliphatic region demonstrate very similar polarization behaviour that indicates the presence of protonated protons.

Table 1. a) Signal intensities and contact times of selected peaks from a) downfield and b) upfield regions.

a)

τ_{CP}	Peak #6	Peak #10	Peak #17	Peak #19
25 μs	43,12	67,12	71,58	88,81
50 μs	67,72	90,87	82,33	92,92
100 μs	91,47	100	91,14	100
200 μs	100	98,33	100	92,06
300 μs	97,55	92,08	98,64	83,63
400 μs	92,6	83,98	91,54	79,03
500 μs	86,36	79,51	89,52	71,73
600 μs	80,87	73,93	87,22	67,06
800 μs	70,82	64,91	74,09	58,49
1 ms	62,16	56,38	64,55	50,31

b)

τ_{CP}	Peak #22	Peak #32	Peak #34	Peak #35
25 μs	90,25	88,47	87,74	75,85
50 μs	100	96,14	95,95	90,27
100 μs	99,78	100	100	100
200 μs	93,57	96,03	95,3	97,16
300 μs	86,7	90,92	88,88	89,63
400 μs	80,66	84,55	83,25	83,98
500 μs	74,9	79,16	77,26	77,38
600 μs	70,24	74,46	71,9	71,62
800 μs	60,91	64,99	62,75	62,45
1 ms	53,94	56,96	54,66	53,86

Normalized intensities of the chosen peaks from the downfield and upfield regions are presented in the Table 1a, b respectively. The maximum intensity of methine carbons at around 66 ppm are achieved with 50 μs, while for methyl carbons the most suitable τ_{CP} should be around 100 μs. The extremum of the carbons at the downfield region of the *sandarac* is achieved with contact time of 200 μs (peaks #6, 17).

5. D. I. 3. IRCP Experiments

IRCP represents a better approach than simple CP-MAS for a detailed and complete insight into the aliphatic region where a strong overlapping of signals is observed. IRCP experiments are generally selective to rigid CH_2 and CH sites as their normalized intensity signal tends, respectively, to a negative value (-1/3) or to 0 as a function of τ_i [35, 36].

On the contrary, the signal of mobile CH_3 and/or quaternary carbons remains positive. Figure 7a, b shows some IRCP experiments for the aliphatic region and arene region respectively at selected inversion times. Signals for rigid CH and CH_2 groups change rapidly during the first tens of microseconds, like signals around 110 and 125 ppm. The peak at ~110 ppm becomes negative and has a relative intensity of one-third of that before polarization inversion, while the peak at ~125 ppm is nearly zero in 50 μs. After 50 μs, the broad signals of the upfield region invert, with the exception made for sharp components within peaks at 13.6, 41.1, 43.2 and 46.1 ppm.

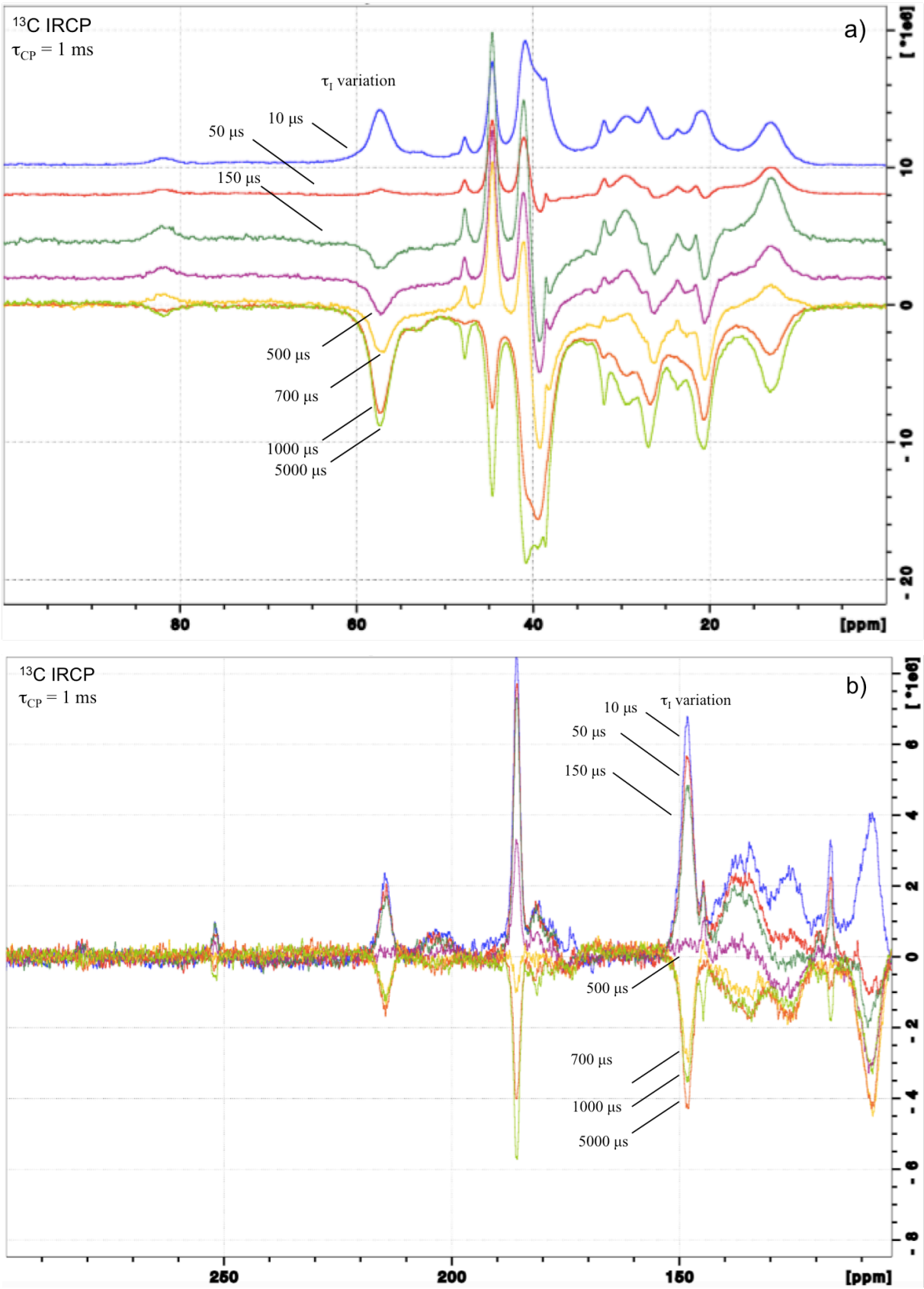

Figure 7. IRCP spectra recorded at various inversion times in the a) aliphatic and b) aromatic regions for the *sandarac* resin (*Kremer*).

Thus, IRCP technique allows distinguishing different kinds of carbon resonances, especially between CH and CH_2. In a wide range of τ_i values (50 – 200 μs) the rigid methine and methylene signals are easily recognized. For the samples of the *sandarac* resin, where the different kinds of carbon – 13 have wide chemical – shift distributions, spectral overlap makes the analysis especially challenging for such samples. Nevertheless, obtained results indicate that this technique is quite promising even for such complex samples.

5. D. II. Comparison of ^{13}C solid-state NMR spectra of the *sandarac* resin from different suppliers (from *Kremer, Okhra, Color Rare, La Marchande de Couleurs, L'Atelier Montessori, Hevea*)

Six samples of the *sandarac* resin from different suppliers were characterized by solid-state ^{13}C NMR spectroscopy. Figure 8 contains six representative spectra of *Kremer*, *Okhra*, *Color Rare*, *La Marchande de Couleurs*, *L'Atelier Montessori*, *Hevea*.

A general qualitative attribution can be proposed for each spectral domain. The upfield region (0-100 ppm) is characteristic of sp^3 carbon atoms, indicating the presence of a broad distribution of CH_x (x = 1-3) sites. This region possesses the most distinctive spectral characteristics with its seven broad peaks representing saturated carbons.

Further region with deshielding effects (100-160 ppm) is characteristic of sp^2 carbon atoms in C = C double bonds with signals between 140 and 160 ppm. In the downfield region (170-225 ppm), C = O groups are carboxylic acid moieties (186 ppm) or ketones and aldehydes (200-220 ppm) resonate.

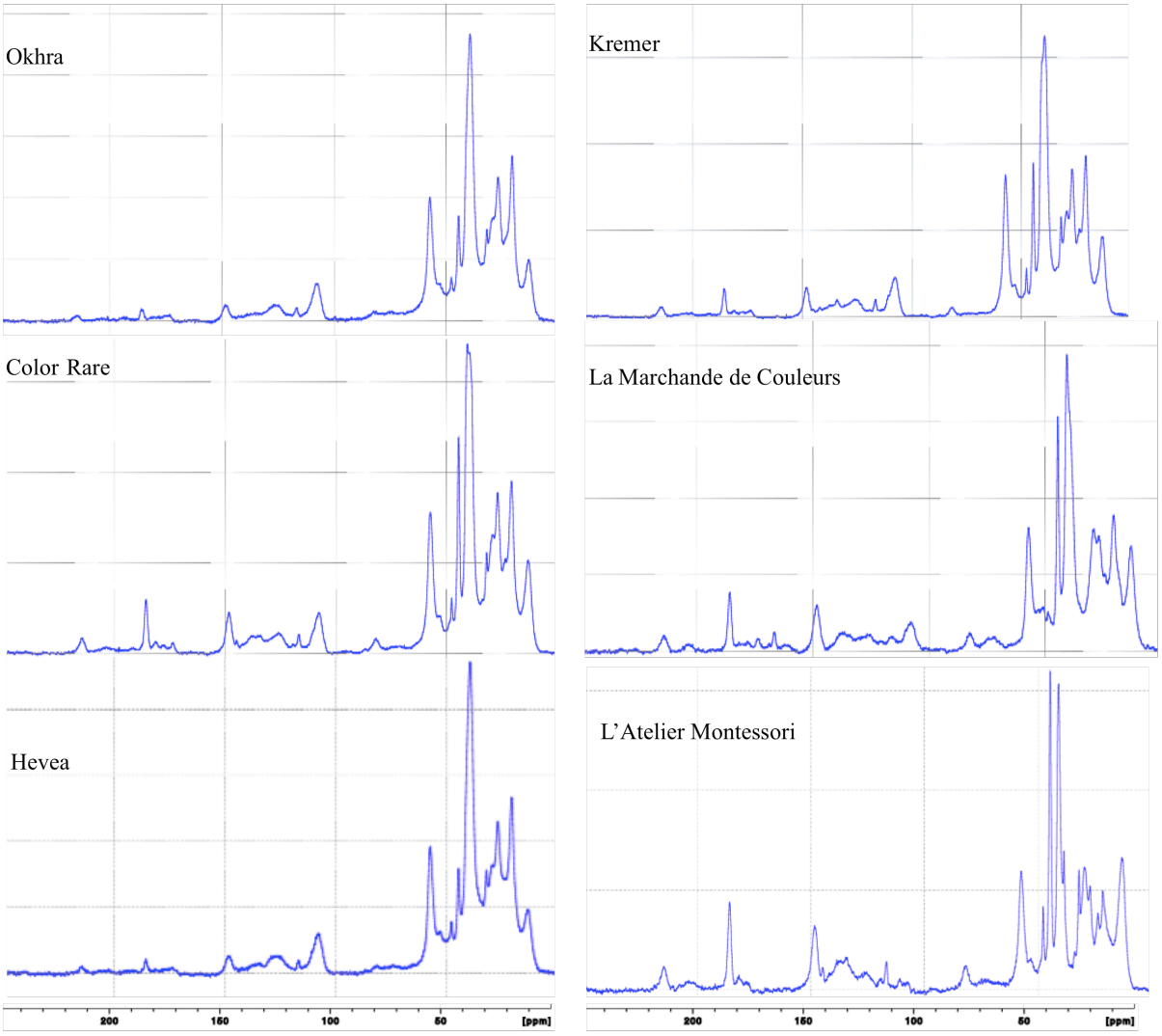

Figure 8. The ^{13}C spectra of the *sandarac* resin from *Kremer*, *Okhra*, *Color Rare*, *La Marchande de Couleurs*, *L'Atelier Montessori*, *Hevea*.

Very similar spectra were obtained for samples from *Kremer* and *Okhra*. Their characteristic resonances include the seven peaks in the aliphatic region of the spectrum and the strong exomethylene ($C=CH_2$) resonances at δ 107.5 and 148.1. There is only one significant resonance in the carbonyl region at δ 186 of carboxylic acid.

The most outstanding aspects of the sample from *Color Rare*, in comparison with *Kremer* and *Okhra*, are broad peak at δ 81.9 in the CP - spectrum and the six- or seven-peak pattern (one often is a shoulder) in the unsaturated region of the spectrum.

A major difference from the rest of the samples is shown by the sandarac from *La Marchande de Couleurs*. Even the large peaks form the saturated region change little within the rest of five resins, while the spectrum from *La Marchande de Couleurs* demonstrates

different pattern. The peak at δ 47.6 disappears, and that near δ 39.5 increases to become the second largest. The dominant peak is always the one near δ 40.8.

The spectrum of *Hevea* has the dominant peak at about δ 39.6, medium peaks at δ 20.9 and 57.3, a shoulder at δ 29.0, and a sharp peak at δ 48.2. The spectra exhibit exomethylene peaks that are relatively small in comparison with the rest of the samples.

In the last sample, *L'Atelier Montessori*, the first two peaks of the alkene region at δ 107.5 and 116 as usually correspond to terminal-chain and unsubstituted - exocyclic alkenes (=CH_2). The carboxylic acid resonance at δ 186 is slightly reduced. Except for the differences in the carboxylic acid resonance and the exomethylene resonance at 108 ppm, the spectral patterns of L'Atelier Montessori and Hevea are very similar.

Thus, solid-state ^{13}C provide some straightforward distinctions of six resin samples. These conclusions based on NMR patterns are in general agreement with those found by the GC – MS analyses, what will be precise in the chapter summarising the methods of analyses applied to the *sandarac* resin.

5. E. ^{1}H, ^{13}C Liquid-state NMR analyses of the *sandarac* resin

In this part of the research the initial liquid-state NMR study of the *sandarac* resin is presented, in order to explore the applicability of ^{1}H, ^{13}C liquid-state NMR spectra to the resins' characterization. We report herein for the *sandarac* resin the one-dimensional ^{1}H, ^{13}C liquid-state NMR spectra and the two-dimensional (COSY) spectra that provide ^{1}H - ^{1}H and ^{1}H – ^{13}C connectivities.

The *sandarac* resin originated from diterpenoids exuded by certain plants maturates over time through polymerization, cross-linking, and oxidation resulted in a robust, rock-like product that is stable to moderate temperatures and chemical conditions. The *sandarac* is partially soluble in some organic solvents, but, as a predominantly hydrocarbon material, it is insoluble in water.

Although solid-state ^{13}C NMR spectroscopy offers the advantages of allowing potentially all species to be characterized in bulk without regard to solubility, there are a number of disadvantages [37]. In many cases peaks are broad in the solid-state ^{13}C NMR spectrum. The magic angle spinning procedure cannot approach the resolution of spectra taken in solution. As a result, many peaks merge and potential spectral distinctions are lost. The solid-state ^{13}C method does not distinguish alkene resonances (from carbons of double

bonds) from arene resonances (from carbons in aromatic rings). This drawback applies to spectra taken of solutions as well as of solids. The ^{13}C experiment is inherently less sensitive than the ^{1}H experiment and consequently requires more sample and longer spectrometer times. Many resin samples are not solid and hence cannot be powdered and placed in the sample cell. Although in theory such materials may be examined, in practice samples that remain sticky or gummy are excluded.

In light of these drawbacks to the ^{13}C experiment, we decided to explore the utility of solution ^{1}H methods to resin's analysis. In the case of the *sandarac* resin, ^{1}H spectroscopy offers a number of potential advantages, which for the most part mirror in inverse the disadvantages of ^{13}C methods listed above [38, 39]. Spectra taken of solutions normally possess very high resolution, allowing peaks to be resolved to a much greater extent. The alkene and arene regions are distinct in the ^{1}H spectrum. Proton NMR spectroscopy is much more sensitive because of the larger gyromagnetic ratio of the proton. Spectra then may be obtained when much less sample is available, and spectral throughput is very high. Since materials are dissolved, it makes no difference whether they are sticky, gummy, or dry solids. Finally, the availability of two - dimensional methods enables spectral properties to be defined not only based on chemical shifts but also in terms of structural connectivities.

5. E. I. Identification of peaks correlation by means of two-dimensional COSY spectra of the *sandarac* resin

^{1}H- and ^{13}C spectra of the *sandarac* resin (*Kremer*) are presented respectively on Figures 1 and 2.

The ^{1}H spectrum of the resin is dominated by the saturated hydrocarbon alkane region (δ 0.6 - 2.0). In general, pimarane and abietane alkane regions have an undifferentiated envelope that forms the base for various sharp peaks that constitute the largest peaks in the spectrum. The resin sample from *Kremer* exhibits, on top of the envelope, three very large sets of peaks, centered at about δ 0.6, 0.8 and 1.2. The δ 1.2 set is the largest.

The region of alkanes with electron-withdrawing substituents such as double bonds and heteroatoms (δ 2.0 - 4.0) begins from the low-frequency end as part of the tail of the saturated alkane envelope and grades into separate peaks on the baseline. The *sandarac* shows three small shoulder peaks present at δ 2.1, 2.2, and 2.7 and one small, broad peak at the end of the alkane envelope at δ 2.5.

The alkene region is quite well pronounced and has peaks at δ 5.4, 5.8, and 6.3, with smaller peaks at δ 4.8, 5.1, and 5.6. The carbonyl region in general is less intense than the

alkene region, with significant peaks at δ 9.2 and 9.6, a group of peaks around δ 9.8, and bigger peaks at δ 10.

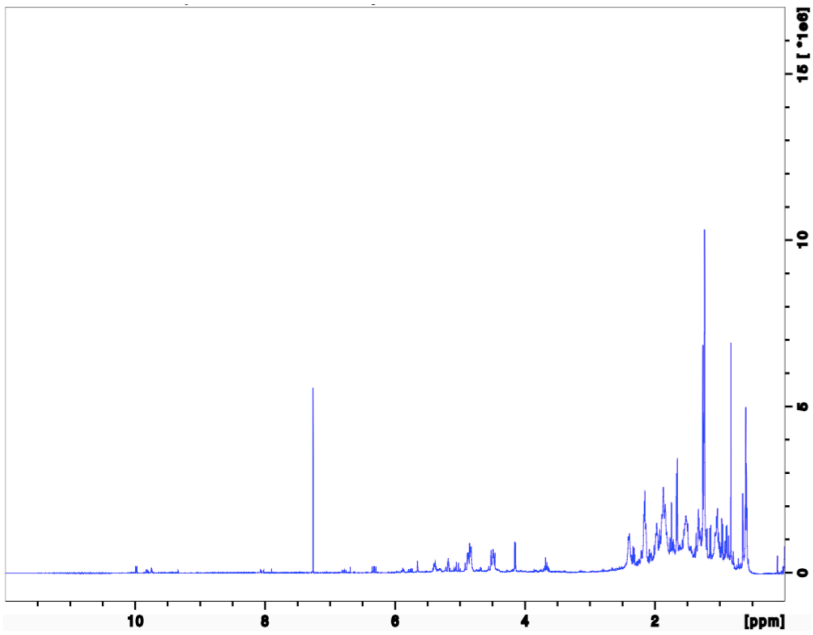

Figure 1. 500 MHz ^{1}H spectrum of the *sandarac* resin (*Kremer*) in $CDCl_3$.

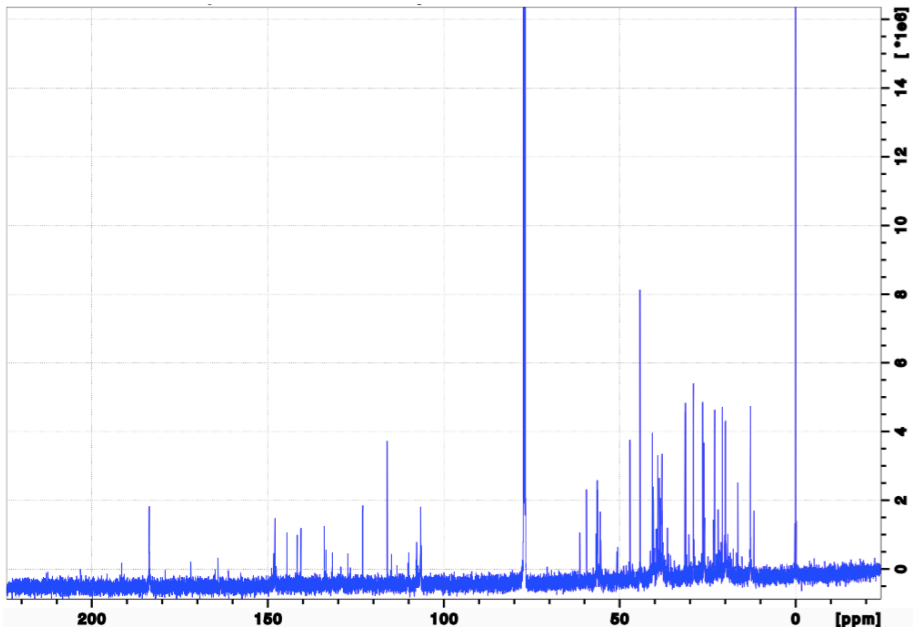

Figure 2. 500 MHz ^{13}C spectrum of the *sandarac* resin (*Kremer*) in $CDCl_3$.

The comparison of the *sandarac* resin and communic acid spectra reveals the presence of all resonances of the communic acid in the resin spectrum (Figure 3). Especially, well defined signal of double of doublets at δ 6.34.

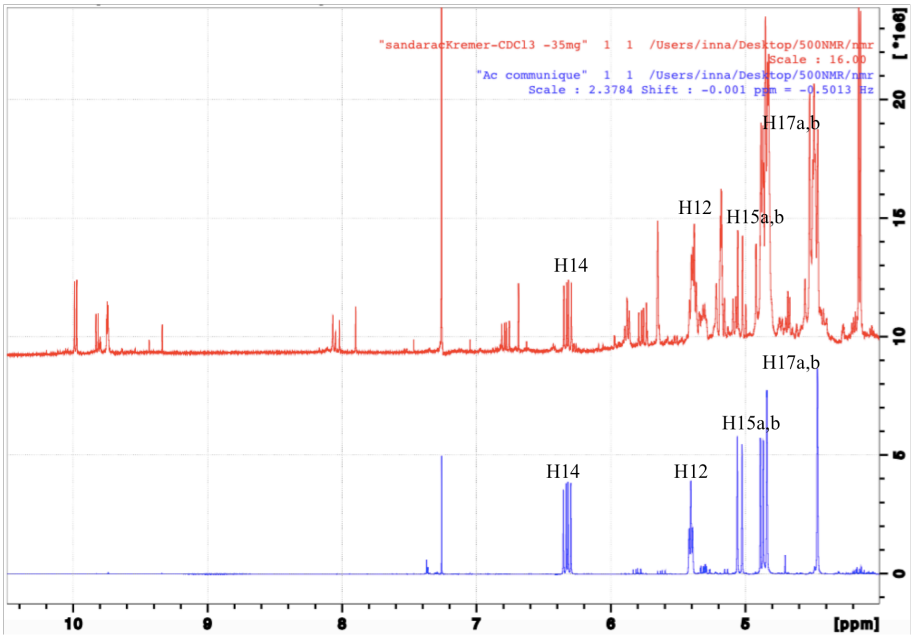

Figure 3. 500 MHz ^{13}C spectra of the *sandarac* resin (*Kremer*) and the communic acid in $CDCl_3$ (4 – 11 ppm).

There are three notable features to the ^{13}C spectrum: the carboxyl resonance of the communic acid at δ 184.2 is diagnostic of the *sandarac* Kremer, but there are no carbonyl resonances from aldehydes and ketones above δ 200. The most intense resonances are found in the saturated region, δ 0 – 60. These are from saturated carbons typical of terpenoid hydrocarbons. There are weaker resonances in the region in which saturated carbon that is substituted with electron-withdrawing groups such as oxygen functionalities (δ 60–110) resonates. The unsaturated region δ 100–160 contains resonances from carbons of double bonds. Singly substituted alkene carbons (C—HC=CH—C) resonate in the range δ 120–145, unsubstituted alkene carbons ($C=CH_2$) at δ ca. 110, and disubstituted alkene carbons (>C=C) at δ ca. 150.

The COSY spectra of the *sandarac* resin (*Kremer*) are rich in cross-peaks. Many of these occur within the saturated alkane region, between pairs of protons with chemical shifts between δ 0.5 and 2.7. Although many of these peaks no doubt represent important connectivities, we have chosen to ignore them diagnostically. The region forms an overlapping, almost continuous block of peaks. It is possible that cross-peaks may coincide without deriving from the same pairs of protons. Moreover, connectivities within saturated chains are less distinctive than others. Consequently, we have considered cross-peaks only of hydrogens shifted by electronegative groups (EWG), by alkenic protons, and by aromatic protons, within and between these groups and with saturated alkane hydrogens.

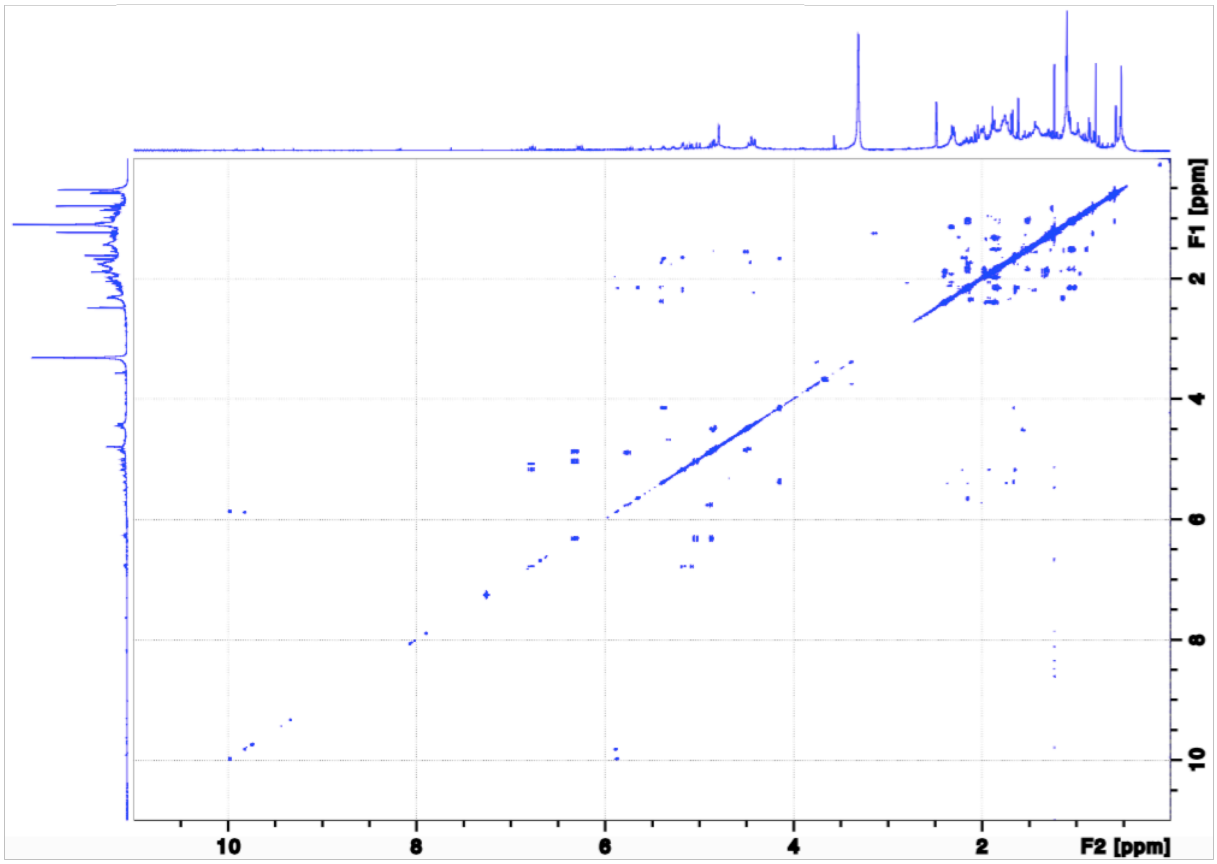

Figure 4. 500 MHz COSY spectrum of the *sandarac* resin (*Kremer*) in $CDCl_3$.

Several cross-peaks are found in the spectrum of *Kremer*: δ 1.3/2.7, 1.7/2.5, 2.4/4.7, 2.7/4.7, 6.6/4.5. Two peaks (1.3/2.7 and 6.6/4.5) are found in all species except *La Marchande de Couleurs*. Several peaks are unique to the spectrum of *Kremer*: δ 1.3/4.9, 1.3/3.7, and 2.5/5.6.

5. E. II. Comparison of ^{1}H, ^{13}C liquid-state NMR spectra of the sandarac resin from different suppliers (from *Kremer, Okhra, Color Rare, La Marchande de Couleurs, L'Atelier Montessori, Hevea*)

In order to find out the qualitative differences among different *sandaracs* and to correlate these results with the comparative analyses of *sandaracs* by GC-MS and ^{13}C solid-state NMR, the *sandarac* resin from six different suppliers (from *Kremer, Okhra, Color Rare, La Marchande de Couleurs, L'Atelier Montessori, Hevea*) was analysed and compared by ^{1}H, ^{13}C liquid-state NMR.

The Figure 5 illustrates the comparative ^{1}H spectra for all six species. Five of the analysed resins have very similar ^{1}H spectra (*Kremer, Okhra, Color Rare, L'Atelier Montessori, Hevea*).

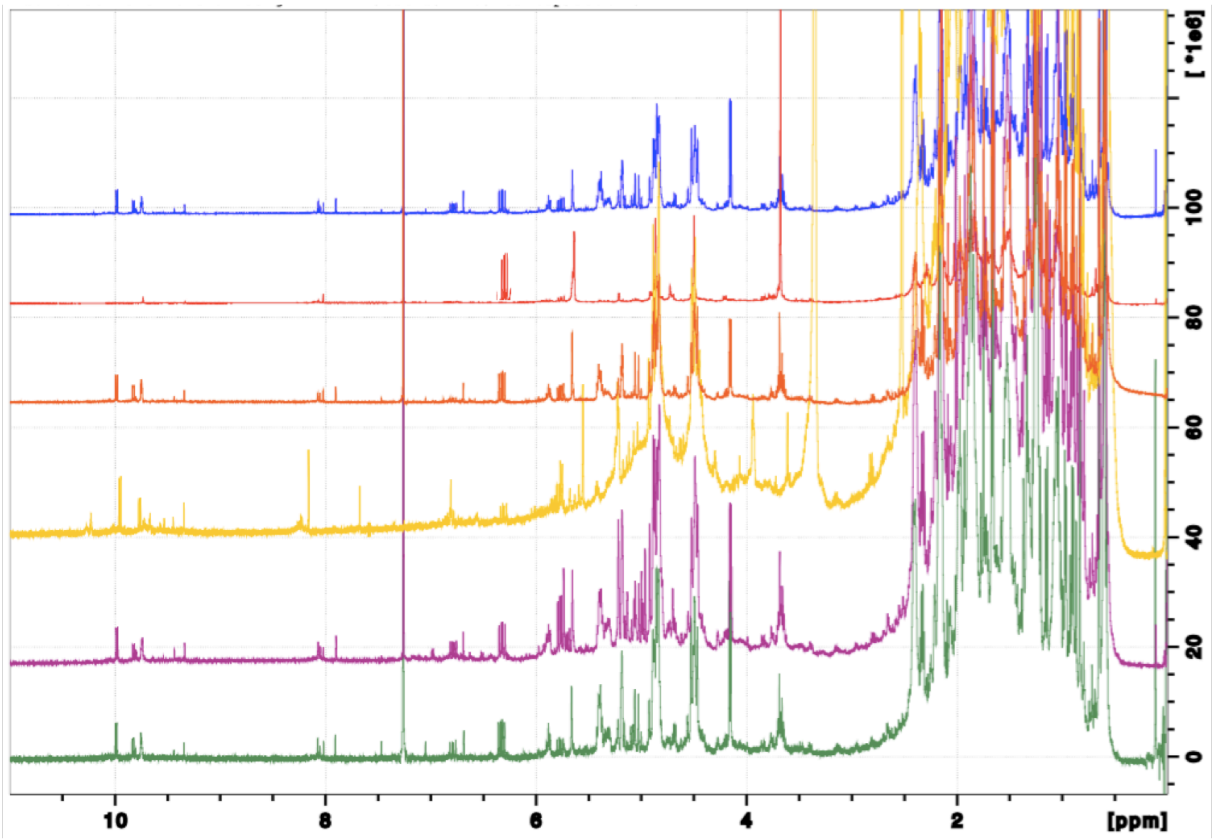

Figure 5. 500 MHz ^{1}H spectra of the *sandarac* resin (*Kremer* (blue), *Okhra* (yellow), *Color Rare* (green), *La Marchande de Couleurs* (red), *L'Atelier Montessori* (orange), *Hevea* (purple) in $CDCl_3$.

Several specific 1D peaks are found throughout all the species of the *sandarac*. In the saturated region, the three large groups of peaks at δ 0.6-0.9, 1.1-1.3, and 1.5-1.7 are present in almost every species, that at δ 1.5-1.7 lacking only in *La Marchande de Couleurs*. The peak at δ 0.8 is present in all but *La Marchande de Couleurs.* A fourth set of peaks found around at δ 1.8 is present in all species, including *La Marchande de Couleurs*.

The alkene region has four highly conserved groups of resonances at δ 4.8, 5.1-5.4, and 5.8. The peak at δ 4.9 is absent in two spectra from *Okhra* and *La Marchande de Couleurs*. That at δ 5.1-5.2 is present in five species. That at δ 5.3-5.4 is absent in only two spectra, both from *Colore Rare* and *La Marchande de Couleurs*.

The aromatic region is nearly identical for every species of the *sandarac*. Three important groups of peaks at δ 6.3, 7.1 and 7.5 are almost universal in all species (one such peak is missing in *La Marchande de Couleurs*). Two small peaks at δ 7.9 and 8.1 are present in most species.

Almost a dozen COSY cross-peaks are found in nearly all the *sandarac* samples. We omitted all cross-peaks between pairs of peaks in the saturated region, with a cutoff at about δ 2.5. Within this rectangular block of cross-peaks, there are numerous overlaps, representing

ambiguous connectivities between alkane neighbours. Cross-peaks outside the region, however, are well defined, including between saturated alkanes and those with electron-withdrawing groups (EWG). Four such cross-peaks are found at 1.3/2.9, 1.4/2.7, 1.8/2.7, and 2.2/2.8. There are two frequently observed cross-peaks between saturated protons and alkenes, at 1.7/5.5 and 2.8/4.7. A cross-peak between two alkene protons at 4.8/5.8 is highly conserved, as are two cross-peaks between aromatic protons at 4.9/6.3 and 7.0/7.2. Another aromatic cross-peak is observed somewhat less frequently at 7.3/8.7.

Although there are a few peaks that differ, the COSY spectra of the analysed samples are very similar, except the spectrum of *La Marchande de Couleurs*.

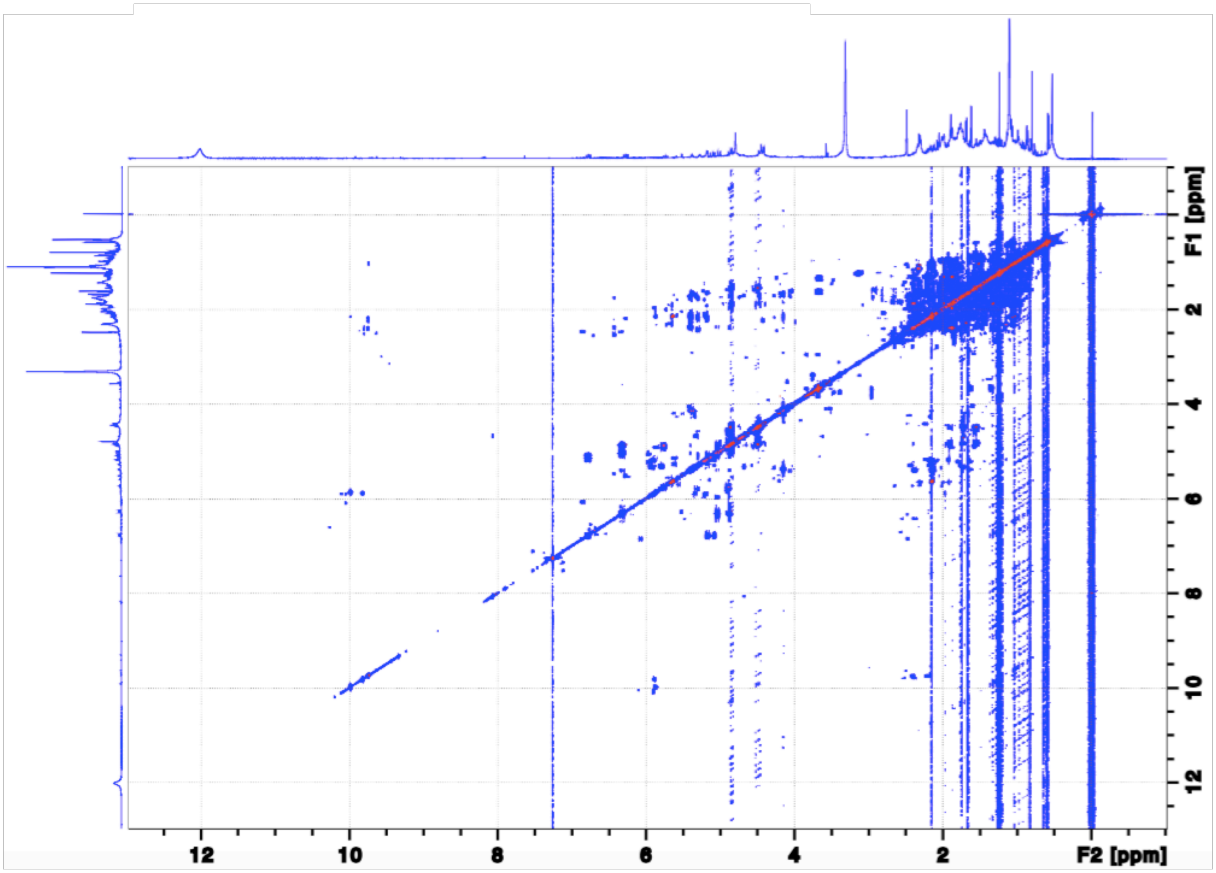

Figure 6. 500 MHz COSY spectra of the *sandarac* resin (*Kremer* (blue), *Okhra* (yellow), *Color Rare* (green), *La Marchande de Couleurs* (red), *L'Atelier Montessori* (orange), *Hevea* (purple) in $CDCl_3$.

Okhra. Its ^1H spectrum very closely resembles those of *Kremer*. Indeed, there is an almost peak for peak coincidence (Figure 7). The alkene region for *Okhra* is of smaller intensity in comparance with *Kremer*, but the patterns are identical. The aromatic region is the same within both samples. One modest difference between the spectrum of *Okhra* and *Kremer* is the low intensity of the trio of peaks near δ 0.9 and the group of peaks near δ 1.0.

Resonances from saturated alkanes dominate the spectra of the *sandarac* from *Okhra*. The alkane envelope is topped by three prominent sets of peaks respectively centered approximately at δ 0.9, 1.2, and 1.5. The sets around δ 0.9 and 1.6, however, have more contributing peaks than for *Kremer*. Whereas the spectra of *Kremer* tend to have well-defined maxima in these regions, those of the *Okhra* have several peaks of similar intensity. The EWG region also is different. The *Kremer* spectra contained two small peaks in this region at δ 2.2 and 2.4 and a broad peak at δ 2.1. The *Okhra* spectra do not contain the same peak at δ 2.1, but have a number of additional peaks, from δ 2.0 to 2.4. The spectra of *Okhra* also have an extremely intense peak at δ 3.4, not present in the spectrum of *Kremer*. The spectra of *Okhra* species have a series of modes peaks in the alkene region from δ 4.4 to 6.5. *Okhra* exhibits a significant, sharp peak at δ 6.7 (alkenic or aromatic), seen only in this species. The aromatic region is of comparable intensity to that of the alkenic regions, in contrast to *Kremer*. Although of stronger intensity, the aromatic region of the *Okhra* is almost identical to those of *Kremer* samples, implying nearly identical aromatic structures in both lumps.

Numerous COSY cross-peaks are common to both Kremer and Okhra species: 1.2/2.7, 1.5/2.9, 2.0/5.3, 1.9/2.1, 2.2/5.6, 2.5/2.7, 4.9/5.2 and 6.7/6.9.

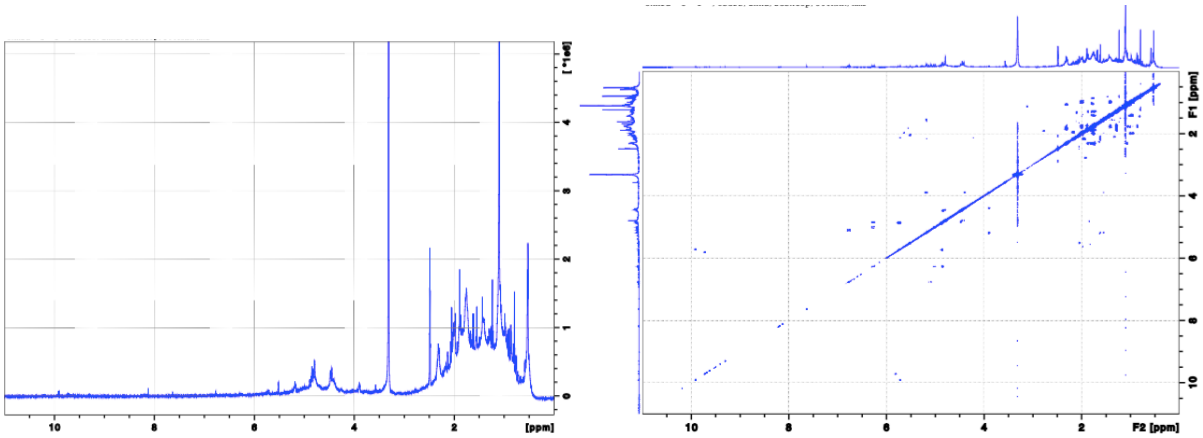

Figure 7. 500 MHz ^{1}H spectrum (left) and COSY spectrum (right) of *Okhra*.

Color Rare. This *sandarac* is characterized by a very well-pronounced alkene region, like the species from *Kremer* and *Okhra* (Figure 8). The aromatic region maintains the highly conserved pattern present in the two previously discussed samples. The alkane region of *Color Rare* most closely resembles that of *Kremer*. Although similar in the alkane and arene regions, the alkene region of this sample is much stronger than that of the others and contains a series of broad peaks at δ 3.3, 3.5, 3.6, 3.9, 5.5 and 5.6. Its broad peak in the EWG region at

δ 3.3 is found in none of the analyzed samples. The COSY spectra contain the standard *sandarac's* cross-peaks and the 2D spectra of the *Color Rare* show only minor differences.

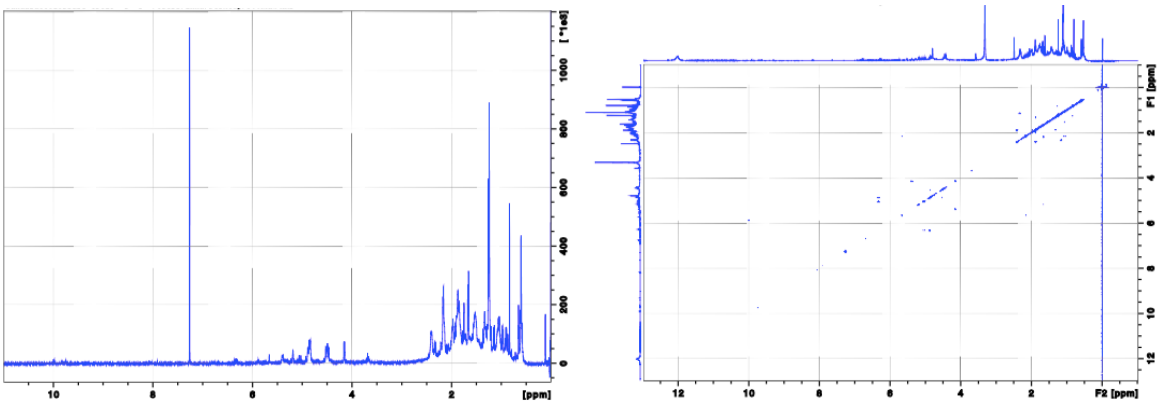

Figure 8. 500 MHz ^{1}H spectrum (left) and COSY spectrum (right) of *Color Rare*.

La Marchande de Couleurs. The samples from *La Marchande de Couleurs* exhibited an unusual physical characteristic. In contrast to samples from the other *sandaracs*, these samples produced slightly cloudy solutions in chloroform. The cloudy material settled, aggregated, and floated to the top of the tube but did not represent a large proportion of the total sample.

The alkane region as usual is dominated by the large set of peaks at δ ca. 1.2, as illustrated in Figure 9 for *La Marchande de Couleurs*. When the entire alkane region is considered, the spectra of *La Marchande de Couleurs* are similar to the rest five species. The resonances at δ ca. 0.9 for *La Marchande de Couleurs* consist of three peaks, whereas remaining five samples have more. *La Marchande de Couleurs* has a large peak at δ 1.1 and then tails to the baseline by δ 2.5 with no further prominent peaks. *La Marchande de Couleurs* exhibit a broad peak at δ 1.8, which is found neither in *Kremer* nor in any other examined species. The peak at δ 2.1 is shared by almost all the species. There are two important peaks in the EWG region, which exhibits a unique pair of singlets at δ 3.3 and 3.6, not present in other *sandaracs*.

The sample from *La Marchande de Couleurs* has significant alkene absorptions, in contrast to the rest of the species. *La Marchande de Couleurs* exhibits four peaks at δ 4.3, 4.9, 5.5 and 5.6. Though weaker, the singlet at δ 5.6 is also seen in the *Kremer* spectra and very weakly in the spectra of *Okhra*. The spectrum of *La Marchande de Couleurs* is distinguished by the absence of peaks in the region δ 6.5-7.2, which is populated in the spectra of the other three species (for example, a double of doublets at δ 6.7 and a pair of peaks at δ 6.9). The aromatic functionalities in *La Marchande de Couleurs* samples do not appear to be conserved, although it has a small but distinct probably aldehyde peak at δ 9.6.

The *La Marchande de Couleurs* COSY spectra exhibit several cross-peaks in common with *Kremer, Okhra, Color Rare, L'Atelier Montessori* and *Hevea*. The cross-peaks at 1.8/2.2, 2.1/2.5, and 5.0/5.8 are present in every species of these six samples. The large peak at 5.1/6.3 is present in the spectra of five of the six species, lacking only in *La Marchande de Couleurs*. Several peaks are unique to *La Marchande de Couleurs*, thus in principle, it may be distinguished from from all other species by the 2D spectra. The cross-peak at 4.4/4.9 results from the pair of singlets noted in the one-dimensional spectrum of *La Marchande de Couleurs.*

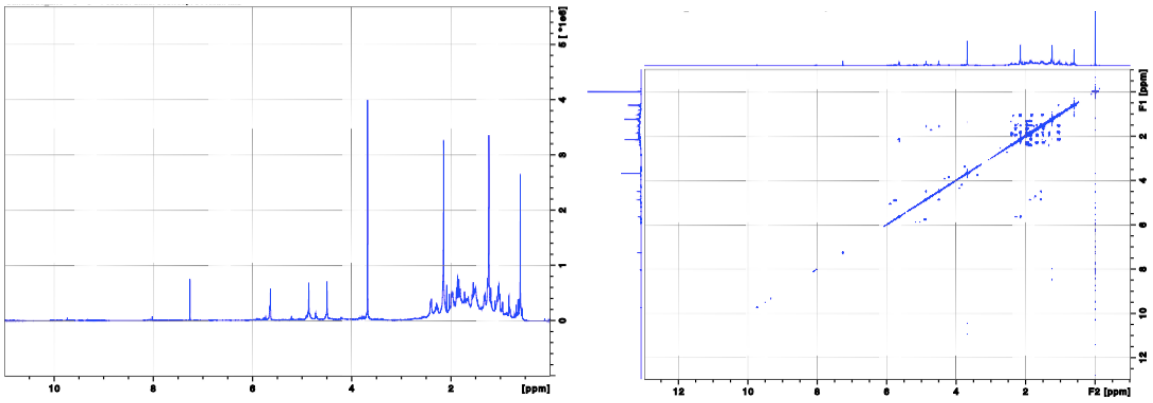

Figure 9. 500 MHz ^{1}H spectrum (left) and COSY spectrum (right) of *La Marchande de Couleurs*.

L'Atelier Montessori. This sample exhibits the same four peaks in the aromatic region as seen in all previous species, at δ 7.4, 7.8, 8.0 and 8.2 (Figure 10). The spectrum of *L'Atelier Montessori* has two small peaks at δ 6.9 and 7.1, also present in all other spectra. *L'Atelier Montessori* contains the broad peak at δ 2.8, which represents the end of the saturated alkane region (or the beginning of the EWG region) and has been observed in all species except *La Marchande de Couleurs*. Its spectra also contain a peak at δ 3.7, which varies from very weak to modest in *Kremer*, *Okhra* and *Color Rare*. As in all *sandarac* samples, the alkane region dominates the spectra of *L'Atelier Montessori*. The largest peak set as usual is at δ 1.2. There are differences in this region, particularly in the number of peaks at δ 0.7 and 1.0, but there is no discernible pattern. In many cases the region δ 1.8 - 2.5 forms a plateau of peaks. The envelope descends rapidly to nearly zero by δ 2.6, followed in all cases by the peak previously noted at δ 2.8.

The EWG region is generally empty, except for the peak common to the *sandarac* at δ 3.7. *L'Atelier Montessori* exhibits a strong, sharp peak at δ 3.7, which was seen in all of the species described thus far. A less broad version of this peak also was observed for *La Marchande de Couleurs*.

In general, the alkene region is well pronounced in the *L'Atelier Montessori*. One common pattern is the peak sets at δ 4.9 (at least four peaks of nearly equal intensity), δ 5.2 (a pair of peaks), δ 5.4 (a pair of peaks), and δ 5.8 (a singlet). These sets are common to other *sandarac* samples described thus far.

There are seven COSY cross-peaks that are common to all five species, except *La Marchande de Couleurs*: 1.2/2.7, 1.2/2.3, 1.7/5.3, 1.9/2.9, 2.5/5.4, 4.3/5.4 and 6.8/5.2. The peaks at 4.3/5.4 and 6.8/5.2 have been dominant across the most of the *sandarac's* spectra. Several other cross-peaks are found commonly here as well as in several other spectra: 0.7/1.4 in four (except *La Marchande de Couleurs* and *Color Rare*) and 9.8/6.1 in five (except *La Marchande de Couleurs*).

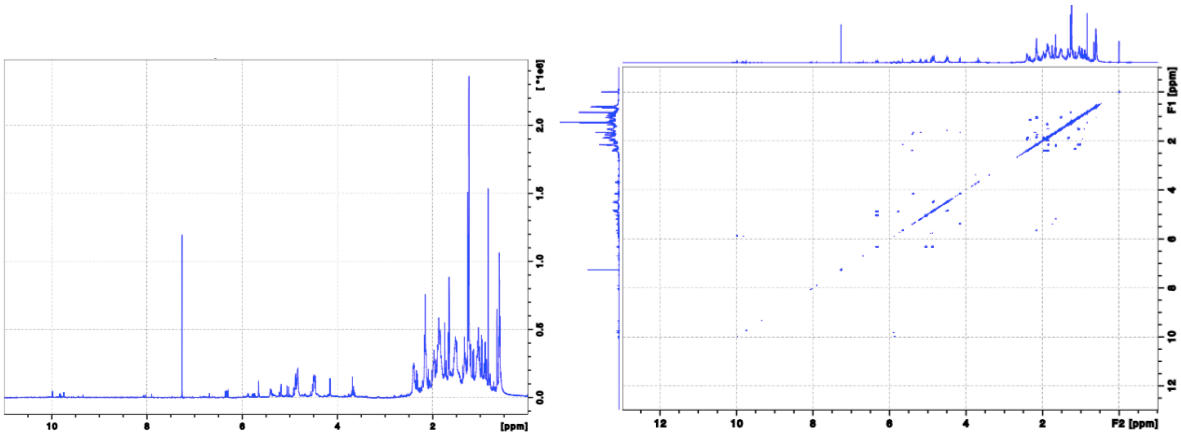

Figure 10. 500 MHz ^{1}H spectrum (left) and COSY spectrum (right) of *L'Atelier Montessori*.

Hevea. Its 1D ^{1}H spectrum very closely resembles those of *L'Atelier Montessori*. The alkenic regions of *Hevea* and of *L'Atelier Montessori* are almost identical.

The alkene region for *Hevea* is intermediate between the strong intensity of *Kremer* and the weak intensity of *Okhra*, but the patterns are identical. As in many of the species, the aromatic region is the same. One modest difference between the spectrum of *Hevea* and that of the other species is the low intensity of the trio of peaks near δ 0.2 and the group of peaks near δ 0.9.

The 2D cross-peaks observed for *Hevea* in general are those that are highly conserved throughout the *sandaracs*. There are no unique cross-peaks. Most of the nine observed cross-peaks are found in nearly all the six spectra. Only 1.7/ 5.3 and 5.2/5.9 are missing.

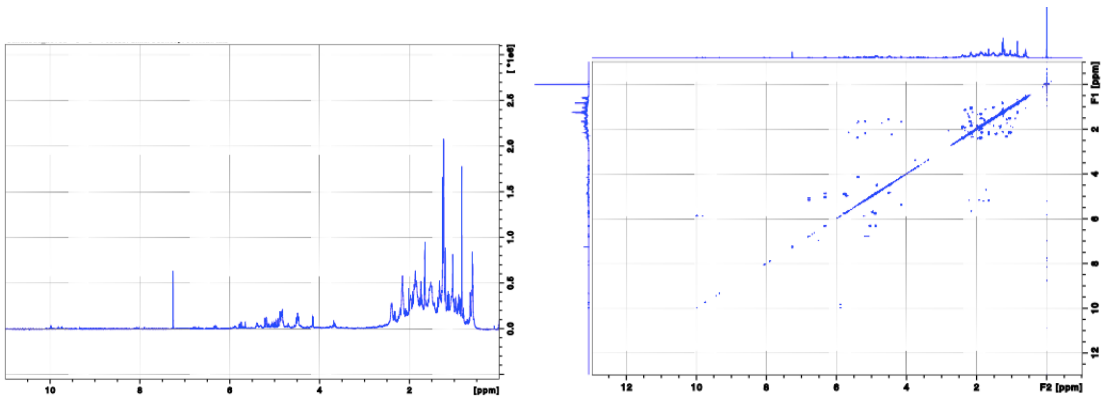

Figure 11. 500 MHz ^{1}H spectrum (left) and COSY spectrum (right) of *Hevea*.

Conclusion

To conclude, several analytical methods were accomplished in order to define the molecular organization of the commercial *sandarac* resin and its main component communic acid. While other research groups already studied the diterpenoid part of the resin, the polymer part was not analyzed by non-destructive methods yet. The only method applied to the analysis of the reticulated fraction of the *sandarac* resin was the pyrolysis, which is a destructive technique. Pyrolytic treatment of the reticulated sample breaks the polymer and leaves fragments, such as bicyclic acids without a side chain, that could possibly come from any original compound. Thus, in this study we applied several non-destructive methods, such as MALDI-TOF, ESI-Orbitrap, liquid- and solid-state NMR, for the analysis of polymerized fraction of the resin. IRCP pulse sequence in solid-state NMR was particularly useful in revealing the rigid character of the sample as a whole. MALDI-TOF and ESI-Orbitrap have shown the polymer massif characterized by several clusters.

The deeper overview of the results obtained by the analytical methods applied is given in the next chapter.

5. F. References

1. Dietemann P (2003) Towards More Stable Natural Resin Varnishes for Paintings. The Aging of Triterpenoid Resins and Varnishes.
2. Daher C, Pari C, Le Hô AS, Bellot-Gurlet L, Échard JP (2010) A joint use of Raman and infrared spectroscopies for the identification of natural organic media used in ancient varnishes. J. Raman Spectrosc. 41: 1494–1499.
3. Laroche MF (2007) Hemisynthese de meroterpenes issus de dichrostachys cinerea.
4. Azémard C, Vieillescazes C, Ménager M (2014) Effect of photodegradation on the identification of natural varnishes by FT-IR spectroscopy. Microchem J. 112: 137–149.
5. Silverstein RM, Webster FX (1998) Spectrometric Identification of Organic Compounds. John Wiley & Sons: New York.
6. Kwan EE, Huang SG (2008) Structural Elucidation with NMR Spectroscopy: Practical Strategies for Organic Chemists. Eur. J. Org. Chem. 2671–2688.
7. Feller RL (1994) Accelerated Aging. Photochemical and Thermal Aspects. Michigan.
8. Mellott MB, Searcy K, Pishko MV (2001) Release of protein from highly cross-linked hydrogels of poly(ethyleneglycol) diacrylate fabricated by UV polymerization. Biomaterials. 22: 929-941.
9. Christian Decker. The Use of UV Irradiation in Polymerization. Polymer International 45 133-141.
10. de la Rie ER (1988) Photochemical and Thermal Degradation of Films of Dammar Resin. Studies in Conservation, 33 (2): 53-70.
11. Pastorova I, Van der Berg KJ, Boon JJ, Verhoeven JW (1997) Analysis of oxidised diterpenoid acids using thermally assisted methylation with TMAH. J Anal Appl Pyrolysis. 43:41–57.
12. Dietemann P, Higgitt C, Kalin M, Edelmann MJ, Knochenmuss R, Zenobi R (2009) Ageing and yellowing of triterpenoid resin varnishes - Influence of aging conditions and resin composition. Journal of Cultural Heritage. 10: 30-40.
13. Dietemanna P, Edelmanna MJ, Meisterhansb C, Pfeiffera C, Zumbühlc S, Knochenmussa, Zenobia RR (2000) Artificial Photoaging of Triterpenes Studied by Graphite-Assisted Laser Desorption/Ionization Mass Spectrometry. Helvetica Chimica Acta. 83: 1766 - 1777.
14. Romero-Noguera J, Martín-Sánchez I, Doménech-Carbó MT, Osete-Cortina L, López-Miras MM, Bolívar-Galiano F (2014) Analytical characterisation of the biodeterioration

of diterpenoid labdanic varnishes used in pictorial techniques: Sandarac and Manila copal. International Biodeterioration & Biodegradation. 90: 99-105.

15. Clifford DJ, Hatcher PG (1995) Structural transformations of polylabdanoid resinites during maturation. Org. Geochem. 23 (5): 407-418.
16. Scalarone D, Lazzari M, Chiantore O (2003) Ageing behaviour and analytical pyrolysis characterisation of diterpenic resins used as art materials: Manila copal and sandarac. J. Anal. Appl. Pyrolysis. 68 – 69: 115 – 136.
17. Lakshmi Hima Bindu MR, Angala Parameswari S, Gopinath C (2013) A Review on GC-MS and Method Development and Validation. International Journal of Pharmaceutical Quality Assurance. 4 (3): 42-51.
18. Marinach C, Papillon MC, Pepe C (2004) Identification of binding media in works of art by gas chromatography–mass spectrometry. Journal of Cultural Heritage. 5: 231–240.
19. Pastorova I, Van der Berg KJ, Boon JJ, Verhoeven JW (1997) Analysis of oxidised diterpenoid acids using thermally assisted methylation with TMAH. Journal of Analytical and Applied Pyrolysis. 43: 41–57.
20. Osete-Cortina L, Doménech-Carbo MT (2005) Analytical characterization of diterpenoid resins present in pictorial varnishes using pyrolysis–gas chromatography–mass spectrometry with on line trimethylsilylation. Journal of Chromatography A. 1065: 265–278.
21. Berg KJ van den, Boon JJ, Pastorova I, Spetter LFM (2000) Mass spectrometric methodology for the analysis of highly oxidized diterpenoid acids in Old Master paintings. J. Mass Spectrom. 35: 512–533.
22. Kutnink MA, Hawkes WC, Schaus EE, Omaye ST (1987) An Internal Standard Method for the Unattended High-Performance Liquid Chromatographic Analysis of Ascorbic Acid in Blood Components. Analytical Biochemistry. 166: 424 – 430.
23. Armenini GB (1977) On the true precepts of the art of painting. Ayer Publishing.
24. Merrifield MP (1849) Medieval and Renaissance treatises on the arts of painting: original texts with English translations.
25. Cennini C, Tambroni G (1844) A treatise on painting. Lumley.
26. Klaas Jan van den Berg. Analysis of diterpenoid resins and polymers in paint media and varnishes with an atlas of mass spectra.
27. Colombini MP, Modugno F (2009) Organic Mass Spectrometry in Art and Archaeology. Wiley.

28. Vahur S, Teearu A, Haljasorg T, Burk P, Leito I, Kaljurand I (2012) Analysis of dammar resin with MALDI-FT-ICR-MS and APCI-FT-ICR-MS. J Mass Spectrom. 47(3): 392-409.
29. Zenobi R, Knochenmuss R (1998) Ion formation in MALDI mass spectrometry. Mass Spectrom. Rev. 17: 337.
30. Zumbul S, Knochenmuss R, Wu1lfert S, Dubois F, Dale MJ, Zenobi R (1998) A Graphite-Assisted Laser Desorption/Ionization Study of Light-Induced Aging in Triterpene Dammar and Mastic Varnishes. Anal. Chem. 70: 707-715.
31. Lambert JB, Wu Y, Santiago-Blay JA (2005) Taxonomic and Chemical Relationships Revealed by Nuclear Magnetic Resonance Spectra of Plant Exudates. J. Nat. Prod. 68 (5): 635–648.
32. Bennett AE, Rienstra CM, Auger M, Lakshmi KV, Griffin RG (1995) Heteronuclear decoupling in rotating solids. J. Chem. Phys. 103 (16): 6951 – 6958.
33. Massiot D, Fayon F, Capron M, King I, Le Calve S, Alonso B, Durand JO, Bujoli B, Gan G, Hoatson G (2002) Modelling one- and two-dimensional solid-state NMR spectra Magn. Reson. Chem. 40: 70–76.
34. Alemany LB, Grant DM, Pugmire RJ, Alger TD, Zilm KW (1983) Cross Polarization and Magic Angle Sample Spinning NMR Spectra of Model Organic Compounds. 1. Highly Protonated Molecules J. Am. Chem. SOC. 105 (8): 2133-2141.
35. Baccile N, Laurent G, Babonneau F, Fayon F, Titirici MM, Antonietti M (2009) Structural Characterization of Hydrothermal Carbon Spheres by Advanced Solid-State MAS ^{13}C NMR Investigations. J. Phys. Chem. C. 113: 9644–9654.
36. Baccile N, Falco C, Titirici MM (2014) Characterization of biomass and its derived char using ^{13}C-solid state nuclear magnetic resonance. Green Chem. 16: 4839–4869.
37. Lambert JB, Wu Y, Santiago-Blay JA (2005) Taxonomic and Chemical Relationships Revealed by Nuclear Magnetic Resonance Spectra of Plant Exudates. Journal of Natural Products. 68 (5): 635–648.
38. Lambert JB, Wu Y, Santiago-Blay JA, Wuc Y, Levya AJ (2015) Examination of amber and related materials by NMR spectroscopy. J. Magn. Reson. Chem. 53: 2–8.
39. Spyros A (2016) Liquid-State NMR in Cultural Heritage and Archaeological Sciences. Springer International Publishing.

6. Discussion

6. A. Introduction

As previously mentioned the purpose of this study was to combine several analytical methods that would give a clear picture on the chemical composition of the *sandarac* resin that has been widely used throughout history for artistic purposes. Thus, in this chapter we discuss the usefulness of each analytical method applied for the molecular characterization of the *sandarac*, the necessity of each of them and in what extent these analytical approaches complement each other.

Additionally, a practical goal of this work is to give an overview on the commercial resin *sandarac* that is brought to market from different suppliers today. Thus, further in the chapter, a summary on the comparative analysis of different lamps of resins is provided. This information would be useful first of all for the artists who are the major potential clients of the resin suppliers.

And finally, a description of the varnish elaboration in the laboratory is given, which has shown the significance of having exclusively fresh resin, just recently extracted, as told in the recipe of the 'perfect varnish' by Leonardo da Vinci.

6. B. Synthesis on the analytical methods applied

The first goal of the presented PhD research work was to give a molecular characterization of the *sandarac* resin and its principal component communic acid. Thus, following this purpose, in this study several analytical approaches, comprising mass-spectrometric (GC-MS, MALDI-TOF and ESI-Orbitrap) and spectroscopic methods (FTIR, 1D, 2D ^{1}H and ^{13}C liquid- and solid-state NMR), were applied to the analysis of the resin of interest and its main compound. In order to give an insight on the communic acid polymerisation and to prove that this diterpenoid is responsible for the *sandarac* resin reticulation, the UV aged samples of freshly extracted communic acid were studied as well by FTIR, ESI-Orbitrap and liquid-state NMR analyses.

As mentioned in the Bibliography part the *sandarac* resin was recommended in many recipes for the varnish preparation, most of which included preliminary heating of the resin and then subsequent heating of the resin-solvent mixture as a whole. On this evidence, we

thought it would be informative as well to study the chemical modifications within the resin after its thermal treatment. Thus, thermally treated *sandarac* resin was analysed by GC-MS and compared to the analyses of non-heated resin.

The choice of the above listed methods of analyses is argumented by the following reasons. Analytical techniques, such as FTIR and GC-MS, are already well-established methods for the samples of resin nature. As told in the Bibliography part two main publications dedicated to the *sandarac* resin applied gas chromatography – mass spectrometry analysis as the most suitable and appropriate technique for this type of samples [1, 2].

On other hand, application of 'soft' ionization methods of mass-spectrometry for high molecular weight compounds is a relatively unstudied area for natural resin samples. Only two publications pioneered 'soft' ionization techniques for triterpenoid resins (dammar and mastic) [3, 4]. Thus, in this research we explored for the first time the possibility to apply these methods of analyses for diterpenoid resins.

Solid-state NMR analyses were widely applied to amber studies [5, 6], but fresh or commercial resins were not studied by this technique to our knowledge. So, NMR analyses with different pulse sequences applications, such as cross-polarization and IRCP technique, were evaluated in the view of its 'suitableness' for diterpenoid resin *sandarac*.

It is essential to specify that different analytical approaches are applied to samples in order to resolve the ambiguities in some points posing doubts or to get the final confirmation of the proposed structure/composition based on the previous analyses made [7]. Many analytical techniques require sample derivatization, which in its turn modifies a sample in the extent that comparison of results obtained by different analytical methods is no longer correct, because in reality different samples are being analyzed.

First of all, in our study, we analyzed isolated communic acid to get a full characterization of the compound. By means of 2D NMR the ambiguities with C5/C9 and C6/C7 assignments were resolved (Figure 1).

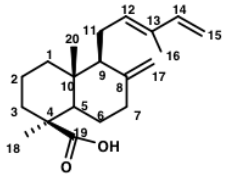

Figure 1. Communic acid.

Aged under UV samples of the communic acid were analysed by combination of mass-spectrometric and spectroscopic methods: ESI-Orbitrap, IR and liquid-state NMR spectroscopy.

IR analysis is a reliable approach as it does not require any sample modification. The IR spectrum of the aged communic acid has revealed the weakening of peaks corresponding to double bonds of the compound (Figure 1 in the chapter **4. D. I.**). Concretely, the intensity diminution of the band at 1606 cm^{-1}, indicating the prior engagement of the conjugated C = C bonds. This conversion of double bonds into saturated carbon chain according to the classical reaction of polymerisation (Figure 2) provoked respectively changes in the CH region (3200 - 2400) of the spectrum as also previously described in [8].

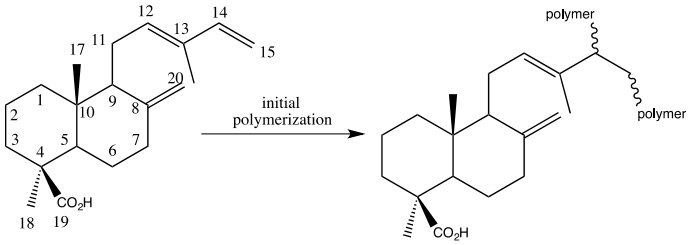

Figure 2. Polymerisation of communic acid.

Mass-spectrometric analysis of the aged communic acid by electrospray ionisation imposed two major requirements for the sample preparation: firstly, its solubilisation in the solvent; secondly, ionisation of the sample components in the ionisation chamber. The first requirement has been fulfilled, since prepared solutions were completely transparent and no formation of the precipitate was observed. The second demand is frequently a problem for all analyses of non-polar compounds and the formation of a polymer generally tends to reduce the polarity of the system [9]. Thus, the spectra obtained for the aged communic acid didn't show the formation of a polymer most likely because of the ionisation difficulties. Nevertheless, new signals corresponding to possible oxidations, such as O-atoms incorporation or simultaneous loss of H by allylic oxidation, have been detected up to m/z 364 in the commuic acid aged samples spectra obtained by ESI-Orbitrap (Figure 4 in the chapter **4. D. II.**).

ESI-Orbitrap analyses of the aged communic acid were followed by liquid-state NMR studies. The major difficulty that was met during these analyses was the poor solubility of the samples. This problem was aggravated as well by little quantities of the communic acid in hands, due to the low yields while the compound extraction. Among three tested deuterated

solvents ($CDCl_3$, DMSO, ethanol-d6) suitable for NMR analyses the most satisfactory solubility was reached with deuterated chloroform. As a result, the liquid-state NMR spectra, obtained for aged samples, have shown appearance of new peaks in the zone of carbons with sp^2–hybridisation and a significant complication of the saturated region of the spectrum. The fact to point out is that the non-aged communic acid is still present in the sample, meaning the conversion into the polymer was not complete. The incomplete conversion of the communic acid into its polymer might have been caused by insufficient time of irradiation or by the inhomogeneity of the layer exposed to UV light. Anyway, the traces of communic acid are still present in the commercial *sandarac* resin that was definitely stocked for long time.

After studies of non-aged and aged communic acid we pursued the analyses of chemical composition of the *sandarac* resin.

Primarily, the commercial *sandarac* resin has been analysed by mass-spectrometric methods. Based on the knowledge, that its composition can be formally divided into two parts, namely, free diterpenoids and reticulated fraction, two mass-spectrometric approaches have been chosen for the analysis of each part [1]. GC-MS was chosen as a classical method of analyses for resin samples already well recommended in the literature.

GC-MS is the analyses that require a derivatization of the sample, to produce a compound that has properties more amenable to a chromatography column. In this research a silylation was chosen as a type of derivatization reaction. For this kind of derivatization BSTFA (N,O-bis(trimethylsilyl)trifluoroacetamide) and trimethylsilyl chloride, as a catalyst, were used. The general reaction of the formation of trialkylsilyl derivatives is shown in the Figure 3 below.

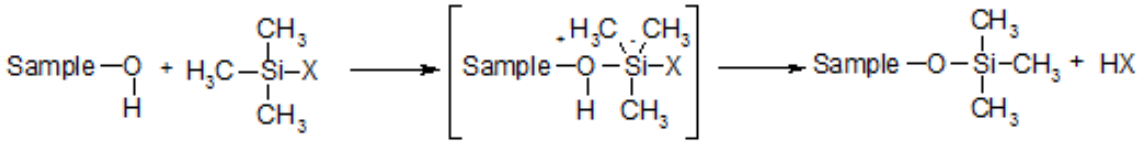

for BSTFA.

Figure 3. The general reaction of the formation of trialkylsilyl derivatives.

During silylation active hydrogen is replaced by an alkylsilyl group (most often trimethylsilyl (TMS)). Compared to their parent compounds, silyl derivatives generally are more volatile, less polar, and more thermally stable. In case of acid derivatization silyl derivatives are formed by the displacement of the active proton in –COOH group [10].

The reaction is viewed as a nucleophilic attack upon the silicon atom of the silyl donor, producing a bimolecular transition state (Figure 3). The silyl compound leaving group (X) must possess low basicity, the ability to stabilize a negative charge in the transition state, and little or no tendency for π (p-d) back bonding between itself and the silicon atom.

The ideal silyl compound leaving group (X) must be such that it is readily lost from the transition state during reaction, but possesses sufficient chemical stability in combination with the alkyl silyl group to allow long term storage of the derivatizing agent for use as required.

Thus, GC-MS analysis detects compounds that were initially derivatized, to precise our case, compounds that possess active hydrogen. So, it's important to mention that, based on the bibliographic background, some acidic components of the resins in nature have tendency to replace their carboxylic function proton by sodium or potassium [4]. That means, that because of this sodium content of the natural resin itself, the active protons of the acid function, that has to be modified by the derivatization are no longer available. The aspect of the proton substitution by sodium in nature has not been yet fully studied and no information on which compounds are more prone to this kind of substitution exists for the time being. But just the fact that it happens, allows concluding that, possibly, not all diterpenoids of the *sandarac* resin were analysed by the detector while GC-MS analyses.

Thereby, the proton substitution by sodium may explain several intensive peaks in the detection region of GC-MS that were nevertheless not detected by this method, but gave signals in spectra obtained by MALDI-TOF. The intense peaks at m/z 300, 301, 302 may come from the sodium adducts, which are highly prone to ionization (Figure 1 in the chapter **5. C. I. 5.**).

The qualitative analysis of the *sandarac* resin by GC-MS was followed by a quantitative study of the resin components. This was an important stage in understanding what is the actual part of the sample being analysed by GC-MS, in the view of its mass range limits. Thus, the application of the method of internal standard revealed that roughly 10-30% of the sample is brought up to the detector and analysed GC-MS.

As mentioned above, the high molecular part of the *sandarac* was analyzed by appropriate for such measurements techniques: MALDI – TOF and ESI-Orbitrap. The most important experimental requirement for both methods is the ionization of the sample. This might be sometimes problematic as these approaches are 'soft' types of ionization and easily ionize only polar polymers [11].

For the *sandarac* resin analyses the mass detection stopped at m/z 900 in case of MALDI-TOF and rose up to m/z 1100 for ESI-Orbitrap. It is highly possible that detected mass ranges are not limited to those figures, but the difficulties with ionization restrained the polymer detection in higher molecular weight ranges.

Further, the resin of interest was subjected to liquid- and solid- state NMR analyses. As with the aged communic acid, the solubility problem has come through for the commercial resin as well. However, in this case we were not limited by the quantity of resin, and good signal/noise ratios in the liquid-state NMR spectra have been reached by dissolution of 40 mg of the resin in $CDCl_3$.

As it was shown on ^1H NMR spectra in the Results part the signals of the communic acid can still be found, indicating that process of polymerisation doesn't happen within the whole sample. Apart from the peaks definitely corresponding to the communic acid, the peaks that are found in the downfield of the ^1H NMR spectra of the *sandarac* resin according to their chemical shifts would be corresponding to compounds with aldehyde or ketone functional groups. These peaks are singlets at 9.34 ppm and 9.74 ppm and two doublets at 9.82 ppm and 9.98 ppm (Figure 1 in the chapter **5. E. I.**). Among the diterpenoids identified by GC-MS, the dihydroagathalic acid is the only diterpenoid that possess the aldehyde group, the proton of which would easily give a peak in far deshielded region.

Finally, solid-state NMR analysis was accomplished to conclude the polymer nature of the major part of the *sandarac* resin. Solid-state NMR gives more representative insight on the sample, as the resin doesn't undergo any chemical modifications, meanwhile it loses greatly in the spectrum resolution. Due to IRCP approach the rigidity of the sample was approved. The IRCP method was particularly useful in revealing the reticulated structure of the aliphatic region, where a strong overlapping of signals is observed. As highlighted in the experimental part, IRCP experiments are generally selective to rigid CH_2 and CH sites as their normalized intensity signal tends, respectively, to a negative value (-1/3) or to 0 as a function of τ_i. On the contrary, the signal of mobile CH_3 and/or quaternary carbons remains positive [12]. Figure 7 in the chapter **5. D. I. 3.** shows IRCP spectra recorded at various inversion times in the aliphatic region; after 150 μs the most of the broad signals invert. This result signifies that the majority of the sample (meaning, the remaining 70% of the resin) is rigid and not mobile.

As a result, the molecular characterization of the *sandarac* resin has been studied by several analytical approaches (IR, GC-MS, MALDI-TOF, ESI-Orbitrap, RMN) that gave an

insight on the resin organization and brought up to the hypothesis that its one-third part is made up of free diterpenoid resins, while the rest is reticulated communic acid.

The following points give the summary of the impact of each analytical method:

- Qualitative GC-MS analyses permitted the identification of six free diterpenoid acids with labdane and pimarane skeletons of the *sandarac* resin.
- Quantification by the method of internal standard allowed defining that the non-polymerised fraction of the *sandarac* resin is less than 1/3 of the sample in total.
- MALDI-TOF and ESI-Orbitrap revealed the 'cluster-type' arrangement of the resin, showing the molecules in the state of oxidation within the cluster. MALDI – TOF approach brought to visualizing spectra with tree clusters of peaks in the m/z range of 300–900. For ESI-Orbitrap the presence of polymer was detected up to molecular weights 1300 Da.
- NMR analyses indicated the rigid nature of the resin, supporting the supposition that the rest 70% of the *sandarac* resin is of polymer character.

6. C. Hypothesis of the communic acid polymerization

Based on the results obtained for the UV irradiation of the communic acid a hypothesis that this diterpenoid polymerizes into the *sandarac* resin can be finally formulated. Indeed, ageing under UV light of the communic acid within a few days has shown how the IR spectrum of the communic acid approaches the spectrum of the *sandarac* resin. Moreover, liquid-state NMR spectrum of the aged communic acid also aims to repeat the shape of the spectrum of the *sandarac* resin. Thus, these experiments have brought us to a conclusion that it is sufficient to have a system of conjugated double bonds to provoke the modifications within the molecule of the diterpenoid.

The hypothesis that the *sandarac* resin is reticulated mainly because of the communic acid polymerization and because of its transformation into polycommunic acid (Figure 2) was already suggested by Scalarone team by means of the pyrolysis–GC-MS analyses. This method allowed to break the polymer due to the pyrolytic treatment and to observe the bicyclic acids (Figure 4) generated by loss of the unsaturated side chain of communic acid. These fragments are produced in a considerable amount and can be used as markers for the *sandarac* resin [1].

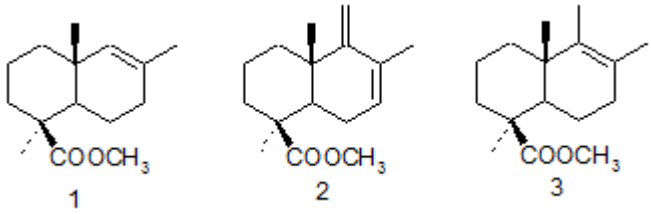

Figure 4. The bicyclic acids detected from the pyrolysis – GC-MS.

In our experiments with thermal treatment of the *sandarac* resin we also observed similar bicyclic acids what indicates that by heating the resin we break its more complicated part into less complex structures.

It is worth mentioning, that without light enhancement the communic acid is rather stable compound. Nevertheless, it was sufficient to expose it to UV light during a day, and a thin layer of the communic acid deposited onto glass microscopic slide became dark yellow in the region of the irradiation. This observation of the physical modification contributes into the theory of paintings yellowing, which concludes that the formation of the polymer enhances colour changing in artworks.

On the other hand, we have the results of ESI-Orbitrap analyses that demonstrated that the polymerization is not the only process going on while ageing the communic acid. Indeed, we were observing not only the formation of the dimmer in the ESI-Orbitrap spectrum of the aged communic acid, but many different peaks forming the clusters. Within each cluster we observed the oxidation processes that were concluded from the repetitive addition of oxygen. Moreover, hydrogen extraction was observed as well within a cluster, bringing us to a hypothesis that while ageing of the communic acid many different chemical processes are likely engaged.

Instead of observing a dimmer of the communic acid that is logically expected from the reaction of polymerization, in the ESI-Orbitrap spectrum we observe a highly saturated massif of peaks.

Thus, the global conclusion would be that the UV irradiation provokes not only polymerization of the communic acid, but many different oxidation and hydrogen extraction reactions. The complexity of the spectra obtained did not allow the identification of numerous compounds formed as a result of communic acid ageing.

Thus the clear mechanism of communic acid modification during its ageing could not be reproduced in the view of the complexity of the spectra obtained. So, the formation of a

polymer resulting from the communic acid ageing will rather stay in a form a hypothesis, than a final conclusion. UV irradiation studies of the communic acid in order to provoke its polymerization have brought to the general hypothesis that the communic acid is diterpenoid responsible for the resin reticulation.

6. D. Comparative studies of the *sandarac* resin from different suppliers

Another important part of the analyses accomplished in this research work is the comparison of different samples of the sandarac resin purchased from different resin suppliers (from *Kremer, Okhra, Color Rare, La Marchande de Couleurs, L'Atelier Montessori, Hevea*). As previously mentioned, this seemed necessary because of the great variability of the chemical content of the *sandarac* resin that existed in the literature [2, 13]. So, in the view of this background, the different *sandaracs* were compared in order to conclude how strongly differs the chemical content of the commercial resin from one supplier to another.

The differences in the chemical composition of the *sandarac* resin, remarked after bibliographic research, were shown mainly by the GC-MS analyses. In this study the comparison of different *sandarac* samples was made by GC-MS, liquid- and solid- state NMR.

The comparison of different *sandarac* samples was made by GC-MS qualitatively and quantitatively as well. Quantitative comparison revealed a remarkable similarity between resins purchased from *Kremer* and *Okhra*. Both of the samples demonstrated a low concentration of sandaracopimaric acid and communic acid, and meanwhile high ratio of agathic acid's derivatives. In the liquid-state NMR spectrum a low concentration of the communic acid would be characterized by a relatively weak intensity of double of doublets at 6.34 ppm. And indeed, this is observed in the liquid-state NMR spectra for these two species (Figure 5).

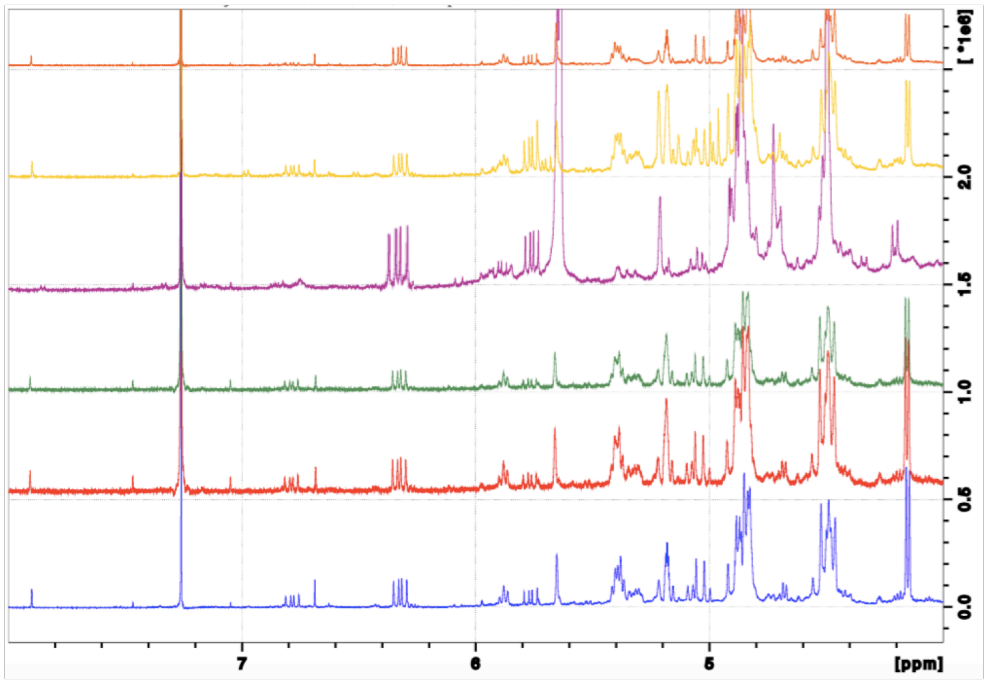

Figure 5. 500 MHz ^{1}H spectra of the *sandarac* resin (*Kremer* (blue), *Okhra* (red), *Color Rare* (green), *La Marchande de Couleurs* (purple), *L'Atelier Montessori* (yellow), *Hevea* (orange) in $CDCl_3$.

Kremer and *Okhra* showed the highest concentration of diterpenoid acids that reaches 30% in comparison with the other resins. This result was supported by IRCP experiment that showed spectra of these two samples to have slightly more mobile nature and a longer time of inversion for IRCP. As shown in the Figure 6, IRCP spectra recorded at the same inversion time τ_i = 40 μs for six samples have inverted peaks at 108.3 ppm for all resins except *Kremer* and *Okhra*.

The remaining samples from *Color Rare*, *L'Atelier Montessori* and *Hevea* revealed an average concentration of free diterpenoids around 20-25%. Their concentration of communic acid is even less than that of *Kremer* and *Okhra*. The resin from *Hevea* contains the least quantity of communic acid that is confirmed by the liquid-state NMR spectrum with a low intensity characteristic peak at 6.34 ppm (Figure 5).

The resin that is standing out of the rest comes from *La Marchande de Couleurs*. GC-MS analyses of this resin showed the presence of only 10% of diterpenoids, signifying the least content of free/mobile molecules in the resin and the shortest time of inversion in IRCP spectra. This result wasn't actually surprising as the physical properties of the *La Marchande de Couleurs* resin (colour, odour, size and shape of lumps) were somewhat different from the other five samples (Figure 12 in the chapter **5. A. II.**)

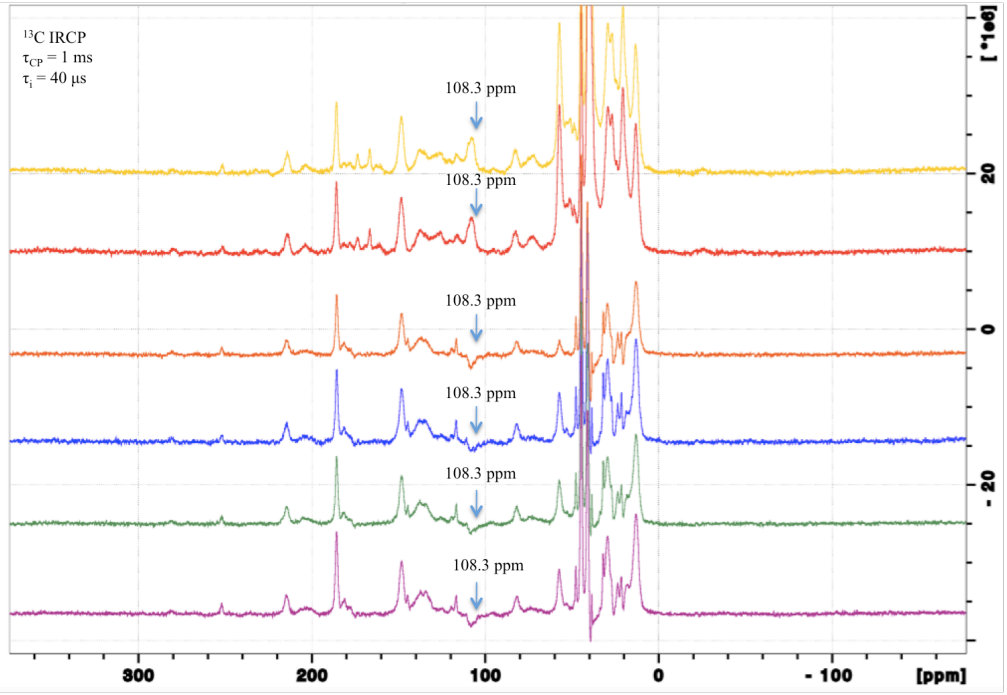

Figure 6. IRCP spectra recorded at τ_i = 40 µs for the sandarac resin (*Kremer* (red), *Okhra* (yellow), *Color Rare* (green), *La Marchande de Couleurs* (blue), *L'Atelier Montessori* (orange), *Hevea* (purple)

According to the hypothesis that is commonly supported in the literature the communic acid is the first diterpenoid to be responsible for the polymerisation of the *sandarac* resin. This brings to the conclusion that the *sandarac* from *La Marchande de Couleurs* is the freshest resin among the others, since its concentration of the communic acid is the highest among the rest resins. That means that the *sandarac* from this supplier still contains communic acid in an excessive quantity relatively to other analysed resins. From the spectroscopic point of view this relative abundance of communic acid is revealed in the ^{1}H liquid-state NMR spectrum by the intensive characteristic peak at 6,34 ppm giving double of doublets (Figure 5).

At first glance at the solid state NMR spectra of all six samples no great difference is remarked (Figure 8 in the chapter **5. D. II.**). Only close analysis of each part of the spectrum (region that is characteristic of sp^3 carbon atoms (0-100 ppm), indicating the presence of a broad distribution of CH_x (x = 1- 3) sites; region that is characteristic of sp^2 carbon atoms in C=C double bonds (100-160 ppm) with signals between 140 and 160 ppm, more specifically due to oxygen bound, O-C=C, sp^2 carbons; and finally, the region of C=O groups in either carboxylic acid moieties (175 ppm) or ketones and aldehydes (200-220 ppm) resonates (170-225 ppm)) reveals the minor differences between the samples. Indeed, the quantitative GC-MS analyses have shown that free diterpenoid molecules dominate only 30% at maximum of

the resin sample. Based only on this fact we could already suppose that the remaining and the major part of the sample is rigid, meaning has a polymer nature. This hypothesis is supported by the inversion times τ_i for the IRCP spectra, which are short enough to conclude that the overall sample composition has rigid character. Thus, the qualitative and quantitative GC-MS analyses along with liquid- and solid-state NMR analyses are in good concordance with each other.

GC-MS and NMR analyses are also in satisfactory agreement with the results showed by MALDI-TOF and ESI-Orbitrap, although a possibility remains that the difficulties with ionization of the polymer didn't allow going higher in the mass range.

Thus this comparative study of different lumps of resin has brought us to such questions as:

- Is *Okhra* supplied by the *sandarac* from *Kremer* in view of their molecular composition similarity?
- Is the *sandarac* from *La Marchande de Couleurs* the real resin from *Tetraclinis articulata* and not coming from the other conifer?
- Is the *sandarac* from *La Marchande de Couleurs* was stored in better conditions in terms of keeping the resin fresh as long as possible since its concentration of the communic acid is the highest among the rest?

Anyway, to answer these questions we would need to go back to the origin of the resins supplied and to obtain their definite botanical references.

6. E. The elaboration of the varnish based on the *sandarac* resin

Based on the background obtained from the analyses of the *sandarac* resin and its principal component communic acid we return to the applicative side of this research – the recipe of Leonardo da Vinci from his collection of writings 'A Treatise on Painting'. Thus several attempts were made to elaborate a varnish based on the commercial *sandarac* resin and to reveal the importance of extracting a fresh resin, as indicated in the recipe.

In order to analyse a natural varnish at first it was necessary to develop a model varnish from recipes found in specialized books and manuscripts. As mentioned before, there are many recipes and these often include mixtures of several resins and media [14 - 17]. We have chosen to elaborate a varnish comprising only one resin *sandarac* and one medium at once. The two types of varnish (alcoholic and fatty) were developed, when possible,

according to the recipes inspired by the manuscripts found and given by technical art historians. Thus, we have adopted technique of the laboratory: the heating plate, suitable glassware, and precise measurements. The heating was carried below the boiling points of the components to allow maximum dissolution while avoiding any loss of solvent (Tb (ethanol) = 79 °C, Tb (linseed oil) = 316 °C).

Preparation of ethanol and linseed oil - varnishes based on the *sandarac* resin

As previously described, the resin has to be solubilised in a solvent to form a varnish. The oil varnishes (so-called 'fat') require heating to allow the dissolution of the resin. If a polar solvent replaces the oil, such as ethanol, the melting of the resin is no more and so-called 'lean' varnish is produced.

Initial tests allowed specifying the protocol of varnish preparation. The *sandarac* resin couldn't be completely dissolved in linseed oil, despite of the fact that many recipes describe 'fat' varnishes based on the *sandarac*. Oppositely, the *sandarac* resin permits to obtain a homogeneous and transparent varnish if the ethanol is used as a solvent.

Nevertheless, besides the analysis of the *sandarac* varnish based on ethanol, the *sandarac* varnish based on oil was studied as well, in order to conclude if there is a partial solubility of the resin in the linseed oil. Two procedures were tried to elaborate the 'fat' varnish: in the first trial 5 gr of the *sandarac* resin (*Kremer*) were first crushed in a mortar and placed in a beaker. 20 ml of the linseed oil (Laverdure) were then added, the whole was heated to 100 °C and kept under manual stirring. The heating time was maintained during one hour. The varnish obtained was then filtered in order to separate the precipitate that didn't dissolve and to remove any impurities.

In the second attempt to obtain oil-based *sandarac* varnish, 5 gr of the *sandarac* resin (*Kremer*) were first heated in the beaker at 100 °C in order to melt the resin. Then, 20 ml of the linseed oil (Laverdure) were then added, the whole was heated to 100 °C and kept under manual stirring. The heating time was maintained during one hour. The varnish obtained was then filtered in order to separate the precipitate that didn't dissolve and to remove any impurities. The precipitate that was separated from the oil was very abundant indicating prior to IR analyses that no dissolution of the resin in the oil occurred.

To prepare alcohol-based varnish, 5 gr of the *sandarac* resin (*Kremer*) were first crushed in a mortar and placed in a beaker, to which 20 ml of ethanol (+99% Aldrich) were added while manual stirring. The varnish obtained was then filtered to remove any impurities.

Observations

The only varnish based on the *sandarac* resin that showed the transparency and homogeneity is the alcohol varnish (Figure 7). With the given resin concentration, the ethanol varnish is easily steered and spread, lacking viscosity.

Although, none of the optimised methods for 'fat' varnish preparation led to a complete dissolution of the *sandarac*, the second procedure demonstrated better homogeneity of the resin-oil mixture. Thus, the latest sample was analysed by FTIR further.

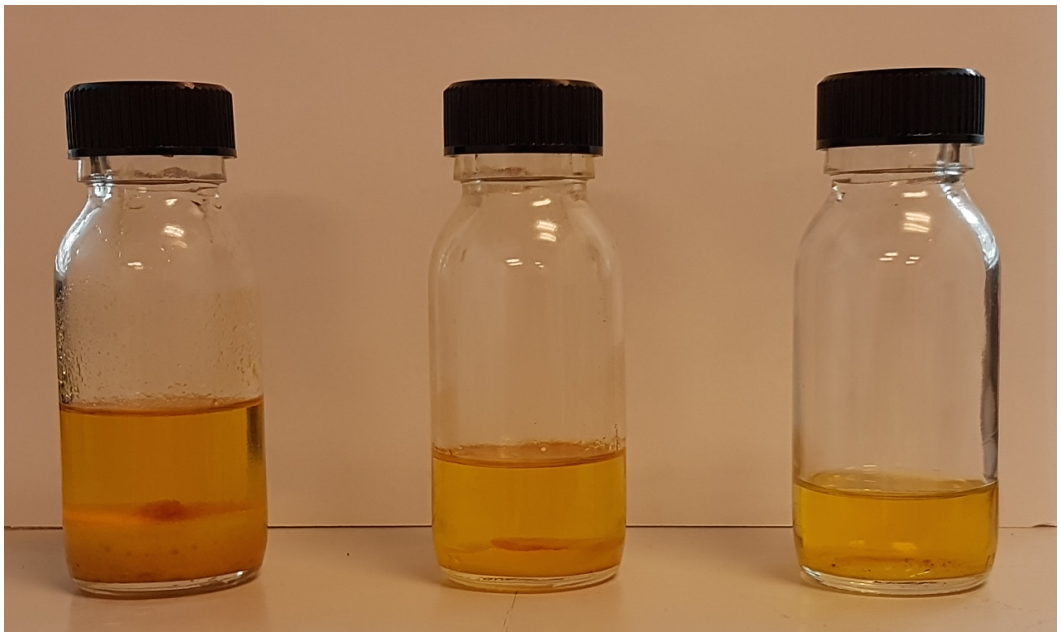

Figure 7. Oil – sandarac varnishes (prepared by two different methods, see text) and ethanol – sandarac varnish (from left to right).

To explain the specific properties of each preparation, we then sought to characterize their chemical nature, mainly by infrared spectroscopy.

Since our samples are liquid or doughy, the required contact between the ATR crystal and the sample is obtained without the additional pressure.

The measurements are carried out at ambient temperature on a Spectrum 2000 spectrometer from Perkin Elmer. For each preparation, 3 spectra of 20 scans are acquired, with a spectral resolution of 8 cm^{-1}.

The analyses by infrared spectroscopy allowed us to verify the nature of the products formed and the possible reactions that may have taken place during the mixtures: oil/ resin/ alcohol.

The spectra obtained by FTIR on the *sandarac* varnishes (one with linseed oil and the other with ethanol) are shown respectively in Figure 8 and 9.

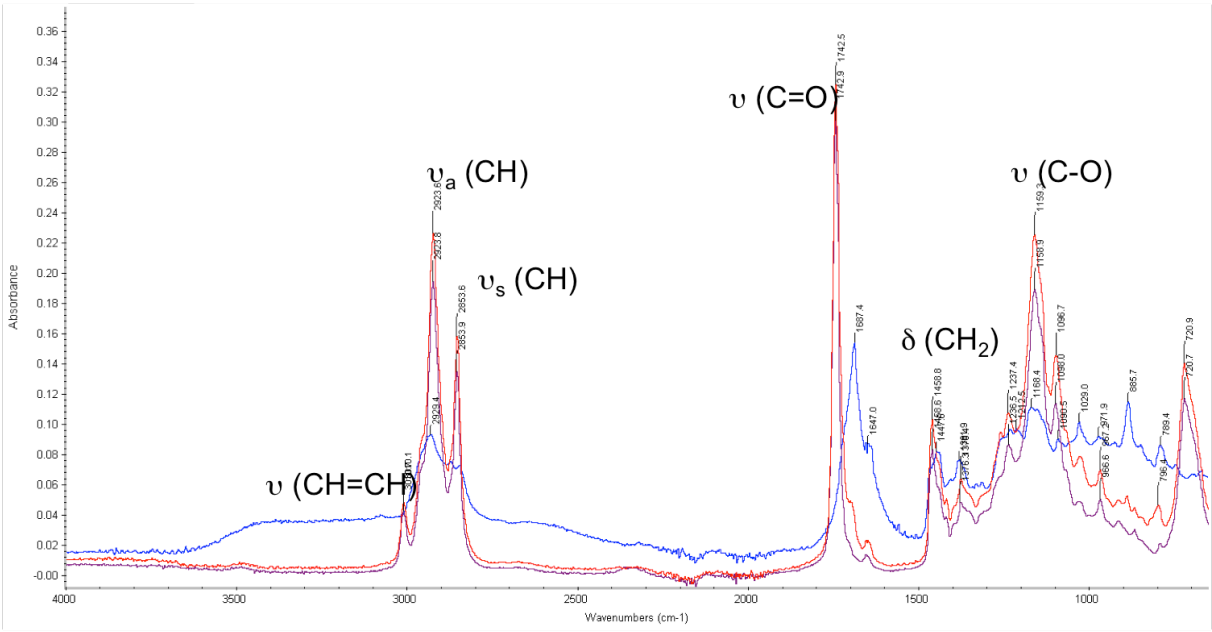

Figure 8. FTIR spectrum of the sandarac resin (Kremer) (blue), linseed oil (purple) and varnish composed of sandarac and oil (red).

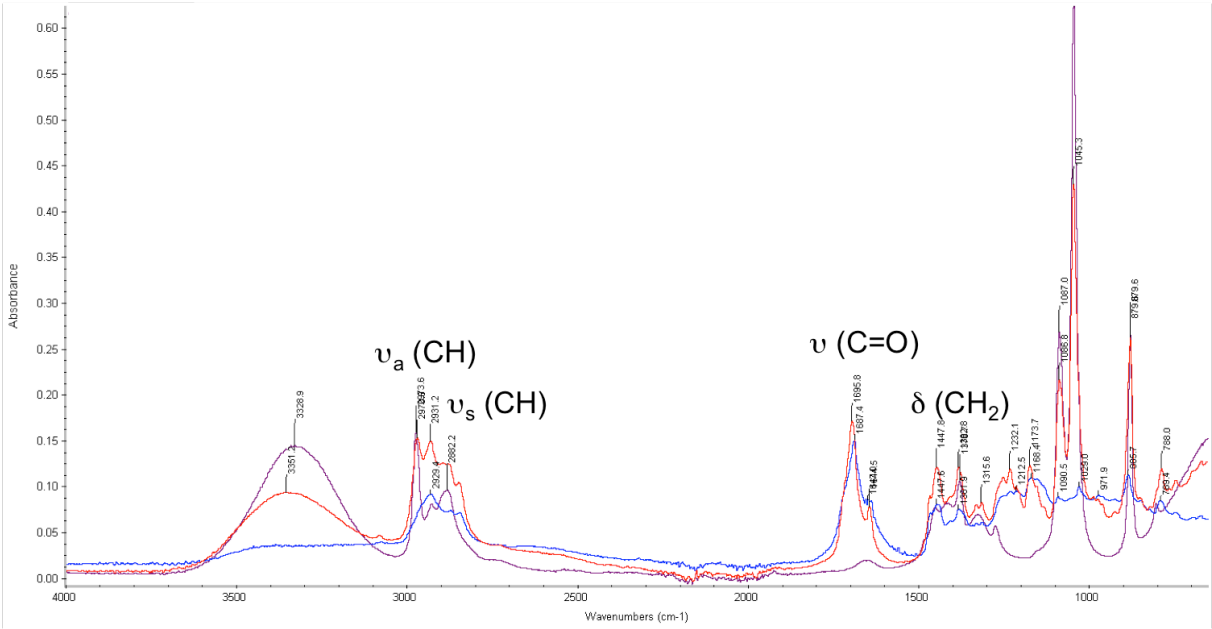

Figure 9. FTIR spectrum of the sandarac resin (Kremer) (blue), ethanol (purple) and varnish composed of sandarac and alcohol (red).

From the Figure 8, showing the spectrum of the 'fat' varnish, it is obvious that the dissolution of the sandarac in oil went to a nearly negligible extent, and the varnish is almost

completely represented by bands corresponding to the linseed oil spectrum. The spectrum of linseed oil has characteristic bands at 2800–3000 cm^{-1}, representing the C-H stretching, a band around 1740 cm^{-1}, corresponding to C=O stretching, and several bands within the region 719–1474 cm^{-1}.

Meanwhile, the spectrum of the alcohol varnish resembles the spectrum that could be reconstituted from the spectra of each component.

A weak band is observed at 3070 cm^{-1} corresponds to the frequency of elongation of the CH groups of vinyl groups. A fine band between 1645 and 1650 cm^{-1} is observed on the *sandarac* spectrum. This band corresponds to the elongation of the C = C double bond. A second thin strip at about 890-900 cm^{-1} is present.

The diterpenoid resins possess a band around 3080 cm corresponding to the oscillatory vibration of the double bond C=C of the vinyl function of pimaranes in coniferous resins. A band centred on 2929 cm^{-1} is observed, coming from the elongation of the CH_2, potentially belonging to vinyl functions present in the pimaranes. The carbonyl band is an intense band with a maximum around 1695 cm^{-1} for the *sandarac* resin.

Thus, these preliminary trials of varnish elaboration showed the importance of the availability of the 'fresh' resin and thus obtained results support the advice given in the recipe, that the resin has to be freshly extracted from the cypress and immediately mixed with the oil. That is why the *sandarac* that is supplied on the market today is normally used for alcohol-based varnishes for musical instruments, and no longer as a fat varnish for artistic purposes.

5. F. The varnish problem

As stated in the Bibliography part varnishes have protective and esthetical functions. They protect the paintings from dust, light and oxygen or pollutants in the atmosphere. More important, however, are their optical properties: they saturate the colours, enhance contrast and give an even gloss to the painting. Varnishes make paintings look clear with more visible details, especially in dark regions [18-20]. They have been used until the late 19^{th} century, when artists began to try out new techniques and materials to find ways to express their thoughts.

In the beginning, resins or mixtures of oils with resins were used as varnish materials. Unfortunately, these varnish materials decompose rather quickly and the films become brittle, breakable and yellow. Yellowing is often the main degradation phenomenon, and a yellowed

varnish can considerably obscure a painting, especially if it consist of many layers and is relatively thick. A strongly yellowed varnish also considerably changes the appearance of a painting. Not only the underlying colours change, but also contrast and balance between the colours, since not all colours change to the same extent. For this reason, the yellowed varnish has to be removed and replaced to restore the initial colours and appearance of the painting.

Varnishes are normally removed by the mechanical and chemical action of a cotton swab drenched in organic solvents. Solvents of sufficient polarity are needed to remove an old and oxidized varnish, and this treatment may damage a painting: swelling and deswelling of the paint layers leads to mechanical stress, and soluble components can be leached out of the paint [21]. These outcomes are even more probable when the new varnish is applied, which is not surprising since amount and residence time of the solvent is even greater [22]. Therefore, the solvent of a new varnish should be as apolar as possible to minimize these effects.

Thus, it becomes obvious that the renewal of a painting's varnish is a severe intervention and should be avoided as far as possible. Consequently, an ideal varnish should be apolar and stable, and it should not oxidize or yellow. Unfortunately, the opposite is true: the commonly used varnish materials, natural resins, are very unstable, oxidize very quickly and yellow considerably. Thus they need to be replaced regularly.

Evidently, the choice of apolar solvent to remove the varnish based on the *sandarac* resin would not be efficient, as seen from its solubility tests. The *sandarac* resin is a 'hard' resin that will definitely require highly polar solvents, such as ethanol, to be dissolved. This explains why the 'perfect varnish' is obtained only from the fresh resin that has been exposed to the environment for a time as short as possible. Moreover, the obtained results for the *sandarac* resin underlines that there is a crucial difference between the resin at its harvest and after its storage without preservation.

Leonardo da Vinci in his recipe demonstrated understanding the fact that the elaboration of a varnish does not begin with an artist buying a resin and applying it as a varnish. In fact, the elaboration of a varnish starts much earlier, with the resin coming out of a tree and being irradiated by the sun. This sunlight irradiation largely influences the properties of the resin, provoking polymerisation on the sites prone to it, such as system of conjugated double bonds not hindered sterically.

Figure 10. Mastic harvest under protection from sunlight. After cutting, the branches are wrapped in aluminum foil to avoid sunlight irradiation. The resin was collected from the foil after 4 days at dusk or dawn to minimize exposure to light [23].

Based on the gained in this study knowledge regarding the *sandarac* resin, we can conclude that the only way to prepare a 'perfect varnish' as in the Leonardo da Vinci's recipe is to collect sandarac resin while preserving it from sun irradiation. Such protection when harvesting has already been done for the mastic resin collection (Figure 10) and described in the PhD thesis of Patrick Dietmann [23]. The reason for harvesting mastic in darkness was to avoid radical formation in the fresh resin and consequently to suppress and slow down oxidation. As a result, harvesting in darkness did reduce the amount of radicals significantly.

The collection of the *sandarac* resin today without protection from sunlight and specific conditions of its further storage (in a dark and cool capacity) with commercial purposes provoked artist to refuse from *sandarac* as a resin for paintings varnish, due to its hardness and low solubility in solvents.

Thus, for further analyses of the *sandarac* resin it would be highly advised to take all the precautions necessary to protect the resin from sunlight and air oxidation.

6. G. References

1. Scalarone D, Lazzari M, Chiantore O (2003) Ageing behaviour and analytical pyrolysis characterisation of diterpenic resins used as art materials: Manila copal and sandarac. J. Anal. Appl. Pyrolysis. 68 – 69: 115 – 136.
2. Romero-Noguera J, Martín-Sánchez I, Doménech-Carbó MT, Osete- Cortina L, López-Miras MM, Bolívar-Galiano F (2014) Analytical characterisation of the biodeterioration of diterpenoid labdanic varnishes used in pictorial techniques: sandarac and Manila copal. Int Biodeterior Biodegrad 90:99–105.
3. Dietemann P, Edelmanna MJ, Meisterhans C, Pfeiffer C, Zumbühl S, Knochenmuss R, Zenobi R (200) Artificial Photoaging of Triterpenes Studied by Graphite-Assisted Laser Desorption/Ionization Mass Spectrometry. Helvetica Chimica Acta. 83: 1766 – 1777.
4. Vahur S, Teearu A, Haljasorg T, Burk P, Leito I, Kaljurand I (2012) Analysis of dammar resin with MALDI-FT-ICR-MS and APCI-FT-ICR-MS. J Mass Spectrom. 47(3): 392-409.
5. Lambert JB (1985) Amber from the Dominican Republic: analysis by nuclear magnetic resonance. Archaeometry. 27(1): 43-51.
6. Lambert JB, Poinar GO (2002) Amber: the Organic Gemstone. Acc. Chem. Res. 35: 628-636.
7. Silverstein RM, Webster FX (1998) Spectrometric Identification of Organic Compounds. John Wiley & Sons: New York.
8. Clifford DJ, Hatcher PG (1995) Structural transformations of polylabdanoid resinites during maturation. Org. Geochem. 23 (5): 407-418.
9. Banerjee S, Mazumdar S (2011) Electrospray Ionization Mass Spectrometry: A Technique to Access the Information beyond the Molecular Weight of the Analyte. International Journal of Analytical Chemistry. 2012: 40.
10. Knapp DR (1979) Handbook of Analytical Derivatization Reactions; John Wiley & Sons, New York.
11. M. Colombini, F. Modugno. Organic Mass Spectrometry in Art and Archaeology. 2009 John Wiley & Sons, Ltd.
12. Baccile N, Laurent G, Babonneau F, Fayon F, Titirici MM, Antonietti M (2009) Structural Characterization of Hydrothermal Carbon Spheres by Advanced Solid-State MAS 13C NMR Investigations. J. Phys. Chem. C. 113: 9644–9654.

13. Scalarone D, Van der Horst J, Boon JJ, Chiantore O (2003) Direct- temperature mass spectrometric detection of volatile terpenoids and natural terpenoid polymers in fresh and artificially aged resins. J Mass Spectrom 38: 607–617.
14. Cameron, J. Oils and Varnishes. (J. & A. Churchill, 1886).
15. Armenini, G. B. On the true precepts of the art of painting. (Ayer Publishing, 1977).
16. Anonyme. In Medieval and Renaissance treatises on the arts of painting: original texts with English translations 643–718 (M.P. Merrifield, 1849)
17. Cennini, C. & Tambroni, G. A treatise on painting. (Lumley, 1844).
18. R.E. De la Rie, "The Influence of Varnishes on the Appearance of Paintings", Studies in Conservation 1987, 32, pp. 1-13.
19. R. De la Rie, "Old Master Paintings: A Study of the Varnish Problem", Anal. Chem. 1989, 61, p. 1228A.
20. R.S. Berns, and R.E. De la Rie, "The relative importance of surface roughness and refractive index in the effects of varnishes on the appearance of paintings", in Preprints of the 13th triennial meeting of the ICOM Committee for Conservation, Vol. I (Ed.: V. R.), James & James (Science Publishers) Ltd., Rio de Janeiro, 2002, pp. 211-216.
21. N. Stolow, "Solvent Action", in "On Picture Varnishes and their Solvents (Eds.: R.L. Feller, N. Stolow, E.H. Jones), National Gallery of Art, Washington D.C., 1985, pp. 47-116.
22. K. Sutherland, "The Extraction of Soluble Components from an Oil Paint Film by a Varnish Solution", Studies in Conservation 2000, 45, pp. 54-62.
23. Dietemann P (2003) Towards More Stable Natural Resin Varnishes for Paintings. The Aging of Triterpenoid Resins and Varnishes.

7. Conclusion

Natural diterpenoid resin *sandarac* was widely used as a varnish on paintings in ancient times. This resin is not stable, but polymerizes, oxidizes, subsequently causing solubility problems, and yellows with time. The latter is of major significance since yellowing obscures a painting and can considerably alter its appearance. As a result, varnishes have to be removed and replaced frequently enough, a harsh treatment that can damage the painting. Thus it is preferable to find ways to improve the performance of varnishes with respect to polymerization and, especially, yellowing. This would reduce the number of varnish replacements necessary, and valuable and unique works of art could be protected [1, 2]. This thesis studied the ageing of diterpenoid resin *sandarac* with the aim to improve the work of restorers and to light out the reality for artists when they are purchasing today commercial resin *sandarac*.

This PhD work, however, showed that commercial resins, usually considered “fresh”, are in an advanced stage of polymerization, and high amounts of oxidized compounds are present. These results were obtained by the combination of analytical methods including those that were not largely used in the field of conservation science: MALDI-TOF/ ESI-Orbitrap and solid-state NMR. Consequently, several ageing studies were performed to study the ageing pathways in UV light and by thermal treatment. In the light of the obtained results, the factors influencing the *sandarac* resins properties and its polymerization behaviour were discussed.

With ageing of natural resins, that are already very complex mixtures of different compounds, mostly terpenoids, their complexity increases even more [3, 4, 5]. In order to understand the ageing behaviour of such complex mixtures, it seemed to be useful to first study the ageing behaviour of individual components. In this research work, the communic acid was chosen as such compound and was artificially polymerized to investigate the changes occurring during reticulation.

Conventionally, the polymerization of the *sandarac* resin was described with a model that postulated the communic acid to be the precursor compound responsible for the resin reticulation. Ageing in UV light meant polymerization proceeding by activation of system of conjugated double bonds. The UV irradiation was believed to be necessary for the initiation of reticulation reactions.

A kinetic study revealed that the polymer concentrations change considerably within days after change of illumination conditions. This explains the rapid polymerization of varnishes and proves that ageing reactions are very dynamic and vigorous.

Ageing of a single communic acid resulted in a remarkably wide variety of products, indicating multiple activation points and progressive reaction of initial product. With following oxidation, a diterpenoid was oxidized in many different locations. A great number of oxygen atoms were incorporated and a large variety of ageing products were observed. Such a complex MS pattern was found for all artificially aged communic acid samples measured by ESI-Orbitrap. Different numbers of oxygen atoms were incorporated, leading to signals with a mass difference of 16 Da. Simultaneous loss of hydrogen (e.g. by allylic oxidation or oxidation from alcohols to acids) [6] leaded to mass increases of 14 Da. Different combinations of 14 and 16 Da increments leaded to signal groups becoming broader and less distinct with increasing mass.

Since ageing of a single communic acid already brought up to a surprisingly large distribution of products, the complex composition of aged *sandarac* is not due to the formation of a few ageing products from a large number of initial compounds, but rather the complexity of the ageing products of each single component.

Qualitative and quantitative analyses by gas chromatography- mass spectrometry (GC-MS) were accomplished for identification of the chemical composition of the *sandarac* resin.

GCMS was found to be valuable tool for the analysis of the diterpenoid fraction of commercial *sandarac* resin. The method of internal standard was applied in order to quantify and assess the sample's diterpenoid content. As a result of quantification, the non-polymerised fraction of the *sandarac* resin is less than 30% of the sample in total.

Six compounds with labdane and pimarane skeletons were identified in the resin. It has been demonstrated as well that the quantitative chemical composition of *sandarac* resin differs from one supplier to another, while the qualitative composition is almost the same. Sandaracopimaric and communic acids are present in all resins. The rest of the diterpenoids is found in the different *sandarac* analysed with various proportions. Dihydroagathic acid was not identified in the *sandarac* from *La Marchande de Couleurs*, but communic acid is present in a larger quantity compared to other resins. The *sandarac* from *L'Atelier Montessori* demonstrated only traces of methyl pinifolic and dihydroagathic acids. We show here a wide range of composition for resins from different suppliers, which can explain the difference existing in the literature concerning *sandarac*. The contradiction that appeared in the previous studies dedicate to the *sandarac* analyses [7, 8, 9] can be explained by this variability.

Another explanation would rely on the potential influence of the resin derivation method. In order to deeper the existing knowledge, it would also be interesting to investigate the true impact of the derivation methods.

The complexity of commercial *sandarac* resin was well reflected by the MALDI-TOF and ESI-Orbitrap mass spectra. As a result, MALDI-TOF mass spectra comprised three clusters of peaks in the m/z range of 300–900, and for the ESI-Orbitrap mass spectra contained five clusters of peaks in the m/z range of 300–1100. The peaks in the clusters corresponded to the oxygenated derivatives of the diterpenoids.

MALDI and ESI were concluded to be complementary ionization sources for the analysis of the *sandarac* resin. In both sources, preferably polar (extensively oxidized) components of the resin were ionized (probably, mostly as Na^+ adducts).

Many of the new insights on the polymerization process of the *sandarac* resin arose from the use of the analytical method newly introduced in the field of conservation science: solid-state NMR including several techniques such as single-pulse, cross-polarization and inversion recovery cross-polarization.

The results obtained from the IRCP experiments revealed the rigid character of the *sandarac* resin samples analyzed and justified the hypothesis that the rest of the sample, which could not be quantified by the method of internal standard, would have a polymeric nature.

Protection from any light during harvest was concluded to dramatically suppress spontaneous polymerization and prevent oxidation of diterpenoids in fresh *sandarac*. Dark harvested *sandarac* would contain no polymer, and that is likely the reason why it is prescribed in the recipe of Leonardo da Vinci from his collection of writings ‘A Treatise on Painting’ to prepare the varnish straight after the resin extraction from the conifer in spring.

Systematic analyses on the natural products that are sold to artists on the market can provide them with a better insight on the materials they are using. Of course, the composition of natural products on the molecular level may differ notably depending on many factors such as geographic and climatic; differences that would impact drastically the artist’s work.

As further perspectives of the presented work we would first of all suggest to keep going with principle of system simplification, as we did here with the communic acid. Choosing a model for the polymerization studies of the *sandarac* resin has shown to be a reliable approach as it allows to understand on the molecular level the changes induced by artificial ageing. Therefore the same strategy would be highly recommend to explore the

polymerization/oxidation processes happening in the other complex resins beyond *sandarac*, such as copal.

During the analyses of the high molecular part of the *sandarac* resin by MALDI-TOF and ESI-Orbitrap many components within the clusters were not identified. So, as a second perspective of this PhD would be the identification of numerous peaks remained non-identified by means of MS/MS fragmentation analyses. This would probably give clear indications on sites of oxidation, hydrogen elimination and other modifications within the clusters.

For the further investigation in this study it would be interesting to study the samples of fresh resin. When collecting the fresh resin from the conifer special precautions are to be taken in order to protect the fresh resin form sun light irradiation and air oxidation, just like in the thesis of Patrick Dietmann [10].

7. A. References

1. De la Rie R (1989) Old Master Paintings: A Study of the Varnish Problem. Anal. Chem. 61(21): 1228A–1240A.
2. Mills JS, White R (1994) The Organic Chemistry of Museum Objects. 2nd ed., Butterworth-Heinemann, Oxford.
3. Boon J, Van der Doelen G (1998) Advances in the Current Understanding of Aged Dammar and Mastic Triterpenoid Varnishes on the Molecular Level. Postprints of Firnis, Material Aesthetik Geschichte, International Kolloquium, Braunschweig. 92-104.
4. Van der Doelen GA, Van den Berg KJ, Boon JJ. "Comparative Chromatographic and Mass-Spectrometric Studies of Triterpenoid Varnishes: Fresh Material and Aged Samples from Paintings", Studies in Conservation 1998, 43, pp. 249-264.
5. Van der Doelen GA, Van den Berg KJ, Boon JJ, Shibayama N, De la Rie RE, Genuit WJL (1998) Analysis of fresh triterpenoid resins and aged triterpenoid varnishes by high-performance liquid chromatography-atmospheric pressure chemical ionisation (tandem) mass spectrometry. Journal of Chromatography. 809: 21-37.
6. Zumbühl S, Knochenmuss R, Wülfert S, Dubois F, Dale MJ, Zenobi R (1998) A Graphite-Assisted Laser Desorption/Ionisation Study of Light-Induced Aging in Triterpene Dammar and Mastic Varnishes. Anal. Chem. 70: 707-715.
7. Romero-Noguera J, Martín-Sánchez I, Doménech-Carbó MT, Osete-Cortina L, López-Miras MM, Bolívar-Galiano F (2014) Analytical characterisation of the biodeterioration of diterpenoid labdanic varnishes used in pictorial techniques: Sandarac and Manila copal. International Biodeterioration & Biodegradation. 90: 99-105.
8. Scalarone D, Lazzari M, Chiantore O (2003) Ageing behaviour and analytical pyrolysis characterisation of diterpenic resins used as art materials: Manila copal and sandarac. J. Anal. Appl. Pyrolysis. 68 – 69: 115 – 136.
9. Scalarone D, Lazzari M, Chiantore O (2003) Ageing behaviour and analytical pyrolysis characterisation of diterpenic resins used as art materials: Manila copal and sandarac. J. Anal. Appl. Pyrolysis. 68 – 69: 115 – 136.
10. Dietemann P (2003) Towards More Stable Natural Resin Varnishes for Paintings. The Aging of Triterpenoid Resins and Varnishes.

Abstract

The chemical composition of *sandarac* resin and its principal component communic acid was investigated by gas chromatography-mass spectrometry (GC-MS), MALDI-TOF (Matrix Assisted Laser Desorption Ionization - Time of Flight), ESI (Electrospray ionization)-Orbitrap, FTIR/ATR (Fourier transform infrared spectroscopy/Attenuated total reflectance), liquid- and solid state NMR (Nuclear magnetic resonance) spectroscopy.

Six compounds with labdane and pimarane skeletons were identified in the commercial resin. The obtained mass spectra were interpreted and the mass spectrometric behaviour of these diterpenoids under EI conditions was described. Quantitative analysis by the method of internal standard revealed that identified diterpenoids represent only 10–30% of the analysed sample.

The polymerization of the *sandarac* resin was described with a model that postulated the communic acid to be the precursor compound responsible for the resin reticulation. Ageing of a single communic acid resulted in a remarkably wide variety of products, indicating multiple activation points and progressive reaction of initial product. Different numbers of oxygen atoms were incorporated, leading to signals with a mass difference of 16 Da. Simultaneous loss of hydrogen (e.g. by allylic oxidation or oxidation from alcohols to acids) leaded to mass increases of 14 Da.

The *sandarac* resin from different suppliers was analysed (from *Kremer, Okhra, Color Rare, La Marchande de Couleurs, L'Atelier Montessori, Hevea*). The analysis of different lumps of resins showed that the chemical composition differs from one lump to another, varying mainly in the relative distributions of the components.

The complexity of the reticulated fraction of the commercial *sandarac* resin was well reflected by the MALDI-TOF and ESI-Orbitrap mass spectra. As a result, MALDI-TOF mass spectra comprised three clusters of peaks in the m/z range of 300–900, and for the ESI-Orbitrap mass spectra contained five clusters of peaks in the m/z range of 300–1100. The peaks in the clusters corresponded to the oxygenated derivatives of the diterpenoids.

The results obtained from the IRCP (Inversion Recovery Cross-Polarization) experiments revealed the rigid character of the *sandarac* resin samples analyzed and justified the hypothesis that the rest of the sample, which could not be quantified by the method of internal standard, would have a polymeric nature.

Key words: Varnish, sandarac, diterpenoid, communic acid, GC-MS, MALDI-TOF, ESI – Orbitrap, NMR.

Résumé

La composition chimique de la résine *sandaraque* et de son composant principal l'acide communique a été étudiée par chromatographie en phase gazeuse – spectrométrie de masse (GC-MS), MALDI-TOF (désorption-ionisation laser assistée par matrice - temps de vol), ESI (ionisation par électronébuliseur) - Orbitrap, FTIR/ATR (spectroscopie infrarouge à transformée de Fourier/réflectance totale atténuée), spectroscopie de RMN (résonance magnétique nucléaire) à l'état solide et liquide.

Six composés avec des squelettes labdane et pimarane ont été identifiés dans la résine commerciale. Les spectres de masse obtenus ont été interprétés et le comportement en spectrométrie de masse de ces diterpénoïdes dans les conditions de l'impact électronique a été décrit. L'analyse quantitative par la méthode de l'étalon interne a révélé que les diterpénoïdes identifiés ne représentaient que 10 à 30% de l'échantillon analysé.

La polymérisation de la résine sandaraque a été décrite avec un modèle postulant que l'acide communique est le composé précurseur responsable de la réticulation de la résine. Le vieillissement de l'acide communique seul a entraîné une variété remarquablement large de produits, indiquant plusieurs points d'activation et une réaction progressive du produit initial. Des nombres différents d'atomes d'oxygène ont été incorporés, conduisant à des signaux avec une différence de masse de 16 Da. La perte simultanée d'hydrogène (par exemple par oxydation allylique ou oxydation d'alcools en acides) a conduit à des augmentations de masse de 14 Da.

La résine sandaraque de différents fournisseurs a été analysée (de *Kremer, Okhra, Color Rare, La Marchande de Couleurs, L'Atelier Montessori, Hevea*). L'analyse de différents groupements de résines a montré que la composition chimique diffère d'un lot à l'autre, en fonction principalement des distributions relatives des composants.

La complexité de la fraction réticulée de la résine commerciale sandaraque est bien reflétée par les spectres de masse MALDI-TOF et ESI-Orbitrap. En conséquence, les spectres de masse de MALDI-TOF comprenaient trois clusters de pics dans la gamme m/z de 300-900, et ceux d'ESI-Orbitrap contenaient cinq clusters de pics dans la gamme m/z de 300-1100. Les pics dans les clusters correspondent aux dérivés oxygénés des diterpénoïdes.

Les résultats obtenus à partir des expériences RMN par IRCP (Inversion Recovery Cross-Polarization) ont révélé le caractère rigide des échantillons de la résine sandaraque analysés et justifiaient l'hypothèse que le reste de l'échantillon, qui ne pouvait être quantifié par la méthode de l'étalon interne, aurait un caractère polymère.

Mots clés: Vernis, sandaraque, diterpénoïde, acide communique, GC-MS, MALDI-TOF, ESI - Orbitrap, RMN.